Structure and chemistry of two heuweltjies in areas with contrasting aridity in the Olifants/Doorn catchment: Evidence for downward salt movement

by

Magdaleen Hattingh

Thesis presented in fulfilment of the requirements for the degree of

Master of Science in the Faculty of Agriculture

at Stellenbosch University

Supervisor: Prof Catherine E. Clarke[a]

Co-supervisors: Dr Michele L. Francis[a] and Prof Jodie A. Miller[b]

[a] Faculty of AgriSciences, Department of Soil Science

[b]Faculty of Science, Department of Earth Science

April 2022

Declaration

By submitting this thesis electronically, I declare that the entirety of the work contained therein is my own, original work, that I am the sole author thereof (save to the extent explicitly otherwise stated), that reproduction and publication thereof by Stellenbosch University will not infringe any third party rights and that I have not previously in its entirety or in part submitted it for obtaining any qualification.

April 2022

Acknowledgements

Your support network is the solid ground from which you can propel yourself upwards (Anna Barnes). I am grateful for those who willingly and dutifully walked beside me during the completion of my thesis. To Cathy Clarke, Michele Francis and Jodie Miller, if I could one day be half the women you are in science, I would deem myself rich. Thank you for sharing your knowledge, guiding where it was needed and having the patience. Your mentorship and belief in my abilities had a major influence on my growth as a scientist and made all the late nights worth the while.

My mother, the example of a resilient woman that never gives up on any challenge and who showed me how to lead a faith-based life. Thank you for always placing my needs before yours, checking up and motivating on the good and bad days. To my father, thank you for instilling an inquisitive mindset from a young age, for reminding me that I can do anything through hard work and for introducing me to the realm of soil. To my siblings, life would have been pretty mundane without your presence. I appreciate the last-minute help in the lab before curfew, endless hours of crushing dorbank, sharing common interests and making sure I enjoy life between all the hard work.

To my friends, who are my second family, thank you for keeping me sane and balanced throughout these two years. Thank you for carrying the burdens of life with me and making my load a little lighter. May we always support each other's dreams and endeavours.

To lab personnel at soil science (Leana, Faiek and Vumile), thank you for always going the extra mile to make sure I was assisted in the lab the best way possible. To all the colleagues at soil science and Nicola Vermonti at Conservation Ecology, thank you for assisting with field and lab work, sharing, and supporting during overwhelming weeks. You are all destined to achieve great things. To Prof Shayne Jacobs, it was a privilege to have met and spend time with you in the field. May your impact at Conservation Ecology be remembered for years to come. Thank you to Dr Janine Colling at DSI BIOGRIP node for Soil and Water Analysis (hosted at Stellenbosch University), Dr Remy Bucher at iThemba LABS and the Soil, Water and Plant Diagnostics Laboratory at Elsenburg for analytical support.

The financial assistance of the National Research Foundation (NRF) towards this research is hereby acknowledged (Grant Number 118594). Opinions expressed and conclusions arrived at, are those of the author and are not necessarily to be attributed to the NRF.

Abstract

The Olifants/Doorn catchment in the West Coast region of South Africa is variably affected by saline groundwater. Other areas along the coast of southern Africa experience similar mean annual precipitation rates but do not display the same variability in saline groundwater. This suggests additional contributions to groundwater salinisation in the West Coast. Regularly spaced earthen mounds, termed heuweltjies (up to 2 m high and about 32 m wide), occur in abundance in the Olifants/Doorn catchment area. These mounds are characterised by significantly higher salinity levels compared to surrounding soils. Variable saline groundwater seems to spatially correspond with salt affected heuweltjies, suggesting that mound salts might be contributing to groundwater salinisation in the region. Two heuweltjies, one in a semi-arid climate (Klawer) and the another in a more Mediterranean climate (Piketberg), were excavated to determine the morphological properties and distribution of soluble salts and ions within the mounds. The study was conducted to determine and compare if salts in heuweltjies with different mean annual precipitation rates could be contributing to groundwater salinisation of the Olifants/Doorn catchment. The mineralogy, soil texture, electrical conductivity, pH, anion and cation profiles and dissolved silica was analysed to determine if these heuweltjies are potentially contributing to the groundwater chemistry. Dominant salts exclusively present in heuweltjie soils were identified in both the mineralogy and modelling of ion concentrations. Calcite (in both heuweltjies) and gypsum (in the mound in Klawer) were identified to be enriched in mound soils. The less soluble calcite was saturated at closer to the surface compared to more soluble gypsum at greater depths in both mounds. This sequence of precipitation of increasing soluble salts suggested that the net direction of water movement occurs downward in mounds of both high rainfall and lower rainfall areas. The clay mineralogy did not support the parent material as a provenance. Additionally, increased coarse soil texture with depth and large macropores of heuweltjies indicated that groundwater is an unlikely cause of mound salinity. The chemical signature of salts indicated a marine origin. Concentrated hotspots of ions and minerals within biogenic features of mound soils suggested that burrowing fauna are responsible for accumulating marine-derived salts in heuweltjie soils. Preferential flow paths that aid solute movement were observed in gravelly dorbank, fractured platy dorbank and as termite channels and rodent burrows in the mound centres of both Piketberg and Klawer. This study reinforced the hypothesis that heuweltjie salts are generated within mounds, possibly through biological activity, and that salts are potentially translocated to the groundwater through preferential flow paths in mounds of the Olifants/Doorn catchment.

Opsomming

Die Olifants/Doorn opvangsgebied aan die Weskus van Suid-Afrika word variërend deur sout grondwater geaffekteer. Die groter kus streek van suidelike Afrika ontvang soortgelyke gemiddelde jaarlikse reënval, maar toon nie dieselfde mate van variasie in sout grondwater nie. Dít dui daarop dat addisionele bydraes tot grondwater versouting in die Weskus plaasvind. Eweredig gespasiëerde grondhopies, bekend as heuweltjies (tot 2 m hoog en 32 m breed), word geredelik aangetref in die Olifants/Doorn opvangsgebied. Heuweltjies word gekenmerk deur sout inhoude wat noemenswaardig verskil van die omliggende gronde. Dit wil voorkom asof die variërende sout grondwater ruimtelik ooreenstem met die voorkoms van heuweltjies, wat daarop dui dat die hope moontlik tot die versouting van grondwater in die gebied bydra. Twee heuweltjies, een in ‘n semi-droog klimaat (Klawer), en die ander in ‘n Meditereense klimaat (Piketberg), is gemonster om die morfologiese eienskappe en verspreiding van oplosbare soute en ione in die hope te bepaal. Die studie is uitgevoer om te bepaal en te vergelyk, of oplosbare soute in heuweltjies, wat verskillende gemiddelde jaarlikse reënval ontvang, moontlik kan bydra tot grondwater versouting in die Olifants/Doorn opvangsgebied. Die mineralogie, grond tekstuur, elektriese geleiding, pH, anioon en katioon profiele en opgelosde silika is bepaal om vas te stel of heuweltjies potensieel tot die grondwater chemie bydra. Dominante soute wat uitsluitlik teenwoordig was in heuweltjie gronde was geïdentifiseer in beide die mineralogiese samestelling en deur modellering van ioon konsentrasies. Kalsiet (in beide heuwletjies) en gips (in die Klawer heuweltjie) was teenwoordig in heuweltjie gronde. Die minder oplosbare kalsiet was versadig by nader aan die oppervlak in vergelyking met die meer oplosbare gips teenwoordig dieper in die gronde van beide heuweltjies. Hierdie volgorde van presipitasie van toenemend oplosbare soute dui daarop dat die netto waterbeweging afwaarts is in heuweltjies van beide hoër- en laer reënval areas. Die klei mineralogie het nie ‘n soutbron afkomstig van die moedermateriaal ondersteun nie. Daarbenewens het ‘n toename in growwe tekstuur gronde met diepte en die groot makroporieë van die heuweltjies, aangedui dat die grondwater ‘n onwaarskynlike bron is vir die soutinhoud van die heuweltjies. Die chemiese samestelling van die soute in heuweltjies het daarop gedui dat die soute ‘n mariene oorsprong het. Gekonsentreerde areas van ione en minerale in assosiasie met biogeniese kenmerke van die heuweltjie gronde, het daarop gedui dat fauna wat plantmateriaal versamel, verantwoordelik is vir die opbou van soute met ‘n mariene oorspong, in gronde van die heuweltjies. Voorkeurvloei roetes wat die vervoer van opgeloste stowwe bevoordeel was waargeneem in gruisagtige dorbank, plaatagtige dorbank met breuke, en as termiet kanale en knaagdier tonnels in

heuweltjie kerne van beide Piketberg en Klawer. Hierdie studie het addisionele ondersteuning gebied tot die hipotese dat die soute wat kenmerkend is aan heuweltjies binne die hope gegenereer word, moontlik deur biologiese aktiwiteit, en dat hierdie soute potensieel na die grondwater getranslokeer word deur voorkeurvloei roetes in heuweltjies van diie Olifants/Doorn opvangsgebied.

Table of Contents

List of Figures

List of Tables

1 Introduction

Salinisation has long been a widespread global problem (Pitman and Läuchli, 2002; Bouchaou et al., 2008; Vengosh, 2014). Concerningly, salinisation is predicted to increase exponentially in the 21st century due to climate change that will bring about rising sea levels, increased groundwater abstraction and higher evaporation rates (Daliakopoulos et al., 2016). The process of salinisation constitutes the concentration of dissolved salts in soil and water, and is driven by either natural or anthropogenic mechanisms (Salama et al., 1999). Mechanisms of natural (primary) salinisation include; evaporative concentration (Vengosh, 2014; Alvarez et al., 2015), atmospheric deposition of marine aerosols (Bergh and Compton, 2015) or windblown dust (Gamboa et al., 2019), seawater intrusion (Vengosh and Rosenthal, 1994; Daliakopoulos et al., 2016), and weathering of parent material, carbonates or silicates (Blum et al., 1998; Nell and van Huyssteen, 2014). Anthropogenic (secondary) factors of salinisation are mainly attributed to the use of saline irrigation water (Daliakopoulos et al., 2016), wastewater discharge and overfertilisation (Vengosh, 2014).

In semi-arid and arid dryland environments salinisation commonly occurs due to insufficient rainfall for annual leaching of salts (Vengosh and Rosenthal, 1994; Hillel, 2004; Vengosh, 2014). Salinisation particularly limits the supply of potable fresh water in these areas as groundwater aquifers are the main water source (Vengosh and Rosenthal, 1994; Vengosh et al., 1999). One of the biggest concerns related to salinisation is its detrimental effect on agricultural crop productivity and the threat it poses through the decline of arable agricultural land (Pitman and Läuchli, 2002; Smith and Compton, 2004; Nell and van Huyssteen, 2014). Multiple primary and secondary drivers can play a role in an area which introduces complexity. Furthermore, region-specific salinisation mechanisms are poorly understood (Bouchaou et al., 2008). Consequently, understanding all the mechanisms contributing to salinisation of groundwater and soils poses a challenge but has important implications in resource management of saline affected soils and groundwater (Bouchaou et al., 2008).

The West Coast of South Africa is such an area where possible regional drivers of salinisation have not received adequate attention. Groundwater in the West Coast region is variably saline (Miller et al., 2018). The region has overall low precipitation rates and high evaporative rates in some areas (Miller et al., 2018). Additionally, it has been predicted that the West Coast will be highly affected by climate change (Archer et al., 2009; Ziervogel et al., 2014). The West Coast also experiences increased demands for groundwater abstraction for agricultural use due

to frequent droughts and accompanied insufficient surface water sources (Miller et al., 2018; van Rooyen et al., 2021). These factors all pose major challenges with regards to the management of water resources along the West Coast.

Although some areas in sub-humid and humid zones of South Africa contain salt-affected soils, areas of highest soil and groundwater salinity and sodicity are found in the semi-arid regions of the western part of the country (Nell and van Huyssteen, 2014). The Olifants/Doorn and Berg River catchments (Figure 1.1) the West Coast region show weakly to moderately or severely saline groundwater (Miller et al., 2018; Watson et al., 2020a; van Rooyen et al., 2021), whereas the Buffels River catchment (Figure 1.1) shows moderately to severely saline groundwater in the northern parts of the West Coast (Miller et al., 2018; van Gend et al., 2021).

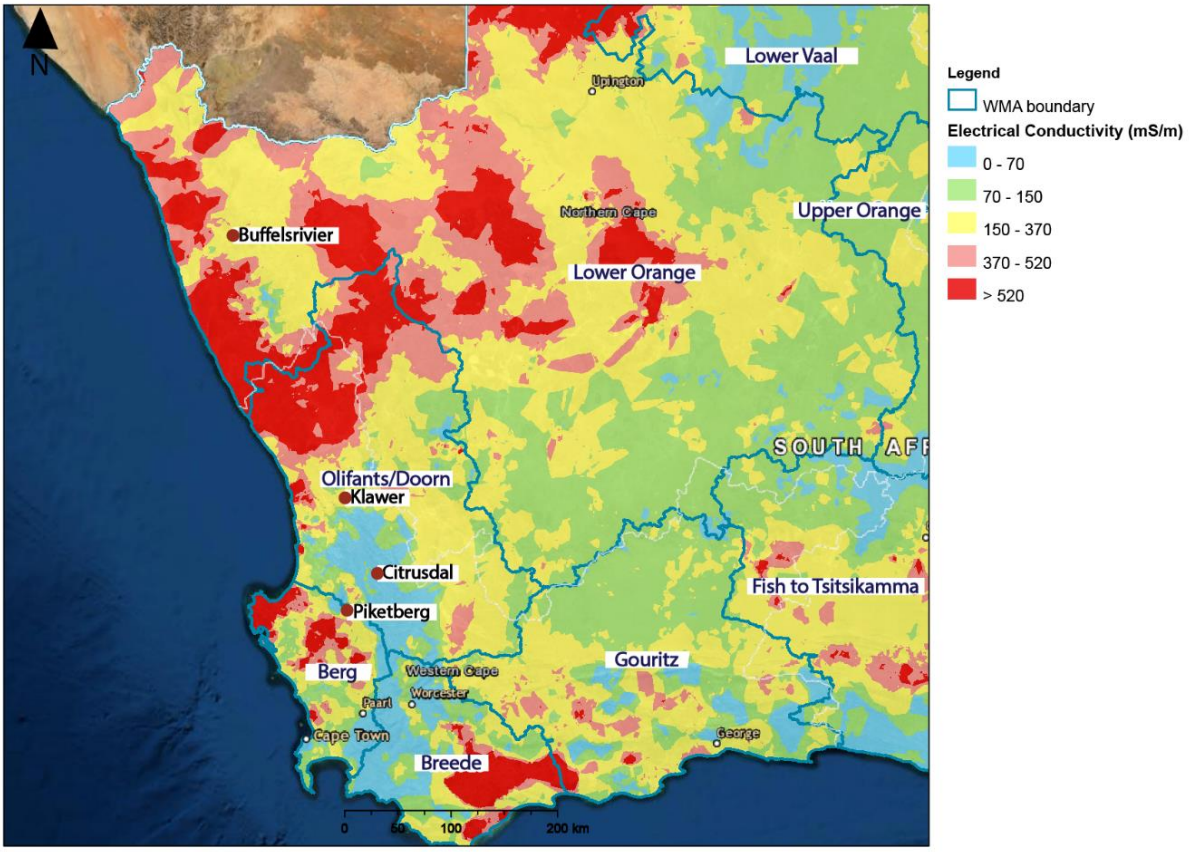

Figure 1.1: A map of the EC (mS/m) of catchments (outlined in blue) of the southwestern parts of South Africa with important town locations (indicated with red dots) in featured catchments (Buffels River, Olifants/Doorn, and Berg River catchments) of this study. Adapted from CapeFarmMapper version 2.6.4 (Product of the Western Cape Department of Agriculture) Ground water quality resource layer supplied by Department of Water and Sanitation.

Variable groundwater salinity is not as pronounced in similar geological profiles and climatic regions of southern Africa. This implies that other regional factors are possibly contributing to the salinisation of groundwater in the West Coast.

A recent study in the Buffels River catchment of the West Coast suggested that the variable groundwater salinity in the catchment can spatially be correlated to the occurrence of heuweltjies (van Gend et al., 2021). Heuweltjies (little hills or hillocks) are described as large, regularly spaced biogenic mounds. These dome-shaped mounds are easily identified on satellite imagery (Figure 1.2) due to distinct vegetation patterns or vegetation sparseness on the mounds. Differences in vegetation types or densities are a result of soil water, nutrients or salinity (Ellis, 2001; Schmiedel et al., 2015).

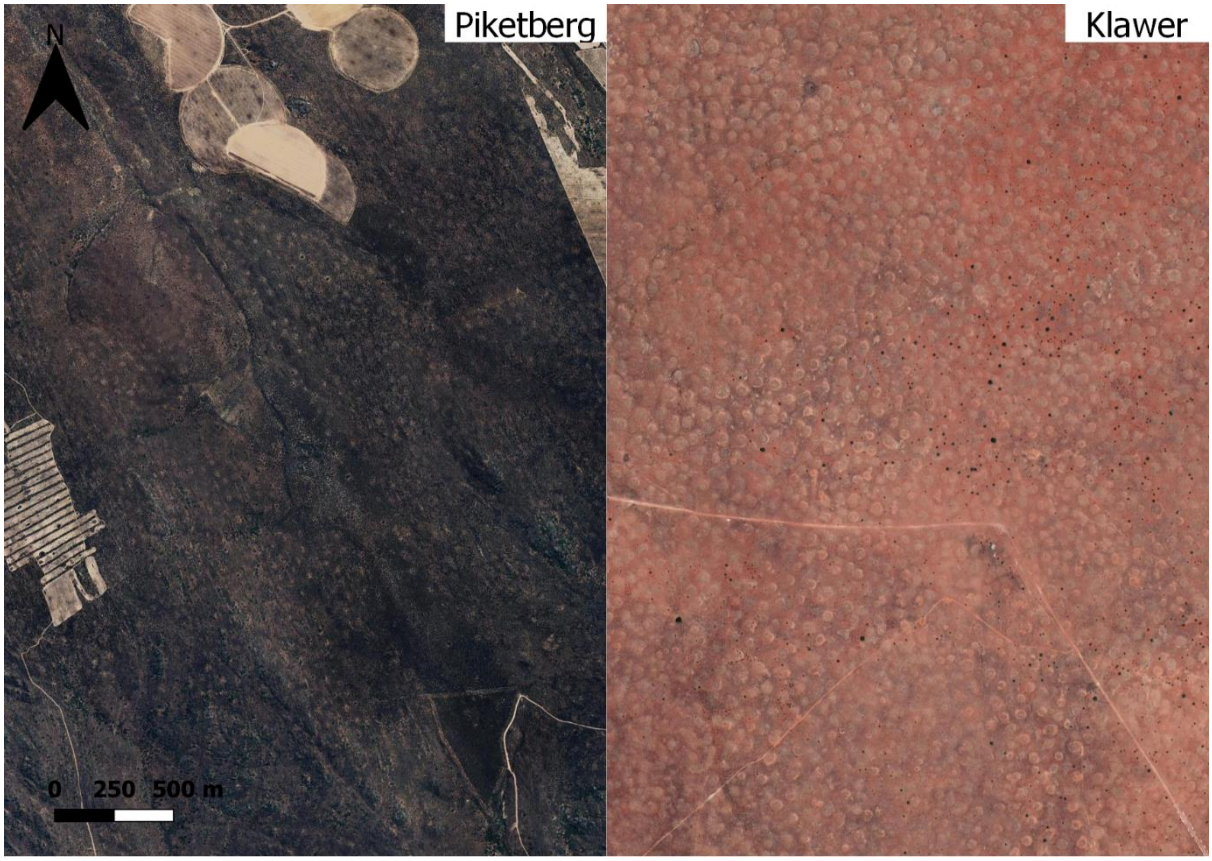

Figure 1.2:Abundance of heuweltjies near Piketberg and Klawer in the Olifants/Doorn catchment.

The origins of heuweltjies, although somewhat ambiguous, are widely attributed to paleo and modern termite activity (Lovegrove and Siegfried, 1989; Moore and Picker, 1991; Cramer and Midgley, 2015; Cramer et al., 2017; McAuliffe et al., 2019a). The modern termite species associated with heuweltjies is the southern harvester termite *Microhodotermes viator*

(Latreille), although its exact role in mound formation remain speculative (McAuliffe *et al.*, 2019a; McAuliffe *et al.*, 2019b).

Heuweltjies represent 14-25% of the land surface (Lovegrove and Siegfried, 1989; Picker et al., 2007) and are enriched with nutrients and salts compared to their surrounding sediments (Midgley and Musil, 1990; Kunz et al., 2012). Heuweltjies in the Buffels River were shown to have salinity levels an order of magnitude higher than that of the surrounding inter-mound soils (van Gend et al., 2021). In the Buffels River catchment, McAuliffe *et al.* (2014) found that heuweltjie soils had extreme salt contents (>5000 ppm) at half meter depth which increased two to three times in some cases at a depth of 1 m. In Vanrhynsdorp, poor vegetation growth on eroded heuweltjies was attributed to exposure of subsoils with salt contents an order of magnitude higher than surface soils and was compared to non-eroded, vegetated mounds or inter-mound soils with lower salt contents Midgley and Musil (1990) compared nutrient contents between heuweltjie and inter-heuweltjie soils in the Worcester – Robertson valley and found that heuweltjie soils were significantly enriched with nutrients, especially Ca, compared to inter-mound soils. Synonymous with the previous references to nutrient and salt accumulation, heuweltjie soils are characterised by higher pH values than the surrounding soils and are often associated with central carbonate and silica accumulation (Ellis, 2002; Midgley et al., 2002; Francis et al., 2007, 2013; Kunz et al., 2012; Schmiedel et al., 2016; Francis and Poch, 2019; McAuliffe et al., 2019a; b).

Even though termite mounds also contain salts and basic cations (Watson, 1969; Erens et al., 2015; McAuliffe et al., 2019a), the possibility of termite mounds contributing to groundwater salinity has not received attention. In contrast, infiltration studies on termite mounds are extensive. Large macropores created by termites through tunnelling have been shown to allow increased infiltration and preferential flow through mounds during rainfall events (Léonard and Rajot, 2001; Turner et al., 2006; Beven and Germann, 2013; Bargues Tobella et al., 2014; Ahmed II et al., 2019). Traditionally termite mounds serve as indicators for shallow groundwater in some parts of Africa (Ahmed II et al., 2019). Some termites harvest groundwater through tunneling further than 80 m deep, enriching their mounds with micronutrients (Mills and Sirami, 2018). However, in Australia and Botswana, termites have also been demonstrated to modify groundwater chemistry (Barnes et al., 1992; Vogel et al., 2004). In both Botswana and Australia nitrate fixing bacteria present in termite mounds were suggested to contribute to nitrogen enrichment in unconfined aquifers (Barnes et al., 1992; Vogel et al., 2004).

Vermooten (2019) established a downward migration of salts in heuweltjies of the Buffels River catchment and Van Gend et al. (2021) indicated that spatially, saline heuweltjies overlap with saline groundwater in the same region. Based on this it was hypothesised that heuweltjies contribute to groundwater salinity following the mechanism in Figure 1.3. It was suggested that salts concentrated in heuweltjies originate from a marine source and are unlikely to be derived from groundwater capillary rise (Vermooten, 2019; van Gend et al., 2021).

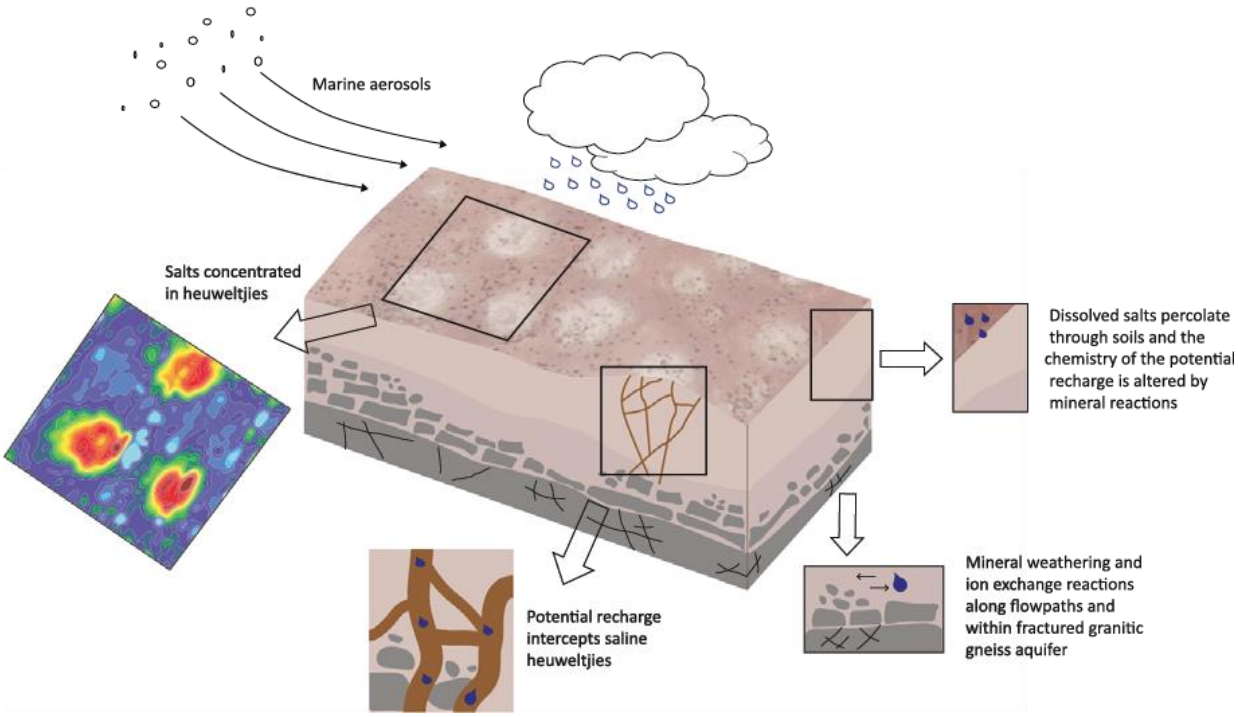

Figure 1.3: Mechanism proposed for the contribution of heuweljie salts to groundwater salinisation (van Gend et al., 2021). Salts originating from marine aerosols are concentrated in heuweltjies during drier periods where subsequent precipitation flushes salts from the heuweltjie soils through preferential flow paths and fractured aquifers into the groundwater system.

It is unclear whether the salts in heuweltjies that occur in other catchments along the West Coast with higher annual rainfall compared to the Buffels River catchment, could potentially be contributing to groundwater salinity in a similar way (Figure 1.3). Also poorly understood is the origin of salts concentrated within heuweltjies as both atmospheric and groundwater sources of salts are plausible. Although previous studies suggested a marine origin (Vermooten, 2019; van Gend et al., 2021), the source and distribution of salts within heuweltjies warrant further investigation in heuweltjies of other areas. Therefore, this study aimed at investigating the salt composition, origin, and distribution in heuweltjies of the Olifants/Doorn catchment in the West Coast.

The Olifants/Doorn catchment (Figure 1.4) covers an area of 56 446 km^2 (DWAF, 2005). The Olifants River, with Doring (Koue Bokkeveld and Doring areas) and Sout (Knersvlakte area) tributaries are the major rivers draining the Olifants/Doorn catchment (Soderberg and Compton, 2007). The Olifants and Doring rivers flow through the Olifants River Valley which mainly hosts large- and small-scale farms. Two sites in the Olifants/Doorn catchment were identified for investigation in this study. A higher rainfall site north of Piketberg (in the Sandveld sub catchment) and a lower rainfall site north of Klawer (in the Lower Olifants sub catchment) (Figure 1.4). The Olifants River Valley is highly dependent on groundwater as a municipal and agricultural water source (DWAF, 2005). However, groundwater salinity has been recognized as an intensifying water quality problem in the Olifants/Doorn catchment and further degradation of water resources is becoming an increasing concern in the area (Soderberg, 2003). Climate models have predicted that the Western Cape will become warmer and drier than present (DEA, 2013) and annual rainfall might decrease by as much as 15% in parts of the Olifants/Doorn catchment (DWAF, 2005). This will cause strain on the already limited water resources of the Olifants /Doorn catchment and apply further pressure on the agricultural and municipal sectors to manage water resources in a sustainable manner (Knüppe and Meissner, 2016).

Figure 1.4: The catchment locations (outlined in blue) of the southwestern parts of South Africa with important town locations (indicated with red dots) in featured catchments (Buffels River, Olifants/Doorn, and Berg River catchments) of this study. Adapted from CapeFarmMapper version 2.6.4 (Product of the Western Cape Department of Agriculture).

A range of field and analytical techniques were implemented to gather information about the soil and salt profiles of two excavated heuweltjies in the Olifants/Doorn region. These techniques include detailed field observations, pH(H_2O), and electrical conductivity (EC) measurements, soil texture analysis, mineralogy, ion profiling, and dissolved silica analysis.

1.1 Problem statement

The West Coast is the most arid region of South Africa and subsequent droughts increase the dependence of populations on groundwater as a primary water source in this region (Knüppe and Meissner, 2016; Watson et al., 2020a). Besides groundwater depletion, the intensified abstraction of groundwater due to the dry climate could cause increased salinisation with

detrimental effects on groundwater management and potability (Watson et al., 2020a). All the factors that contribute to salinisation in the West Coast are poorly understood and quantified which makes the implementation of mitigation strategies all the more difficult (Knüppe and Meissner, 2016). Although non-uniformity of saline groundwater in the Buffels River drainage basin was suggested to be influenced by downward migration of salts in saline heuweltjies (Vermooten, 2019; van Gend et al., 2021), it is not clear whether a similar conclusion can be made in other, less arid, areas of the West Coast.

The solution in determining if heuweltjies can be regarded as primary contributors to salinisation in the larger West Coast lies in investigating the nature of heuweltjie salts in multiple climatic zones within the region. This can be achieved by replicating similar studies done in the Buffels River, within the Olifants/Doorn catchment. Therefore, heuweltjies in the Olifants/Doorn catchment will also be characterized in terms of the sediment makeup, dominant heuweltjie salts, where the salts are hosted in the heuweltjies, and if salt movement is occurring in a specific direction within heuweltjies. Once it can be established if heuweltjies contribute to groundwater salinisation throughout the larger West Coast, strategies can be implemented by local farmers and communities to manage groundwater resources in a more sustainable way.

1.2 Aims and objectives

The main aim of this study was to determine the net direction of salt movement within two heuweltjies located in areas with differing mean annual rainfall and to establish possible mechanisms of salt entry into the mounds. The goal was to determine the dominant salts within the mounds and their distribution to address whether heuweltjie salts could be contributing to groundwater chemistry, or vice versa. To address the movement and distribution of salts in heuweltjies of the Olifants/Doorn catchment, the following objectives and key questions were stipulated:

Objective 1: To describe and determine the morphological, physical and mineralogical properties of the two heuweltjies, with key questions being:

- What are the morphological properties and types of heuweltjie soils? How do they compare to inter-heuweltjie soils?
- Is there a difference in soil texture between heuweltjie and inter-heuweltjie soils and how would this affect solute and water movement in the mounds?

- What type of clay and other minerals are present within the heuweltjies and do these minerals suggest a source of salts or base rich minerals in the parent material?

Objective 2: Determine the vertical and horizontal distribution of solute components of mound and inter-mound soils and establish a net direction of solute movement, with key questions:

- What are the chemical properties and prevalent anions and cations in the mounds and how do they relate to depth?
- Do saturation indices of increasingly soluble salts represent an upward or downward trend in saline water movement?

Objective 3: Identify possible sources of salt enrichment in mound soils, with key questions:

- How do salt profiles correspond to biogenic features in the mounds?
- Is there evidence of salt movement along preferential flow pathways?
- Are there marine or continental influences in the soluble component composition?

1.3 Thesis structure

This thesis consists of a further four chapters following the introduction (Chapter 1). Chapter 2 consists of the materials and methods which deals with the procedure of site selection, sampling and analytical techniques implemented for achieving said objectives. The results chapter (Chapter 3) is structured to begin with the morphological and physiochemical characteristics of mounds building up to the chemical analysis of each heuweltjie. Chapter 4 contains the discussion of the results and is structured to speak to each of the objectives of this study. The first section of the discussion aims at characterising the textural and mineralogical differences of mound and inter-mound soils, and to establish if heuweltjies contain base rich parent material. The second section focuses on establishing a net direction of solute movement within both mounds. The third section investigates the source and preferential flow of heuweltjie salts in both Piketberg and Klawer. A last section of the discussion explores the implications of heuweltjie salts potentially moving towards the groundwater system in the Olifants/Doorn catchment. The final chapter contains the general conclusions and research recommendations (Chapter 5).

1.4 Background

1.4.1 A brief overview on Heuweltjies

Heuweltjies are typically dome shaped with heights between 1 to 2.5 m and average diameters of around 10 to 30 m (Lovegrove and Siegfried, 1986, 1989; Moore and Picker, 1991; Francis et al., 2013; Cramer and Barger, 2014). The ages of these mounds have been estimated between 20 000 to 35 000 years using ^{14}C dating of the calcite horizons (Midgley et al., 2002; Potts et al., 2009). Heuweltjie distribution is limited to the arid and semi-arid sparsely vegetated Namaqualand and the western and southern Cape coasts in Succulent Karoo and Fynbos biomes in South Africa (Lovegrove and Siegfried, 1989; Moore and Picker, 1991; Picker et al., 2007). Their distribution is mainly restricted to mountain valleys, West Coast lowlands and inland flats but they are mostly absent from mountainous areas (Lovegrove and Siegfried, 1986; Picker et al., 2007). The termite species *M. viator* (Latreille), associated with heuweltjies, is endemic to the Cape provinces in South Africa as well as southern parts of Namibia and their distribution is related to vegetation types, feeding habits and nest structures (Coaton and Sheasby, 1974). *M. viator* (Latreille) is colloquially known as *houtkapper* (wood cutter) or *stokkiesdraer* (stick carrier) as its distribution is confined to scrubby vegetation (Coaton and Sheasby, 1974). *M. viator* (Latreille) is characterized by subterranean hives from which narrow galleries extend and their superficial storage chambers link to foraging ports often visible through rings of cut vegetation encircling them. Soil dumps (termed frass) are regular on the surface of mounds and comprises of dark organic debris and excrement mixed with soil that is aggregated by saliva (Coaton and Sheasby, 1974).

Although the origin of heuweltjies remain somewhat of an enigma, their presence has attracted widespread scientific attention due to their indisputable influence on the variation in vegetation in the biomes they form part of (Midgley and Musil, 1990; Booi, 2011; Kunz et al., 2012; Schmiedel et al., 2015, 2016; Francis and Poch, 2019). The vegetation patterning is largely ascribed to heuweltjies having vastly different soil properties in comparison to surrounding soils (Midgley and Musil, 1990; McAuliffe et al., 2019a; b). Chemical and physical properties of heuweltjies allow them to have elevated nutrient and water contents increasing local faunal biodiversity (Midgley and Musil, 1990; Kunz et al., 2012; McAuliffe et al., 2014; Bekker et al., 2016). Heuweltjies also have higher clay or silt content, less gravel in their topsoil, and therefore an overall better water holding capacity than the surrounding soils (Kunz et al., 2012; Schmiedel et al., 2015).

Heuweltjies commonly have petrocalcic layers at about 0.5 to 1 m below the mound surface (Ellis, 2002; Potts et al., 2009; Francis et al., 2013; McAuliffe et al., 2018). Petrocalcic layers consist of indurated horizons cemented by calcium carbonate that can be either platy or massive and are very hard (WRB, 2014). Petrocalcic horizons are usually thicker than 10 cm and sometimes occur in association with petroduric (Si cemented) horizons in more arid regions (WRB, 2014). Ellis (2002) speculated on the degree of hardpan cementation in heuweltjies and related it to termite activity. In areas of very low rainfall termite activity is low or even relict and mounds have petrocalcic to petroduric central hardpans. Higher rainfall areas (250 to 450 mm) show termite activity limited to the center of active mounds where these have hypocalcic to hypercalcic horizons in the center or are base rich compared to inter-mound soils (Ellis, 2002).

Heuweltjies are commonly situated on landforms with non-calcareous parent material (Francis and Poch, 2019; McAuliffe et al., 2019a) and processes responsible for carbonate accumulation in heuweltjies are poorly understood (McAuliffe et al., 2018). A few studies argue that *M. viator* plays a direct role in the accumulation of base rich (especially Ca^{2+}) organic matter in heuweltjies leading to the formation of non-lithogenic calcite (Ellis, 2002; Francis et al., 2013; McAuliffe et al., 2014, 2018, 2019a; Francis and Poch, 2019). It has been proposed that Ca rich plant materials are centralized in heuweltjies through transport by *M. viator* promoting the formation of calcic horizons (Francis et al., 2013). However, regional soil forming abiotic processes are also responsible for the redistribution of non-lithogenic calcite, closing pores to form a petrocalcic horizons (Francis and Poch, 2019). Vertical and lateral movement of soil water in low rainfall regions result in the successive dissolution and precipitation of calcite causing calcite cappings and pendants in some heuweltjies (Francis and Poch, 2019).

Mean annual rainfall will determine the fate of Ca and C as a regional soil forming process and will either cause soluble minerals to precipitate or leach to greater depths (Francis and Poch, 2019). This is evident in heuweltjies of non-calcareous parent material that are calcareous in the lower rainfall area of Robertson but non-calcareous in the higher rainfall area of Stellenbosch (Bekker et al., 2016). Other nutrients such as P and C are also concentrated in lower rainfall heuwetjies of the Succulent Karoo compared to heuweltjies in higher rainfall soils of the Fynbos biome (Booi, 2011).

1.4.2 Geology of the Olifants/Doorn catchment and study areas

The Olifants River Valley lies within a well-defined valley superimposed on substrate geology comprising a dramatic synclinal fold. The mountains flanking this valley reach elevations of up to 1800 m above mean sealevel (a.m.s.l) (Partridge and Maud, 1987; Soderberg and Compton, 2007). Westwards along the coast of the Olifants/Doorn catchment, rolling hills and sand dunes make up the topography where the Sandveld sub catchment lies to the south of the catchment (DWAF, 2005). Deep alluvial deposits of the Sandveld overlying bedrock provide significant groundwater resources as a primary aquifer (Watson et al., 2020b). To the north, elevations range between 500-900 m a.m.s.l which constitutes the low relief part of the Olifants/Doorn catchment (Partridge and Maud, 1987; DWAF, 2005). The substrate geology of the Olifants/Doorn catchment is dominated by the Palaeozoic Table Mountain Group (TMG) of the Cape Supergroup. Sandstone and shale formations of the Cape Supergroup make up the synclinal structures building the high mountainous terrain (Soderberg and Compton, 2007). In the eastern and northern areas of the Olifants/Doorn catchment, the Palaeozoic to Mesozoic Karoo Supergroup overlies the TMG strata whereas the Precambrian Vanrhynsdorp Group, as the basement geological unit, is overlain by the TMG that outcrops in the east. Shales of the Precambrian Malmesbury Group and TMG sandstone variably underlies the coastal platform which contains more recent alluvial sediments, marine and calcrete or ferricrete deposits (DWAF, 2005).

1.4.2.1 Piketberg site

Fluvial, shallow marine or estuarine and aeolian deposits from both the Quaternary Sandveld and West Coast Groups occurs as unconsolidated coastal platform deposits (Roberts et al., 2011) in the study area north of Piketberg (Figure 1.5). The Ordovician Peninsula Formation (Figure 1.5) has an average thickness of 2000 m (Johnson et al., 2006) and consists of quartzitic sandstone with high quartz content (98.8 wt% SiO_2) and minor minerals of feldspar and mica (Soderberg and Compton, 2007). The Ordovician Piekenierskloof Formation (Figure 1.5), approximately 800 mm thick, consists of conglomerate at the base followed by coarse-grained sandstone, mudrock, and conglomerates (SACS, 1980; Johnson et al., 2006). The Precambrian Piketberg Formation (Figure 1.5) of the Malmesbury Group outcrops between Piketberg and Relinghuys and mainly consists of feldspatic sandstone, greywacke and conglomerate with interlayered phyllite and occasional single layers of limestone (SACS, 1980; Rozendaal et al., 1994).

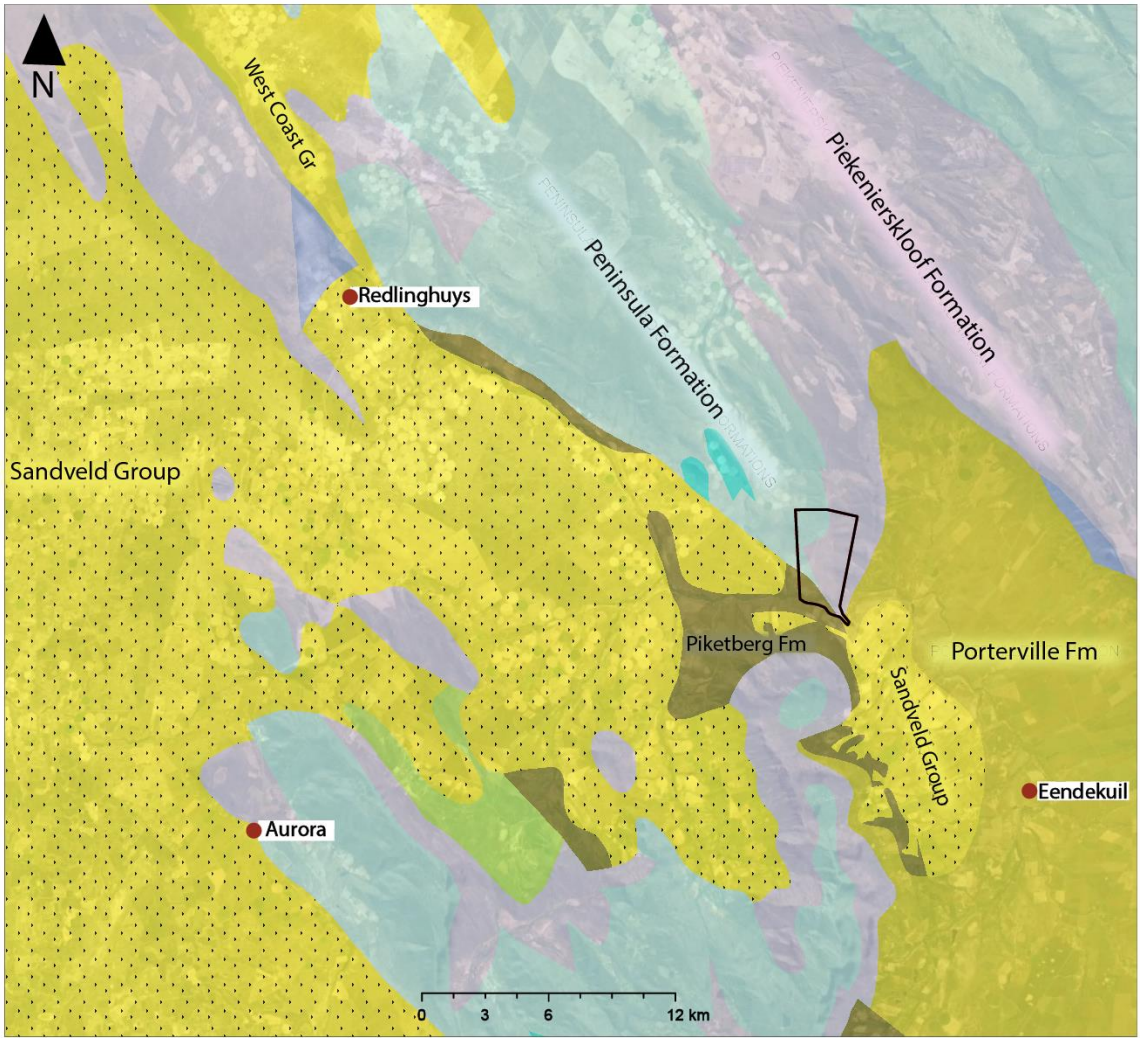

Figure 1.5: Major geological units of the study area north of Piketberg. Farm boundaries of study area indicated in black. Adapted from CapeFarmMapper version 2.6.4 (Product of the Western Cape Department of Agriculture) Geology resource layer supplied by SACS (1980). Coordinates: 32°34'54.8"S 18°46'21.3"E

1.4.2.2 Klawer site

The basal units of the Precambrian Gifberg Group (Figure 1.6) consists of limestone and marble that occurs as crests and anticlines (SACS, 1980; Gresse, 1986). Limestone grades to marble with increased depth which is followed by green, red or purple phyllite with interlayers of mudstone and quartzite displaying intense folding (SACS, 1980). The Precambrian Flaminkberg Formation (Figure 1.6) constitutes a thin (30 m) hard blueish quartzite layer with shale and conglomerate-like properties in some places (SACS, 1980; Gresse, 1986). The Precambrian Knersvlake Subgroup (Figure 1.6) progresses the Flaminkberg Formation and consists of mudstone, siltstone and shale with interlayes of sandstone, grintstone and

conglomerate (SACS, 1980). The Silurian Nardouw Subgroup (Figure 1.6) consists of folded quartzitic sandstone (arenite) containing 90.2 to 95.6 wt% SiO_2 often stained orange and black from oxidation of trace amounts of Fe and Mn from the groundwater (Soderberg, 2003). The Late Quaternary Masotcheni Formation (Figure 1.6) described by Botha (2021) consists of sheetwash, colluvium and hillslope cover and was previously labelled as alluvium, colluvium or sand on geological maps (SACS, 1980). Sheetwash colluvium is predominantly sandy and occurs in shallow basins on ridge crests and low slopes in the Cedarberg mountains of the Cape Fold Mountains geomorphic province (Botha, 2021). Intercalated paleosol horizons are common between sheetwash colluvium deposits and these deposits are sometimes associated with mineralogically distinct 'heuweltjies', indicating a history of complex geomorphology that correlates with the Masotcheni Formation.

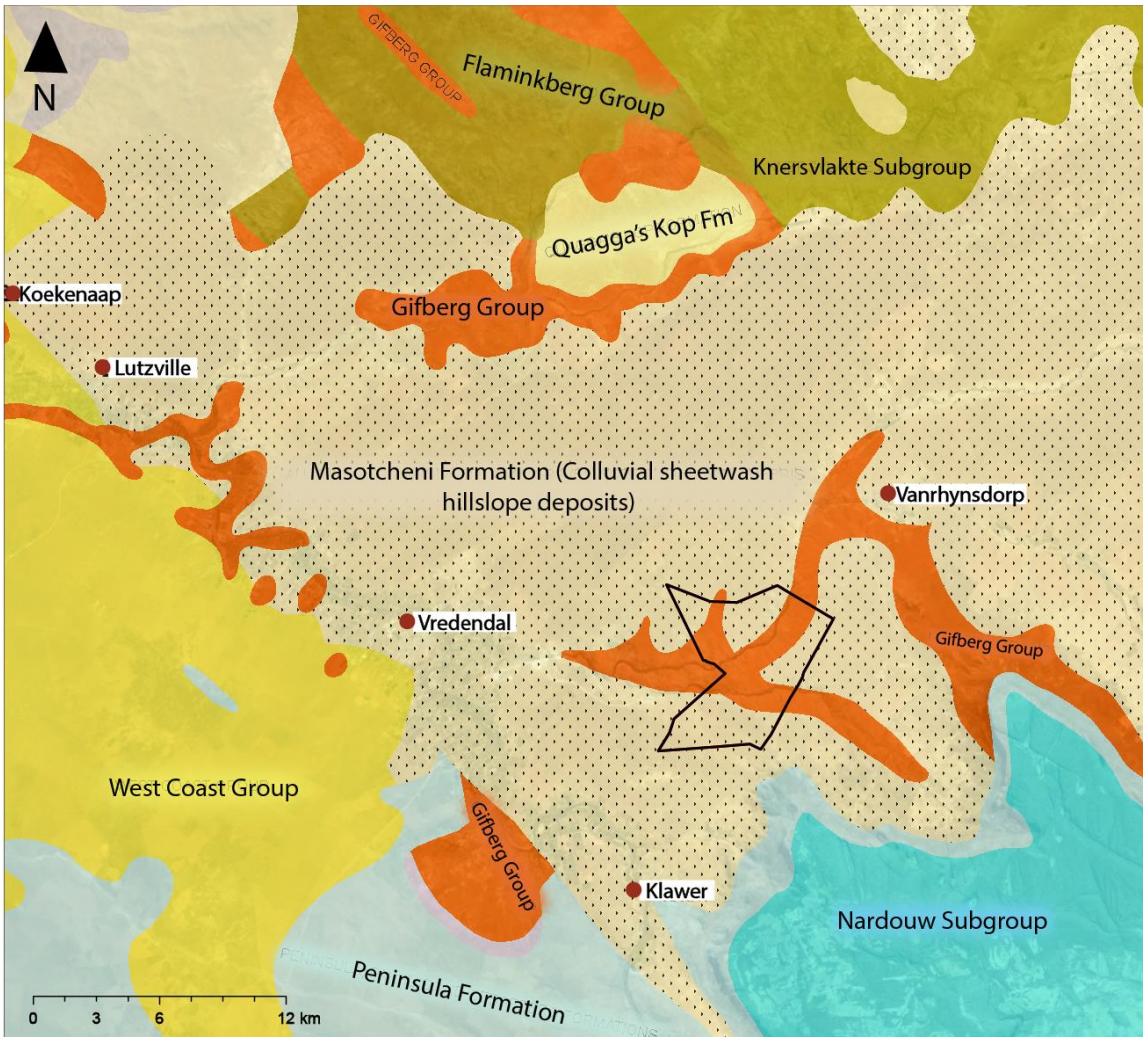

Figure 1.6: Major geological units of the study area north of Klawer. Farm boundaries of study area indicated in black. Adapted from CapeFarmMapper version 2.6.4 (Product of the Western Cape Department of Agriculture) Geology resource layer supplied by SACS (1980). Coordinates: 31°40'26.8"S 18°41'51.7"E

1.4.3 Climate of the Olifants/Doorn catchment

The Olifants/Doorn catchment is situated in a warm temperate (with dry hot summers) climates in the middle and south-western areas to arid desert (cold and hot) climates in the rest of the catchment (Beck et al., 2018). The Pleistocene era is accepted as the beginning of the Mediterranean climate of South Africa and consequent aridification of the west coast of South Africa (Dingle et al., 1983). The climate of the Olifants/Doorn catchment is subjected to much variation due to topographical changes. Temperatures range from -3˚C to 3˚C minimum in July and 39˚C to 44 ˚C maximum in January (DWAF, 2005). Inland mean annual temperatures increase to the north and are higher compared to the coast owing to the cold Benguela Current of the West Coast (Desmet, 2007). Maximum temperatures (>35˚C) are reached when hot, dry berg winds from the interior plateau sweep down the escarpment (Desmet, 2007). The catchment lies in a winter rainfall area where rainfall is derived from cold westerly fronts from the southern oceans occurring between May and September (Desmet, 2007; Davis et al., 2016). Mean annual precipitation (MAP) varies greatly (Figure 1.7) and is orographic in nature reaching up to 1500 mm in the Cedarberg mountains to the south-west where it decreases dramatically to 200 mm to the immediate north, east and west of the mountains and less than 100 mm in the far north of the catchment (DWAF, 2005). Alternative sources of moisture are generated from the Benguela Current in the form of coastal fog in summer months and heavy dew falls during mid-winter (Desmet, 2007; Davis et al., 2016). Average mean evaporation (measured by Symon's pan) varies from 1500 mm in the south-west to 2200 mm in the drier, northern areas of the Olifants/Doorn catchment (DWAF, 2005).

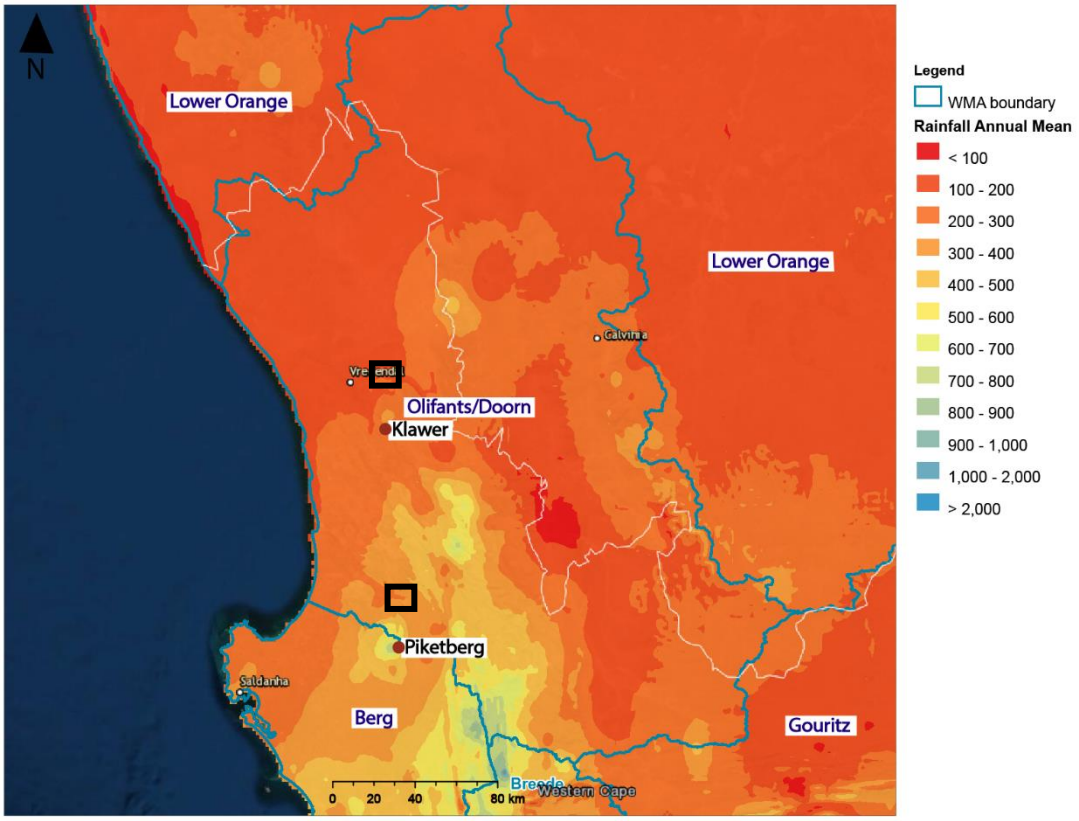

Figure 1.7: Mean annual precipitation rates of the Olifants/Doorn catchment (DWAF, 2005). Black boxes indicate the study areas. Adapted from CapeFarmMapper version 2.6.4 (Product of the Western Cape Department of Agriculture).

1.4.4 Vegetation of the Olifants/Doorn catchment

The Olifants/Doorn catchment is host to the Fynbos Biome to the south-west which borders the Succulent Karoo Biome in the middle, south-eastern and northern parts of the catchment (Figure 1.8). The Nama Karoo Biome occurs as a small area in the northern-most part of the catchment (Mucina and Rutherford, 2006). The Succulent Karoo and Fynbos Biomes are a part of the Greater Cape Floristic Kingdom (Jürgens, 1991), receiving global attention for its uniqueness and species richness (Cowling et al., 1999; Luther-Mosebach et al., 2012). The Fynbos Biome comprises of three distinct vegetation types namely, fynbos (as the main vegetation type), renosterveld and strandveld. These vegetation types characteristically contain evergreen shrubs that are small-leaved and of which regeneration is related to periodic fires (Mucina and Rutherford, 2006). The climate of the Fynbos Biome is typical of a Mediterranean region, with dry summers and wet, mild winters where vegetation types of this biome are adapted to grow on mostly leached, low nutrient soils (Soderberg, 2003). The Fynbos biome is supported by regions with parent material of sandstone, quartzite, granite, shales, young

limestones and gneisses to a marginal extent (Mucina and Rutherford, 2006). The Succulent Karoo Biome is termed as such due to the reoccurring feature of succulence throughout the biome but is by no means restricted to succulent plants only (Mucina and Rutherford, 2006). The Succulent Karoo Biome covers a total area of 111 000 km^2 and comprises mostly of flat to gently undulating terrain which includes the western coastal platform, Knersvlakte and Tanqua Karoo (Mucina and Rutherford, 2006). The Succulent Karoo is a semidesert region characterized by an even, mild climate and strong maritime influence. The climatic stability of this region plays an important part in preserving the species diversity of the biome maintaining the uniqueness of the biome (Cowling et al., 1999). The Nama-Karoo is an arid biome classified as a 'hot-desert' and in contrast with the Succulent Karoo is not particularly species rich. The unpredictable rainfall and shallow soils of the Nama-Karoo limits the presence of leaf succulents, perennial grasses and trees (Mucina and Rutherford, 2006).

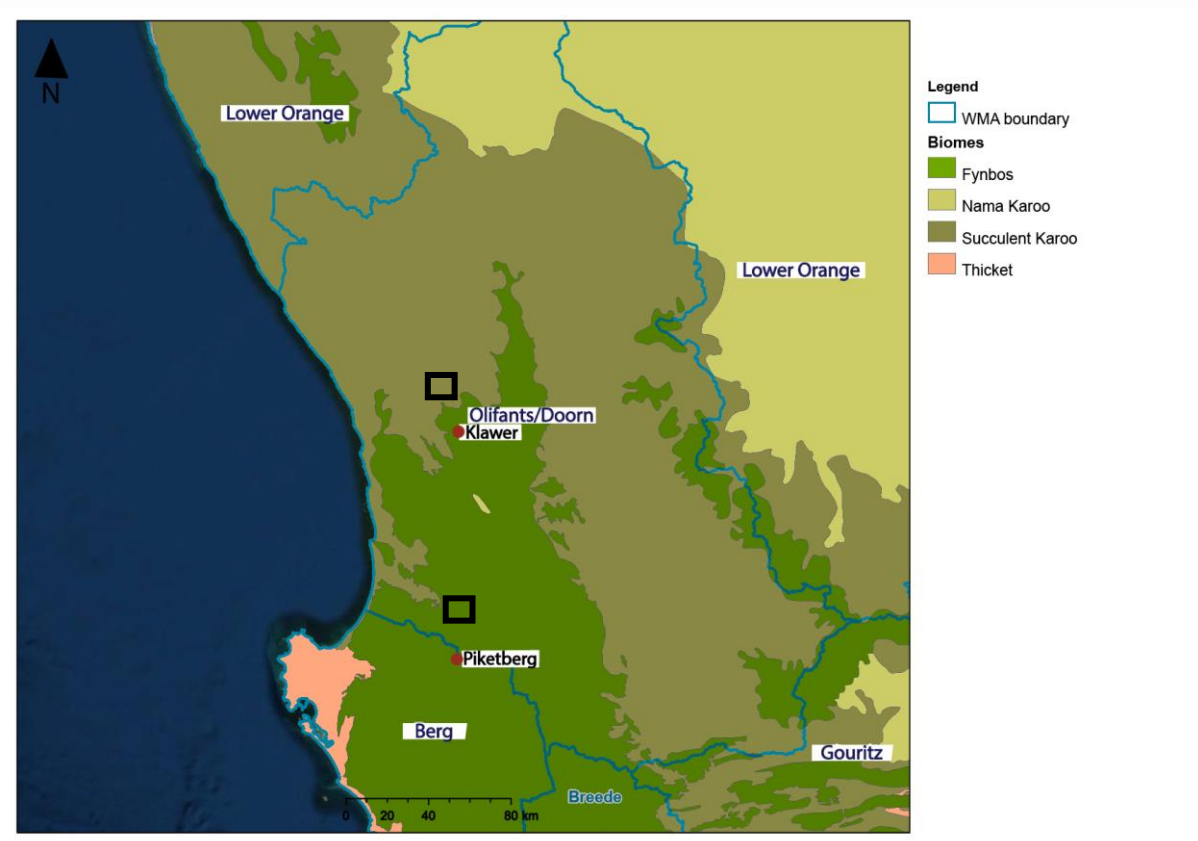

Figure 1.8: Biomes of the Olifants/Doorn catchment (Mucina and Rutherford, 2006). Black boxes indicate the study areas. Adapted from CapeFarmMapper version 2.6.4 (Product of the Western Cape Department of Agriculture).

1.4.5 Soils of the winter rainfall area of the West Coast (South Africa)

The winter rainfall area of the West Coast is an old landscape showing a high degree of terrain diversity, and varied substrate lithologies with large differences in annual precipitation. These factors provide dramatic variation in soil forming processes reflected in the wide range of soils (eutrophic to dystrophic and ancient to recent) of the region (Bühmann et al., 2004 citing Lambrechts, 1983). Generally, the soils of the Fynbos and Succulent Biomes can be distinguished in terms of rainfall. In higher rainfall areas such as the Fynbos Biome regular leaching causes macro- and micronutrient losses whereas soils of the Succulent Karoo Biome accumulate most of the important plant nutrients (Ellis, 1988; Mucina and Rutherford, 2006). The soils, adjacent to the coast of the West Coast area are predominantly regic, grey, calcareous sands of aeolian origin which are followed by interrupted yellow sands in the northern parts (Cowling et al., 1999; Mucina and Rutherford, 2006). Deep, red sandy soils occur in large areas inland of the coast and are calcareous in some places depending on the rainfall and degree of leaching (Mucina and Rutherford, 2006). Heavy textured soils develop in the more mountainous areas to the south on slope-creep from residually weathered shales and contain thin colluvial surface layers (Mucina and Rutherford, 2006). Lithosolic soils are also common in steeper terrains of the southern parts of the West Coast. Clay migration becomes prominent in these soils as slope gradients decrease and rainfall increases, forming clay-rich subsoils (Mucina and Rutherford, 2006). The quartzitic mountain ranges to the south are associated with a range of acidic, iron poor and leached sandy soils developed from colluvial and alluvial accumulation in inter-and intramountain footslopes and valleys (Mucina and Rutherford, 2006).

Many evaporate minerals are also observed in the soils of the northern, drier, parts of the West Coast and include halite, gypsum, calcite, sepiolite and palygorskite (Francis et al., 2007, 2012, 2020; Francis, 2019; Francis and Poch, 2019). Sepiolitic soils are mostly found in calcareous soils of the coastal plain of northern Namaqualand whereas palygorskite soils follow the Orange River to the inland (Francis, 2019). The silicified soils (duripans/dorbank) of the West Coast commonly occur below red sandy soils with varying morphologies and depths depending on the aridity (Fey et al., 2010a). Soils of the more arid northern parts (Namaqualand and Knersvlakte) exhibit silicified layers at shallower depths due to intense evaporation (Francis, 2019). In addition, alkaline conditions in many of these arid soils cause the localized precipitation of Ca, Si and/or Mg with carbonates, sulphates and sepiolite, either in combination or uniquely (Francis et al., 2007, 2012).

1.4.5.1 Calcic soils

Calcic soils are mostly encountered as either soft (calcic) or hardpan (petrocalcic) carbonate horizons (Soil Classification Working Group, 1991). Carbonate-rich horizons are a result of continuous calcium carbonate accumulation over a long period of time resulting in neoformed soft to hardpan carbonates or calcified nodules (Francis et al., 2007; Fey et al., 2010a). Calcic horizons (soft carbonate horizon; Soil Classification Working Group, 1991) are characterized by accumulation of secondary carbonates as calcium carbonate impregnation of the soil matrix and is not cemented (WRB, 2014). Calcite impregnation usually manifests as fine particles (< 1 mm) or coatings, veins and nodules in subsurface horizons (WRB, 2014). Petrocalcic horizons are formed when secondary carbonates of calcic horizons become continuously indurated and cemented as platy or massive hard carbonate horizons (WRB, 2014). The platy or massive (nodular or non-nodular) carbonate layers present as either lamellar calcrete or petrified lamellar calcrete (WRB, 2014). Petrified lamellar calcrete is more cemented than lamellar calcrete and consists of one or more very hard layers, uniform in thickness, and pink to grey in colour (WRB, 2014). Lamellar calcrete varies between a few millimeters to centimeters thick and is pink to white in colour (WRB, 2014).

1.4.5.2 Gypsic soils

In the less Mediterranean, more semi-arid to arid areas of the West Coast (Namaqualand and Knersvlakte north of Klawer) the calcic and petrocalcic horizons occur in association with gypsic and/or petrogypsic horizons where groundwater or soils are enriched with sulphates (Fey et al., 2010a; WRB, 2014). Gypsic horizons present as non-cemented secondary gypsum, accumulated in surface or subsurface horizons as coatings, crystals and powders (WRB, 2014) When gypsic horizons become indurated, massive or platy petrogypsic horizons are formed (WRB, 2014). Lenticular crystals of gypsic soils plug and cement soil pores over time forming root restrictive subsoils (WRB, 2014). The higher solubility of gypsum compared to calcite indicates that more arid climates are required for accumulation compared to calcite accumulation (Fey et al., 2010a). This is evident in the larger distribution of calcic soils in wider climatic ranges compared to gypsic soils (Fey et al., 2010a). Furthermore, gypsum also requires a source of S for formation to occur (Papadopoulos, 1984; Schaetzl and Anderson, 2005).

1.4.5.3 Silicic soils

Silicic soils are also associated exclusively with more arid landscapes and contain a subsurface horizon cemented by silica (Fey et al., 2010a). Silica as a cementing agent is derived from either the groundwater, weathering dust, and transport from upper soils horizon or higher elevation areas (Sommer et al., 2006). The dominant silica cemented horizons of southern Africa are either petroduric horizons (WRB, 2014), equivalent to dorbank in the South African Classification System (Soil Classification Working Group, 1991), or silcretes (Partridge and Maud, 1987). Both dorbank and silcrete form as a result of silica cementation but their morphologies and genesis differ (Ellis and Lambrechts, 1994). Silcrete often occurs as cappings on old landscape positions and is regarded a paleofeature, where dorbank is present in lower lying erosion surfaces and appears to be a horizon forming under current climatic conditions (Ellis and Lambrechts, 1994; Fey et al., 2010a). Dorbank can either be classified as a massive or platy (laminated) type structure where the platy type ranges from a few milimiters to 0.3 m thick and can contain vertical cracks (Ellis and Lambrechts, 1994). The platy dorbank often contains calcium carbonate coatings in-between. Massive dorbank varies between 1 to 5 m or more in thickness and is not commonly associated with vertical cracks (Lambrechts et al., 1978; Ellis and Lambrechts, 1994). In more arid climates (such as the northern parts of the West Coast) dorbank shows a continuous platy or massive cementation, whereas the dorbank of less arid, more Mediterranean climates (south western parts of the West Coast) occur as prism-shaped blocks due to slight expansion and contraction during seasonal changes (Fey et al., 2010a).

1.5 Ion and mineral profiling for determining net direction of water movement

1.5.1 Electrical conductivity (EC)

The EC is influenced by a range of soil physical and chemical properties such as water and salt content, temperature, texture and solution pH (Friedman, 2005). A soil is regarded saline if the EC is greater than 4 dS/m at 25˚C (United States Salinity Laboratory Staff, 1954). Saline soils often display a sequence of horizon chemistry through the position of salts showing the dominant water trend through the profile e.g., upward from an underlying water table. The EC is therefore a valuable measurement that could indicate the net direction of water movement and that of major ions in the soil profile (Bui, 2013).

1.5.2 Salt profiling

The unsaturated zone (UZ) links the groundwater to the land surface and provides storage for water, solutes (such as Cl), and other contaminants (Huang et al., 2016). The solute profile of the UZ can therefor provide much insight into groundwater recharge and the ions that are possibly introduced to the groundwater system (Huang et al., 2016). Ions of salts are not evenly distributed throughout soils and major ion profiling on soluble salts such as Na, Cl and SO_4 versus less soluble salts of carbonates can provide valuable insights to vertical solute movement and accumulation (Huber et al., 2008; Lin and Bañuuelos, 2015). Sulphate has also received much attention in soils due to its mobility, precipitation, availability to plants and microorganisms and its reactivity with soil surfaces with positive charges (Tabatabai, 1987). In soils, SO_4 occurs as soluble salts, insoluble forms (organic and inorganic), or as adsorbed components of colloids (Tabatabai, 1987). The movement of SO_4 in soils depend on its concentration, water movement and reactions with solid phases (Tabatabai, 1987). High soil pH, low clay contents, and monovalent cations of K and Na causes great leaching losses of SO_4 (Tabatabai, 1987). Gypsum will precipitate within soils if solutions with high SO_4 and Ca are present (Papadopoulos, 1984).

Dissolved Si is also an important solute to consider as the presence of soluble Si may lead to the formation of secondary minerals such as neoformed Al silicates, precipitation of amorphous Si, translocation and formation of new horizons or translocation out of soils (desilication) (Sommer et al., 2006). The flux of dissolved Si in soils is regulated by water movement in the form of silicic acid (H_4SiO_4), mainly as monomeric silicic acid, and its movement and location in a soil profile is therefore directly related to water movement (Drees et al., 1989; Sommer et al., 2006). Silica concentrations are independent on pH in soil solutions below pH of 9, where an increase in mobility occurs above pH 9 due to deprotonation of monosilicic acid (Jones and Handreck, 1963; Drees et al., 1989; Sommer et al., 2006). As heuweltjie soils have higher Si contents than surrounding soils (Ellis, 2002) it could suggest that water preferentially moves through heuweltjies rather than surrounding soils.

The determination of gypsum and calcite in the soils of this study will aid greatly in determining the net direction of water movement in heuweltjie soils. The solubility of calcite is less than that of gypsum and even more so when both are saturated in the same soil environment (FAO, 1990). Gypsum and calcium carbonate share a common ion (Ca) and the common ion effect stipulates that if a more soluble salt (gypsum) is introduced to a saturated solution of another

salt (calcite), where both share a common ion, the less soluble salt (calcium carbonate) will precipitate (FAO, 1990; Casby-Horton et al., 2015). Therefore, in soils where both calcium carbonate and gypsum occur, the more soluble gypsum will occur at greater depths compared to calcium carbonate in the profile, if the net direction of water occurs downward (Casby-Horton et al., 2015). Should the reverse direction (upward) of water movement occur in the soil profile, through capillary rise from a water table, the more soluble gypsum would precipitate at shallower depths than that of calcium carbonate (Casby-Horton et al., 2015). The carbonate-gypsum precipitation sequence further indicates the likely source of these minerals in soils, i.e., deposition from above or from the groundwater (Casby-Horton et al., 2015).

1.6 Knowledge gaps

At present most literature confirms that heuweltjies are characterized by elevated levels of salts. However, it is unclear what the impact of these salts are on the groundwater system of the West Coast, where mounds are found in high densities. Currently it is suggested that heuweltjie salts might be contributing to groundwater salinity in the Buffels River drainage basin (Vermooten, 2019; van Gend et al., 2021). It is not certain how the groundwater of the wider West Coast is affected by the elevated concentrations of salts in heuweltjies and what impact climate has on the composition and movement of salts in mounds. Detailed morphological and mineralogical analysis, and ion and salt profiling of entire heuweltjie structures are also lacking. Therefore, this study is not only pivotal to exploring the contribution of heuweltjies to groundwater salinisation in the larger West Coast but also to the complete morphological and chemical characterisation of heuweltjies.

2 Materials and Methods

2.1 Study sites

The higher rainfall site was located on a farm approximately 47 km north of Piketberg in the Western Cape Province (Figure 2.1). The main farming practice is the production and propagation of grapevines. In addition, the farm makes use of the natural vegetation for the grazing of cattle and cultivates grain crops as well as rooibos tea. The main vegetation types on the farm are a part of the Fynbos Biome and include Sandstone Fynbos, Sand Fynbos and Resnosterveld (Mucina and Rutherford, 2006). MAP of this region ranges between 300-400 mm (DWAF, 2005) which was corroborated with data from the farm (approximately 350 mm annually). Mean annual evaporation rates reaches between 1600 and 1700 mm (DWAF, 2005). According to the Köppen-Geiger climate classification (Beck et al., 2018) the area near Piketberg is classified as temperate hot-summer Mediterranean (Csa). The lower rainfall site was located on a farm approximately 16 km north of Klawer in the Western Cape Province (Figure 2.1). The farm is almost entirely used for the grazing of sheep. The main vegetation types on the farm are all a part of the Succulent Karoo Biome and include Vanrhynsdorp Gannabosveld, Knersvlakete Vygieveld, Knersvlakte Quartz Vygieveld, Klawer Sandy Shrubland and Namaqualand Spinescent Grassland (Mucina and Rutherford, 2006). MAP of this region ranges between 100-200 mm (DWAF, 2005) which was corroborated with data from a weather station at Moedverloor (30 km from the study site) recording MAP of 50-100 mm between the years 2017 to 2020 (SASSCAL, 2021). Mean annual evaporation rates reaches between 1600 and 1700 mm (DWAF, 2005). The Köppen-Geiger climate classification (Beck et al., 2018) classifies the area north of Klawer as hot semi-arid (BSh).

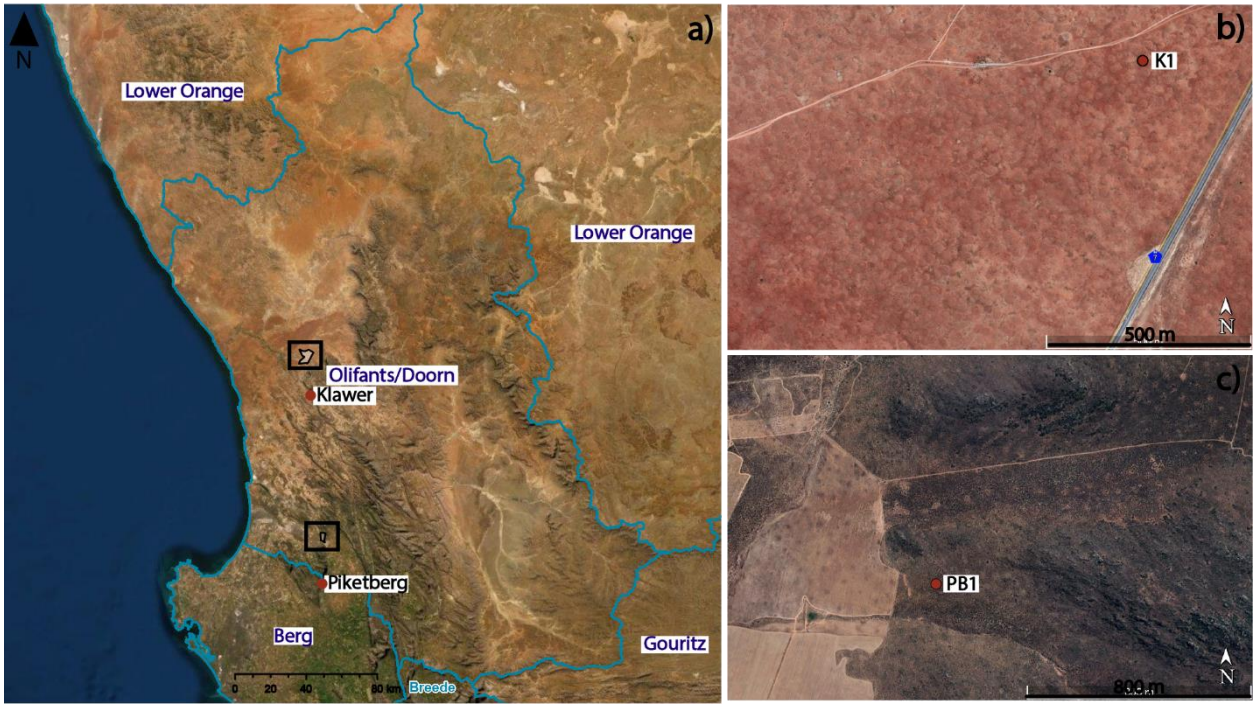

Figure 2.1: a) Black boxes showing the locations of the selected study sites on farms north of Piketberg and north of Klawer in the Olifants/Doorn catchment. b) The heuweltjie selected for excavation on the farm north of Klawer. c) The heuweltjie selected for excavation on the farm north of Piketberg.

2.2 Selection of study site

Preliminary field studies were conducted on both the Klawer and Piketberg sites to select a representative heuweltjie suitable for excavation at each site. A total of 22 heuweltjies (twelve in Piketberg and ten in Klawer) were sampled during the preliminary study (Figure 2.2 and Figure 2.3). Samples were taken using a hand auger and consisted of a topsoil sample (0-20cm) and a subsoil sample, where the depth of the subsoil sample depended on how deep the auger could penetrate the soil. Centre, side and off-mound samples of the topsoil and subsoil of each heuweltjie were taken for comparison of changes in salinity and pH(H_2O) within and between mounds. Heuweltjies selected for excavation were done so based on the typical chemistry (higher pH(H_2O) and EC on the mound compared to inter-mound soil) and representative morphology (faunal activity and distribution of flora). The accessibility of the mound for an excavator was also considered to prevent unnecessary damage to natural vegetation. The heuweltjie (HK6) selected on the farm near Pikeberg was situated next to a rooibos tea field and will from here on be referred to as PB1 (Figure 2.2). The heuweltjie (K1) selected on the farm near Klawer was situated close to the N7 between Klawer and Vanrhynsdorp and will be referred to as K1 (Figure 2.3).

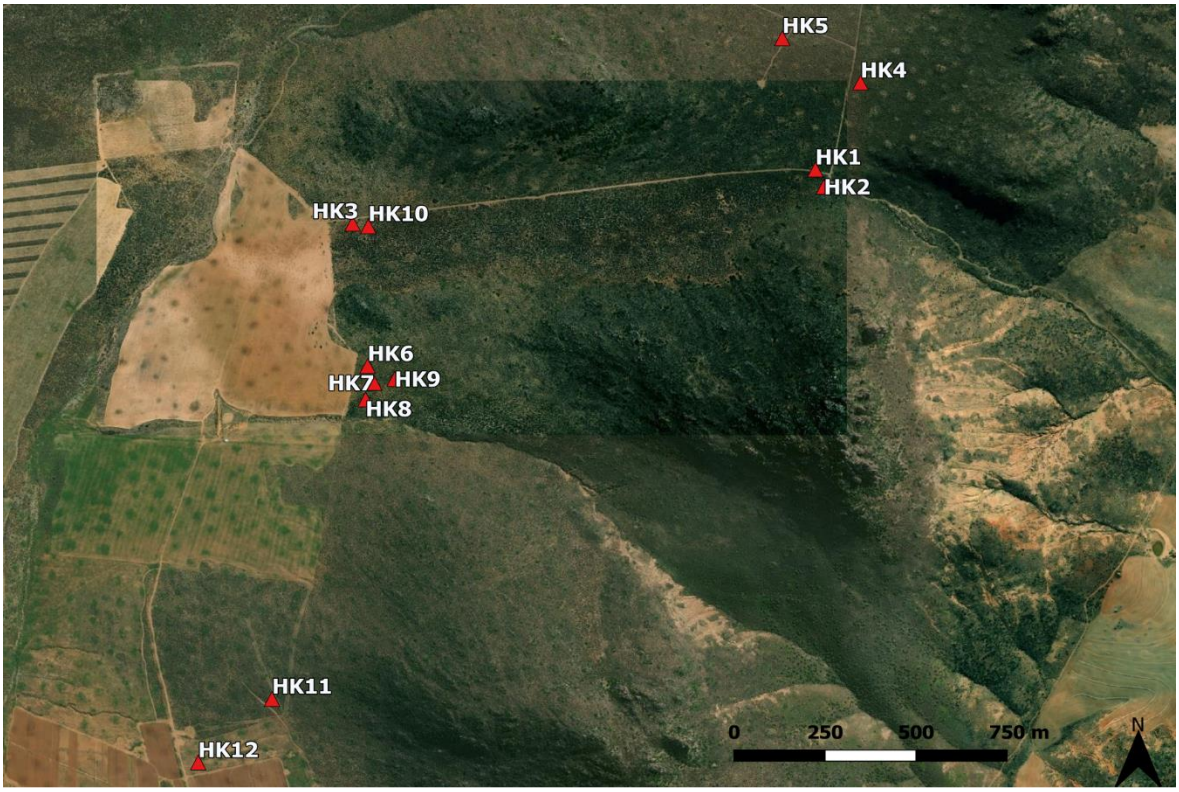

Figure 2.2: The twelve (HK1-12) preliminary sampled heuweltjies on the farm near Piketberg (HK6 indicates the heuweltjie selected for excavation at this site).

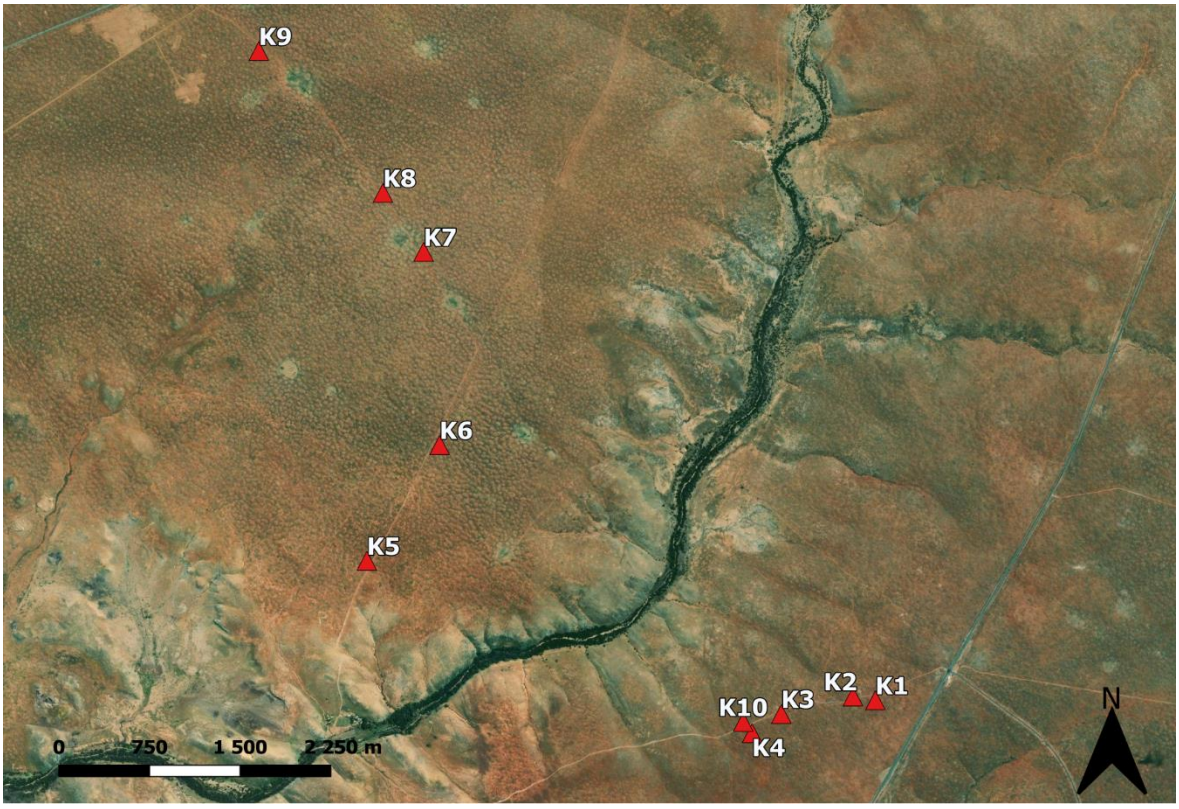

Figure 2.3: The ten (K1-10) preliminary sampled heuweltjies on the farm between Klawer and Vanrhynsdorp (K1 indicates the heuweltjie selected for excavation at this site).

2.3 EMI survey

An electromagnetic induction (EMI) survey was conducted at the site selected in Piketberg using a DF Instrumental CX Mini Explorer 2 attached to a quad bike (Figure 2.4). The EMI survey was conducted to measure the difference in apparent electrical conductivity (EC_a) between the heuweltjie and inter-heuweltjie soils. The instrument is fitted with three transmitters that produces electromagnetic pulses which penetrates the soil at depths of 25 cm, 50 cm, and 90 cm respectively. The pulses interact with material at the set depths and return pulses are produced that is sent to a receiver at one end of the instrument. After data collection EC_a grids were produced by Kriging using Surfer® Version 21.1.158.

Figure 2.4: A DF Instrumental CX Mini Explorer 2, attached to a quad bike, used to measure electrical conductivity during the electromagnetic induction survey.

2.4 Sample collection

The heuweltjie near Piketberg was sampled during cool and slightly wet conditions at the end of winter (August 2020). The heuweltjie near Klawer was samples during warmer, dry, windy, summer conditions at the start of summer (November 2020).

2.4.1 Excavation of heuweltjies

The heuweltjie near Piketberg (PB1) was excavated on the 3rd of August 2020 using a EX65 Hitatchi ZX200LC excavator. The heuweltjie near Klawer (K1) was excavated on the 23rd of November 2020 using a Volvo EC240BLC excavator fitted with a rock bucket as dorbank was expected. The heuweltjies were excavated by digging a 2-3 m deep trench through the centre of the mound to create a cross-section of the heuweltjie. The trench depth was dependent on how limiting the dorbank was in Klawer and the sandstone boulders in Pikerberg. PB1 was excavated in a north to south direction (Figure 2.5) and K1 was excavated in a north-east to south-west direction (Figure 2.6). The direction of excavation was based on where inter-heuweltjie spaces were largest between the selected mound and other heuweltjies to prevent possible overlap during excavation and sampling. Partial excavation of inter-heuweltjie areas was important for comparison of both mound and inter-mound soil samples with regards to chemistry, mineralogy, and texture. The shallow nature of the dorbank in the K1 inter-heuweltjie areas and sandstone boulders in the PB1 inter-heuweltjie areas prevented the inter-mound soils from being excavated as deep as soils within the mound.

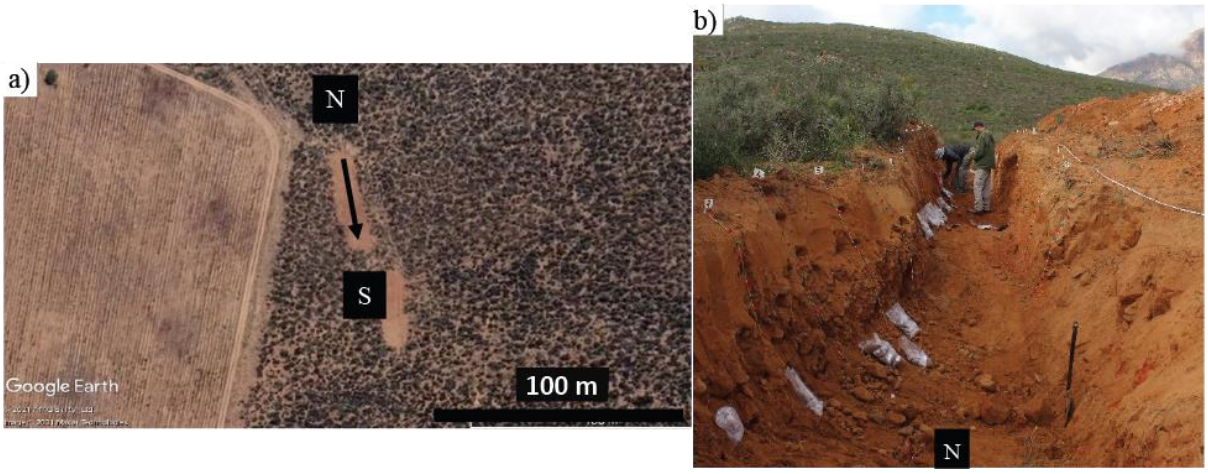

Figure 2.5: The trench dug through the mound and inter-mound soils of the heuweltjie at Piketberg (PB1) using an excavator. a) The north to south direction of excavation (indicated by arrow) on a Google Earth Pro™ image. b) The trench through PB1 from a north to south perspective.

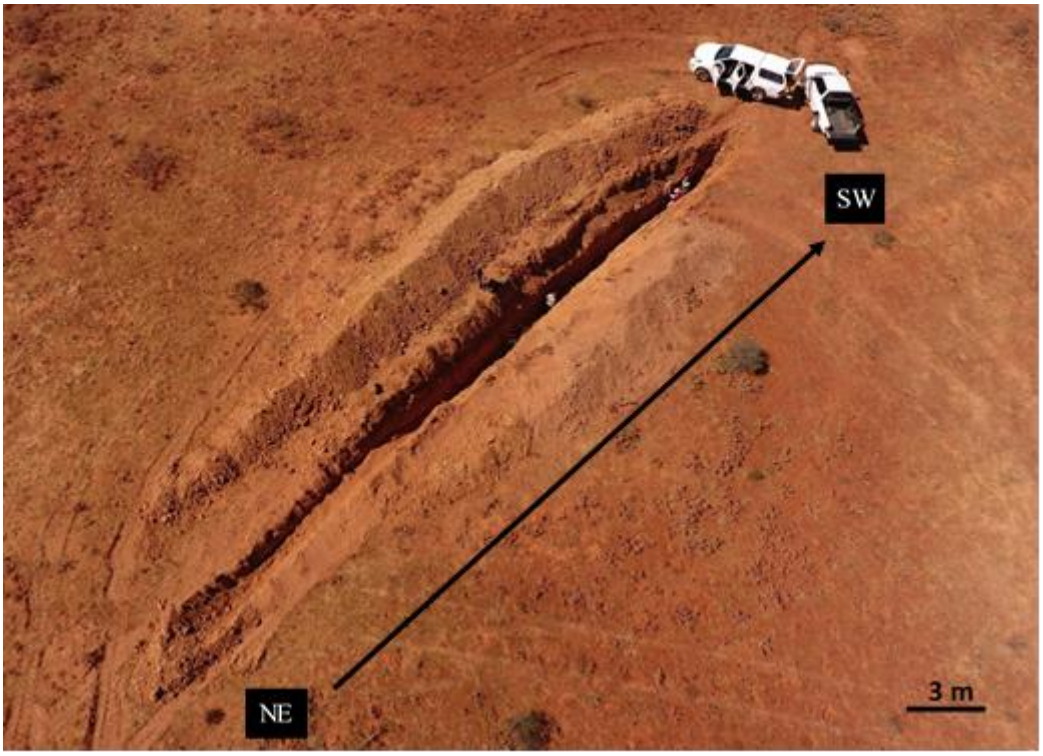

Figure 2.6: A drone image of the trench dug (using an excavator) through the mound and inter-mound soils of the heuweltjie (K1) between Klawer and Vanrhynsdorp. The trench was made in a north-east to south-west direction (indicated with arrow). Drone image supplied by Jannick Nieuwoudt.

2.4.2 Procedure of Sampling excavated heuweltjies

Detailed sampling, documentation and analysis of the wall faces of PB1 and K1 was done. A specific wall of the heuweltjie cross-section was chosen to sample by considering the morphological features visible on the walls. The south-east wall was selected for sampling for K1. During the excavation of PB1 the topsoil of the west wall was inadvertently partially removed. However, the west wall had morphological features that was deemed important to sample. Consequently, both the east wall and partially the west wall was sampled for PB1, and the sampling depth was adjusted for the west wall based on the amount of topsoil that was removed.

Prior to sampling, the selected cross sectioned walls were measured and marked with flags at 1 m intervals as seen in Figure 2.5b. Modal profiles were then identified at specific representative 1 m interval profiles of both inter- and heuweltjie soils for detailed classification, texture, mineralogy, and chemical analysis. Modal profiles were identified at 4, 13, 19, and 35 m on the east wall of PB1 and 6, 12 and 15 m on the west wall of PB1. For K1, modal profiles were identified at 2, 8, 11, 17, 21, 26 and 30 m on the south-east wall.

Soil samples were taken of each horizon at almost every meter of the selected heuweltjie and inter-heuweltjie cross-sectioned walls. Samples of PB1 were taken in a north to south direction from 0-40 m on the east wall and 6-23 m on the west wall. Samples of K1 were taken in a north-east to south-west direction from 0-30 m. Sampling within silica cemented horizons proved to be difficult and subsequently sample sizes ranged from 300-500 g for pH(H_2O) and EC screening and chemistry and 2-3 kg for modal profile samples. Between 2-9 samples were collected at each profile depending on the depth to the excavated floor and the number of distinct horizons. All samples were placed in individual plastic bags, labelled, and then double bagged to prevent contamination. A total of 210 samples were collected at PB1 and 154 samples at K1. Areas where bioturbation and preferential flow paths were prevalent were also sampled to determine if the salt content was higher within these features. Dorbank was sampled using a pickaxe in both heuweltjies.

Each profile was photographed and the soil texture, soil classification and soil colour (using Munsell Soil Colour Charts) were determined in field for the selected modal profiles. Detailed profile descriptions were made and diagnostic horizons were assigned according to both the Guidelines for Soil description (FAO, 2006) and South African taxonomic system of soil classification (Soil Classification Working Group, 1991). The presence of carbonates, Mn oxides and sepiolite were tested for using 10% HCl, 10% H_2O_2 and methyl orange (Mifsud et al., 1979), respectively. Sketches of heuweltjie walls were made in field and the depth of each horizon, feature and other notable morphologies were documented in detail. The in-field detailed sketches of each heuweltjie wall were digitised using QGIS Version 3.14.0.

2.4.3 Sample labels

All sample numbers were written in the following format:

AX-Y-Z

Where AX refers to the specific heuweltjie or trench wall, either PB1E, PB1W or K1 for Piketberg east and west walls and Klawer respectively; Y indicates the cross-section distance, in meters, from the north end of the heuweltjie (eg. 0 – 40 m on PB1E); Z refers to the depth in cm where samples were taken within each profile. For example, where a sample was taken at a cross-section distance of 2 m at a depth of 40 cm in the east wall of the heuweltjie near Piketberg, the sample is labelled as PB1E-2-40 (Figure 2.7). Labels using only AX-Y indicates

the entire soil profile at the specific cross-section distance. PB1E-2 refers to the whole profile at two meters of the cross-section distance.

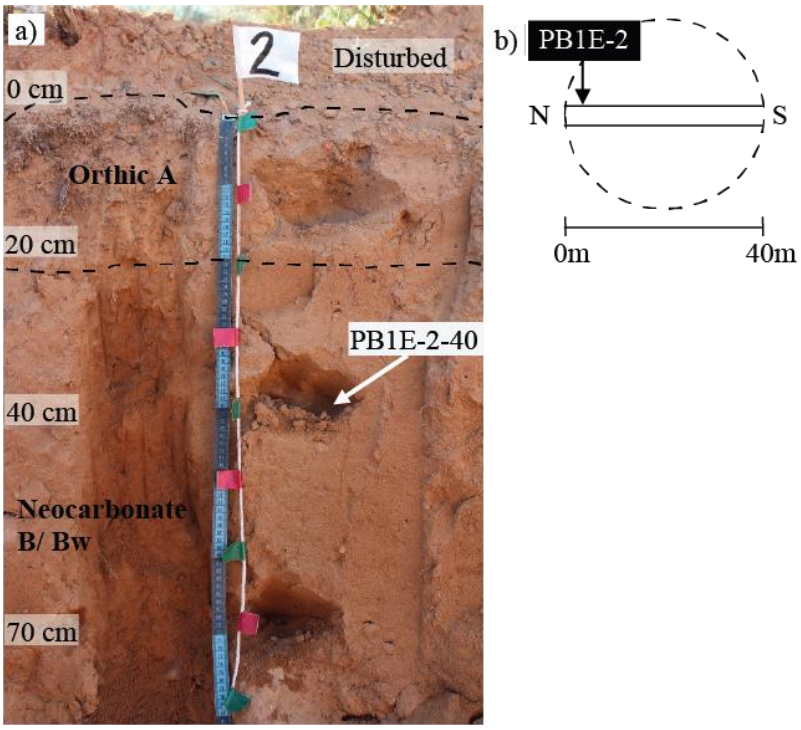

Figure 2.7: Sample label on the east wall of the heuweltjie near Piketberg at the cross-section distance profile of 2 m and depth of 40 cm (PB1E-2-40). a) The full profile at 2 m of PB1E with sample lable example at 40 cm. b) Location of the 2 m profile in relation to the cross-section distance of the whole trench from 0-40 m.

2.5 Sample Analysis

The samples collected from Piketberg and Klawer were taken to Stellenbosch University where they were air dried and sieved through a 2 mm sieve. Samples containing dorbank were crushed with a porcelain mortar and pestle to ensure no dorbank fragments remained. Care was taken not to crush coarse fragments and calcite nodules.

2.5.1 Soil texture

A total of 76 samples collected from the selected modal profiles at Piketberg and Klawer were subjected to soil texture analysis. Pre-treatment procedures of samples prior to particle size analysis was followed as outlined in Soil Classification Working Group (1991). Carbonates, silica-cementing agents, and organic matter (OM) was removed. Iron was not removed from samples as the clay in samples would be used to determine clay mineralogy using x-ray diffraction (XRD).

After pre-treatments, samples were dispersed using Calgon. The silt and clay fractions of solutions were transferred to 1000 ml measuring cylinders and sand fractions were separated and oven dried. The suspension temperatures of the soil solutions in the measuring cylinders were used to determine sedimentation rates of silt and clay for collection. Crucibles containing collected clay and silt fractions were oven-dried and weighed. Sand, silt and clay fractions were used to determine soil texture following the calculations of the Soil Classification Working Group (1991). Incomplete removal of carbonates from samples K1-21-290 and K1-26-275 led to failure to disperse and the soil texture could not be determined for these samples.

2.5.2 Clay mineralogy

Silt and clay suspensions in the measuring cylinders used for soil texture analysis were further utilized to collect clay for mineralogy. The top 200 ml of the measuring cylinders were collected, and divided in two separate glass beakers, after shaking and waiting approximately 8 hours. The cylinders were refilled with deionised water, shaken again, and a second aliquot of 200 ml was collected after 8 hours. The procedure was repeated 5-7 times per sample so that enough clay was collected for mineralogy. Clay samples in the two beakers were then flocculated using a few drops of 5M $MgCl_2$ and 3M KCl respectively. The clay was transferred to separated centrifuge tubes, washed further with 2M $MgCl_2$ and 1M KCl respectively and washed free of excess chloride using 0:1; 1:3; 1:1; 3:4 and 1:0 70% ethanol: deionised water ratios. The clay was oven-dried at 40˚C to remove excess water, powdered, placed in small paper envelopes, and sent to iThemba LABS for analysis. A step-size of 0.05 and step time of 40 seconds was specified during XRD analysis using a Burker D8-Advance multi-purpose X-ray diffractometer with tube voltage and current at 40kV and 40mA (Francis et al., 2013).

Graphs of count vs degrees two theta (˚2theta) were plotted for each sample and peaks were labelled using d-spacings converted from ˚2theta tables. The d-spacings were assigned to peaks according to minerals present in the sample. Untreated bulk and feature samples were also sent in for mineralogy at iThemba LABS using the same method and specifications. Bulk samples were milled using a ball mill and feature samples using a mortar and pestle.

2.5.3 Sample screening for chemical analysis

All samples collected during the excavation of heuweltjies were subjected to pH(H_2O) and EC measurements for sample screening. EC_w and pH(H_2O) measurements were made in the same suspensions of 1:2.5 soil to deionised water ratios. Soil-water suspensions were obtained by

adding 25 ml water to 10 g of soil and shaking for 30 minutes (Sonmez et al., 2008). Suspensions were allowed to settle for 30 minutes and analysed for pH(H_2O) and EC_w using an Eutech pH700 pH meter and Jenway 4510 Conductivity meter, respectively. 1:2.5 EC_w values were converted to saturated paste EC_e using the equations outlined by Sonmez *et al.*, 2008. Sample screening was performed to select representative samples for further detailed chemical analysis.

2.5.4 Solution chemistry

The samples collected from modal profiles at Klawer and Piketberg were all included for detailed chemical analysis along with profile samples selected at least every second or third meter, where possible, for both the east and west walls in Piketberg as well as Klawer. Sample selection amounted to a total of 180 samples used for anion and cation analysis from both sites. Selected samples were used to obtain 1:1 soil-water extracts as 150 ml deionised water was added to 150 g of soil (Rhoades, 1996). Throughout sample analysis low density polyethylene (LDPE) bottles and polypropylene tubes were used to shake, extract, dilute and store samples as glassware could cause silica contamination. Samples were shaken in bottles for an hour using a mechanical shaker, extracted through suction filtration using Buchner funnels with highly retentive filter paper and collected in 250 ml bottles (Rhoades, 1996). The extracts were then filtered using 0.45 µm cellulose acetate syringe filters and diluted in a 1:1 extract to deionised water ratio to prevent precipitation of carbonates.

Diluted extracts were transferred to conical polypropylene tubes for anion and cation analysis and 50 ml bottles for pH(H_2O), EC, phosphate, and dissolved silica analysis. Extracts were refrigerated and kept dark during storage and transport between analyses to prevent microbes from metabolising ions. Major cations and anions (Ca^{2+}, Mg^{2+}, Na^{+}, K^{+} Cl^{-}, and SO_4^{2-}) were analysed using Ion chromatography at the DSI BIOGRIP Node for Soil and Water Analysis unit of Stellenbosch University's Central Analytical Facility (CAF). Iron (Fe^{2+}) and manganese (Mn^{2+}) were analysed using Inductively coupled plasma mass spectrometry (ICP-MS) at the Soil, Water and Plant Diagnostics Laboratory at Elsenburg. Alkalinity, pH(H_2O), EC, phosphate and dissolved silica was analysed in the Department of Soil Science laboratories of Stellenbosch University. All anion and cation concentrations were multiplied by 2 to correct for dilution.

2.5.4.1 Alkalinity, pH(H_2O) and EC

Measurement of EC using the saturated paste extract method (EC_e) is the recommended method for estimating absolute soil salinity as it is closely related to in-field moisture conditions (USDA, 1954; Rhoades et al., 1989). Soil-water suspensions of different soil to water ratios (1:1, 1:2, 1:2.5, 1:5 and 1:10) are also used widely to determine relative soil sainity (EC_w), but, unlike saturated pastes, do not mimic natural soil conditions (USDA, 1954; Sonmez et al., 2008; Aboukila and Norton, 2017). 1:1 soil-water suspensions were used during this study as it easier to prepare, to extract, and is less time consuming than performing saturated paste extracts which allows for faster throughput (USDA, 1954; McKenzie et al., 1983; Zhang et al., 2005; Sonmez et al., 2008). Sample extracts were analysed for alkalinity, pH(H_2O) and EC directly after extraction of the 1:1 soil-water suspensions. Alkalinity was determined using a calibrated Metrohm 702 SM Titrano automatic titrator. A 10 ml sample was titrated using a standard 0.01M HCl solution and the alkalinity was determined in mg/L CaCO3 equivalents using the equation [1]:

$$Alkalinity\ (mg/L) = \frac{N_{HCl} \times V_{HCl}(ml)}{V_{sample}(ml)} \times Mr_{CaCO_3} \times 1000 \qquad [1]$$

Where N_{HCl} is the normality of HCl; V_{HCl} is the millilitres of 0.01M HCl titrated in the sample; V_{sample} is the 10 ml sample used during the titration and Mr_{CaCO_3} is the equivalent weight of $CaCO_3$ (50 g/mole). An Eutech pH700 pH meter and a Jenway 4510 Conductivity meter was used to measure pH(H_2O) and EC of each sample extract, respectively. Alkalinity and EC measurements were corrected for dilution by multiplying with two.

2.5.4.2 Phosphate analysis

Phosphate was analysed using the ascorbic acid molybdenum blue method as indicated by Murphy and Riley (1962). Prior to analysis all glassware used for phosphate analysis was treated with sulfuric acid and rinsed to prevent contamination. Standards of 0.05, 0.1, 0.2, 0.3, 0.5, 0.7 and 1 mg/L phosphorus (as P) were prepared using a potassium dihydrogen phosphate stock solution. The mixed reagent was prepared as required by mixing a 4% ammonium molybdate solution with 5N sulfuric acid, adding 0.1M ascorbic acid to the mixture, and lastly adding a potassium antimonyl tartrate solution (1mg Sb/ml). An aliquot of 40 ml sample was pipetted into 50 ml volumetric flasks, 8 ml of mixed reagent added, and filled to the 50 ml mark with deionised water. Blue colour development was allowed, and sample absorbances were measured 10 minutes after adding the mixed reagent. Standard solutions were analysed

following the same procedure as indicated for the unknowns. The mixed reagent was also added to a blank containing deionised water and the blank absorbance was subtracted from all sample and standard absorbances. Absorbances of both standards and unknowns were measured at a wavelength of 882 nm using a Jenway 7315 UV Scanning Spectrophotometer.

Standard phosphate solution concentrations and absorbances were used to draw a standard curve with a linear line of best fit forced through zero.

2.5.4.3 Dissolved silica analysis

Solutions used during silica analysis were all stored in LDPE plastic bottles to prevent contamination from glassware. A sodium metasilicate stock solution was prepared as indicated by Yang *et al.* (2015) and the pH was adjusted to 1.5 as emphasized by Jones and Dreher (1996). Standard solutions of 0.1, 0.2, 0.3, 0.4, 0.6, 1.0, 1.4 and 1.8 mg/L silica, as silicic acid (H_4SiO_4), were prepared. Standards were prepared by pipetting the correct amount of stock solution directly into a 50 ml polypropylene centrifuge tube. Samples were treated in a similar manner by pipetting 1 ml of sample into 50 ml centrifuge tubes. Samples and standards were all diluted to 20 ml using deionised water.

Standards and sample unknowns were analysed using the blue silicomolybdous acid procedure outlined by Jones and Dreher (1996). A reducing solution was prepared by dissolving sodium bisulphite in deionised water and mixing with a sodium sulphite and 1-amino-2-naphthol-4-sulfonic acid solution. The reducing solution was kept refrigerated between analyses and prepared as required. A 10 ml aliquot of both H_2SO_4 and ammonium molybdate were added to the diluted samples and/or standards in centrifuge tubes. After waiting two minutes, 5 ml of both tartaric acid and the reducing agent were added, and the tubes were mixed immediately. Absorbances were measured 30 minutes after adding the reducing agent, allowing the blue colour to develop. The procedure was also followed for a blank containing deionised water and the blank absorbance was subtracted from all sample and standard absorbances. A Jenway 7315 UV Scanning Spectrophotometer was used to measure the absorbances of standards and unknowns.

Standard silica solution concentrations and absorbances were used to draw a standard curve with a linear line forced through zero. The equation of the line was used to determine the unknown silica concentrations of samples. As standard solutions were analysed by directly

pipetting stock solution into centrifuge tubes and adding reagents, sample concentrations were multiplied by 50 to correct for dilution.

2.6 Data analysis

2.6.1 Heuweltjie pH(H_2O) and EC screening

Shapiro-Wilk tests for normality showed that most data were not normally distributed and validated the use of the non-parametric Kruskal-Wallis test. Kruskal-Wallis non-parametric tests were performed on both pH(H_2O) and EC measurements of 22 heuweltjies screened in Piketberg and Klawer. pH(H_2O) and EC were grouped into sample locations (heuweltjie centre, heuweltjie side, and inter-heuweltjie) and depths (topsoil and subsoil samples). Multiple comparisons were performed on significant Kruskal-Wallis tests that was grouped by sample location using the Nemenyi post-hoc test.

2.6.2 Soil texture of heuweltjie and inter-heuweltjie soils

Shapiro-Wilk tests revealed that not all sand, silt and clay percentages of heuweltjie and inter-heuweltjie soils were normally distributed. One-way ANOVA's (Analysis of variance) were conducted on parametric data and Kruskal-Wallis test on non-parametric data of the sand, silt and clay percentages of both heuweltjie and inter-heuweltjie soils of Piketberg and Klawer. Three depth groups were used to group soils with similar morphologies for comparison of sand, silt and clay percentages of grouped depths within and between heuweltjie and inter-heuweltjie soils. Multiple comparisons were performed on significant One-way ANOVA (Tukey's HSD post hoc test) and Kruskal-Wallis tests (Nemenyi post-hoc test) to identify which grouped depth differed significantly for both heuweltjie and inter-heuweltjie sand, silt and clay percentages, respectively. Ion activities and saturation indices

2.6.3 Ion activities and saturation indices

The computer program PHREEQC Interactive 3.6.2-15100 was used to calculate ion activities of major solutes and saturation indices of minerals identified in the XRD patterns in section 2.4.3. As Al^{3+} was not measured directly, activity was calculated using PHREEQC by equilibrating Al concentration with Kaolinite or illite. Illite was used where kaolinite was absent, as derived from the clay mineralogy in section 2.4.3. Common minerals associated with heuweltjies were also included in SI calculations. Using several aqueous models PHREEQC is able to execute speciation calculations and determine saturation degrees for species in solution

with respect to mineral phases (Parkhurst and Appelo, 2013). PHREEQC is a useful tool when trying to understand how solute concentrations are influenced by chemical processes (Appelo and Postma, 2005).

The Specific Ion Interaction Theory activity coefficient model or SIT database (SIT.dat) was used to calculate solute activities and mineral SI. Sepiolite was added as a phase using the PHASES block in PHREEQC as it is absent from the SIT database. The Debye-Hückel theory is implemented to calculate activity coefficients for solutes in PHREEQC up to solution ionic strengths of seawater (Appelo and Postma, 2005). The ionic strengths of the 1:1 soil-water extracts, that ranged between 0.0003 and 0.2832, all fell below that of seawater (~0.67; Nordstrom *et al.*, 1979). Consequently, the soil-water extracts conform to the sodium chloride dominance criteria in PHREEQC which indicates that the SIT model was sufficient to use for speciation calculations of sample soils. Equilibrium constants (log K) and solubility equations of minerals in the SIT database of PHREEQC with the addition of sepiolite are displayed below (Table 2.1)

Table 2.1: Equilibrium constants and solubility equations of common minerals associated with heuweltjies used in mineral saturation calculations in PHREEQC.

Mineral	*Solubility equation*	*log K*	*Source*
Calcite	$CaCO_3 = Ca^{2+} + CO2$	-8.48	(Plummer and Busenberg, 1982)
Gypsum	$CaSO_4 \cdot 2H_2O = Ca^{2+} + SO_4^{2-} + 2H_2O$	-4.61	(Garvin et al., 1987)
Halite	$NaCl = Na^{+} + Cl^{-}$	1.59	(Chase, 1998)
Hydroxyapatite	$Ca_5(OH)(PO_4)_3 = 5Ca^{2+} - 7H^{+} + 3H_2(PO_4)^{-} + H_2O$	14.35	(Nancollas, 1984)
Quartz	$SiO_2 = H_4(SiO_4) – 2H_2O$	-3.74	(Richet et al., 1982)
Amorphous Silica	$SiO_2 = H_4(SiO_4) – 2H_2O$	-2.71	(Gunnarsson and Arnórsson, 2000)
Dolomite	$CaMg(CO_3)_2 = Ca^{2+} + Mg^{2+} + 2CO_3^{-2}$	-17.12	(Hemingway and Robie, 1994)
Sepiolite	$Mg_2Si_3O_{7.5}(OH) \cdot 3H_2O + 4H^{+} + 0.5H_2O = 2Mg^{+2} + 3H_4SiO_4$	15.76	(Stoessell, 1988)

Chloride was selected to use as a measure for the degree of evaporative concentration (Eugster and Jones, 1979). Chloride is maintained at constant over the widest concentration range within the eight principal solutes that dominate the chemistry of natural water (Eugster and Jones, 1979). The conservative nature of chloride can be ascribed to minor anion exchange and that it remains in solution until halite saturation (Eugster and Jones, 1979). Therefore, chloride can be a reliable measure of evaporative concentration limited up to halite saturation (Eugster and Jones, 1979). Evaporative concentration was evaluated by plotting the logarithm of anion and cation activities of samples against that of chloride ($\log[Cl^-]$), where square brackets denote activity. As the SI is a numerical index, it also allows for mineral stability to be plotted against the independent salinity variable of $\log[Cl^-]$ (Francis, 2008). Mineral saturation was evaluated by plotting the SI of minerals against $\log[Cl^-]$ and $pH(H_2O)$.

Correlations were validated of each log[Ion] or log[SI] against $\log[Cl^-]$ or $pH(H_2O)$ using Spearman's rank correlation coefficient (r_s). Spearman's rho of the 1:1 soil water extract data was calculated separately for PB1 and K1. Specific mineral saturation indices selected for display were done so based on bulk sample mineralogy. Although Pearson product-moment correlation coefficient (r) is commonly used to assess linear relationships between two variables, some assumptions must be met to properly deduce the strength of association (Schober and Schwarte, 2018). One such assumption is that of bivariate normality where both variables should follow a normal distribution as Pearson's correlation is sensitive to non-normal data (Kowalski, 1972). Spearman's coefficient, used to assess monotonic relationships, is more robust against outliers and does not require data to be normally distributed (Caruso and Cliff, 1997). Linearity of monotonic relationships can be assessed visually as with scatter plots (Anscombe, 1973). Spearman's correlation coefficients and p-values (t-tests) for analysis of significance were determined using RStudio Version 1.2.5033 at a 95% confidence level.

2.6.4 Interpolated maps

Major ion concentrations, SI values, $pH(H_2O)$ and EC were interpolated as maps for both PB1 and K1. The aim of creating interpolated maps was to visually assess the relative distribution of ions and SI of minerals throughout heuweltjie soils. The distribution of ions and SI would give insight to identify trends in ion concentrations and salt saturation with depth and within specific features. QGIS Version 3.14.0 was used to create a digital surface model which was used as a gridding extent during interpolation in Surfer® Version 21.1.158.

All data points were interpolated using directional ordinary kriging and the direction (diagonal 30-60˚, horizontal 0˚; 180˚, or vertical 90˚; -90˚) of best fit was determined using linear variograms. Directional ordinary kriging is implemented when data shows anisotropy i.e. when spatial variability of data changes more within a specific direction (Goovaerts, 1997). Variograms are used to validate spatial autocorrelation of data in Surfer® and can indicate prediction errors during interpolation. High prediction error would occur where no datapoints are present and low prediction error would occur where data points are close to each other or at the borders of heuweltjie extents. Most of the heuweltjie soils were non-uniform and changed more in specific directions. The spatial variation cannot fully be accounted for while kriging and predictions of ion concentrations and mineral saturation indices are expected to be poor.

The best variogram model fit was chosen separately for each interpolation and the parameters used are indicated in Appendix A. Figure 2.8 shows examples of the best linear variogram model fit for the pH(H_2O) and EC of K1. The direction parameter is used to set the direction (diagonal, horizontal, or vertical) in which a dataset shows the best fit and the tolerance refers to the width of the angle of consideration from the specified direction. When variogram models are fitted for interpolation the objective is to capture major spatial attributes of features and overfitting should be avoided (Goovaerts, 1997). Model fit or R^2 values are poor for all interpolated maps due to the discontinuous nature of heuweltjie soils and their chemistry. However, overfitting the model could cause loss of important spatial attributes of features in heuweltjie soils and was avoided as cautioned by Goovaerts (1997). All variogram parameters are attached in Appendix A.

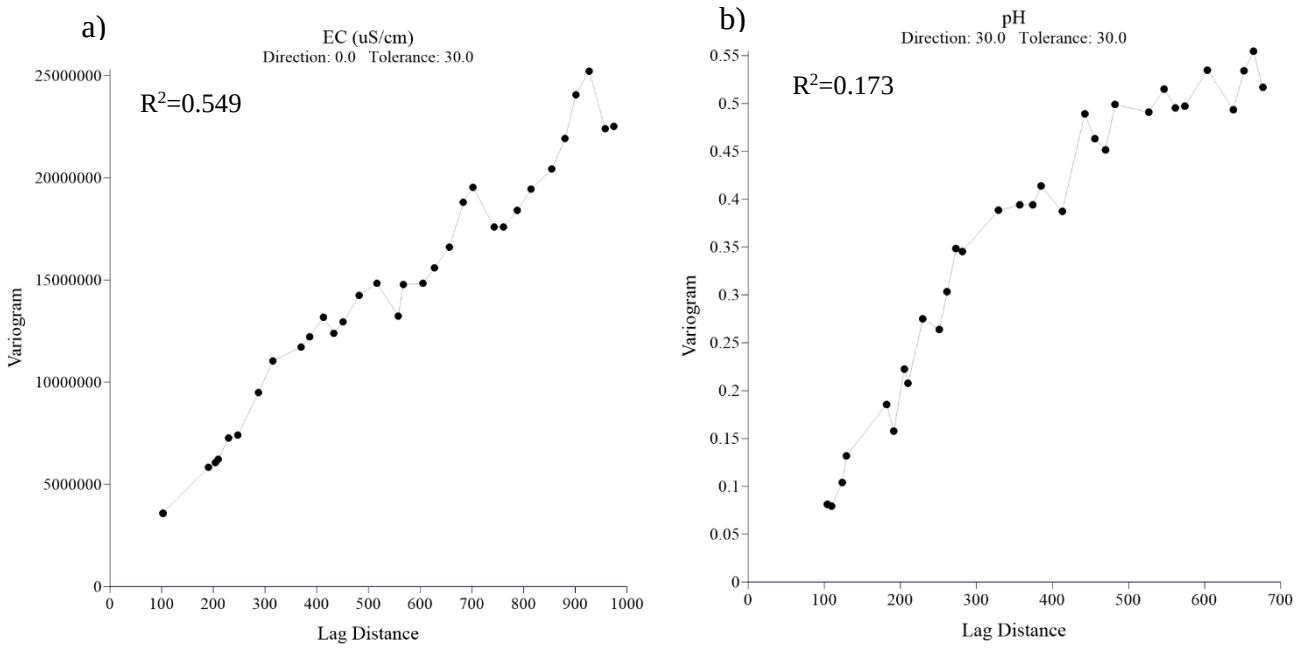

Figure 2.8: Best fit linear variograms for the 1:1 soil:water extract EC (a) and pH (b) of the K1 heuweltjie.

3 Results

3.1 Heuweltjie pH(H_2O) and EC screening

Screening results of heuweltjies in Piketberg and Klawer are displayed in the following section and overall significant trends of average pH(H_2O) and EC measurements for the centre, side, and inter-mound samples are reported. Screening results for individual heuweltjies in both Piketberg and Klawer are attached in Appendix B.

3.1.1 Piketberg heuweltjies

The pH(H_2O) (P=0.015) and EC (P=0.012) of the topsoil samples were significantly higher in the centre of the heuweltjies in Piketberg compared to inter-mound samples (Figure 3.1). Similarly, pH(H_2O) (P=0.024) and EC (P=0.001) of subsoil samples were also significantly higher in the centre of the mounds compared to side and inter-heuweltjie samples (Figure 3.1). A few mound centres and sides showed increases in EC and/or pH(H_2O) with depth.

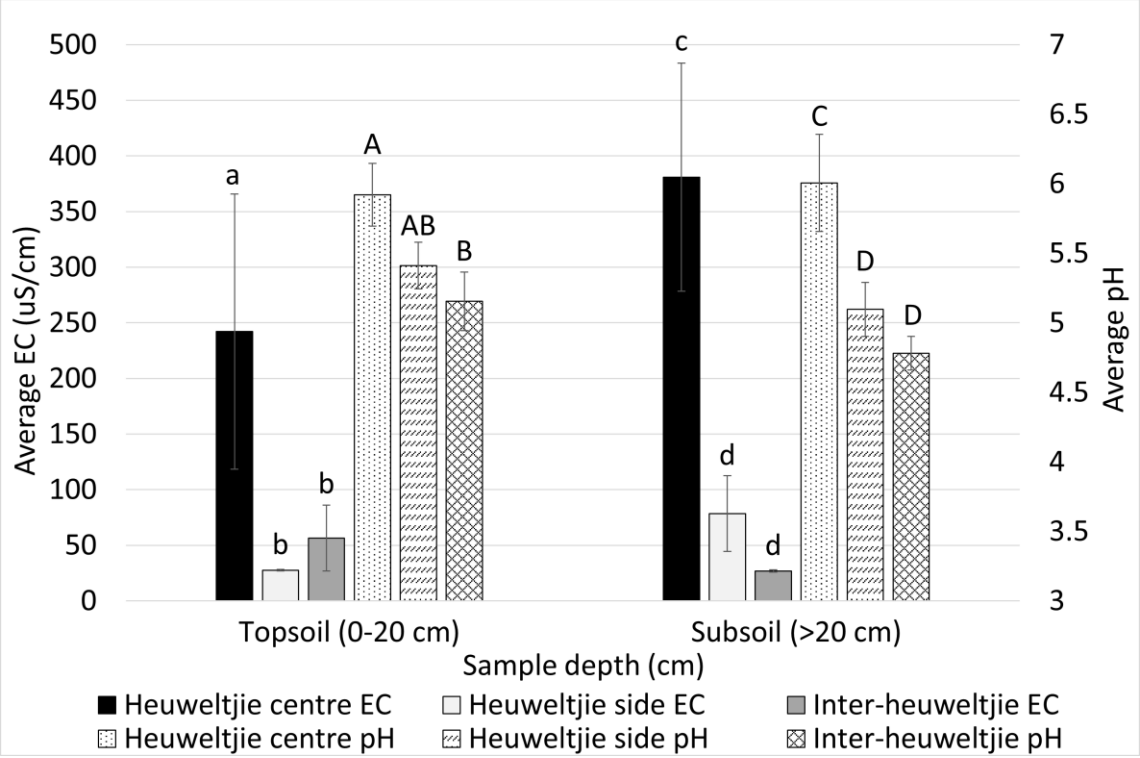

Figure 3.1: Average EC (uS/cm) and pH(H_2O) of heuweltjie centre, side, and inter-heuweltjie topsoil (0-20 cm) and subsoil (>20 cm) samples of twelve heuweltjies sampled in Piketberg. Lowercase letters indicate significance for average EC (uS/cm) and uppercase letters indicate significance for average pH.

3.1.2 Klawer screening

Klawer heuweltjies only showed a significant higher EC (P=0.034) in the centre of mound topsoils compared to side topsoil samples and no significant difference between heuweltjie soils and inter-mound soils (Figure 3.2). However, the topsoil pH(H_2O) (P<0.001) of heuweltjie centre and side samples were significantly higher compared to inter-heuweltjie topsoil samples (Figure 3.2). Subsoil samples of the inter-mound soils could not be obtained as dorbank was present at shallow depths in the inter-heuweltjie soils of all heuweltjies. An increase in EC with depth was observed in the centre and sides of heuweltjies as subsoil samples in mounds had a higher EC compared to topsoil samples.

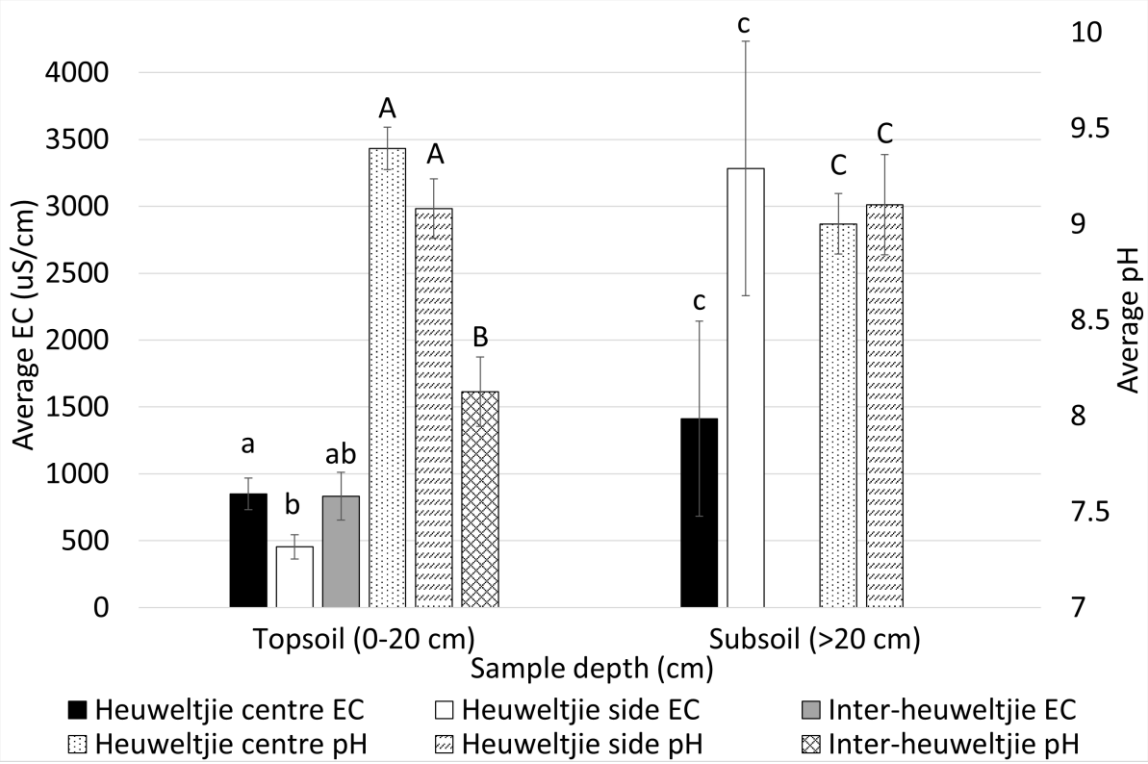

Figure 3.2: Average EC (uS/cm) and pH(H_2O) of heuweltjie centre, side, and inter-heuweltjie topsoil (0-20 cm) and subsoil (>20 cm) samples of ten heuweltjies sampled in Klawer. Lowercase letters indicate significance for average EC (uS/cm) and uppercase letters indicate significance for average pH.

3.2 Profile and feature descriptions

Heuweltjie wall-sketches indicate depths of major soil morphological changes and specific feature locations (termite frass chambers, termite channels, carbonate enrichment and dorbank extents). For each profile, the surface of the mound serves as the highest (zero depth) point. Sketches were exaggerated vertically but depths and cross-section profiles are shown true to field measurements. Tables containing each modal profile description, diagnostic horizon and the soil codes are attached in Appendix B. The descriptions below serve to highlight the major features within and surrounding the modal profiles from each heuweltjie.

3.2.1 Piketberg heuweltjie (PB1)

The heuweltjie and inter-heuweltjie topsoil in Piketberg were unconsolidated and showed signs of soil formation or weathering (Ne/Bw). Inter-heuweltjie subsoils consisted of colluvial material (UC) with high gravel content (sandstone gravel, stones, and boulders) and the occurrence of clay tongues. Heuweltjie subsoils transitioned from loose dorbank (Db/Bqm) nodules to termite channels (Db/Bkqm) with varying degrees of induration and secondary carbonate accumulation (calcareous Db/Bkqm). The parent material in PB1 was identified as aeolian sands overlying colluvial material with weathering sandstone.

3.2.1.1 East-wall of PB1(PB1E)

Figure 3.3 shows the detailed sketch of the east-wall of the PB1 heuweltjie trench with a vertical exaggeration of eight. However, depths on the y-axis are shown unexaggerated. Heuweltjie soils containing gravelly dorbank in the subsurface horizons started between PB1E-7 and PB1E-8 and continued up to the profile at PB1E-30. The heuweltjie soils corresponded with the start of a ring of *Mesembryanthemum* plants (colloquially known as ‘vygies’) around the sides of the mound (indicated with dotted lines above the mound surface in Figure 3.3).

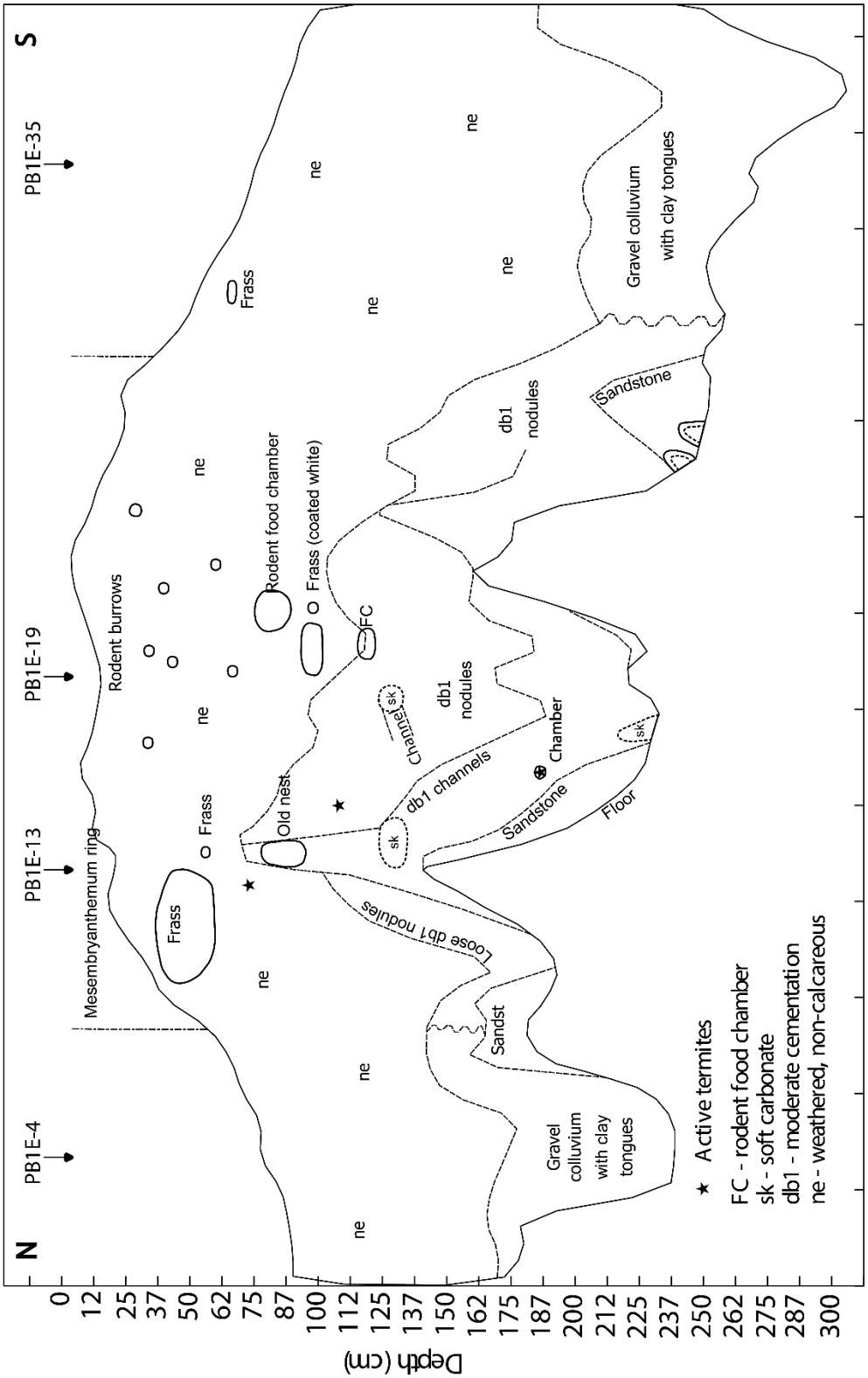

*Figure 3.3: A detailed sketch (in a north to south direction) of the east-wall of the trench dug through the mound and inter-mound soils of the heuweltjie in Piketberg (PB1E). The sketch has a vertical exaggeration of x8. Modal profiles are indicated with arrows. Db(Bqm)= silica cementation or induration; sk(Bk)= secondary carbonate accumulation; ne(Bw)= neocutanic/ weathered soils showing signs of colour development; FC= rodent food chamber, *= active termites; frass= termite excrement.*

Inter-heuweltjie profiles of the mound in Piketberg (PB1E-4, 35, and PB1W-6) had bleached sandy orthic A horizons that gradually transitioned to brownish yellow neocutanic B-horizons (5-7% clay) likely of aeolian origin. Aeolian horizons abruptly transitioned to an unconsolidated colluvial layer consisting of rock, stone, and gravel sandstone fragments with red, finely structured, discontinuous clay tongues (15-20% clay) between fragments. No secondary carbonates were present in any of the inter-heuweltjie soils. Figure 3.4 shows an example of an inter-heuweltjie soil at the profile at 4 m on the east wall.

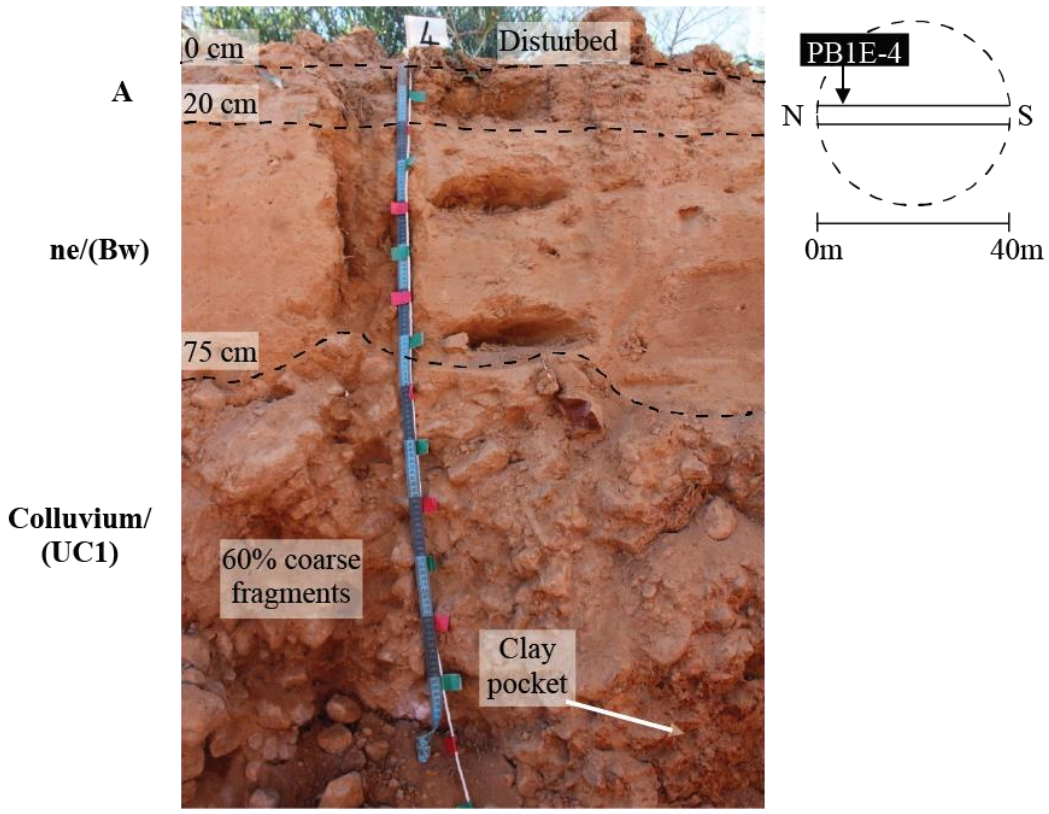

Figure 3.4: Detailed image of inter-heuweltjie soil profile at PB1E-4, Ne/Bw = neocutanic B-horizon/weathered B-horizon showing colour development; UC1 = unconsolidated colluvial slope deposit.

Figure 3.5a, Figure 3.7a, Figure 3.10a and Figure 3.11a following in this section all show examples of heuweltjie soils. Heuweltjie soils (PB1E-8 to 30 and PB1W-12 to 21.5) had apedal sandy orthic A-horizons (5-10% clay) gradually transitioning to loamy sand/sandy loam (7-15% clay), yellowish brown, slightly hard, neocutanic B-horizons with occasional termite channels, frass chambers, and indurated nodules. Neocutanic horizons showed a clear transition to reddish yellow, loose, nodular, gravelly dorbank and/or slightly indurated dorbank with less clay (5-10%) and discontinuous secondary carbonate impregnation in selected profiles (PB1E-13, 17, 18 and PB1W-16 to 19). The loose nodular dorbank horizon abruptly transitioned to moderately or highly indurated dorbank containing abundant medium to large, indurated termite channels in PB1E-12 to 27, PB1W-12 to 15, and PB1W-21.5. Dorbank throughout heuweltjie soils were cemented by silica and enriched in Mn oxides present as veins or coatings on nodules and indurated channels.

Figure 3.5a shows the heuweltjie modal profile at a cross-section distance between 13 and 14 m. At a depth of 20 cm a large frass chamber was present above an old, silicified nest in the orthic A-horizon (Figure 3.5a). Also present above the silicified nest in the neocutanic B-horizon were hard indurated spheres, some containing roots with a sandy texture, and others silicified with no roots (Figure 3.5c). The indurated spheres were observed throughout the loose dorbank layer in the mound. The silicified nest extended between depths of 30 to 80 cm and contained abundant, highly indurated, medium, and large termite channels (Figure 3.5e). Below the silicified nest the loose dorbank layer continued with carbonate accumulation starting at 90 cm and extending to the base of the trench. Active new termite channels, evident in the granular soil structure, were present at a depth of 100 cm in the carbonate impregnated, loose dorbank (Figure 3.5f). Another large (1.5 cm diameter), highly indurated channel was observed at a depth of 115 cm at 14 m cross-section distance with surrounding carbonate and Mn oxide enrichment (Figure 3.5d).

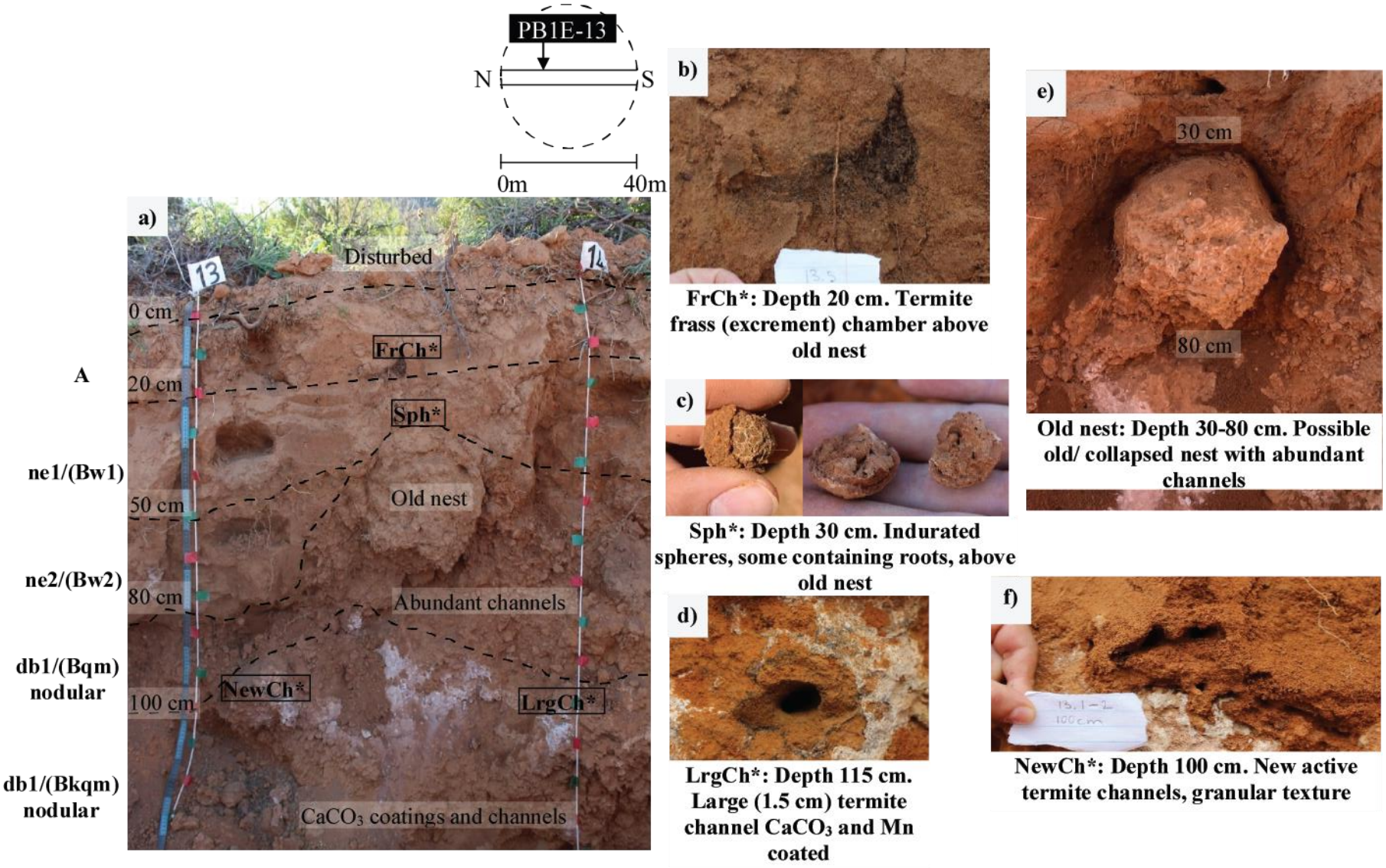

*Figure 3.5: Detailed images of heuweltjie soil profile at PB1E-13 and surrounding features. a) Full heuweltjie profile at 13m; b) Frass chamber above paleo nest; c) spherical root structure removed above nest; d) large, indurated termite channel at 115 cm; e) Exposed paleo nest with abundant channels between 30-80 cm depth; f) new active termite channels with no induration and granular texture. Ne/Bw = neocutanic B-horizon/weathered B-horizon showing colour development; db1/Bqm= moderate Si cementation; Bkqm = Si and carbonate cementation. * Indicate the location of enlarged features in the profile.*

At a depth of 180 cm in profile PB1E-16 a large termite chamber occurred with many dead, rotting termites in the chamber within the loose, nodular dorbank (Figure 3.6a and c). The chamber exterior was enriched in Mn oxide and the interior with organic matter (Figure 3.6c). Prior to exposing the channel, active termites were observed at the chamber (Figure 3.6b). The day after sampling, termites patched up the open chamber as seen in the granular structure (Figure 3.6d).

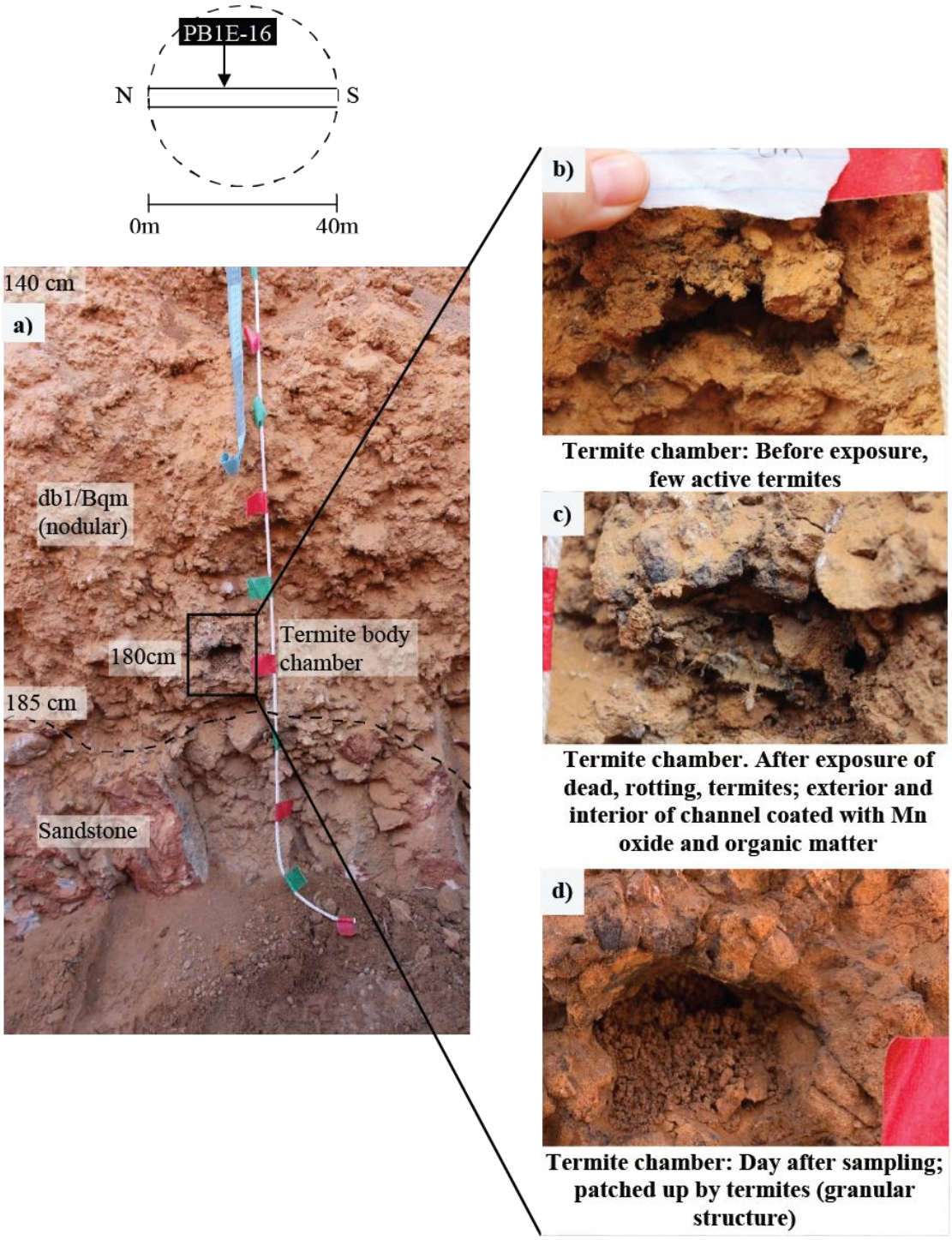

Figure 3.6: Large termite body chamber at profile PB1E-16. a) The nodular db1/Bqm that hosted the termite chamber with sandstone rocks and boulders starting at 185 cm; b) Chamber before exposure with active termites; c) Chamber after exposure of deceased, rotting, termites, and Mn and organic matter channel coatings; d) Chamber patched up by termites (granular structure) a day after sampling. Db1/Bqm = moderate Si cementation.

The heuweltjie soil profile at PB1E-19 had a nodular, loose dorbank layer with many Mn oxide coatings that started at 80 cm and extended down to 145 cm (Figure 3.7a and d). The nodular dorbank abruptly transitioned to highly indurated channels that continued down to the start of the colluvium at a depth of 170 cm.

Between PB1E-18 and PB1E-19 in the nodular, loose dorbank, large, indurated channels were present at depths between 100 and 170 cm with localized carbonate accumulation occurring at 100 cm (Figure 3.7b). Multiple large rodent burrows and a rodent food pile was observed between PB1E-19 to PB1E-20 within the neocutanic and nodular, loose dorbank B-horizons (Figure 3.7c). These burrows and occasional food piles were present throughout the cross-sections of 19 to 24 m in mainly the neocutanic horizons and upper nodular dorbank horizons of the heuweltjie (Figure 3.3). Active rodents were observed in some of the burrows.

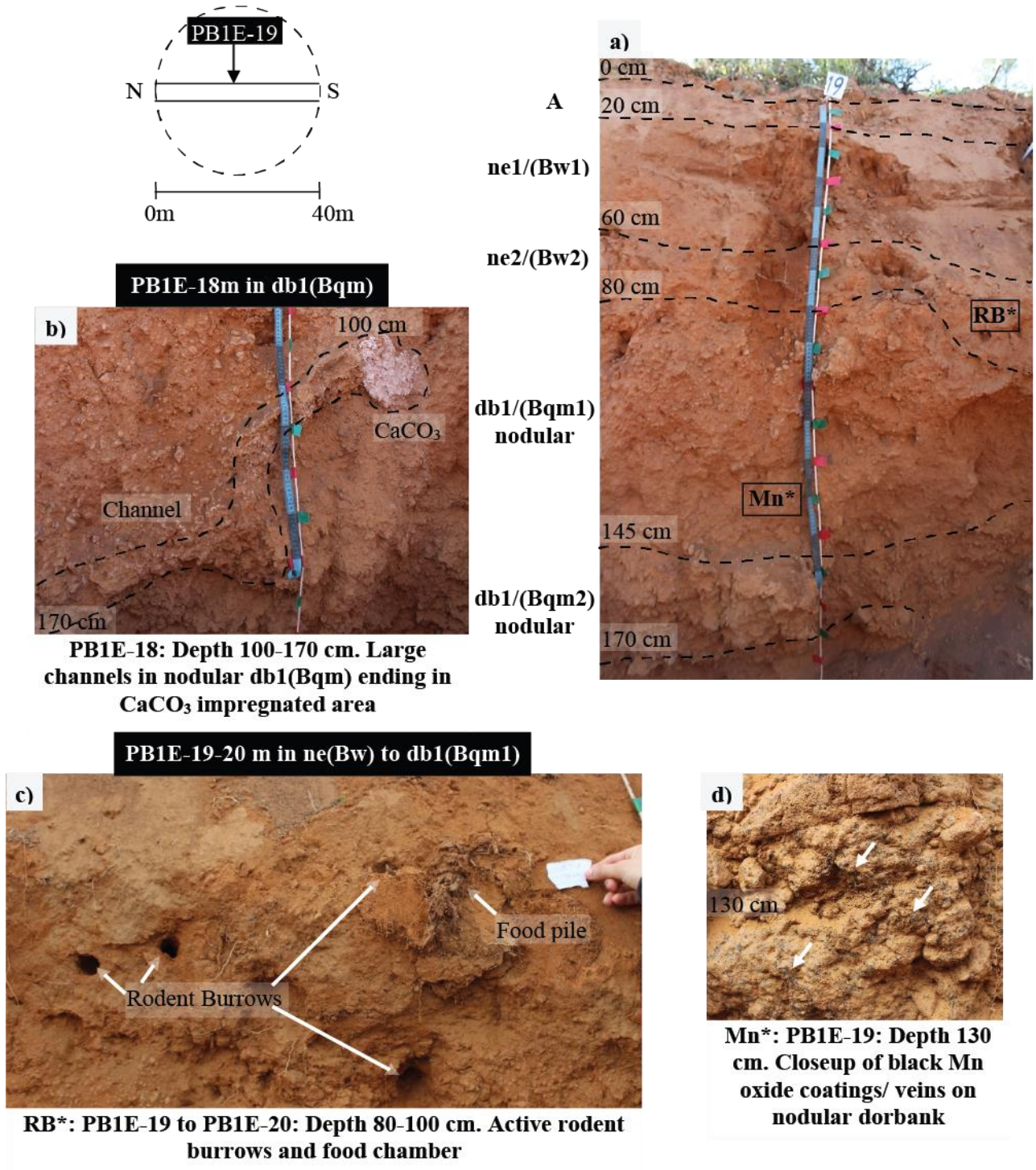

*Figure 3.7: Detailed images of the heuweltjie soil modal profile at PB1E-19 and surrounding features. a) The full heuweltjie soil profile at 19m; b) Large channels within the nodular silica cemented horizon ending in carbonate impregnated area between 18-19m; c) Active rodent burrows and rodent food chamber between 19-20m. d) Closeup of the black Mn coatings on nodular dorbank/silica cementation. Ne/Bw= neocutanic/weathered soil showing colour development; db1/Bqm= moderate Si cementation. * Indicate the location of enlarged features in the profile.*

Figure 3.8a shows a large exposed rodent burrow between cross-section distances of 21 and 22 m at depths of 20 to 70 cm in the neocutanic B-horizon. Also observed at profile PB1E-21 was a termite frass chamber in the neocutanic horizon that was coated with a white precipitate or filaments that had no reaction to HCl (Figure 3.8b and c).

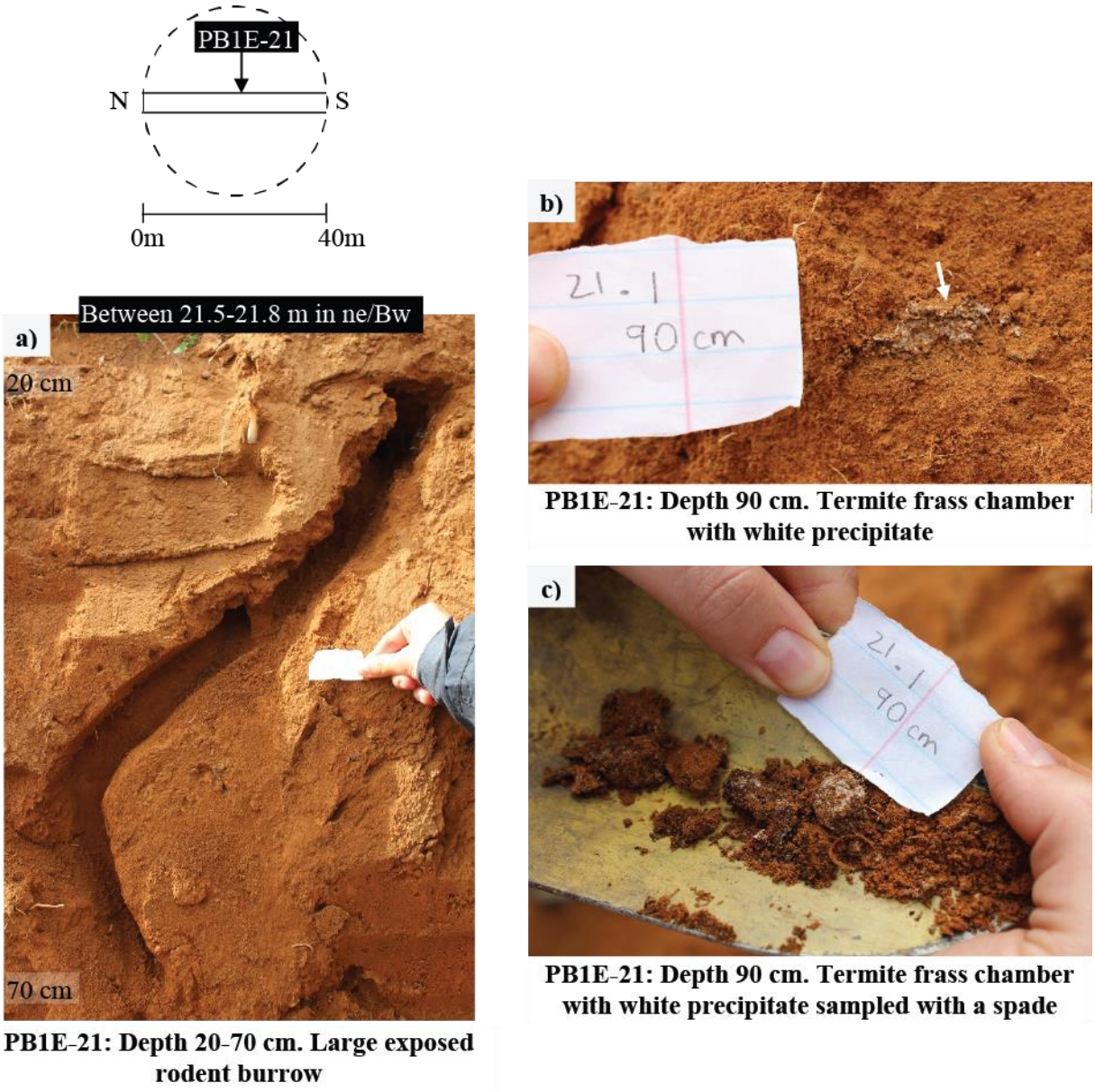

Figure 3.8: Description of features located at PB1E-21. a) Large exposed rodent burrow between cross-section distances of 21 and 22 m in the ne/Bw soil horizon; b) A termite frass chamber with a white precipitate coating the frass in the ne/Bw soil horizon; c) The sampled termite frass chamber showing black frass pellets with some coated in a white precipitate. ne/Bw= neocutanic/weathered horizon

3.2.1.2 West-wall of PB1 (PB1W)

Figure 3.9 shows the detailed sketch of the west-wall of the trench dug through the PB1 heuweltjie with a vertical exaggeration of five but depths are shown unexaggerated. The west wall was only sampled and described from PB1W-6 to PB1W-21.5 where morphologies differed from the east-wall. The sketch was made in a south to north direction, as the perspective would be of someone standing in the trench facing the west-wall. Heuweltjie soils containing gravelly dorbank/Si cementation in the subsurface horizons started between PB1W-9 and PB1W-10 and continued up to the last sampled profile at PB1W-21.5. The west wall contained a large carbonate accumulated horizon within the gravelly dorbank that started at about 15 m (PB1W-15) and extended up to about 19 m (PB1W-19).

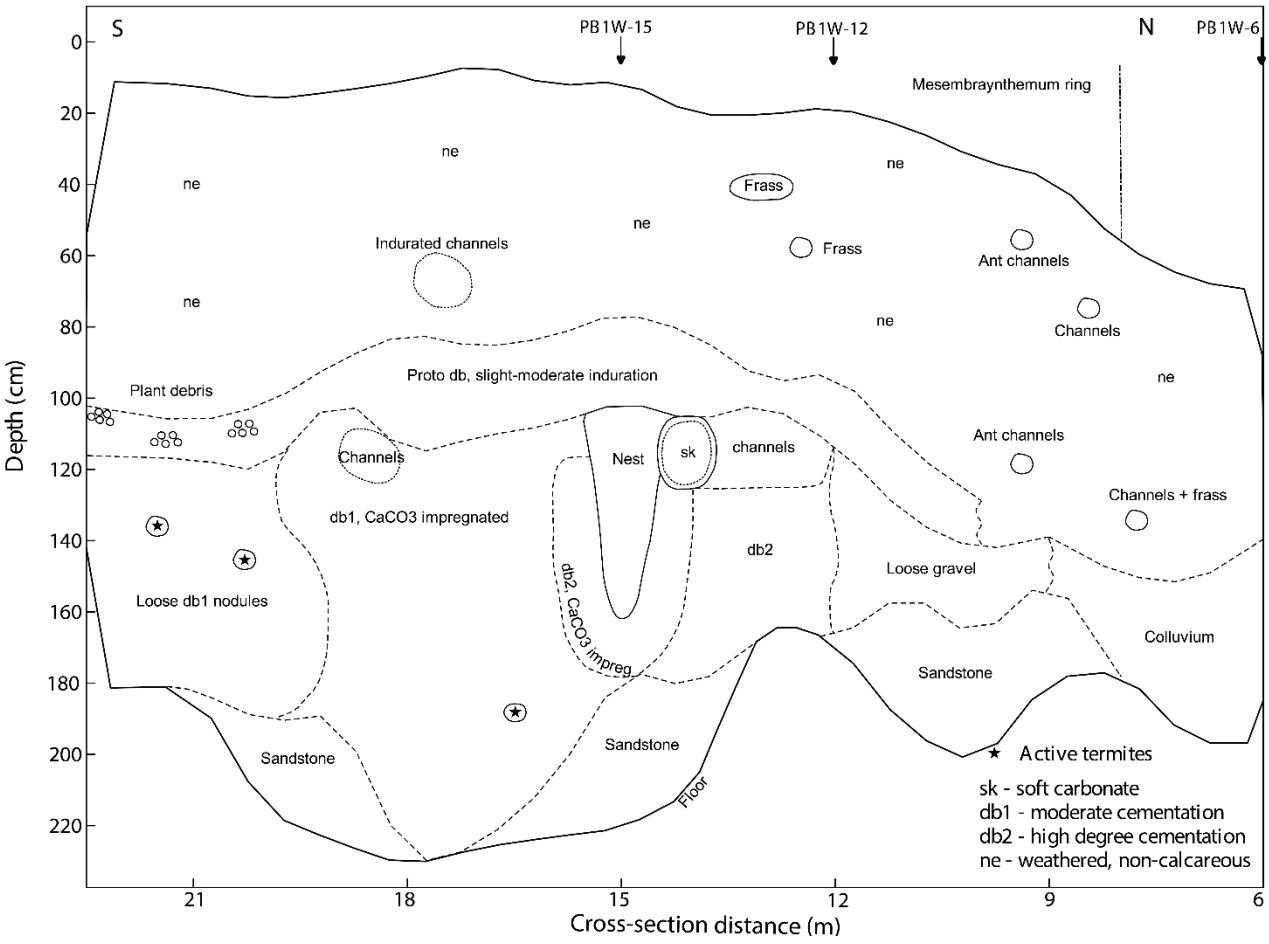

*Figure 3.9: A detailed sketch (in a south to north direction) of the west-wall of the trench dug through the mound and inter-mound soils of the heuweltjie in Piketberg (PB1E). The sketch has a vertical exaggeration of x5. Modal profiles are indicated with arrows. Db (Bqm)= Si cementation or induration; sk(Bk)= secondary carbonate accumulation; ne(Bw)= neocutanic/weathered soils showing signs of colour development; *= active termites; frass= termite excrement chambers.*

At the cross-section of 15 m the loose, nodular dorbank layer between 80 and 130 cm was surrounded by highly indurated, calcareous nodular dorbank that contained abundant channels (Figure 3.10a and c). The loose, nodular dorbank in this profile was observed to be an area that could have hosted a nest. The highly indurated, calcareous nodular dorbank surrounding the old nest area at 15 m graded (in a horizontal direction) to loose, nodular dorbank visibly impregnated with carbonates on both sides. The soft carbonate horizons started at 14.5 and 15.5 m cross-section distances on either side (Figure 3.10a and c; *sk1 and *sk2). The soft carbonate horizon at 14.5 m (*sk2) cross-section distance occurred within depths of 90 to 130 cm in the loose, nodular dorbank (Figure 3.10b). The area was encapsulated by a thin silicified outer film with many Mn oxide coatings. Many channels and pores were present within and around the carbonate accumulated area. At 15.5 m cross-section distance the soft carbonate (*sk1) started at 65 cm depth and extended to the trench floor at 190 cm (Figure 3.10a and c). This area marked the start of a large carbonate impregnated horizon on the west wall of the Piketberg heuweltjie trench.

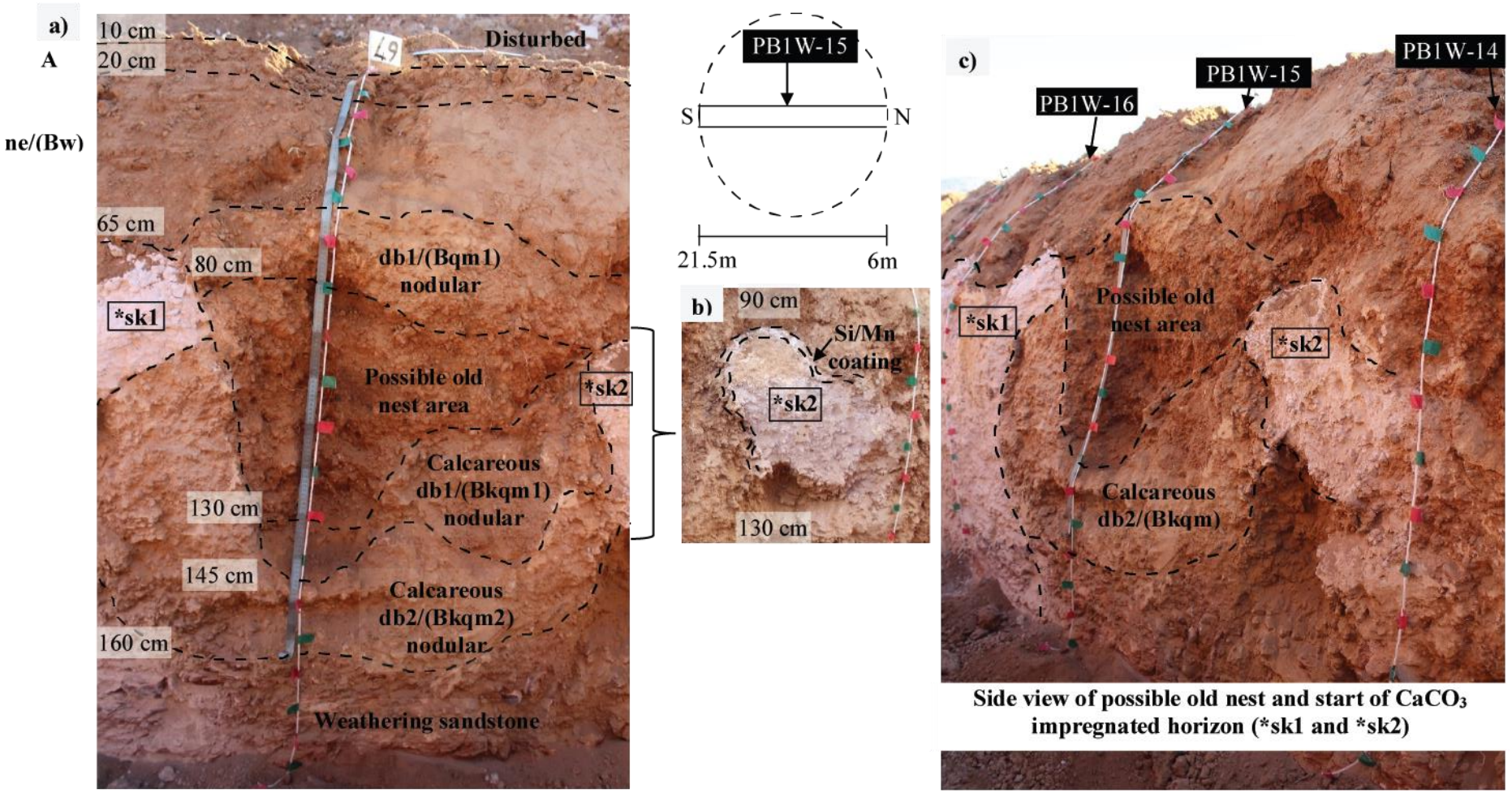

*Figure 3.10: Detailed image of the heuweltjie modal profile at PB1W-15 with an area that possibly hosted an old/paleo nest and secondary carbonate accumulation. The top 10 cm of the profile was removed during excavation. a) Shows the entire profile at PB1W-15; b) Area of secondary carbonate accumulation between PB1W-14 and PB1W-15 with a Si and Mn indurated outer coating; c) Side view of the profile at PB1W-15 showing secondary carbonate accumulated areas and a possible old nest area. Ne/Bw= neocutanic/weathered B-horizon showing signs of colour development; db/Bqm= moderate (db1) to high (db2) Si cementation or induration; Calcareous db/Bkqm= Carbonate and Si cementation; sk= soft carbonate/secondary carbonate accumulation. * Indicate the location of enlarged features in the profile.*

Figure 3.11 shows the extent of the carbonate impregnated horizon on the west wall of the Piketberg heuweltjie trench. Secondary carbonate accumulation occurred within the moderately indurated, loose, nodular dorbank layer of the wall starting at a cross-section distance of about 16.5 m and extending up to about 19 m (Figure 3.11a). A thin silicified film was observed around parts of the outer edges of the horizon which also contained abundant Mn veins. The carbonate accumulated horizon started at depths ranging from 60-100 cm and extended down to the trench floor (Figure 3.11a). At profile PB1W-19, and between profiles PB1W-17 to PB1W-18, above the carbonate accumulated horizon, areas of moderate induration with a high concentration of channels were observed (Figure 3.11a, b, and c). Between PB1W-16 and PB1W-17 at a depth of 180 cm many active termite channels were observed with termites removing frass and plant matter (Figure 3.11d). The pile of termite frass indicated in Figure 3.11d was generated within 16 hours of placing the spade below the channels. Figure 3.11e shows the termite channels at 180 cm depth between PB1W-16 and PB1W-17 that was patched up or blocked by termites a day after sampling the channels.

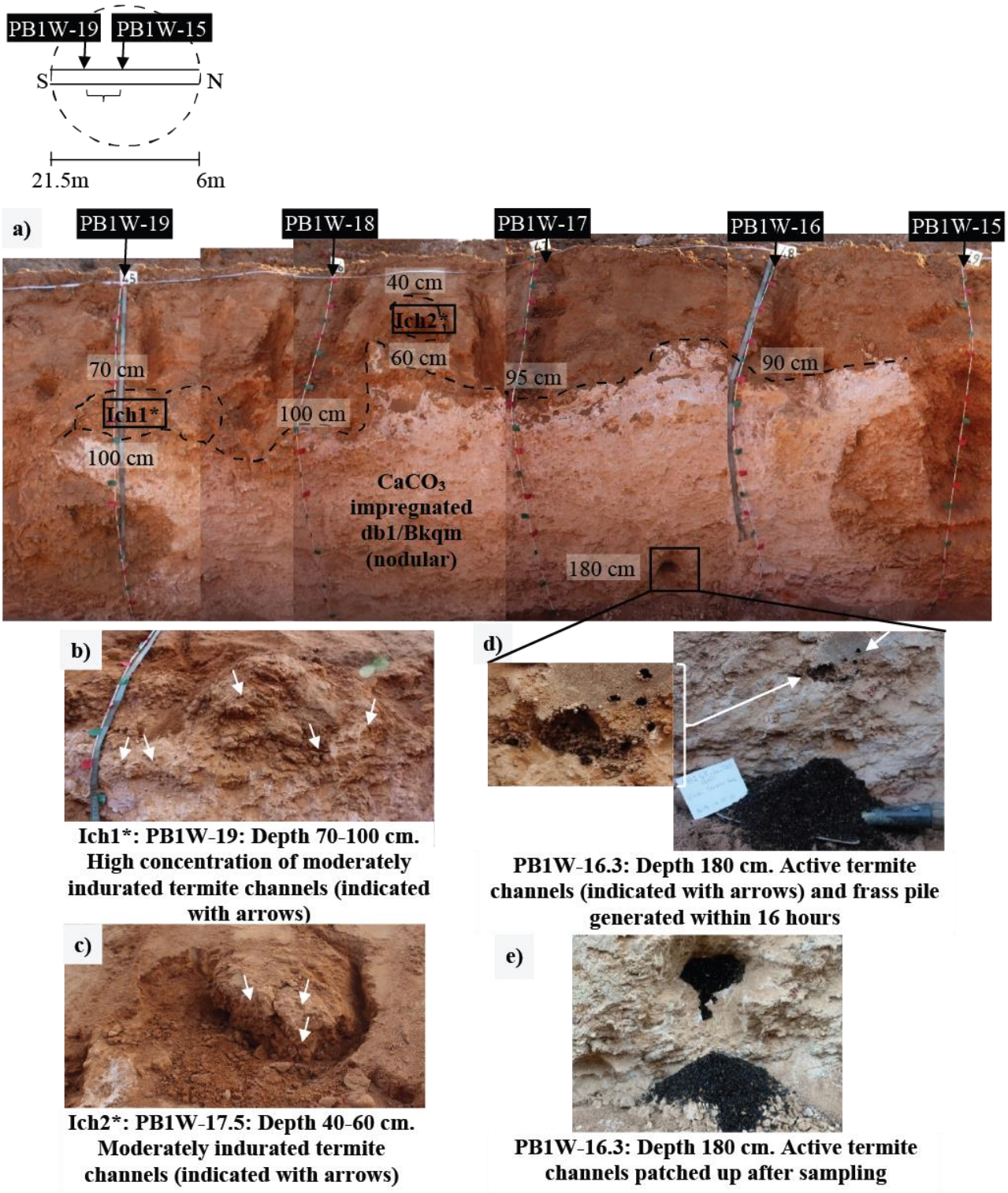

Figure 3.11: A profile mosaic showing the horizon of secondary carbonate accumulation on the west-wall of the trench through the heuweltjie in Piketberg (PB1W). a) The extent of the nodular, moderately indurated dorbank/Si cemented horizon (db1/Bkqm) with secondary carbonate accumulation. The shallowest initial depth was at 60cm and the horizon extended to the trench floor between profiles PB1W-15 to PB1W-19; b and c) Areas of moderate induration above the carbonate accumulated horizon with a high concentration of channels; d) Large active termite channels at 180 cm depth between PB1W-16 and PB1W-17 and a frass pile generated by termites within 16 hours; e) Patched up channel the day after sampling the channels and frass. Calcareous db1/Bkqm= moderate Si cementation and secondary carbonate accumulation.

Figure 3.12 shows the large active termite channel located at a depth of 145 cm within the profile of PB1W-21.5. Figure 3.12a shows the location of the channel within the moderately indurated, nodular dorbank horizon of the profile. Active termites were observed at or leaving the channel (indicated with arrows in Figure 3.12b) and on the floor of the trench at PB1W-21.5 (Figure 3.12c). The channel exterior was visibly coated with carbonates and the channel interior was lined with Mn oxides and organic matter (Figure 3.12d).

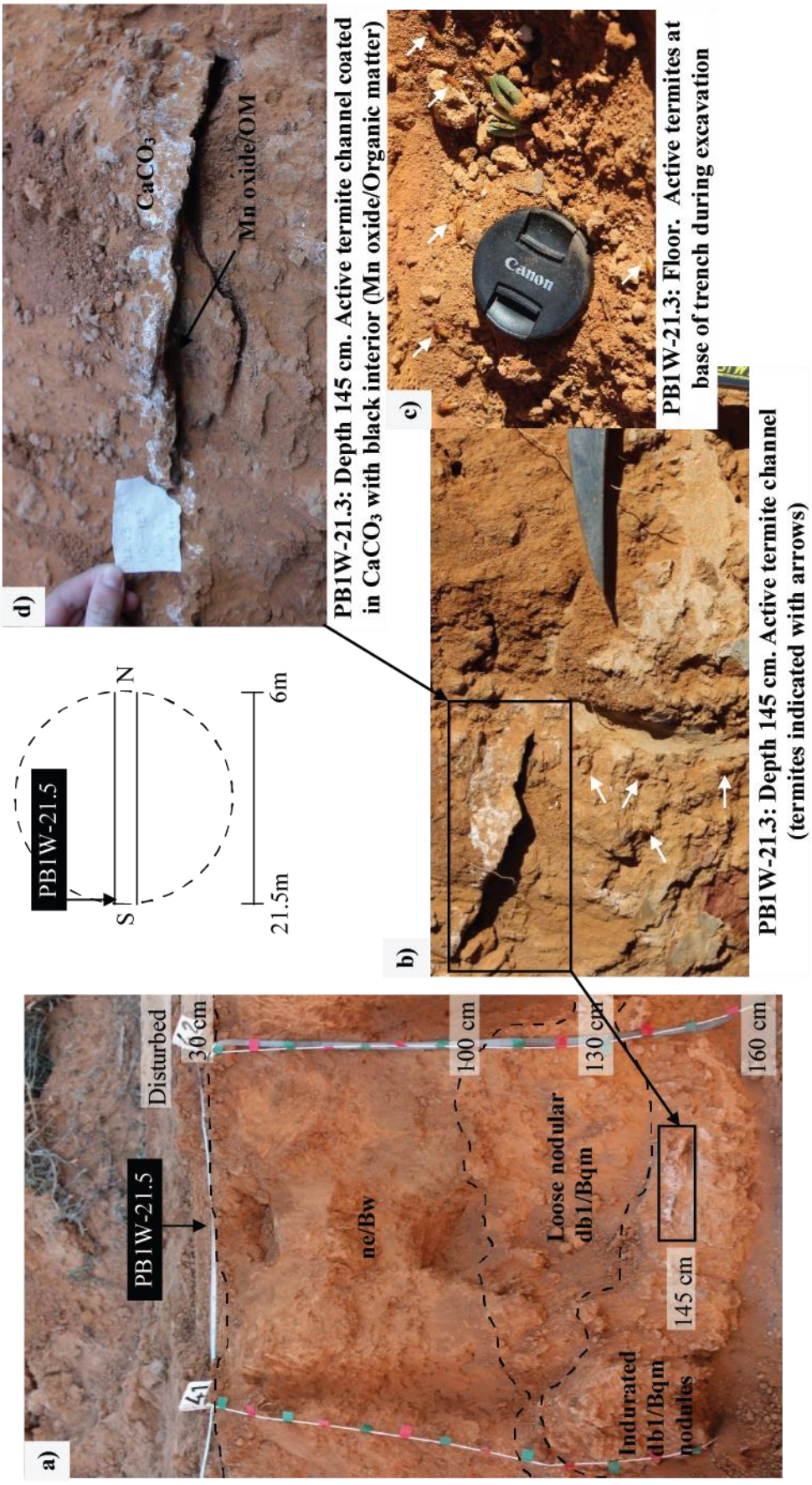

Figure 3.12: Feature description of the large carbonate coated, active termite channel at profile PB1W-21.5 within the indurated dorbank/Si cemented nodules at a depth of 145 cm. a) Shows the position of the large termite channel within the profile at PB1W-21.5 (the top 30 cm of the profile was removed during excavation); b) Active termites observed leaving the large channel indicated with arrows; c) Active termites observed at the floor of the trench at profile PB1W-21.5; d) A closeup of the large termite channel showing visible carbonate coatings around the channel and the black Mn-oxide/organic matter channel interior. Ne/Bw= neocutanic/weathered B-horizon showing signs of colour development; db1/Bqm = moderate silica cementation.

3.2.2 Klawer heuweltjie (K1)

The inter-heuweltjie soils in Klawer were unconsolidated and showed some signs of soil formation or weathering (ne/Bw). Heuweltjie topsoils were mainly unconsolidated calcareous material with signs of soil formation and secondary carbonate accumulation (nc/Bk). Inter-heuweltjie subsoils consisted of highly indurated, poorly fractured platy dorbank/Si cemented horizon (db/Bqm) overlying unconsolidated, moderately indurated material with many lime nodules (nc/Bkqm). As a result of the highly indurated, poorly fractured platy dorbank the excavator could not dig the inter-heuweltjie soils as deep as the heuweltjie soils. Heuweltjie subsoils consisted of various forms of calcareous dorbank/Si cemented (calcareous Db/Bkqm) horizons with varying degrees of cementation. The calcareous dorbank horizons include (as depth increases); loose gravelly dorbank, vesicular indurated dorbank with many biocasts and pedotubules, highly indurated, fractured platy dorbank, and unconsolidated, moderately Si-indurated material with many lime nodules (granular dorbank). The parent material of the Klawer heuweltjie was established to be aeolian sands overlying in-situ weathering granite.

Figure 3.13 shows the detailed sketch of the south-east wall of the K1 heuweltjie trench with a vertical exaggeration of four but depths are indicated without exaggeration. Heuweltjie soils containing various forms of dorbank/Si-cementation started between K1-6 and K1-7 and extended until between K1-26 and K1-27. Modal profiles are indicated with arrows on the sketch (Figure 3.13).

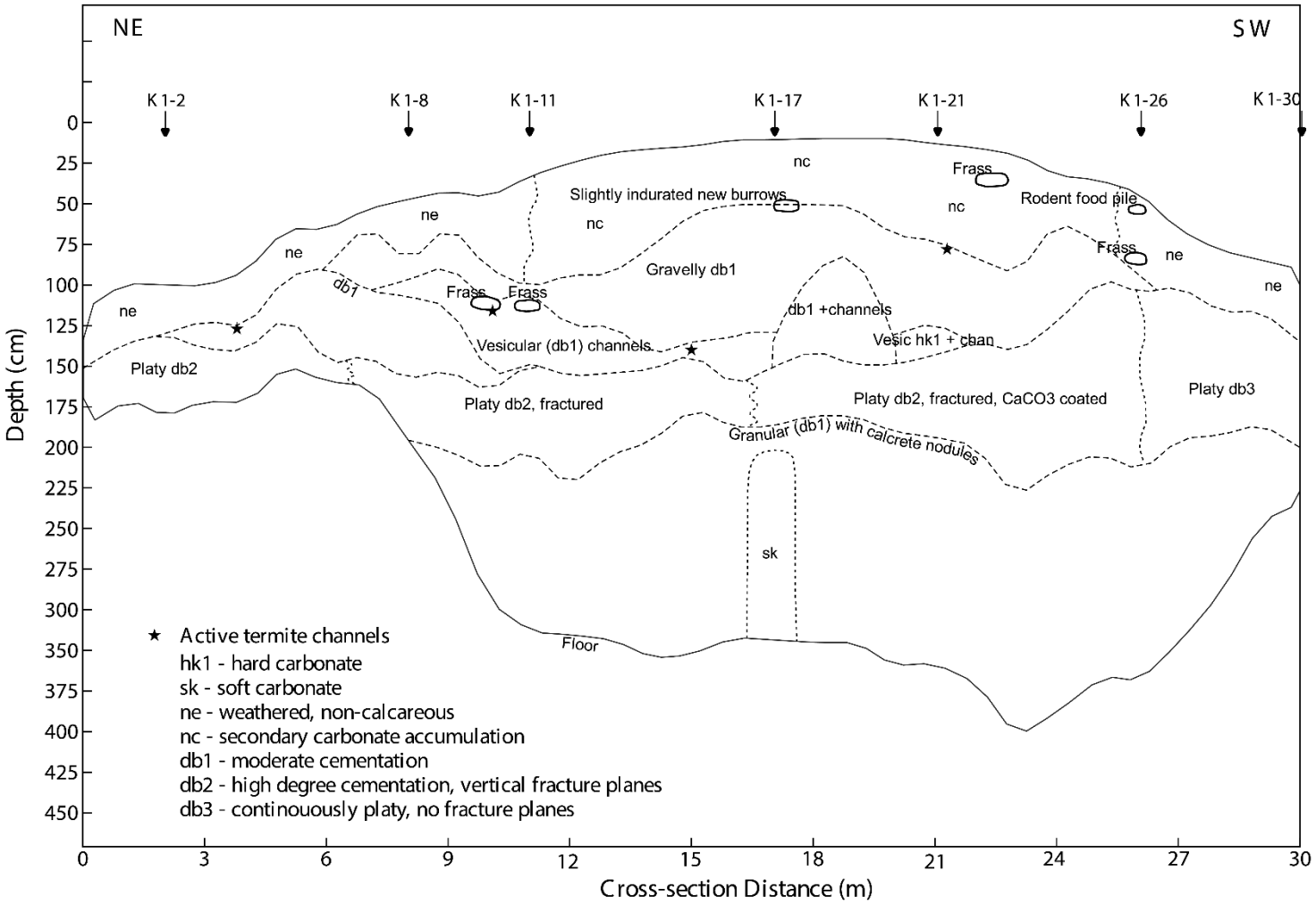

*Figure 3.13: A detailed sketch (in a north-east to south-west direction) of the south-east wall of the trench dug through the mound and inter-mound soils of the heuweltjie in Klawer (K1). The sketch has a vertical exaggeration of x4. Modal profiles are indicated with arrows. Db(Bqm)= silica cementation or induration; sk(Bk)= secondary carbonate accumulation; hk(Bkqm)= silica and carbonate cementation; ne(Bw)= neocutanic/ weathered soils showing signs of colour development;, *= active termites; frass= termite excrement.*

Figure 3.14 shows an example of an inter-heuweltjie profile of K1. Inter-heuweltjie soils of K1 had orthic A-horizons with an apedal structures, loose consistencies, yellowish red colours, and sandy textures (5 to 10% clay). Gradual or clear transitions occurred to neocutanic B-horizons, with slightly harder consistencies, brown or yellowish red colours, and loamy sand textures (10 to 13% clay). Neocutanic horizons abruptly transitioned to hard, reddish brown, continuous, Si cemented, platy dorbank that had no fracture planes and was massive. The platy dorbank contained many distinct coarse black, brown, and white Mn oxide and Si mottles and nodules. Platy dorbank transitioned to calcareous dorbank that was hard, Si cemented, and either strong granular, or weak platy, with reddish yellow colours. The calcareous dorbank also contained lime nodules and was the only horizon in inter-heuweltjie soils to contain carbonates. These horizons were also poorly fractured with many Mn oxide and Si mottles.

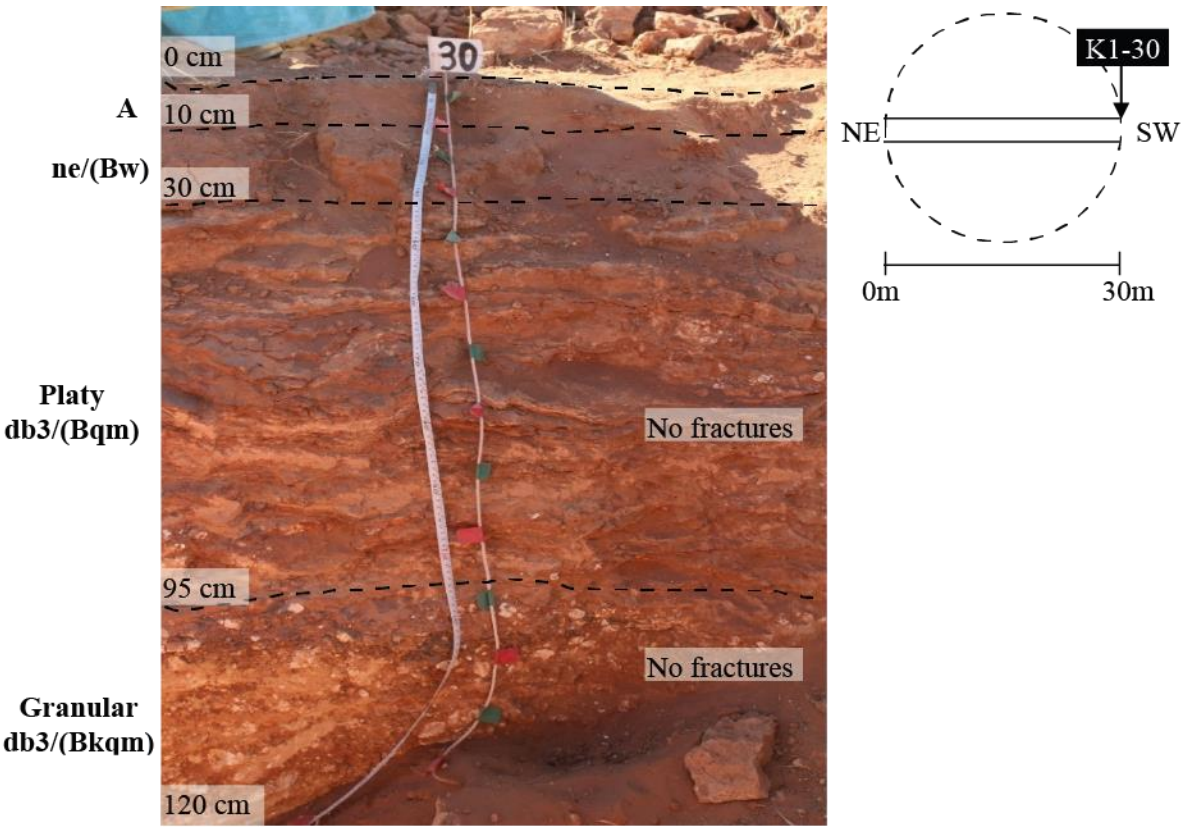

Figure 3.14: Detailed image of the inter-heuweltjie modal profile at K1-30. Ne/Bw= neocutanic /weathered B-horizon showing signs of colour development; db3/Bqm= highly indurated, Si-cementation (platy), no fractures; db3/Bkqm= carbonate and Si cementation (granular), no fractures.

Figure 3.15b shows an enlargement of the Si and Mn oxide nodules and mottles present in the poorly fractured dorbank of the transition profile (Figure 3.15a) at 8 m cross-section distance. The Si and Mn oxide nodules and mottles occurred throughout the platy and granular dorbank that extended across the heuweltjie and inter-heuweltjie soils. The Si nodules showed the presence of sepiolite during field observations (positive methyl orange test, (Mifsud et al., 1979)). Profiles K1-8 and K1-26 were regarded as transition profiles as they displayed soil morphologies with both, heuweltjie (few biocasts and pedotubules in the neocutanic horizons), and inter-heuweltjie (poorly fractured dorbank and absence of carbonates in most horizons) soil characteristics (see Figure 3.15 and Figure 3.20).

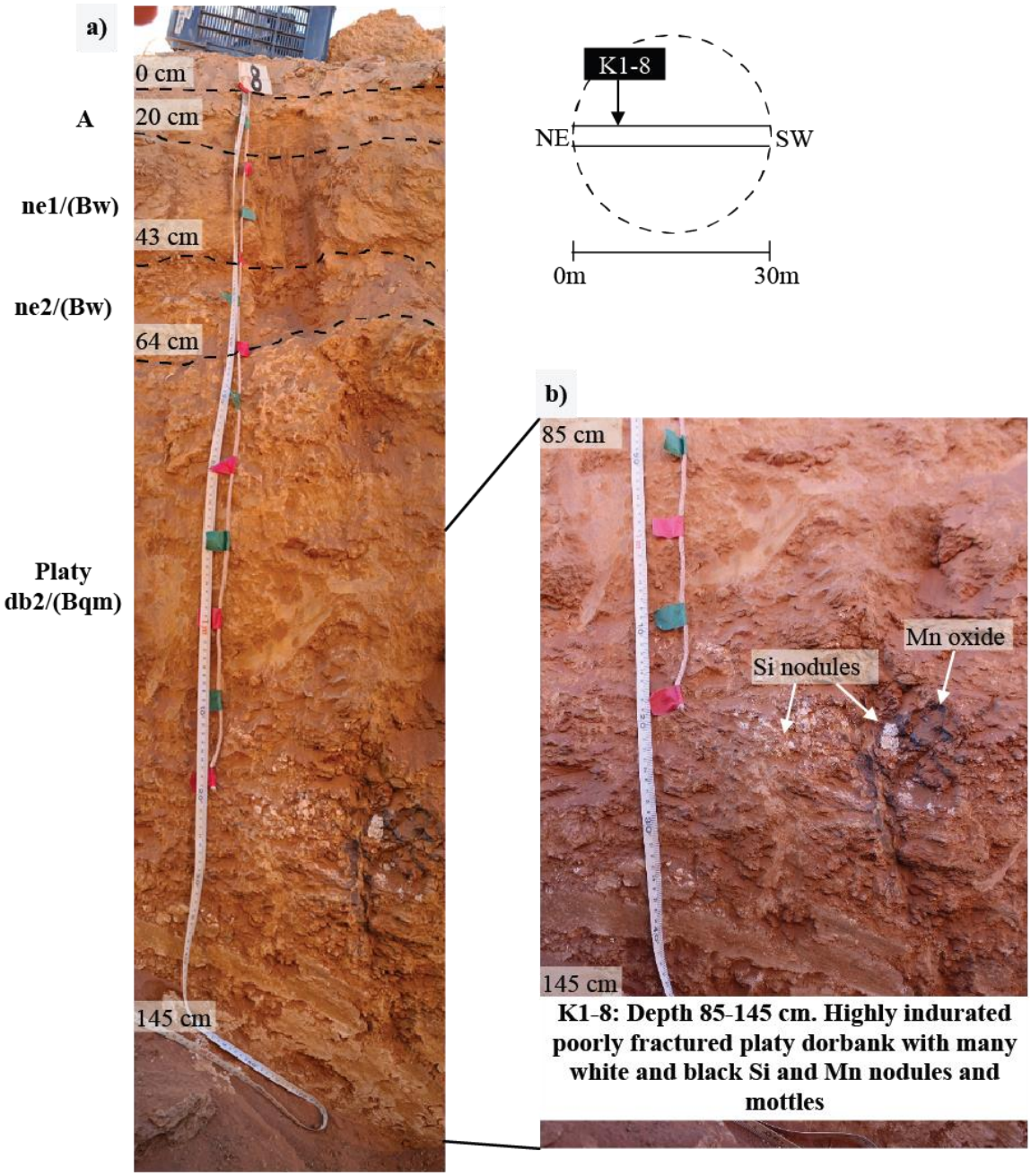

Figure 3.15: Detailed image of heuweltjie modal profile at K1-8. a) The entire profile at K1-8; b) Close-up of the highly indurated, poorly fractured, platy dorbank/Si cemented horizon containing many Si and Mn oxide nodules, mottles and cutans. Ne/Bw= neocutanic /weathered B-horizon showing signs of colour development; db2/Bqm= highly indurated, Si-cementation.

Figure 3.16 to Figure 3.19 that follow in the rest of this section represent the heuweltjie soils of K1. Heuweltjie soils had orthic A-horizons with a loose consistency, massive apedal structure, reddish yellow or yellowish red colour, and fine loamy sand textures (13% clay). A-horizons gradually transitioned to neocarbonate B-horizons with reddish yellow and pink colours, massive apedal structures, loamy sand or sandy loam textures (12-15% clay), and few coarse pedotubules or biocasts. Gradual to abrupt transitions occurred to discontinuous, hard, Si and carbonate cemented vesicular dorbank. Vesicular dorbank had reddish yellow colours with many coarse pedotubules and biocasts, and abundant active, and old indurated termite channels. Platy dorbank followed below vesicular horizons and was notably more fractured compared to inter-heuweltjie dorbank. This was particularly evident between K1-17 and K1-21 in the centre of the heuweltjie (seen in Figure 3.18 and Figure 3.19). The platy dorbank was continuous, moderately cemented, with red to reddish yellow colours, and many Mn and Si mottles. Gradual transitions occurred from platy to weakly granular dorbank with many, green calcite nodules, and Mn oxide mottles in the slightly indurated, clayey, soil matrix. The granular dorbank was continuous with yellowish red colours and many coarse gravel fragments, mainly consisting of calcite nodules. Carbonate accumulation was evident throughout almost all horizons in heuweltjie profiles.

Figure 3.16 shows an example of the heuweltjie profile at K1-10 containing a few biogenic features. A termite frass chamber was observed between 60-75 cm in the vesicular indurated dorbank (Figure 3.16b). Below the frass chamber a slightly indurated, active termite channel was removed at 75 cm (Figure 3.16c). The K-10 profile marked the start of the granular structured dorbank horizon with many calcite nodules (Figure 3.16a). The calcite nodules were highly indurated due to Si and carbonate cementation (Figure 3.16c) and coatings reactedwith methyl orange indicating the presence of sepiolite.

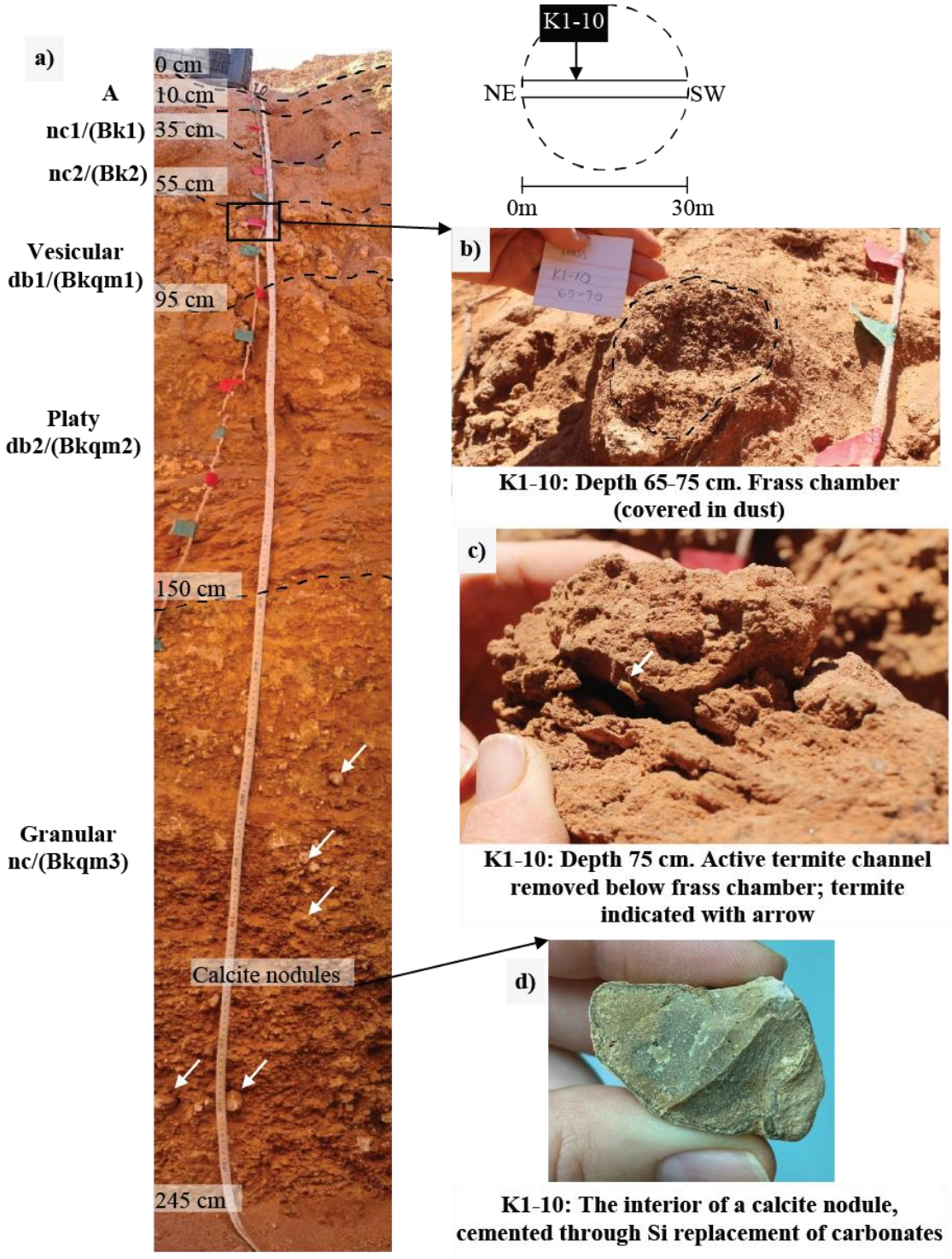

Figure 3.16: Detailed image of features at profile K1-10. a) The location of the features within profile K1-10; b) A frass chamber covered in dust at 60-70 cm depth; c) An active termite channel removed below the frass chamber at 75 cm depth; d) A close-up of the calcite nodules found in the nc/Bkqm3 horizon of the profile. Ne/Bw= neocutanic /weathered B-horizon showing signs of colour development; db/Bqm= Si cementation; calcareous db/Bkqm= carbonate and Si cementation (platy or vesicular); nc/Bkqm= neocarbonate B-horizon/unconsolidated material with secondary carbonate accumulation and slight nodular pan Si cementation.

Figure 3.17a shows the profile of K1-11 containing a large horizon of discontinuous, vesicular indurated dorbank. An enlarged image of the vesicular horizon is shown in Figure 3.17b, indicating many pedotubules and biocasts with abundant medium and small channels.

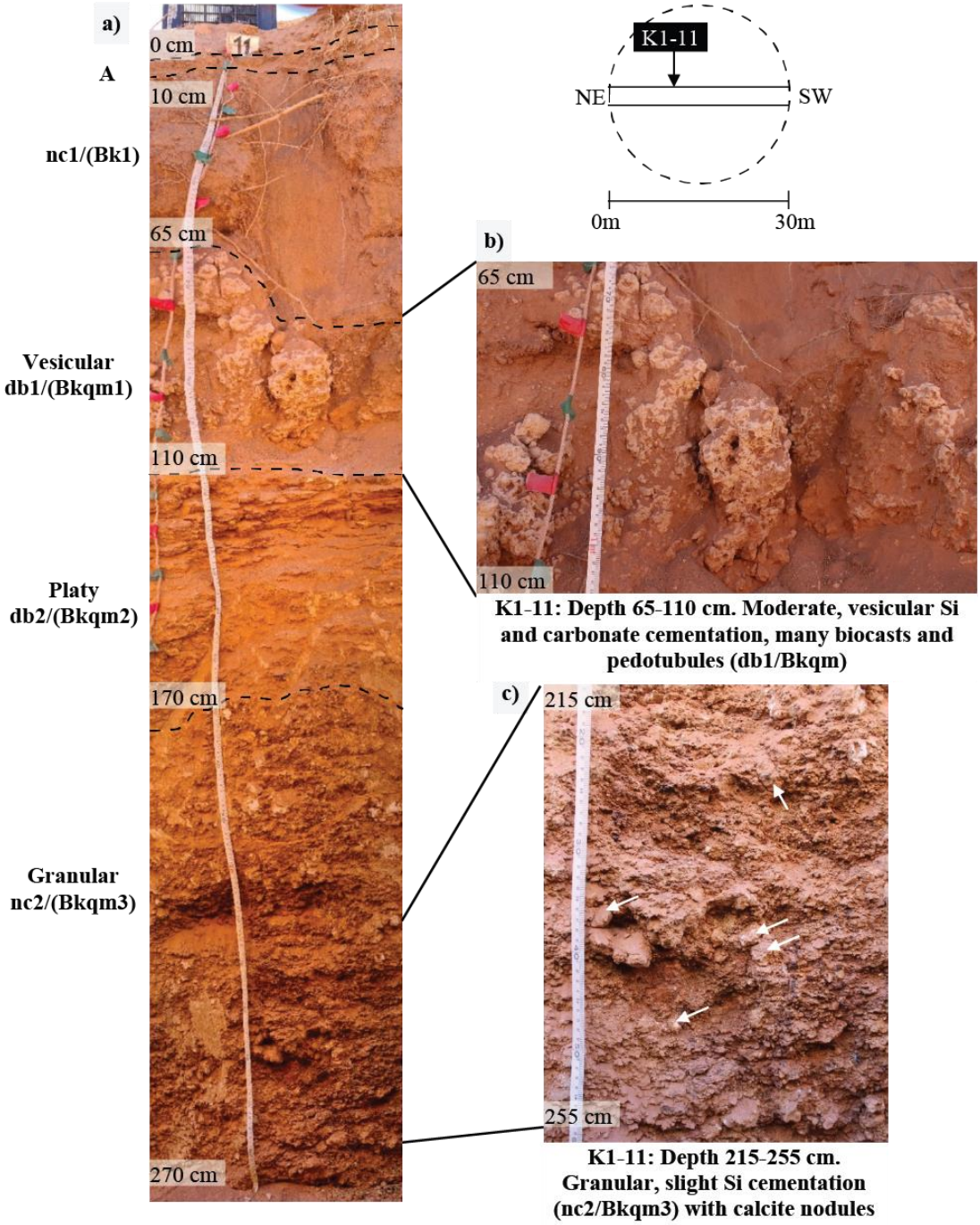

Figure 3.17: Detailed image of heuweltjie modal profile at K1-11. a) Profile at K1-11; b) Moderate, vesicular Si and carbonate cementation between 65-110 cm with many biocasts and pedotubules; c) A close-up of the unconsolidated, weak granular, slight nodular Si cemented horizon with many calcite nodules. Nc/Bk= neocarbonate /carbonate accumulated horizon; calcareous db/Bkqm= carbonate and Si cementation (platy or vesicular); nc/Bkqm= neocarbonate B-horizon/unconsolidated material with secondary carbonate accumulation and slight nodular pan Si cementation.

Profile K1-17 represented the morphology of K1 in the centre of the mound (Figure 3.18) At depths of 40 cm and 100 cm in profile K1-17 new, slightly indurated, termite channels were observed in the neocarbonate and vesicular dorbank horizons (Figure 3.18a and d). The vesicular horizon comprised of abundant loose and fragmented biocasts, and pedotubules wich was not as cemented compared to the corresponding horizon in K1-11(Figure 3.17). Figure 3.18a and b show the highly fractured platy dorbank observed in the centre of K1. Many fracture planes were visible and platy dorbank had a looser consistency compared dorbank on the heuweltjie edges and inter-heuweltjie soils. Platy dorbank also seemed to be slanted in a downward angle in the centre of the mound compared to inter-mound platy dorbank. The granular dorbank and some parts of the platy dorbank in K1-17 contained white powdery carbonates dominating the soil matrix (Figure 3.18a and c).

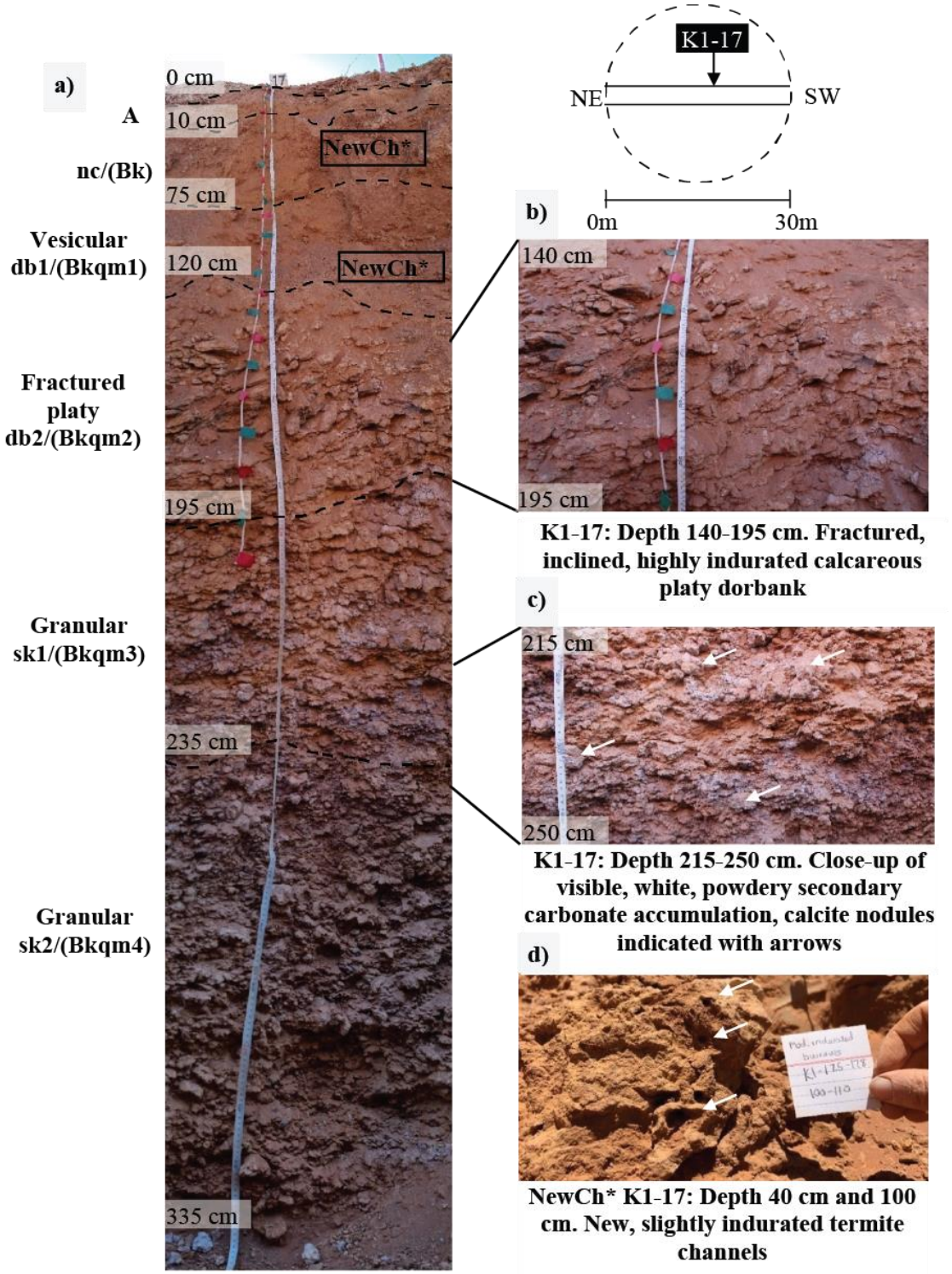

Figure 3.18: Detailed image of heuweltjie modal profile at K1-17. a) The full profile at K1-17; b) Fractured, inclined, highly indurated, platy, calcareous db2/Bkqm2 horizon; c) An image showing a close-up of the visible, white powdery secondary carbonate accumulated horizon with many calcite nodules; d) New, slightly indurated termite channels at 40 cm and 100 cm depths. Nc/Bk= neocarbonate /carbonate accumulated horizon; calcareous db/Bkqm= carbonate and Si cementation (platy or vesicular); sk/Bkqm= soft carbonate B-horizon/unconsolidated material with visible, white powdery, secondary carbonate accumulation and slight nodular pan Si cementation.

At K1-21 the profile again contained highly fractured platy dorbank, however, powdery white carbonates, although present, were not visible to the unaided eye in this profile (Figure 3.19a). K1-21 contained a vesicular dorbank horizon as in K1-11, cemented by Si and carbonates, that had a very hard consistency and many indurated channels (Figure 3.19c). Also present in K1-21 in the neocarbonate horizon were slightly indurated, active termite channels, presumably extending from the vesicular dorbank horizon (Figure 3.19b).

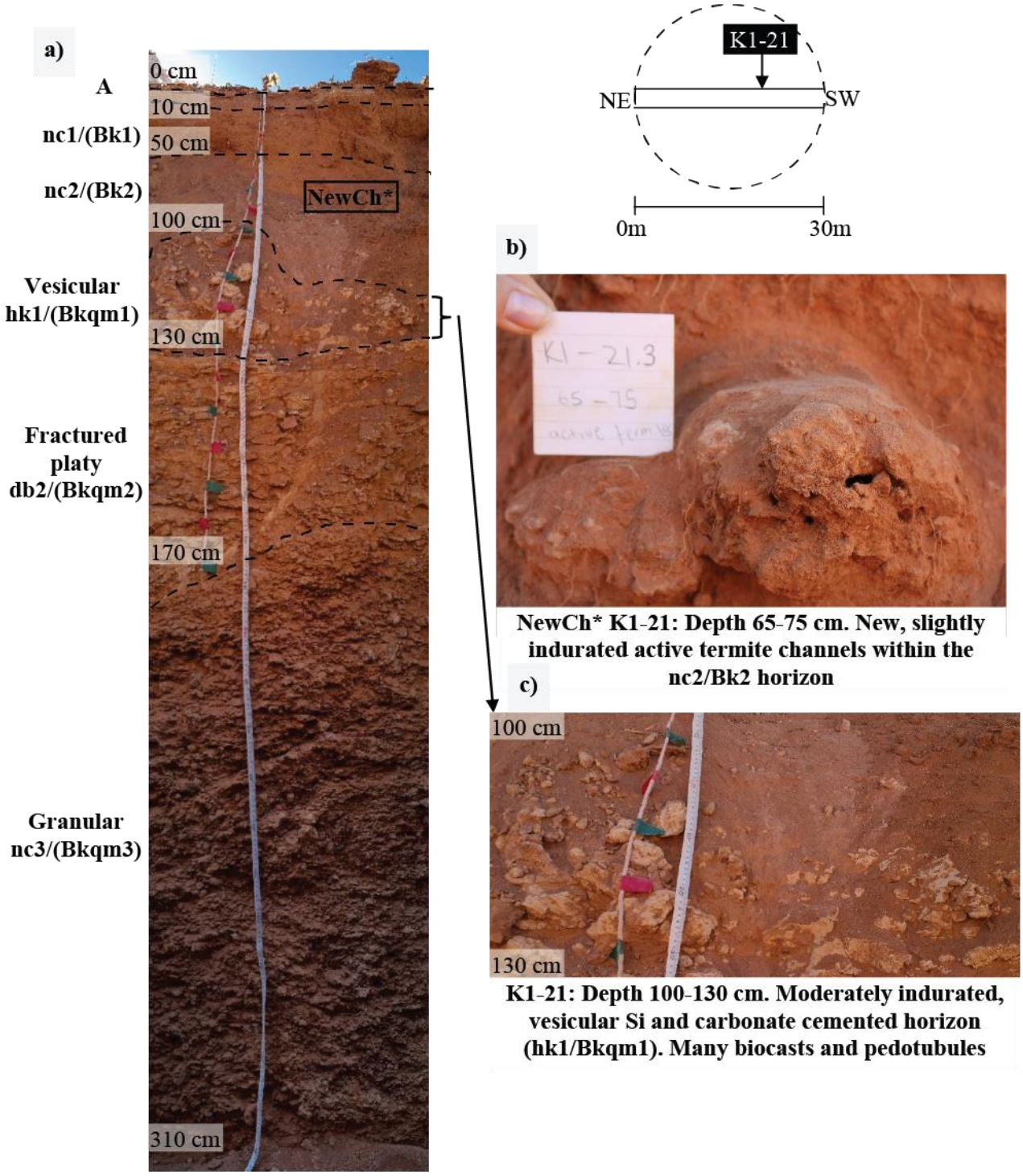

Figure 3.19: Detailed image of heuweltjie modal profile at K1-21. a) The full profile at K1-21; b) New, slightly indurated active termite channels between 65-75 cm depth.; c) Enlarged image of the vesicular, moderately indurated hard carbonate/Si and carbonate cemented horizon with many biocasts and pedotubules. Nc/Bk= neocarbonate /carbonate accumulated horizon; hk/Bkqm= hard carbonate/carbonate and Si cemented horizon (vesicular); calcareous db/Bkqm= carbonate and Si cementation (platy); nc/Bkqm= neocarbonate B-horizon/unconsolidated material with secondary carbonate accumulation and slight nodular pan Si cementation.

The profile at K1-26 shows a transition profile between heuweltjie and inter-heuweltjie soils (Figure 3.20a). Carbonates were only present in the granular dorbank/neocarbonate horizon and both fractured and poorly fractured dorbank was present (Figure 3.20c). A termite frass chamber and rodent food pile was observed at 25 cm within the neocutanic horizon of the K1-26 profile, indicated in Figure 3.20b. A rodent was also observed at the bottom of the K1-26 profile during excavation.

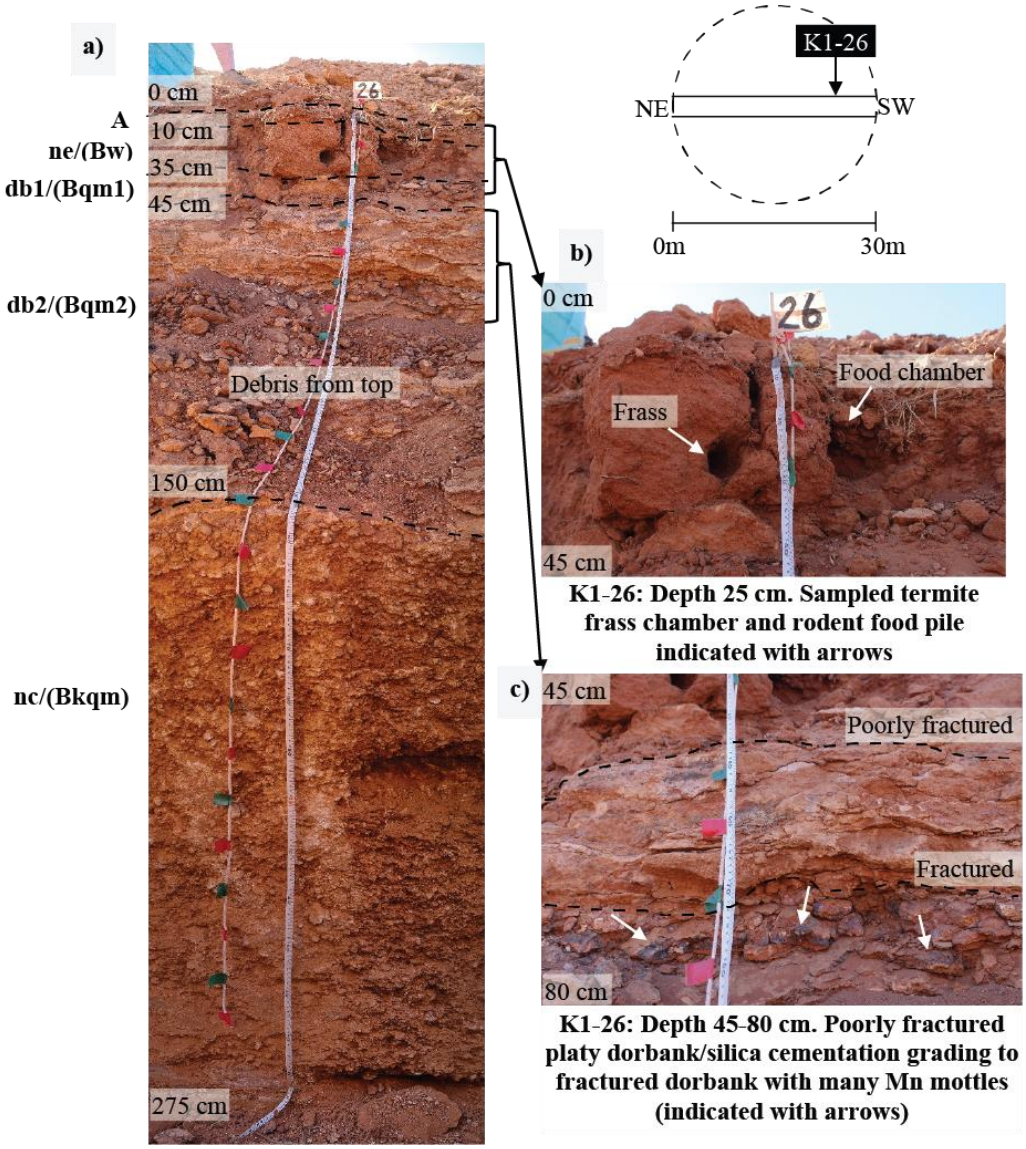

Figure 3.20: a) Detailed image of the heuweltjie/ inter-heuweltjie transition modal profile at K1-26. A rodent was found at the bottom of the profile during excavation; b) Enlargement of the top 0-45 cm to indicate a sampled termite frass chamber and rodent food pile at 25 cm; c) Close-up of the highly indurated, poorly fractured (grading to fractured) platy dorbank/Si cemented horizon containing many Mn mottles. Ne/Bw= neocutanic /weathered B-horizon showing signs of colour development; db2/Bqm= highly indurated, Si-cementation; nc/Bkqm= neocarbonate B-horizon/unconsolidated material with secondary carbonate accumulation and slight nodular pan Si cementation.

3.3 Soil texture

Soil particle and texture analysis of modal profiles in Piketberg and Klawer is shown in this section. Raw soil texture data is added in Table 9.1, Table 9.2 and Table 9.3 of Appendix C.

3.3.1 Piketberg heuweltjie (PB1)

Most of the modal profile soils in PB1 were either sandy loams or loamy sands (Figure 3.21 and Figure 3.22;). Samples consisting mainly of dorbank had coarse sandy textures. At profiles PB1E-13, PB1E-19, PB1W-12, and PB1W-15 heuweltjie soils transitioned from sandy loams to either loamy sands or sands as clay percentage decreased with depth. Heuweltjie topsoil had a finer texture and/or finer sand grade in comparison to most inter-heuweltjie topsoil (Figure 3.21 and Figure 3.22). Heuweltjie soils up to 80 cm depth had significantly lower average sand and higher average silt and clay percentages than heuweltjie subsoils and inter-heuweltjie soils up to 80 cm (Figure 3.23). However, heuweltjie soils below 80 cm depth (mostly consisting of gravelly dorbank) had significantly higher average sand and lower average silt and clay percentages than the heuweltjie topsoil and inter-heuweltjie soils (Figure 3.23). Consequently, the texture of heuweltjie soils become coarser as the transition to dorbank occurs (Figure 3.21 and Figure 3.22). In contrast, an increase in clay percentage with depth occurs in the inter-heuweltjie profiles as soil textures transitioned from loamy sands to sandy loams or sandy clay loams in profiles PB1E-4, PB1E-35, and PB1W-6 (Figure 3.21 and Figure 3.22).

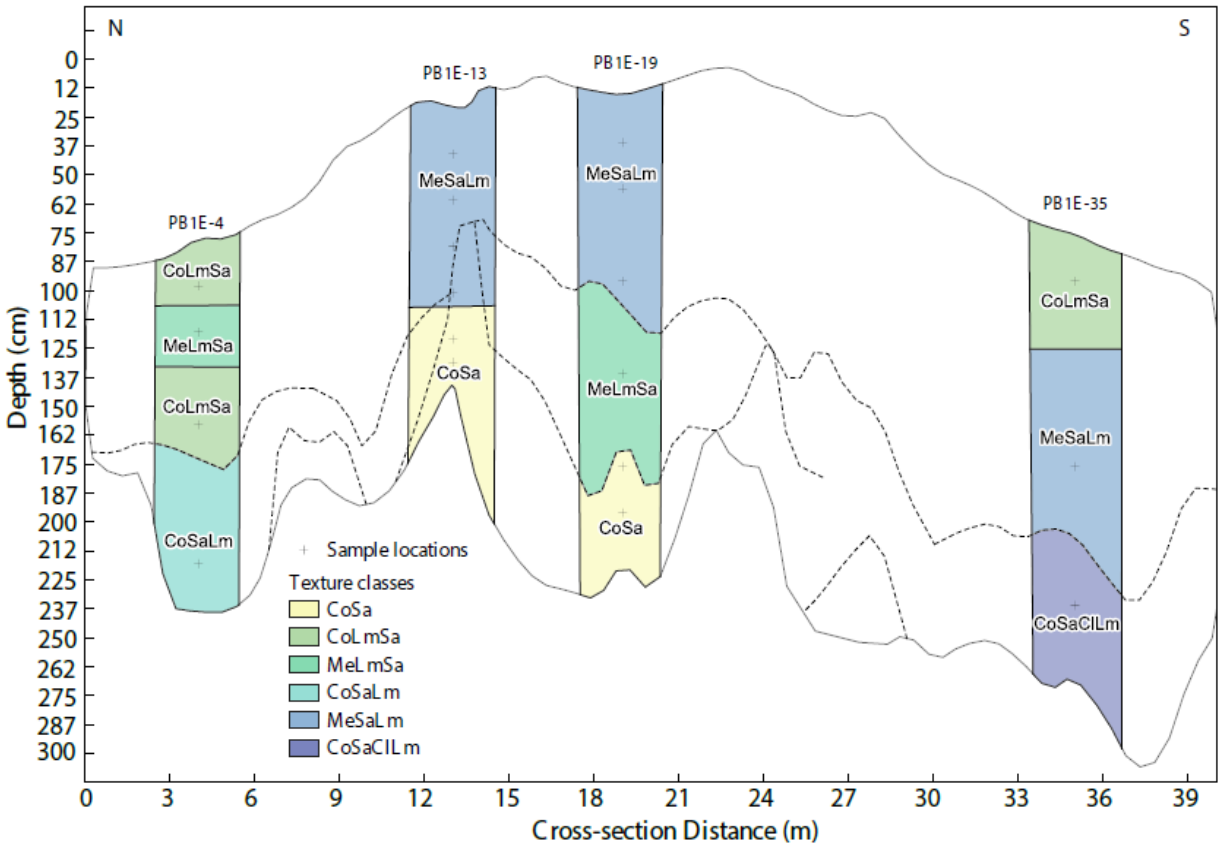

Figure 3.21: PB1E soil texture as shown on the heuweltjie cross-section. Heuweltjie depths are at a x8 exaggeration. Colours indicate a difference in sand grade. Co= coarse; Me= medium; Lm= loam; Sa= sand; Cl= clay.

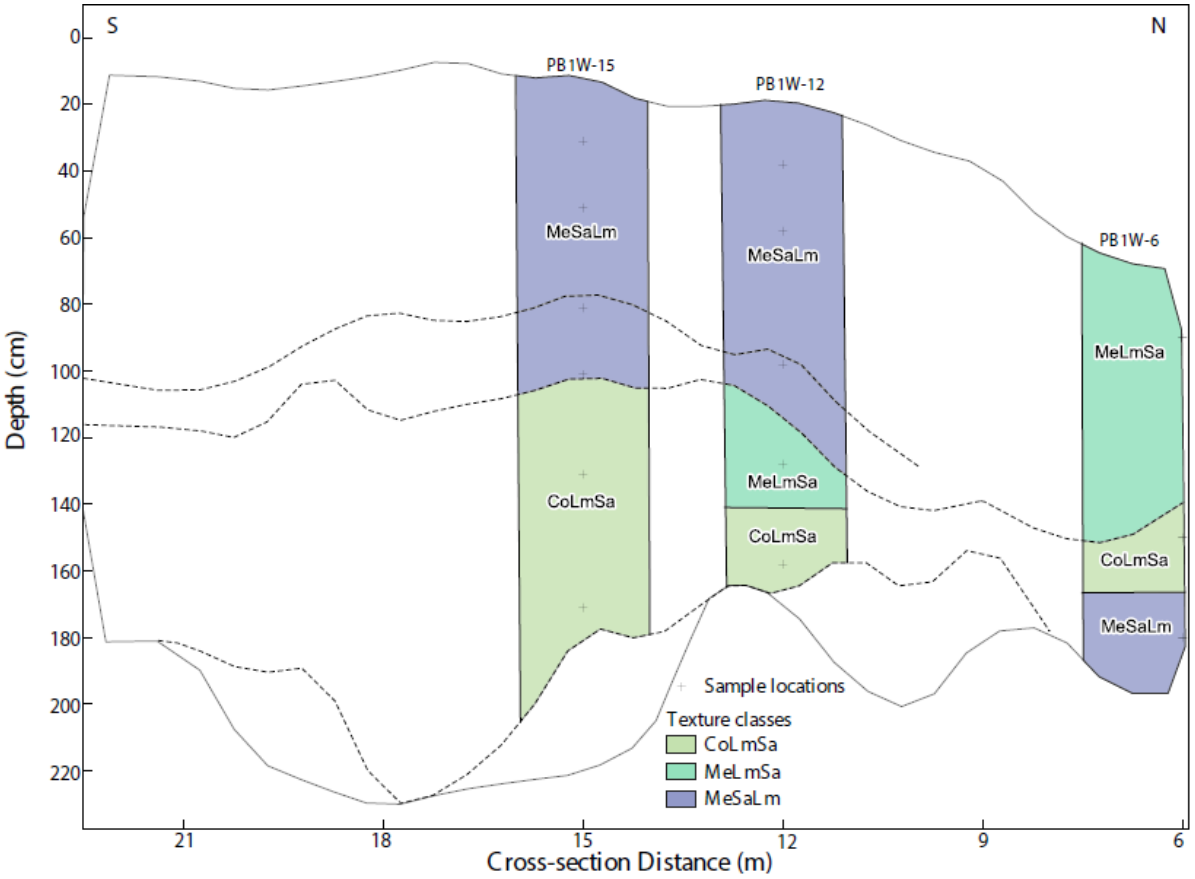

Figure 3.22: PB1W soil texture as shown on the heuweltjie cross-section. Heuweltjie depths are at a x5 exaggeration. Colours indicate a difference in sand grade. Co= coarse; Me= medium; Lm= loam; Sa= sand.

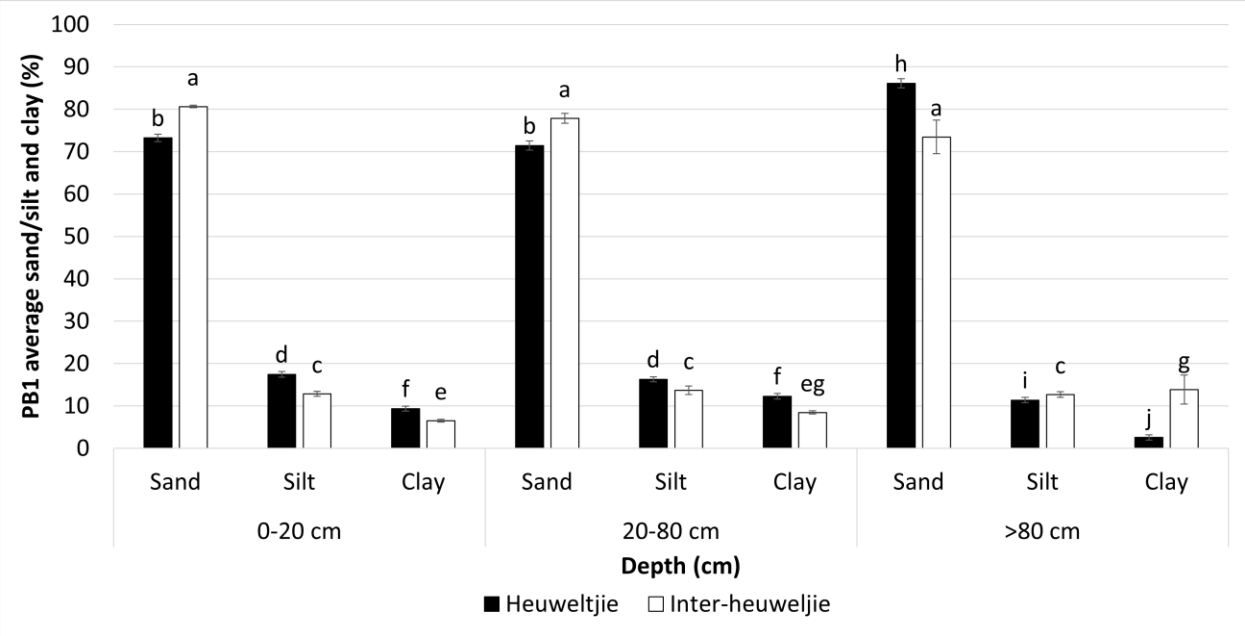

Figure 3.23: Average sand, silt and clay percentages of 0-20 cm, 20-80 cm and >80 cm of heuweltjie and inter-heuweltjie soils of PB1.

3.3.2 Klawer heuweltjie (K1)

As in Piketberg most of the modal profile soils in K1 were either sandy loams or loamy sands (Figure 3.24). Again, samples consisting mainly of dorbank had coarse sandy textures. All profiles of K1 showed a decrease in clay percentage with depth as soils transitioned to vesicular and/or platy dorbank (Figure 3.24). This contrasts with the opposing clay trends of mound and inter-mound soils observed in PB1. Furthermore, where samples were analysed in the granular dorbank sediments of K1, clay content tended to increase again (Figure 3.24). Heuweltjie soils (between K1-8 to K1-26) transitioned from fine sandy loams to fine, medium, or coarse loamy sands, or to coarse sands. Further transitions occurred to either coarse sandy loams or coarse sandy clay loams in the granular dorbank. Inter-heuweltjie (K1-2 and K1-30) soils transitioned from medium sandy loams or loamy sands to coarse sands and loamy sands. Heuweltjie topsoil had a finer texture and/or sand grade compared to the inter-heuweltjie topsoil, as seen in Piketberg. The K1 heuweltjie topsoil also had a finer texture and/or sand grade compared to that of the subsoils as sediments became coarser closer to dorbank horizons. Heuweltjie soils between 10-80 cm depth had significantly higher average sand, silt and clay percentages than inter-heuweltjie topsoil between 10-80 cm (Figure 3.25). Average silt percentages of heuwetjie soils up to 80 cm depth was significantly higher compared to heuweltjie soils mostly consisting of dorbank below 80 cm (Figure 3.25).

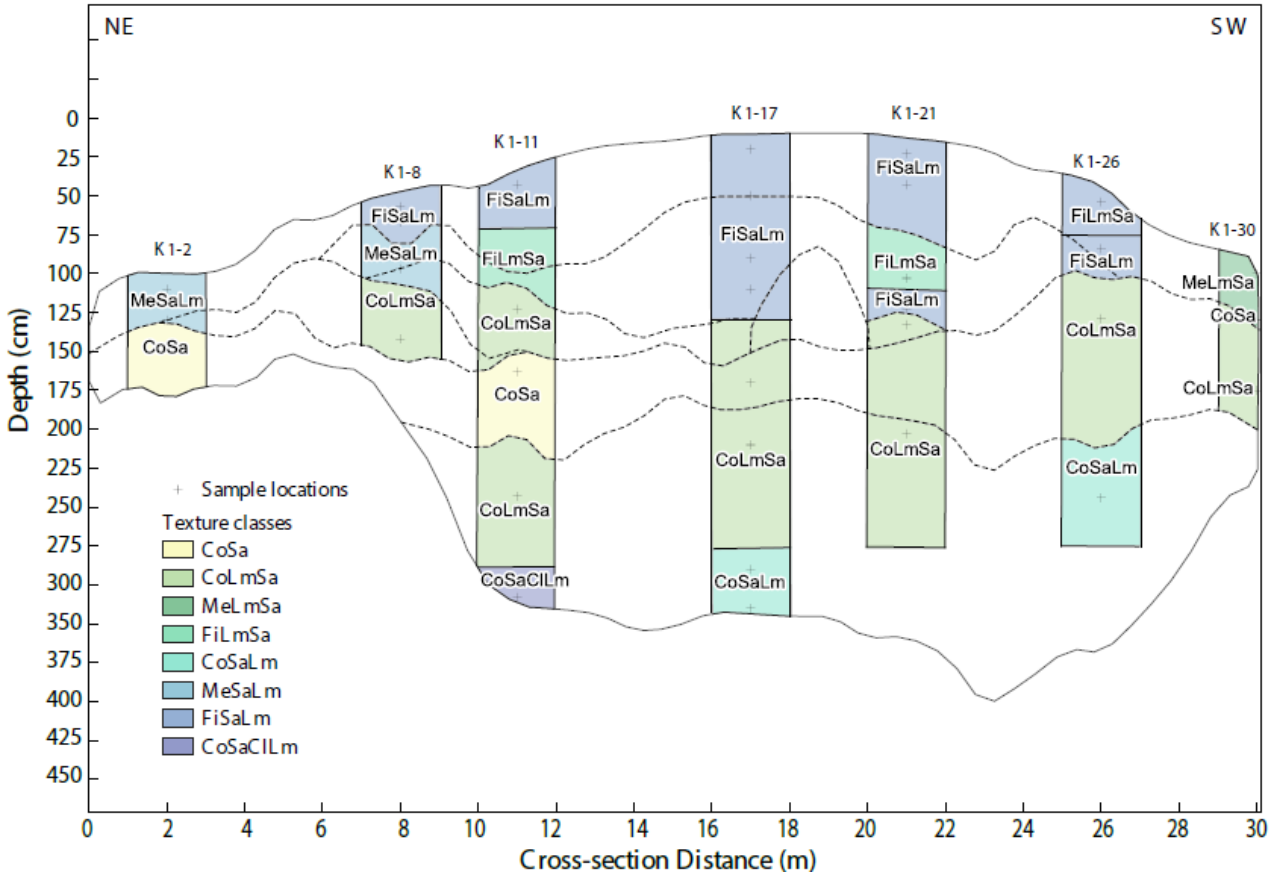

Figure 3.24: K1 soil texture as shown on the heuweltjie cross-section. Heuweltjie depths are at a x4 exaggeration. Colours indicate a difference in sand grade. Co= coarse; Me= medium; Lm= loam; Sa= sand; Cl= clay.

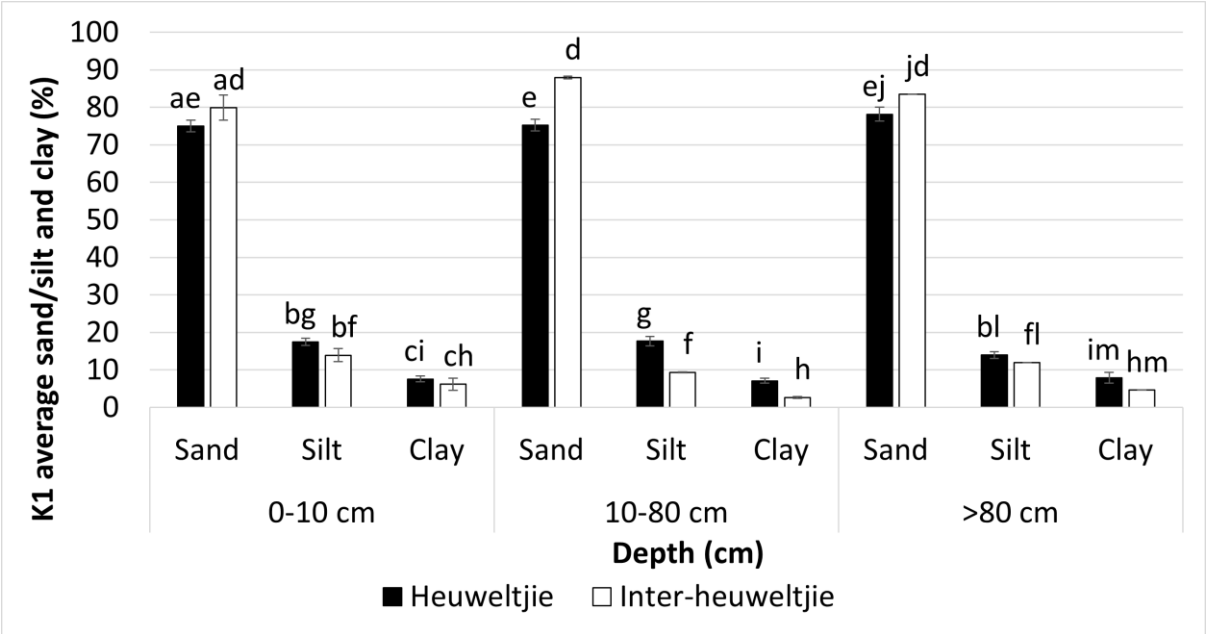

Figure 3.25: Average sand, silt and clay percentages of 0-20 cm, 20-80 cm and >80 cm of heuweltjie and inter-heuweltjie soils of K1.

3.4 Mineralogy

The mineralogy of clay extracts from modal profiles as well as, untreated bulk, and untreated feature samples were determined. X-ray diffraction of all patterns not presented in this section are provided in Appendix B. The mineralogy of samples collected of termites, large termite channels, and termite frass (excrement) are reported as biogenic features in this section.

3.4.1 Piketberg heuweltjie (PB1)

3.4.1.1 Clay mineralogy

3.4.1.1.1 *Inter-heuweltjie and heuweltjie clay mineralogy*

No differences in clay mineralogy were observed within or between inter-heuweltjie (Figure 3.26, Figure 8.9, and Figure 8.10) and heuweltjie (Figure 3.27 and Figure 8.11 to Figure 8.13) modal profile clay extracts of PB1. The predominant clay in Piketberg was kaolinite with an initial peak identified around 0.716 nm (Figure 3.26 and Figure 3.27). Clay sized quartz was also present throughout all clay extracts. The initial peak for quartz was identified around 0.425 nm and a large quartz peak was present at 0.334 nm (Figure 3.26 and Figure 3.27).

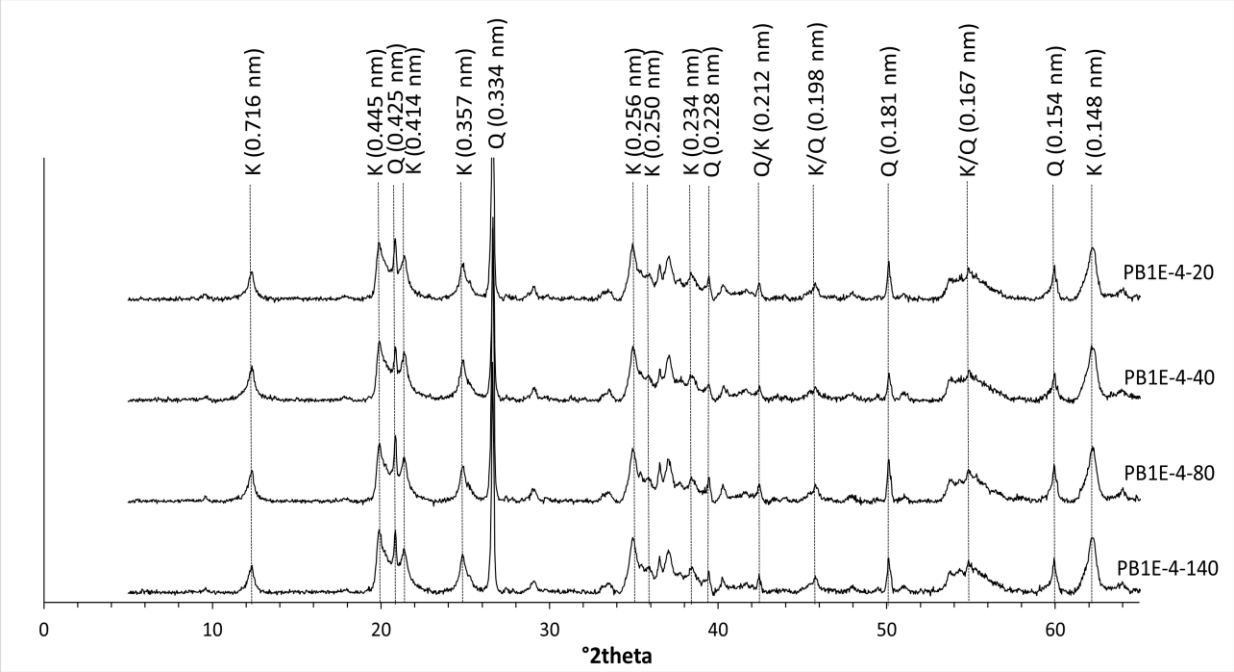

Figure 3.26: XRD pattern indicating peaks labelled with d-spacings (nm) of the $MgCl_2$ treated clay extracts of the inter-heuweltjie soil at profile PB1-4 (K=kaolinite, Q=quartz).

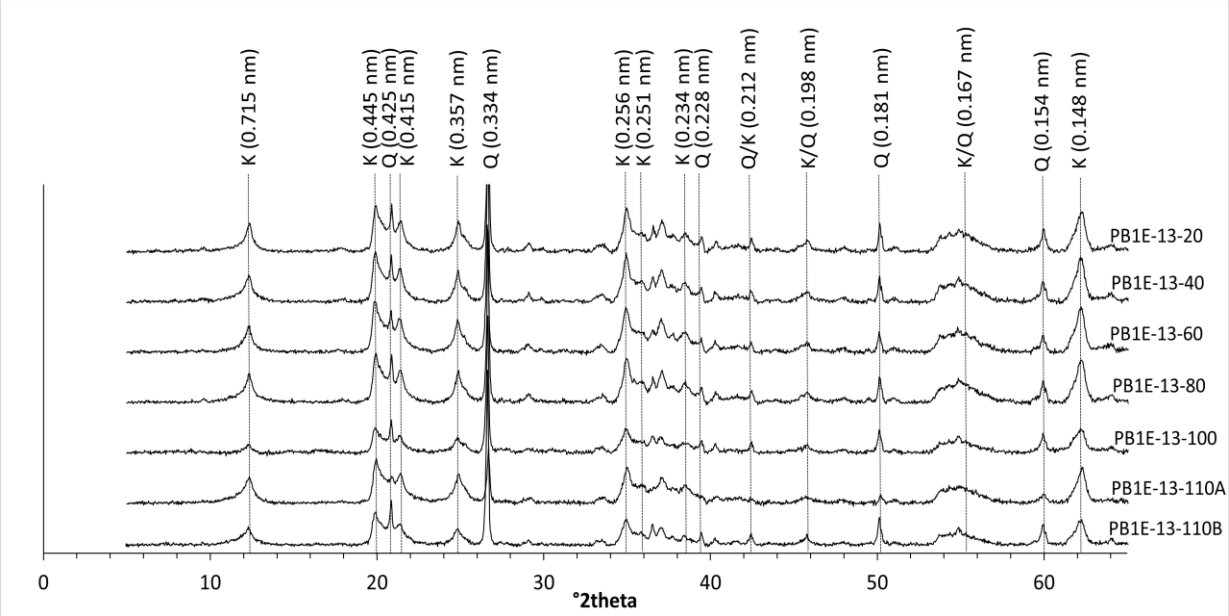

Figure 3.27: XRD pattern indicating peaks labelled with d-spacings (nm) of the $MgCl_2$ treated clay extracts of the heuweltjie soil at profile PB1-13 (K=kaolinite, Q=quartz).

3.4.1.2 Bulk sample mineralogy

Calcite was present in the Piketberg heuweltjie in untreated bulk samples at PB1W-19-100 and PB1W-19-180, from the soft carbonate horizon of the west wall (Figure 3.28). An initial peak for calcite was identified at 0.385 nm and a strong peak was present at 0.304 nm (Figure 3.28). A second carbonate mineral was identified as aragonite in PB1W-16-180 with weak but discernible peaks at 0.327, 0.284, 0.270, and 0.174 nm (Figure 3.28). Kaolinite and quartz were also identified with initial peaks at 0.716 and 0.425 nm respectively.

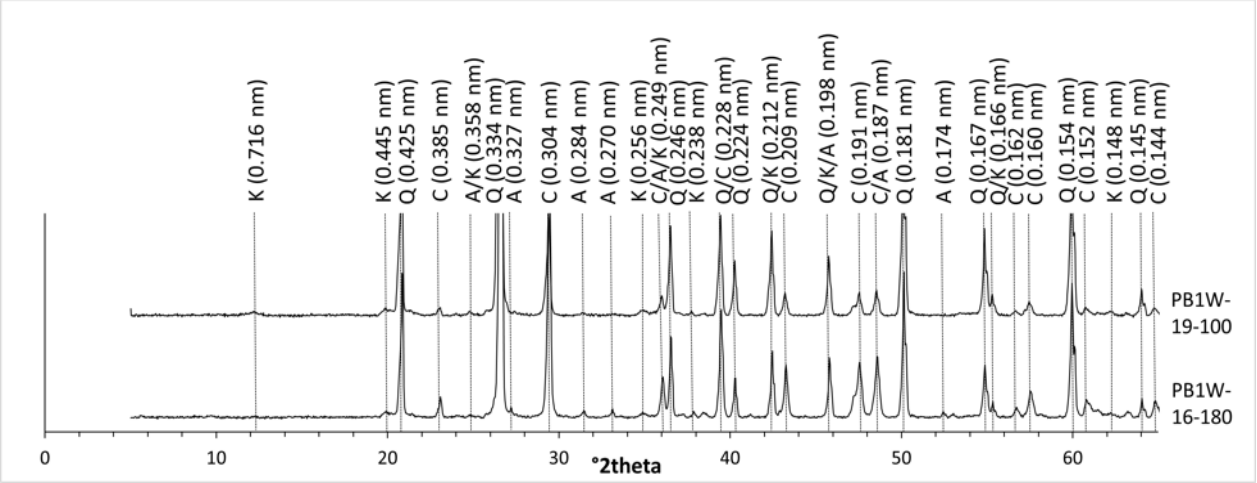

Figure 3.28: XRD pattern indicating peaks labelled with d-spacings (nm) of the untreated bulk samples of the heuweltjie soil sampled at PB1W-19-100 and PB1W-16-180 (K=kaolinite, Q=quartz, C=calcite, A=aragonite).

3.4.1.3 Biogenic feature mineralogy

Calcite was identified in both the large channels sampled at PB1E-14-120 and PB1W-22.5-115 with an initial peak at 0.385 nm (Figure 3.29). A very slight calcite peak was also identified in termites sampled from the trench floor at 22.5 m cross-section distance of the west wall with a weak peak at 0.303 nm (Figure 3.29). The presence of Ca oxalate was observed in termite excrement and frass collected at 21 m cross-section distance on the east wall and 16 m cross-section distance on the west wall of the trench (Figure 3.30). Termite excrement covered with white precipitate or fungal filaments sampled at PB1E-21-90 showed the presence of Ca oxalate as weddellite (dihydrate) with an initial peak at 0.620 nm (Figure 3.30). The fresh frass samples from 180 cm depth and the trench floor at profile PB1W-16 showed the presence of Ca oxalate as whewellite (monohydrate) with an initial peak at 0.593 nm (Figure 3.30). Kaolinite and quartz were also present throughout all biogenic feature samples with initial peaks around 0.714/0.715 nm and 0.425 nm respectively (Figure 3.29 and Figure 3.30).

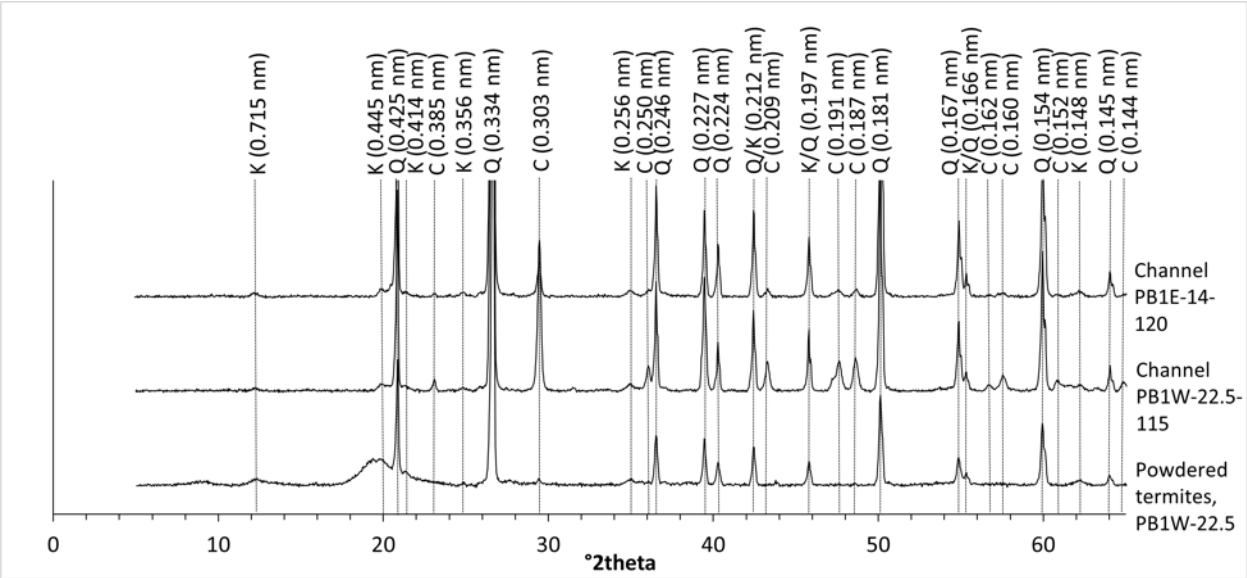

Figure 3.29: XRD pattern indicating peaks labelled with d-spacings (nm) of the untreated channel and termite samples of the Piketberg heuweltjie (K=kaolinite, Q=quartz, C=calcite).

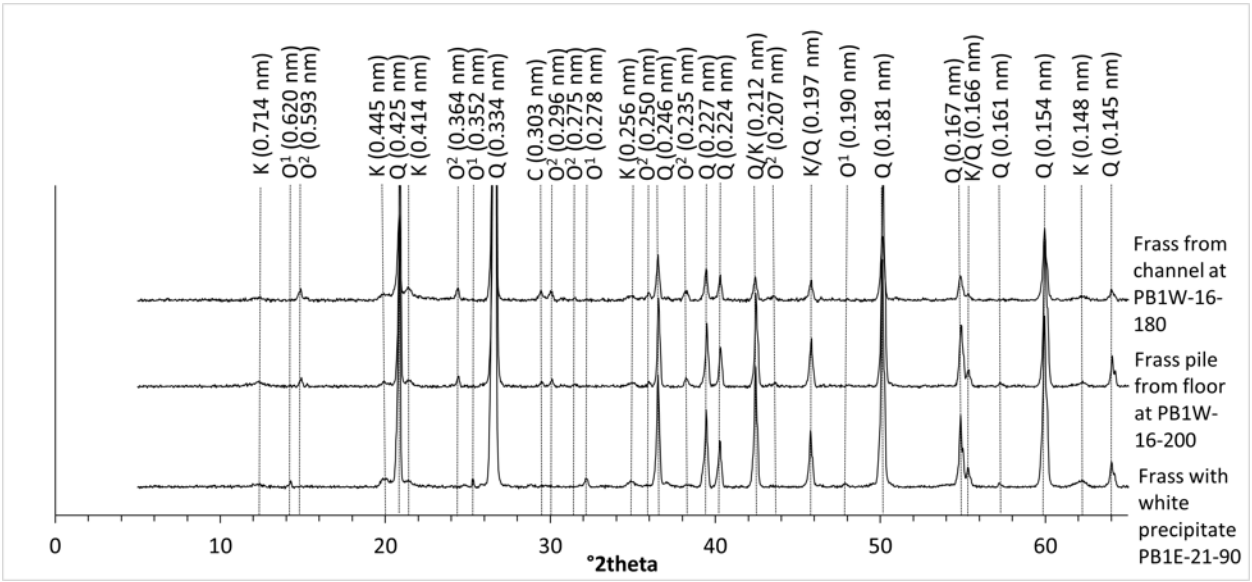

Figure 3.30: XRD pattern indicating peaks labelled with d-spacings (nm) of the untreated termite frass samples of the Piketberg heuweltjie (K=kaolinite, Q=quartz, C=calcite, O^1=Ca oxalate (weddellite), O^2=Ca oxalate (whewellite)).

3.4.2 Klawer heuweltjie (K1)

3.4.2.1 Clay extract mineralogy

3.4.2.1.1 *Inter-heuweltjie clay mineralogy*

Illite was the predominant clay present in all inter-heuweltjie clay extracts analysed from Klawer with an initial peak identified around 0.998/1.012 nm (Figure 3.31 and Figure 8.14). Kaolinite was present in most inter-heuweltjie clay extracts except for K1-30-85 (Figure 8.14). An initial kaolinite peak was present around 0.713/0.717 nm (Figure 3.31). Clay sized quartz was present in all inter-heuweltjie clay extracts with an initial peak around 0.425 nm (Figure 3.31).

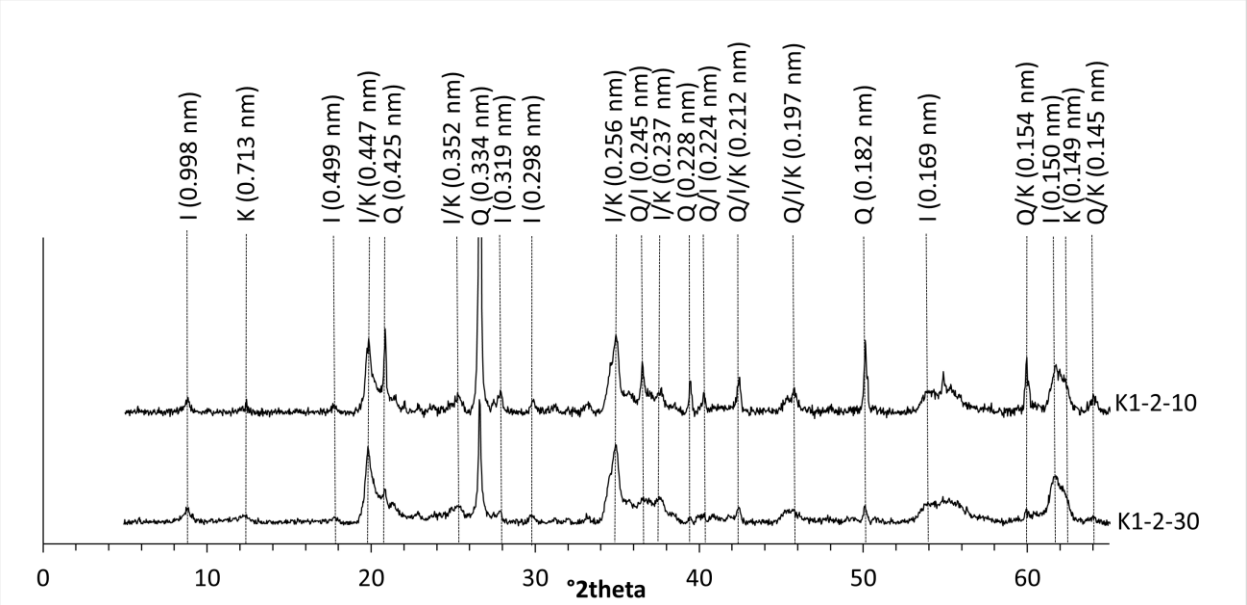

Figure 3.31: XRD pattern indicating peaks labelled with d-spacings (nm) of the $MgCl_2$ treated clay extracts of the inter-heuweltjie soil at profile K1-2 (I=illite, K=kaolinite, Q=quartz).

3.4.2.1.2 *Heuweltjie clay mineralogy*

Illite was identified throughout the heuweltjie K1 with an initial peak around 0.996 nm (Figure 3.32, Figure 3.33, and Figure 8.15 to Figure 8.17). Kaolinite was identified in most heuweltjie clay extracts with an initial peak around 0.716 nm. Kaolinite was absent in K1-11-130 and 275 (Figure 3.32), K1-17-200 and 305 (Figure 3.33), K1-21-190 and 290 (Figure 8.16) and, K1-26-40 to 275 (Figure 8.17). Calcite was present in K1-17-200 (Figure 3.33) and K1-21-120 (Figure 8.16) due to incomplete removal during sample pre-treatment. A weak initial peak for

calcite was identified around 0.383 nm in K1-17-200 and a strong peak around 0.302 nm in K1-17-200 and K1-21-120. Clay sized quartz was present in all heuweltjie clay extracts with an initial peak around 0.425 nm and a strong peak at 0.334 nm (Figure 3.32 and Figure 3.33).

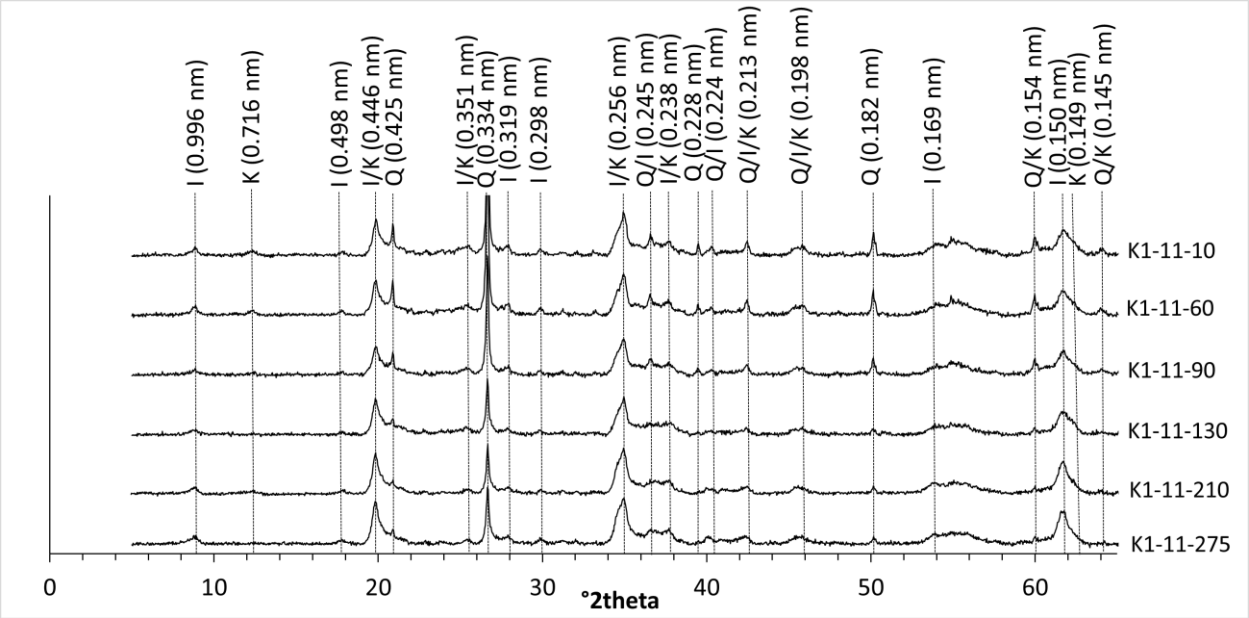

Figure 3.32: XRD pattern indicating peaks labelled with d-spacings (nm) of the $MgCl_2$ treated clay extracts of the heuweltjie soil at profile K1-11 (I=illite, K=kaolinite, Q=quartz).

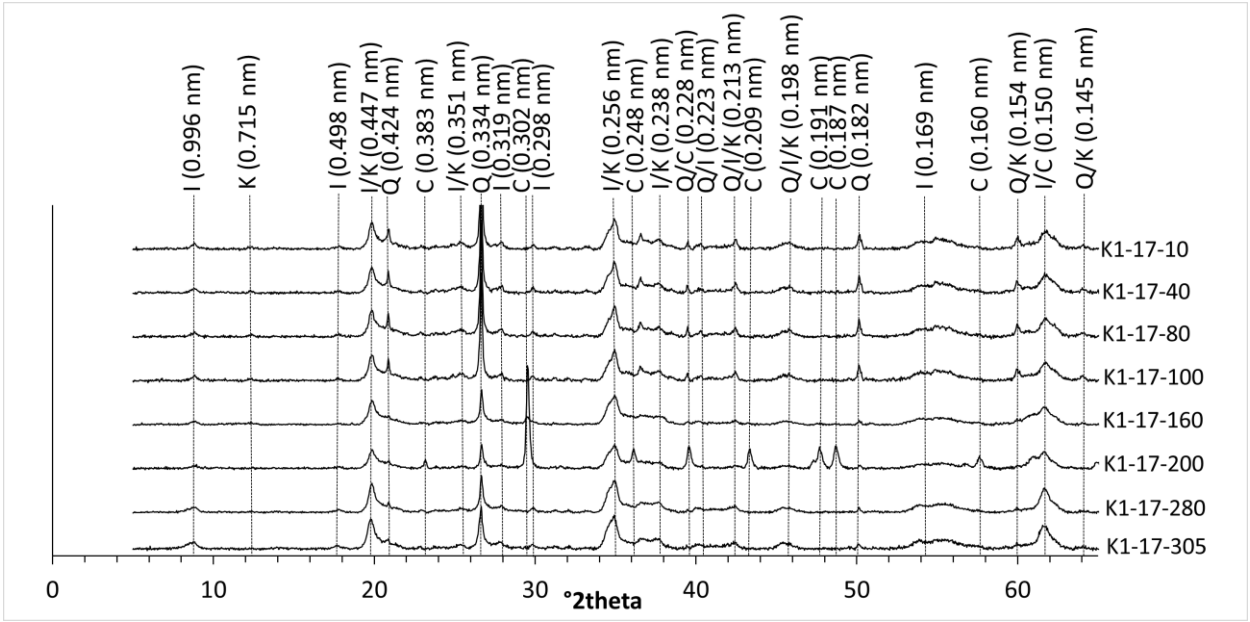

Figure 3.33: XRD pattern indicating peaks labelled with d-spacings (nm) of the $MgCl_2$ treated clay extracts of the heuweltjie soil at profile K1-17 (I=illite, K=kaolinite, Q=quartz, C=calcite).

3.4.2.2 Bulk sample mineralogy

In the profile at 11 m cross-section distance calcite was identified at depths of 90 and 275 cm (Figure 3.34). Albite was present in all samples of K1-11. A weak initial peak for albite (indicated with an F) was identified at 0.404 nm and at 0.303 nm for calcite. Illite and quartz were also present with initial peaks at 1.007 and 0.425 nm respectively.

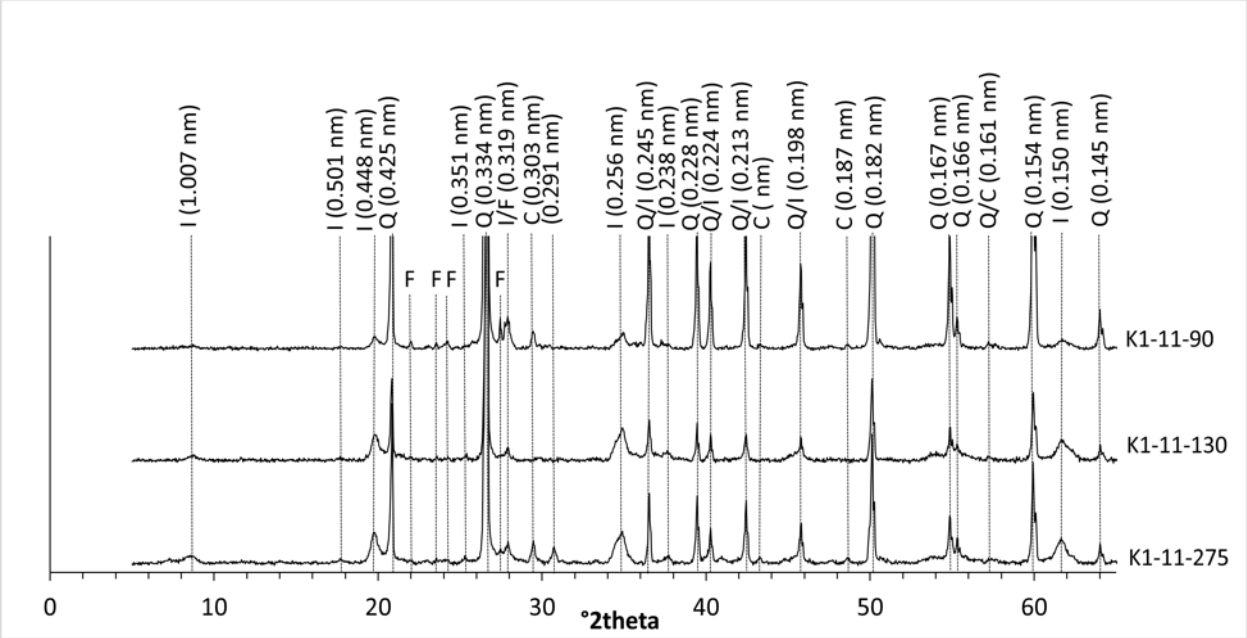

Figure 3.34:XRD pattern indicating peaks labelled with d-spacings (nm) of the untreated bulk samples of the heuweltjie profile K1-11 (I=illite, Q=quartz, C=calcite, F=feldspar (albite)).

Gypsum was identified in the profile at 17 m cross-section distance at depths of 80, 100, and 160 cm only (Figure 3.35). An initial gypsum peak was identified at 0.761 nm. Gypsum was also present at the cross-section distance at 21 m, at a depth of 190 cm. A weak initial peak was identified for gypsum in K1-21-190 at 0.761 nm (Figure 8.18, Appendix B). Calcite and albite (indicated with an F) were present throughout the whole profile at both K1-17 and K1-21 with initial peaks at 0.385 nm and 0.404 nm respectively and a strong peak for calcite at 0.303 nm. Illite and quartz were also present throughout both profiles with initial peaks at 1.007 nm and 0.425 nm.

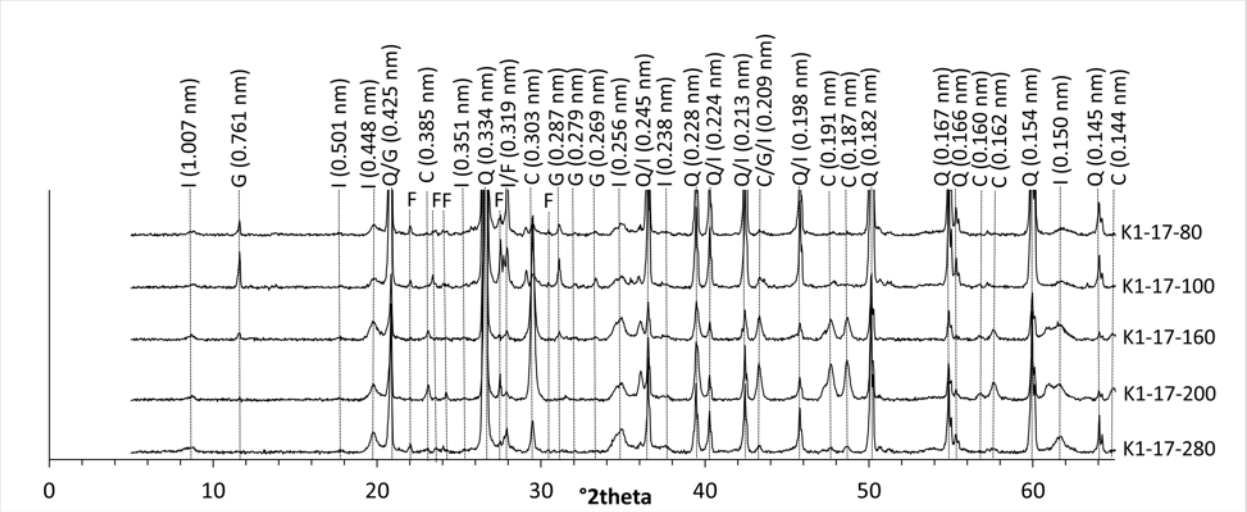

Figure 3.35: XRD pattern indicating peaks labelled with d-spacings (nm) of the untreated bulk samples of the heuweltjie profile K1-17 (I=illite, G=gypsum, Q=quartz, C=calcite, F=feldspar (albite)).

3.4.2.3 Biogenic feature mineralogy

A weak initial peak for Ca oxalate (whewellite) was identified at 0.593 nm in the surface frass pile collected from K1 (Figure 3.36). Illite and quartz were identified in both the surface frass from K1, and frass sampled at K1-26-40 with initial peaks at 1.007 nm and 0.425 nm. The feldspar albite was also identified in both frass samples from K1 and is indicated with the letter F in Figure 3.36.

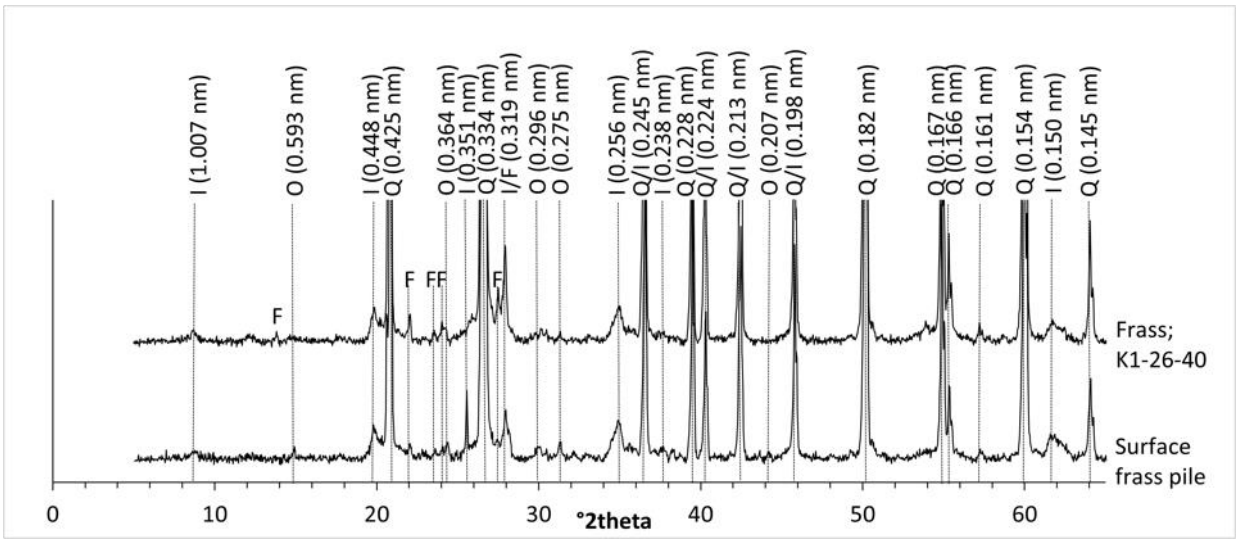

Figure 3.36: XRD pattern indicating peaks labelled with d-spacings (nm) of the untreated termite frass samples of the Klawer heuweltjie (K=kaolinite, Q=quartz, F=feldspar (albite), O=Ca oxalate (whewellite)).

3.5 EMI survey at Piketberg site

In the survey of multiple heuweltjies at the Piketberg site, mounds were clearly delineated by a higher EC_a on the heuweltjie soils compared to the inter-heuweltjie soils at all three depths of 25, 50, and 90 cm (Figure 3.37). The highest EC_a values were grouped together in distinct circular patterns and EC_a values ranged between 0.5 to 32 mS/m. When comparing aerial imagery and field observations of the area, the circular clusters of higher EC_a correspond to those of heuweltjies. At 25 cm depth ECa on the heuweltjie measured around 5.5 to 6.5 mS/m compared to the 0.5 to 1 mS/m of most inter-heuweltjie soils, indicating a five to ten fold increase in heuweltjie soil EC compared to inter-mound soils at the Piketberg site. The EC in the centre of some heuweltjies (>28 mS/m) increased almost twofold compared to the inter-heuweltjie soils (ca 14 mS/m) at 50 cm depth (Figure 3.37). Similarly, at 90 cm a twofold increase in EC occurred on the heuweltjie soils (ca 20 mS/m) compared to most inter-mound soils (ca 10 mS/m). The serrated appearance on the grids of Figure 3.37 can be attributed to soil tillage practices as heuweltjies were located in a field that was previously used for the cultivation of annual crops. Figure 8.19, Appendix B shows the EC_a of a single heuweltjie surveyed in uncultivated natural veld at the Piketberg site. At 25 cm depth the centre of the mound (5.2 to 6.2 mS/m) had an EC five to ten times higher than some of the surrounding inter-mound soils (0.2 to 1.2 mS/m). Confirming, that mound centres at the Piketberg site show a five to ten times increase in EC_a of the topsoil compared to inter-mound soils. The difference in EC between the centre and inter-mound soils at 50 and 90 cm depths were less pronounced. In all heuweltjies surveyed using EMI, EC_a increased from 25 to 50 cm and then decreased from 50 to 90 cm (Figure 3.37 and Figure 8.19).

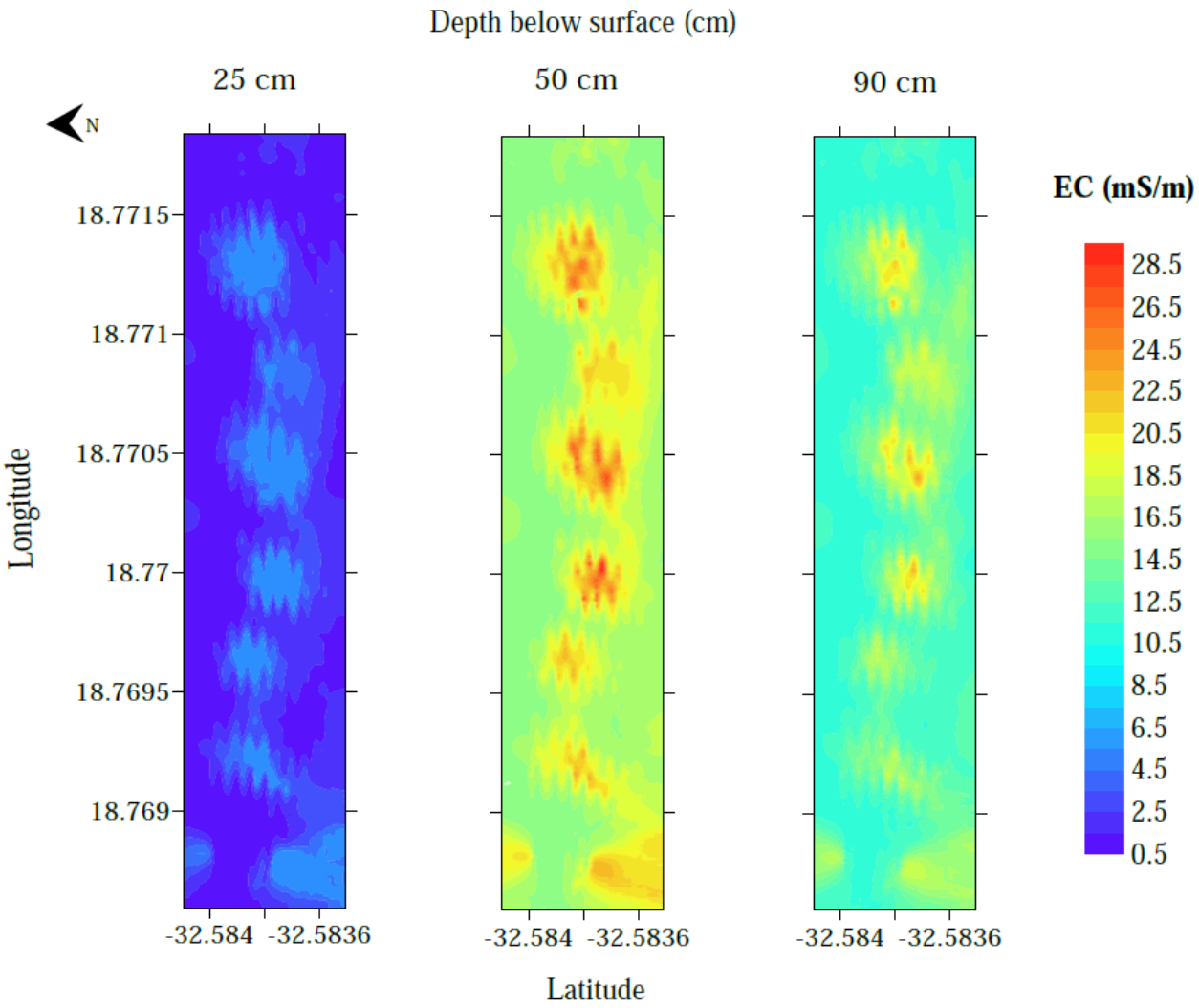

Figure 3.37: Sediment EC (mS/m) at various depths of 25, 50, and 90 cm depths showing EC variation between heuweltjie and inter-heuweltjie soils. Soils were previously tilled resulting in a striped/serrated appearance on the grids.

3.6 Salt and ion variation within heuweltjies

Interpolated maps of PB1W, PB1E, and K1 were created for pH(H_2O), EC, Na, Cl, Ca, SO4, Mg, K, alkalinity, dissolved Si, amorphous Si, halite, calcite, and gypsum. Interpolated maps are discussed according to variation throughout heuweltjies, variation with depth, and relation to mound features. Correlation matrices (Table 3.1 and Table 3.2) were used to validate visual data trends with depth for Piketberg and Klawer heuweltjie, respectively.

3.6.1 Piketberg heuweltjie (PB1)

Data of the east and west walls showed similar trends and will be discussed as PB1, referring to both walls. Interpolated maps of PB1W are attached in Figure 8.20 and Figure 8.21, Appendix B.

Table 3.1: Correlation matrices of 1:1 soil water extract ion concentrations and saturation indices (SI) with sample depth (cm) for the heuweltjie near Piketberg. Spearman's Rho in bold indicate significance (P<0.05).

PB1	pH (H_2O)	EC	Na	Mg	K	Ca	Cl	SO4	PO4	Alka-linity	Dis-solved Si
pH(H_2O)	-										
EC	0.21	-									
Na	**0.33**	**0.95**	-								
Mg	0.12	**0.87**	**0.71**	-							
K	**0.36**	**0.47**	**0.50**	**0.27**	-						
Ca	0.13	**0.87**	**0.70**	**0.95**	**0.32**	-					
Cl	0.13	**0.90**	**0.84**	**0.84**	**0.30**	**0.75**	-				
SO4	0.22	**0.82**	**0.78**	**0.77**	0.45	**0.84**	**0.57**	-			
PO4	**0.31**	**-0.26**	**-0.23**	**-0.25**	**0.36**	**-0.22**	**-0.27**	**-0.18**	-		
Alkalinity	**0.70**	0.30	0.40	0.14	**0.44**	0.12	0.21	0.16	**0.25**	-	
Dissolved Si	**0.73**	**0.32**	**0.38**	**0.24**	0.08	**0.24**	**0.26**	**0.22**	-0.15	**0.46**	-
Depth	0.07	**0.43**	**0.46**	**0.31**	**-0.14**	**0.27**	**0.38**	**0.30**	**-0.60**	**0.10**	**0.46**

	Amorphous Si	Halite	Calcite	Gypsum
Amorphous Si	-			
Halite	**0.46**	-		
Calcite	**0.75**	**0.59**	-	
Gypsum	**0.41**	**0.86**	**0.57**	-
Depth	**0.48**	**0.49**	**0.26**	**0.41**

3.6.1.1 pH(H_2O), EC, and ion concentrations

The pH(H_2O) of PB1 was highest in the centre of the heuweltjie, where pH(H_2O) values ranged between 6.4 and 8, compared to the inter-heuweltjie soils that had pH(H_2O) values ranging between 4 and 5.5 (Figure 3.38a and Figure 8.20a). The highest pH(H_2O) values were associated with areas of secondary carbonate accumulation and indurated termite channels (Figure 3.38a). pH showed no significant correlation with depth (P>0.05) in PB1 (Table 3.1).

EC showed a significant, moderate, positive correlation with depth (r_s=0.43; P<0.05) in PB1 and increased with depth in most heuweltjie and inter-heuweltjie soils (Table 3.1). EC was higher in the centre of the mound compared most inter-mound soils (Figure 3.38b and Figure 8.20b). Na^+ and Cl^- also showed significant, moderate, positive correlations with depth (r_s=0.46/0.38; P<0.05) and increased with depth in most of the profiles (Table 3.1, Figure 3.38c, d, and Figure 8.20c, d). Na^+ and Cl^- were largely concentrated in the centre of the mound. Ca^{2+} and SO_4^{2-} showed similar significant, weak, positive correlations with depth (r_s=0.27/0.30; P<0.05) in PB1 and increased slightly as depth increased (Table 3.1, Figure 3.38e, f, and Figure 8.20e, f). Ca^{2+} and SO_4^{2-} showed the highest concentrations in the centre of the mound compared to most inter-heuweltjie soils (Figure 3.38e, f, and Figure 8.20e, f). The highest EC (>1000 uS/cm), Na^+ (>40 mg/L), Cl^- (>60 mg/L), Ca^{2+} (>12 mg/L) and SO_4^{2-} (>40 mg/L) concentrations were associated with areas with secondary carbonate accumulation, indurated or abundant channels, loose dorbank nodules, and a rodent food pile and burrows between PB1E-19 and PB1E-21 (Figure 3.38b to f, and Figure 8.20b to f). High concentrations were also observed in the pockets of clay conglomerate in the colluvium between PB1E-30 and PB1E-35 (Figure 3.38b to f).

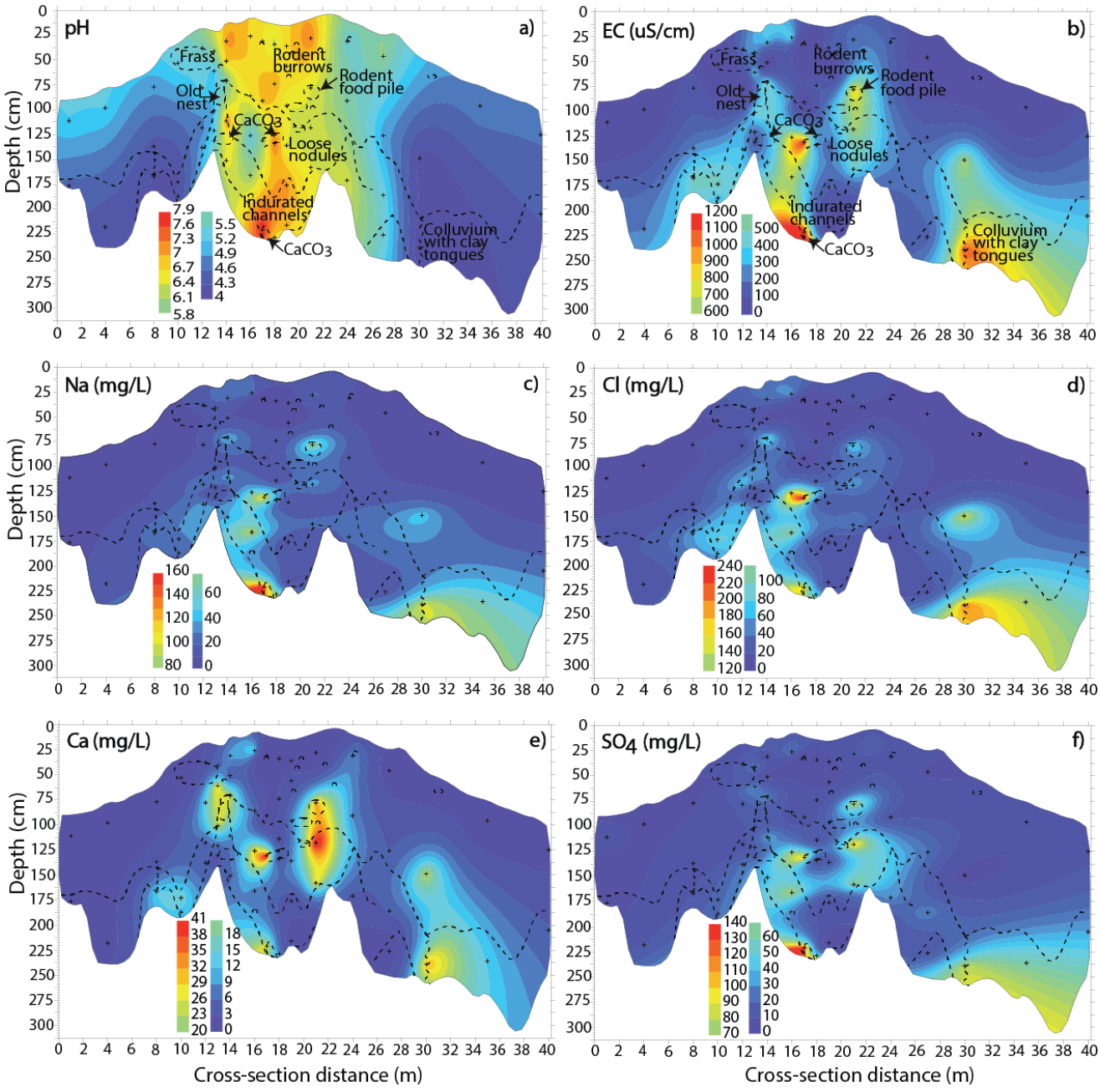

Figure 3.38: Interpolated maps of the east wall of the heuweltjie in Piketberg (PB1E) for a) pH(H_2O), b) EC (uS/cm), and ion concentrations (mg/L) of c) Na, d) Cl, e) Ca, and f) SO4 (similar trends are observed in PB1W, Appendix B).

Mg^{2+} showed a significant, but weak, positive correlation with depth (r_s=0.31; P<0.05) in PB1 (Table 3.1) and Mg^{2+} concentrations increased with depth (Figure 3.39g and Figure 8.20g). Mg also had the highest concentrations in the centre of the mound compared to most inter-heuweltjie soils (Figure 3.39g and Figure 8.20g). The highest Mg^{2+} (>8 mg/L) concentrations were also associated with areas with secondary carbonate accumulation, indurated or abundant channels, and a rodent food pile and burrows between PB1E-19 and PB1E-21 (Figure 3.39g and Figure 8.20g). High concentrations were also observed in the pockets of clay conglomerate in the colluvium between PB1E-30 and PB1E-35 (Figure 3.39g).

K^+ showed an overall significant, weak, negative correlation with depth (r_s=0.-0.14; P<0.05) and decreased with depth in PB1 (Table 3.1). K^+ concentrations were higher in the centre of the mound compared to inter-heuweltjie soils (Figure 3.39h and Figure 8.20h). The higher concentrations of K^+ (>8 mg/L) were mainly associated with areas of secondary carbonate accumulation in loose dorbank nodules, rodent burrows and a rodent food pile (Figure 3.39h and Figure 8.20h). However, the highest K^+ (>24 mg/L) concentration was observed in a few topsoil samples between PB1-14 and PB1-16 (Figure 3.39h and Figure 8.20h). As the area is used for the grazing of cattle, it is possible that these high K concentrations in the few topsoil samples could be attributed to cattle urine, resulting in the negative correlation with depth.

Dissolved Si showed a significant, moderate, positive correlation (r_s=0.46; P<0.05) with sample depth (Table 3.1). Dissolved Si was highest in the centre of the mound compared to inter-mound soils and higher concentrations were observed closer to the base of the trench in the centre of the mound (Figure 3.39i and Figure 8.20i). The highest dissolved Si concentrations (>14 mg/L) were associated with indurated, loose dorbank nodules, indurated channels, and areas of secondary carbonate accumulation (Figure 3.39i and Figure 8.20i).

Alkalinity showed a very weak significant correlation (r_s=0.10; P<0.05) with sample depth in PB1 (Table 3.1). However, on the west wall the alkalinity was higher closer to the trench base in the centre of the mound (Figure 8.20j). Alkalinity was higher in the centre (>16 mg/L) of PB1 compared to inter-mound (<13 mg/L) soils (Figure 3.39j and Figure 8.20j). The highest alkalinity was mainly associated with areas of secondary carbonate accumulation and a higher pH(H_2O) (Figure 3.38a, Figure 3.39j and Figure 8.20a,j). A significant, strong, positive correlation (r_s=0.70; P<0.05) was observed between pH and alkalinity (Table 3.1). Higher alkalinity in the topsoil could also be attributed to cow urine (Figure 3.39j and Figure 8.20j).

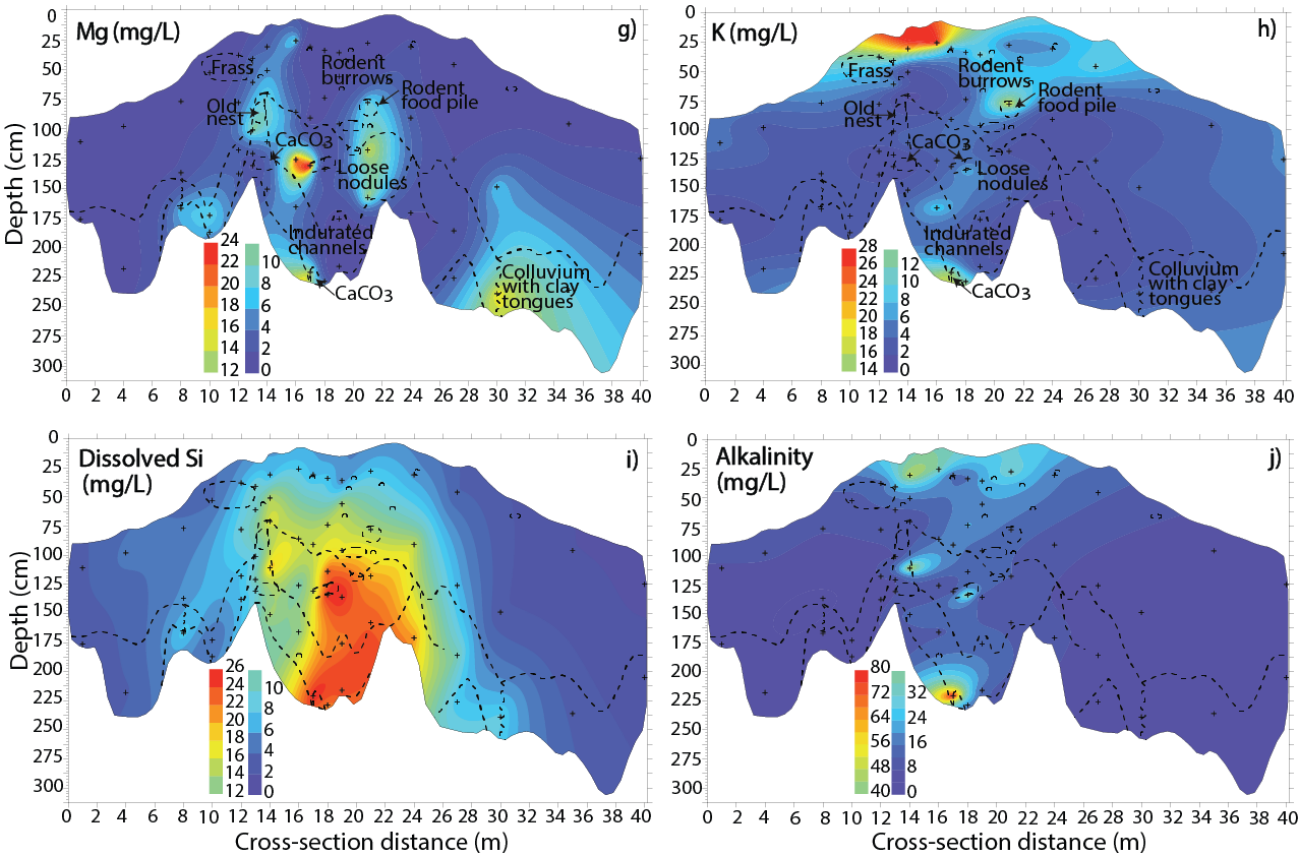

Figure 3.39: Interpolated maps of the east wall of the heuweltjie in Piketberg (PB1E) for ion concentrations (mg/L) of g) Mg, h) K, i) Dissolved Si, and j) Alkalinity (similar trends are observed in PB1W, Appendix B).

3.6.1.1 Mineral Saturation Indices

Amorphous Si followed a similar trend to that of dissolved Si in PB1 (Figure 3.40a and Figure 8.21a). A significant, moderate, positive correlation (0.48; $P<0.05$) existed between the saturation of amorphous Si and sample depth (Table 3.1). The saturation indices of amorphous Si, although all undersaturated, was higher closer to the trench base in the centre of the mound (Figure 3.40a and Figure 8.21a). Amorphous Si was also less undersaturated in the centre of PB1 compared to inter-mound soils and was (Figure 3.40a and Figure 8.21a).

Halite saturation also showed a significant, moderate, positive correlation (r_s=0.49; $P<0.05$) with depth and saturation increased with depth in most profiles of PB1 (Table 3.1). Although undersaturated throughout PB1, halite was less undersaturated in the centre of PB1 compared to most inter-mound soils and was associated with the same biogenic features as Na^+ and Cl^- (Figure 3.40b and Figure 8.21b).

Calcite saturation showed a significant, but weak, positive correlation (r_s=0.26; P<0.05) with sample depth in PB1 (Table 3.1). Profiles between 13 and 24 m in the centre of the mound showed an increase in saturation with depth (Figure 3.40c and Figure 8.21c). Only a few samples, in areas of secondary carbonate accumulation, were at or close to saturation (Figure 3.40c and Figure 8.21c). Calcite saturation indices were higher in the centre of PB1 compared to the inter-heuweltjie soils (Figure 3.40c and Figure 8.21c) and higher saturation indices followed similar trends to pH and alkalinity.

Gypsum saturation showed a significant, moderate, positive correlation (r_s=0.41; P<0.05) with depth and Gypsum saturation indices increased with depth in most profiles of PB1 (Table 3.1). Gypsum remained undersaturated throughout PB1 but was less undersaturated in the centre of the mound compared to most inter-mound soils (Figure 3.40d and Figure 8.21d).

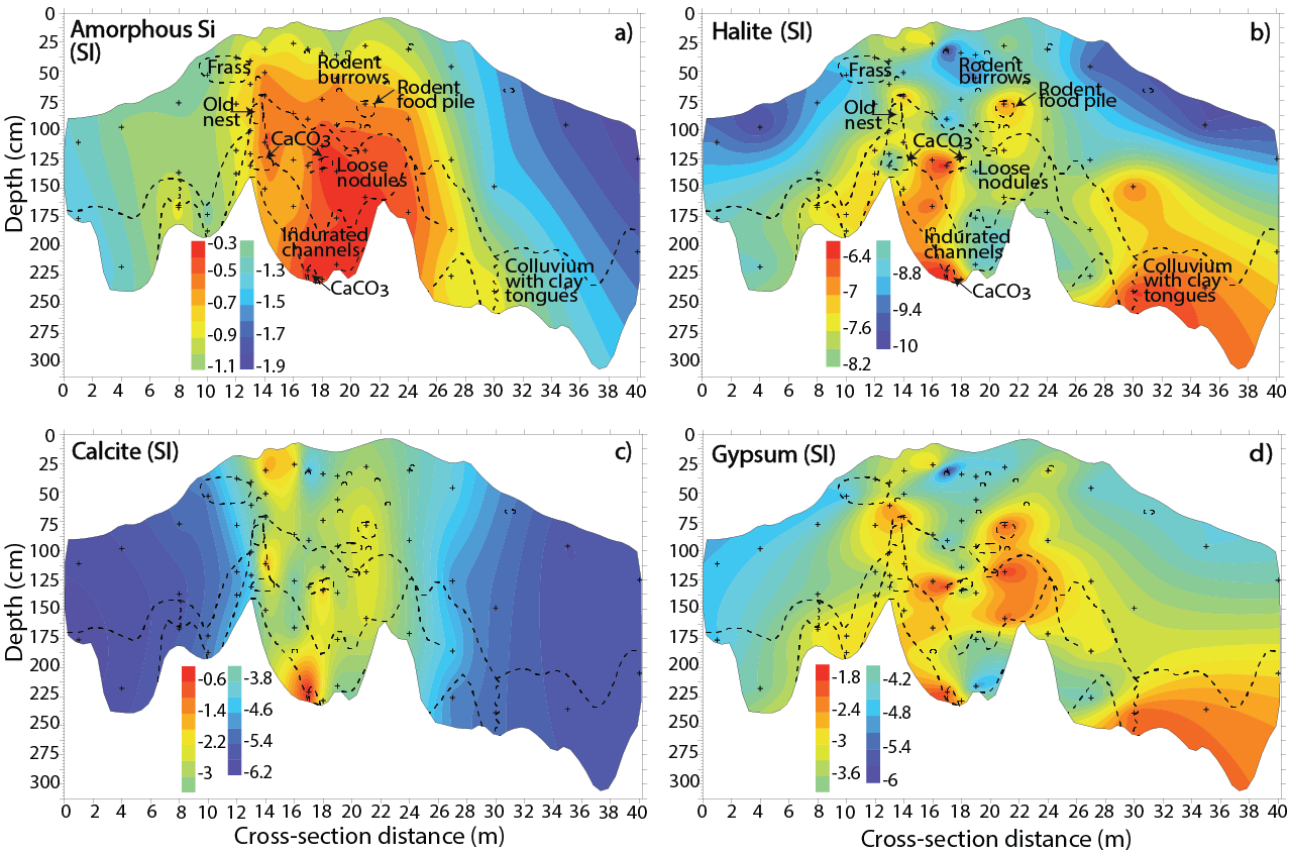

Figure 3.40: Interpolated maps of the east wall of the heuweltjie in Piketberg (PB1E) for mineral saturation indices (SI) of a) amorphous Si, b) halite, c) calcite, and d) gypsum (similar trends are observed in PB1W, Appendix B).

3.6.2 Klawer heuweltjie (K1)

Table 3.2: Correlation matrices of 1:1 soil water extract ion concentrations and saturation indices (SI) with sample depth (cm) for the heuweltjie near Klawer. Spearman's Rho in bold indicate significance (P<0.05).

K1	pH (H_2O)	EC	Na	Mg	K	Ca	Cl	SO4	PO4	Alka-linity	Dis-solved Si
pH(H_2O)	-										
EC	**-0.30**	-									
Na	**-0.28**	**0.97**	-								
Mg	**-0.32**	**0.93**	**0.88**	-							
K	-0.07	**0.89**	**0.88**	**0.81**	-						
Ca	-0.21	**0.71**	**0.59**	**0.82**	**0.59**	-					
Cl	**-0.32**	**0.97**	**0.99**	**0.90**	**0.86**	**0.56**	-				
SO4	-0.19	**0.69**	**0.58**	**0.76**	**0.58**	**0.97**	**0.52**	-			
PO4	**0.34**	**-0.38**	**-0.37**	**-0.33**	**-0.28**	**-0.27**	**-0.37**	**-0.27**	-		
Alkalinity	**0.79**	**-0.38**	-0.33	**-0.37**	-0.25	**-0.35**	**-0.35**	**-0.35**	**0.53**	-	
Dissolved Si	-0.14	0.14	**0.23**	0.07	-0.04	0.01	**0.18**	0.07	-0.11	-0.01	-
Depth	-0.03	**0.75**	**0.77**	**0.65**	**0.78**	**0.35**	**0.77**	**0.33**	**-0.34**	-0.21	-0.01

	Amorphous Si	Halite	Calcite	Gypsum
Amorphous Si	-			
Halite	**0.32**	-		
Calcite	-0.15	0.14	-	
Gypsum	0.22	**0.85**	**0.19**	-
Depth	0.04	**0.65**	0.26	**0.56**

3.6.2.1 pH(H_2O), EC, and Ion concentrations

pH(H_2O) showed no significant correlation with sample depth (P>0.05) in K1 (Table 3.2). However, pH(H_2O) was higher (>8.8) closer to the surface of the mound and decreased (7.2 to 8.4) with depth in the mound centre (Figure 3.41a). Similarly, pH(H_2O) decreased with depth between cross-section distances 0 m to 10 m (Figure 3.41a). However, between 23 m and 30 m cross-section distance, pH(H_2O) showed an increase with depth (Figure 3.41a). The pH(H_2O) was higher in the centre of the mound (9-23 m) compared to most inter-mound soils. The highest pH values (>8.8) were associated with the topsoil in the centre of the mound where secondary carbonate accumulation was observed.

EC, Na^+, and Cl^- showed similar trends within K1, and all had significant, strong, positive correlations (r_s=0.75/0.77; P<0.05) with depth (Table 3.2). EC, Na^+, and Cl^- increased towards the bottom of the trench and was highest in the centre of the mound compared to inter-mound

soils (Figure 3.41b, c, and d). The higher EC (>6000 uS/cm), Na^+ (>1200 mg/L), and Cl^- (>1500 mg/L) measurements were associated with gravelly and vesicular dorbank containing abundant channels and active termites (Figure 3.41b, c, and d), fractured platy dorbank, and granular dorbank in the centre of K1 (Figure 3.41b, c, and d). The highest EC (>16000 uS/cm), Na^+ (>2700 mg/L), and Cl^- (>5000 mg/L) values were observed between K1-14 and K1-15 below active termite channels in the vesicular dorbank at K1-15-130 (Figure 3.41b, c, and d).

Ca^{2+} and SO_4^{2-} concentrations showed similar overall significant, weak, positive correlations with depth (r_s=0.35/0.33; P<0.05) in K1 and increased slightly as depth increased (Table 3.2, Figure 3.41e and f). Ca^{2+} and SO_4 was higher in the centre of the mound compared to inter-mound soils (Figure 3.39e and f). Higher concentrations of Ca^{2+} (>400 mg/L) and SO_4^{2-} (>900 mg/L) were associated with similar biogenic features as EC, Na^+ and Cl^-. The highest concentrations of Ca^{2+} (>900 mg/L) and SO_4^{2-} (>3000 mg/L) were observed in the centre of the mound between K1-15 and K1-19 in the gravelly dorbank, vesicular dorbank with abundant channels, and fractured platy dorbank (Figure 3.41e and f).

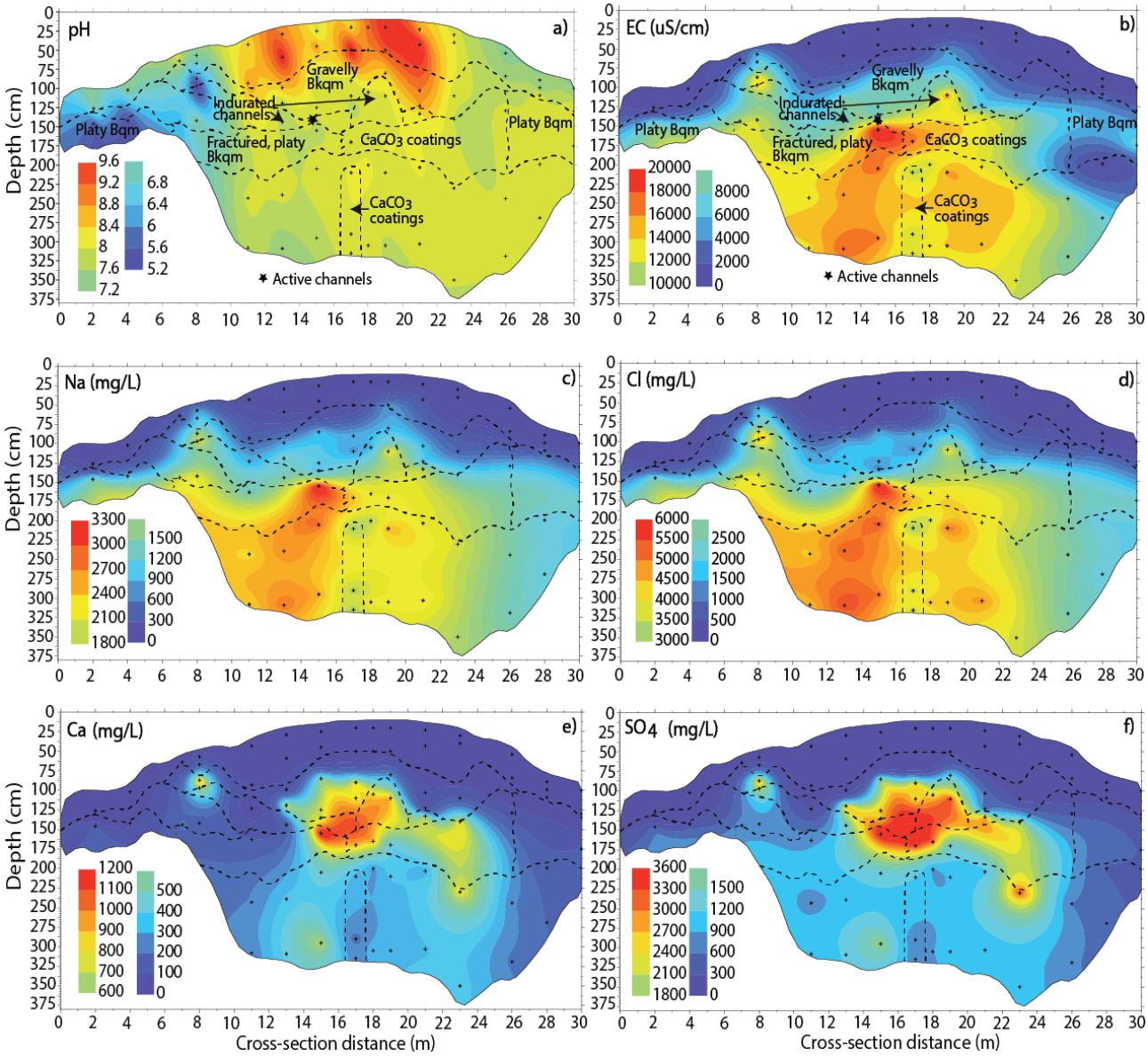

Figure 3.41: Interpolated maps of the heuweltjie in Klawer (K1) for a) pH(H_2O), b) EC (uS/cm), and ion concentrations (mg/L) of c) Na, d) Cl, e) Ca, and f) SO4

Mg^{2+} also increased with depth (Table 3.2, Figure 3.42g) and had a significant, moderate, positive correlation with depth (r_s=0.65; P<0.05). Mg^{2+} was higher in the centre of the mound compared to inter-mound soils (Figure 3.42g). Higher concentrations Mg^{2+} (>160 mg/L) were observed in the centre of the mound between profiles K1-13 and K1-22 in the gravelly dorbank, vesicular dorbank with abundant channels, and fractured and granular platy dorbank (Figure 3.42g). The highest concentration of Mg^{2+} (>480 mg/L) was associated with active termite channels in the centre of the mound and fractured platy dorbank between K1-15 and K1-19 (Figure 3.42g).

K^+ showed an overall significant, strong, positive correlation with depth (r_s=0.78; P<0.05) and increased with depth in K1 (Table 3.2). K^+ concentrations were higher in the centre of the mound compared to inter-mound soils (Figure 3.42h). The highest concentration of K^+ (>110 mg/L) was observed between profiles K1-11 and K1-22 and was mainly associated with fractured platy dorbank and granular dorbank (Figure 3.42h).

Dissolved Si showed no overall significant correlation with depth (P>0.05) in K1 (Table 3.2). However, Si concentrations increased with depth up until the end of the platy dorbank horizon and then decreased towards the base of the trench (Figure 3.42i). The highest Si concentrations (>22 mg/L) were observed in the edges of the mound, and inter-mound soils mostly associated with poorly fractured platy dorbank (Figure 3.42i). Dissolved Si concentrations were lowest (<16 mg/L) in the centre (K17-K21) of the mound were the platy dorbank was highly fractured (Figure 3.42i).

Alkalinity showed no significant correlation with depth (P>0.05) in K1 (Table 3.2). However, alkalinity was higher in the topsoil compared to the subsoils between 10 to 23 m cross-section distances (Figure 3.42j). Alkalinity was highest (>100 mg/L) in the topsoil in the centre of the mound where secondary carbonate accumulation occurred (Figure 3.40j). Alkalinity also had a significant, strong, positive correlation (r_s=0.79; P<0.05) with pH(H_2O) in K1 (Table 3.2).

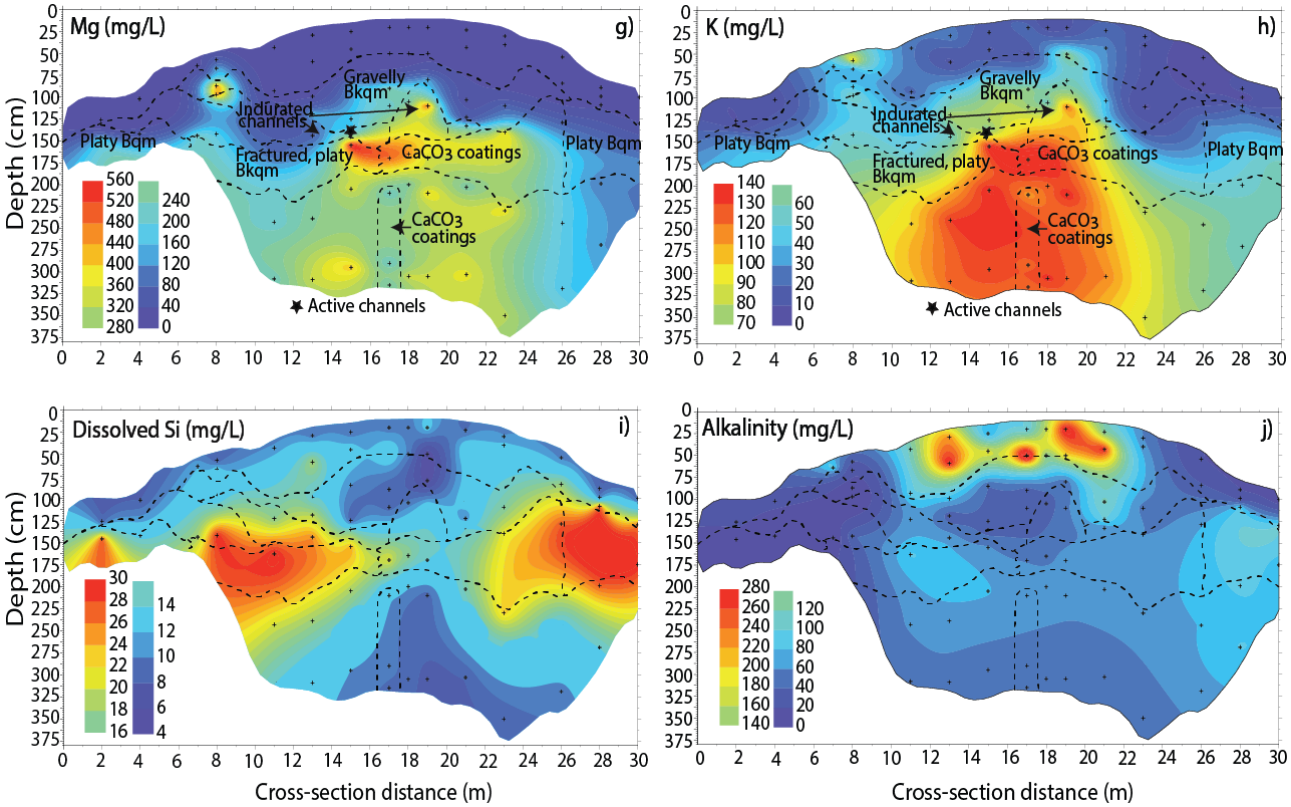

Figure 3.42: Interpolated maps of the heuweltjie in Klawer (K1) for ion concentrations (mg/L) of g) Mg, h) K, i) Dissolved Si, and j) Alkalinity.

3.6.2.1 Mineral Saturation Indices

Amorphous Si saturation followed the same trend to that of dissolved Si in K1 (Figure 3.43a). No significant correlation (r_s=0.04; P>0.05) existed between the saturation of amorphous Si and sample depth (Table 3.2). Saturation indices of amorphous Si, although all undersaturated, was higher closer to the heuweltjie sides and inter-heuweltjie soils than the centre of the mound (Figure 3.43a). Amorphous Si was less undersaturated in the poorly fractured platy dorbank of K1 compared to the rest of the mound and was most undersaturated throughout profiles K1-17 to K1-21 in the centre of the mound (Figure 3.43a).

Halite saturation indices showed a significant, moderate, positive correlation (r_s=0.65 P<0.05) with depth and saturation increased with depth in all profiles of K1 (Table 3.2, Figure 3.43b). Halite was undersaturated throughout K1 but was less undersaturated in the platy and granular dorbank closer to the base of trench, compared to the topsoil (Figure 3.43b).

Calcite saturation showed no significant correlation (r_s=0.26; P>0.05) with sample depth (Table 3.2). However, a few profiles (K1-13 and K1-17 to K1-21) in the centre of the mound showed an overall decrease in saturation with depth (Figure 3.43c). Calcite was predominantly

saturated or supersaturated in K1 with higher saturation indices (>0.4) in the centre of the mound and the lower saturation indices (<-1.2) in the inter-mound profiles (Figure 3.43c). The topsoil in the heuweltjie centre (K1-17, K1-19, and K1-21) had the highest calcite saturation indices (>1.2) and the lowest saturation indices (<-1.2) were observed in the inter-heuweltjie soils (profiles K1-0 to K1-7, and K1-26 to K1-30 of Figure 3.43c). Calcite saturation was consistent with field observations of carbonate presence and followed a similar trend to pH(H_2O) and alkalinity (Figure 3.41a and Figure 3.42j).

Gypsum saturation showed a significant, moderate, positive correlation (r_s=0.56; P<0.05) with depth and increased towards the base of the trench in most profiles of K1 (Table 3.2, Figure 3.43d). Gypsum remained undersaturated throughout most profiles of K1 but was at saturation or supersaturated in the centre of the mound, between profiles K1-12 and K1-23, in the gravelly dorbank, vesicular dorbank with abundant channels, and fractured platy dorbank (Figure 3.43d). Gypsum was also closer to or at saturation (>-0.4) in the centre of the mound compared to the more undersaturated (<-1.2) inter-heuweltjie soils Figure 3.43d). Heuweltjie and inter-heuweltjie topsoil was the least saturated (<-2) with regards to gypsum.

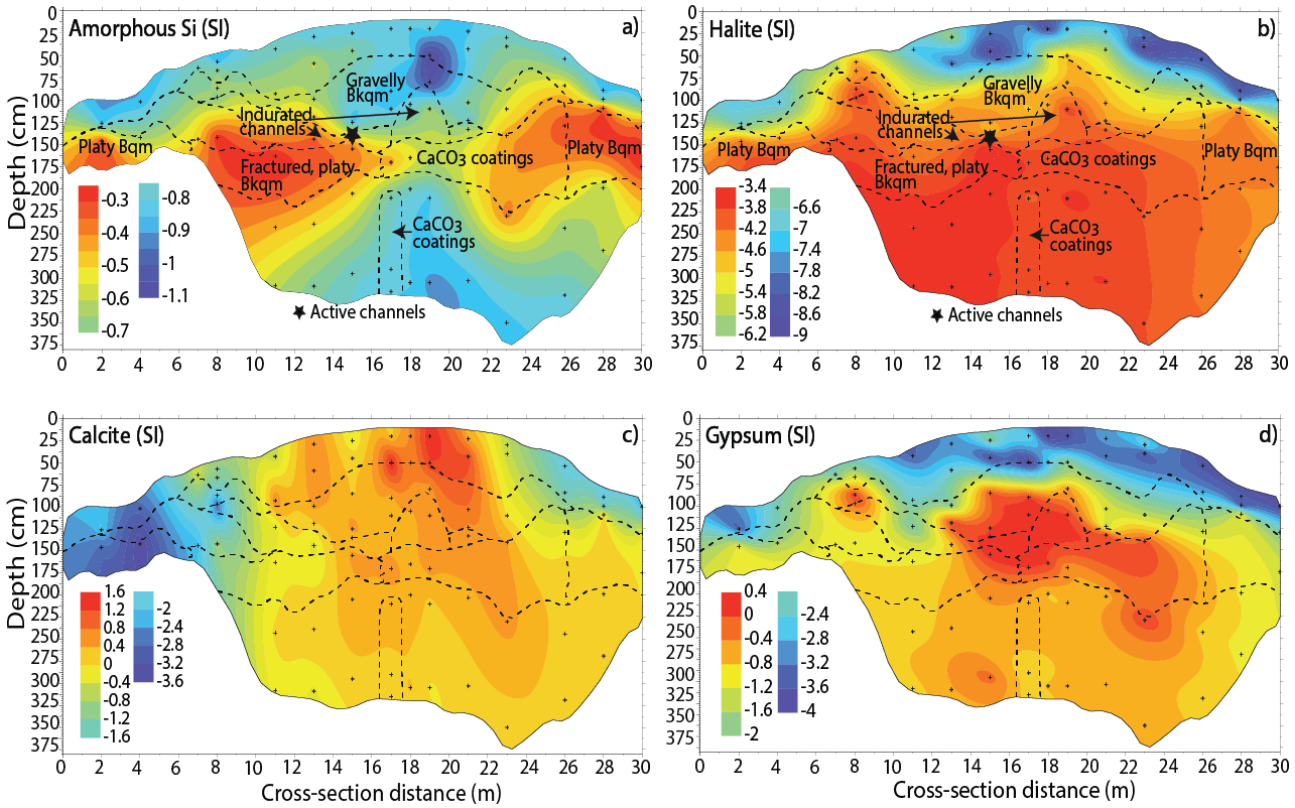

Figure 3.43: Interpolated maps of the heuweltjie in Klawer (K1) for mineral saturation indices (SI) of a) amorphous Si, b) halite, c) calcite, and d) gypsum.

3.7 Ion activities and mineral saturation indices

For this section ion and mineral saturation indices were plotted against Cl^- activity, and mineral saturation indices were also plotted against pH(H_2O). Ion activities were plotted against Cl^- activity because Cl is considered a conservative solute. Consequently, subsequent wetting redissolves Cl^-, its participation in ion exchange is minor, and Cl^- would effectively remain in solution until halite saturation (Eugster and Jones, 1979).

3.7.1 Ion activities and relation to Cl^- activity

The variation in ion activity with Cl^- activity in both the PB1 and K1 water extracts is consistent with the seawater dilution line for Na^+ and Mg^+ (Figure 3.44a- e). Na^+ against Cl^- activity (Figure 3.44a) showed the strongest, significant, positive linear correlation of all solutes in both PB1 (r_s=0.90; $P\leq$0.000) and K1 (r_s=0.97; $P\leq$0.000). Furthermore, Na^+ activities plotted on the seawater dilution line (Figure 3.44a). K^+ activity (Figure 3.44b) showed a weak, but significant, positive correlation with Cl^- activity in PB1 (r_s=0.25; P=0.022) and K^+ activities plotted

slightly above the seawater dilution line in this range. In Figure 3.44b, K^+ increased significantly as Cl^- activity increased in K1 (r_s=0.76; P≤0.001) and activities plotted on or slightly above the seawater dilution line. Ca^{2+}, Mg^{2+}, and SO_4^{2-} activities all showed significant positive correlations (r_s=0.70-0.88; P≤0.001) with Cl^- activity in both PB1 and K1 (Figure 3.44c, d and e). Mg^{2+} activities followed a similar trend to that of the seawater dilution line for both PB1 and K1 (Figure 3.44d). Ca^{2+} and SO_4^{2-} activities plotted parallel to the seawater dilution line but concentrations were elevated compared to that of seawater (Figure 3.44c and e).

HCO_3^- and pH(H_2O) remained constant with increased Cl^- activity in PB1 (P>0.05) with no significant correlation (Figure 3.44f and h). A slight, but significant, decrease (r_s=-0.39/-0.30, P<0.05) was observed in HCO_3^- activity, and pH(H_2O) with Cl^- activity in K1 (Figure 3.44f and h). HCO_3^- mainly plotted above the seawater dilution line in PB1 and K1 and slopes were close to zero in both ranges. In Figure 3.44g, H_4SiO_4 activity showed a weak positive correlation with Cl^- activity in PB1 and K1 (r_s=0.30/0.38; P<0.001). All the H_4SiO_4 activities plotted above the seawater dilution line and concentrations also had slopes close to zero.

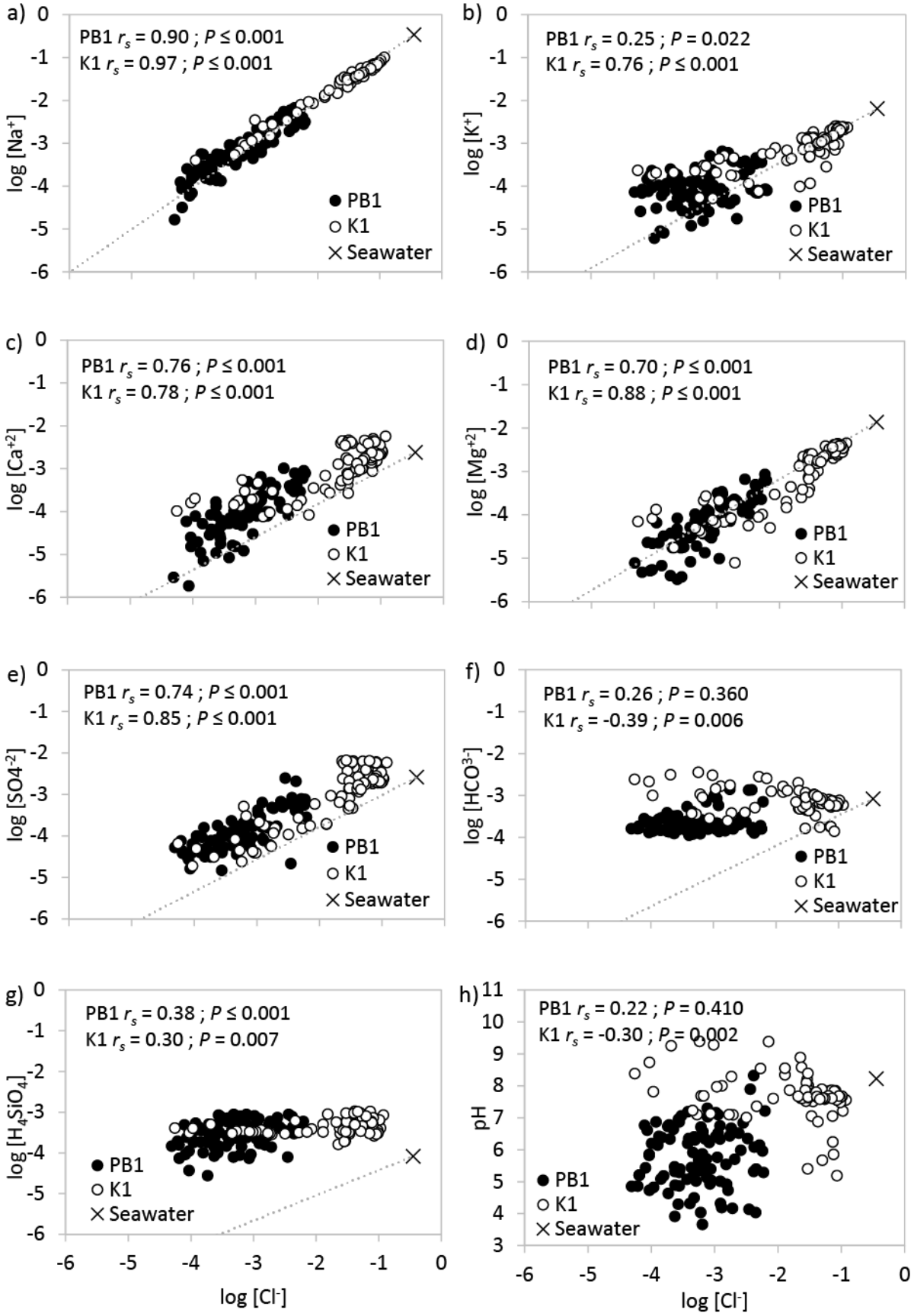

Figure 3.44: Ion activity of a) Na, b) K, c) Ca, d) Mg, e) SO_4, f) HCO_3, g) H_4SiO_4, and h) pH(H_2O) against the ion activity of Cl for the 1:1 soil:water extracts of the heuweltjies in Piketberg (PB1) (black) and Klawer (K1) (white). The composition of seawater is indicated by an X with a dashed line representing the seawater dilution line.

3.7.2 Saturation indices and relation to Cl^- activity

Halite, being the most soluble mineral, was undersaturated in all samples for both PB1 and K1 ranges (Figure 3.45a) and it could be assumed that Cl^- remained in solution. This makes Cl^- a suitable measure for ion concentration in both heuweltjies (Eugster and Jones, 1979). Halite saturation increased significantly (r_s=0.98/0.99; P<0.001) with increased Cl^- activity in both heuweltjies. The saturation indices for calcite remained mostly undersaturated for PB1, except for three samples near or at saturation at the highest ion concentration (log[Cl^-] = -2.2) for the PB1 range (Figure 3.45b). A significant moderate positive correlation existed between the SI of calcite and Cl^- activity (r_s=0.52, P<0.001). This indicates an increase in calcite saturation with ion concentration in the PB1 range until saturation is reached at the highest Cl^- activity. Most of the saturation indices for calcite in K1 were at or near saturation across the entire Cl^- activity range of -4.5 to -1 Figure 3.45b). Gypsum is more soluble than calcite and remained undersaturated for all samples in PB1 and for most samples in K1 (Figure 3.45c). A few samples of the K1 range were at or near saturation with respect to gypsum at the highest ion concentration (log[Cl^-] >-1.5) of the range. Gypsum saturation indices showed a strong positive correlation (r_s=0.81/0.84; P<0.001) with Cl^- activity in both PB1 and K1. Consequently, gypsum saturation increases as ion concentration increase in PB1 and K1 until saturation is reached. However, evaporation does not occur at rates high enough to allow gypsum precipitation in PB1.

Quartz saturation indices remained at or just above saturation (supersaturated) for most samples in PB1 and K1 (Figure 3.45e). In contrast, amorphous Si saturation indices are mostly just below (undersaturated) or near saturation for all samples of both PB1 and K1 (Figure 3.45f). Both quartz and amorphous Si saturation indices were weakly correlated (r_s=0.38/0.29; P<0.05) with Cl^- activity in PB1 and K1 and had slopes close to zero (Figure 3.45e and f). Therefore, quartz and amorphous Si both remain unaffected by an increased ion concentration.

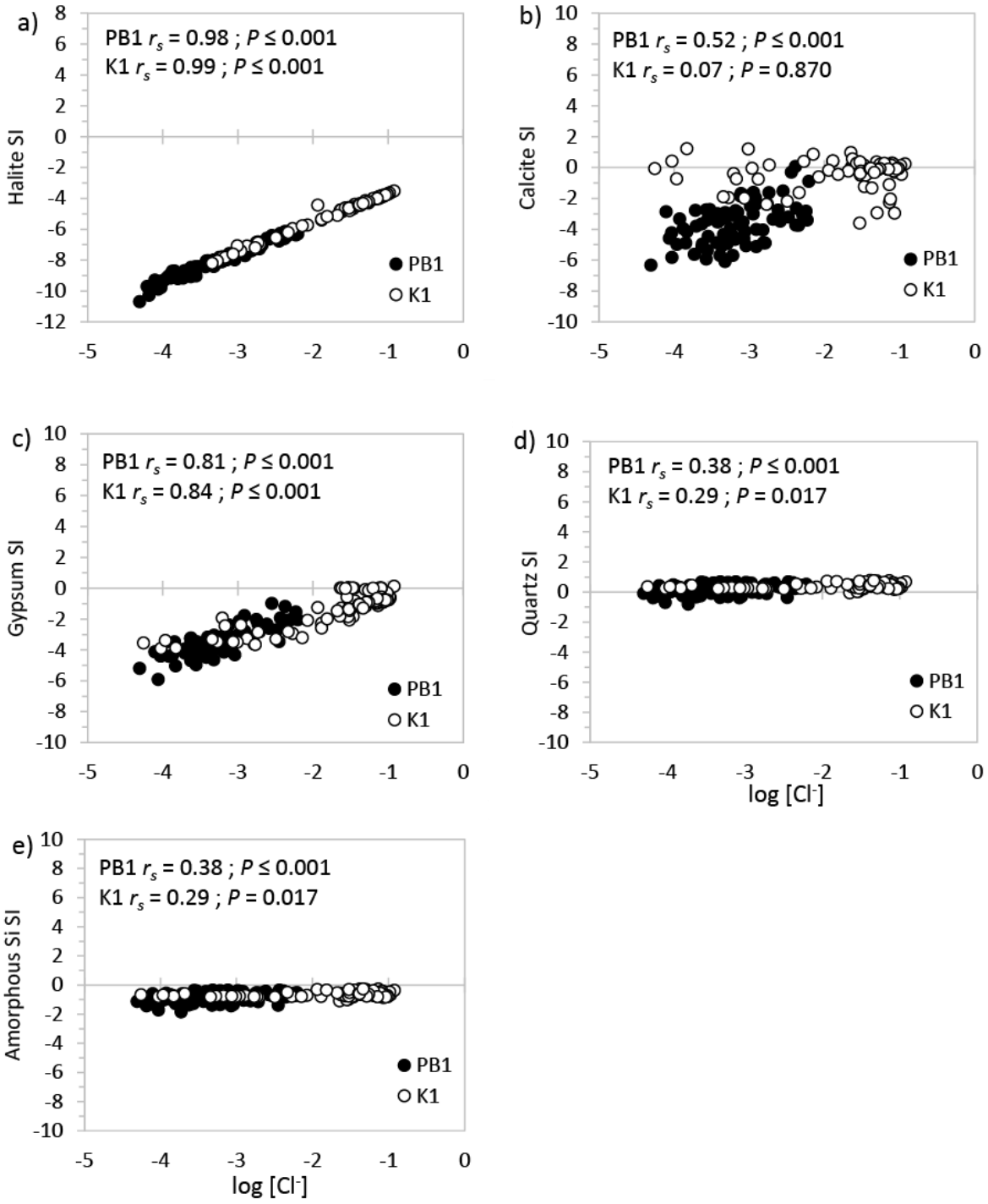

Figure 3.45: Saturation indices of a) halite, b) calcite, c) gypsum, d) quartz, and e) amorphous silica, against the ion activity of Cl for the 1:1 soil:water extracts of the heuweltjies in Piketberg (PB1) (black) and Klawer (K1) (white).

3.7.3 Saturation indices and relation to pH(H_2O)

Halite saturation indices showed no significant (P=0.080), or weak negative (r_s=-0.26; P=0.022), correlation with pH(H_2O) in PB1 and K1, respectively (Figure 3.46a). Therefore, halite saturation is not pH dependent. Calcite saturation indices showed significant, strong, positive correlations (r_s=0.87-0.90; $P \leq 0.001$) with pH(H_2O) in both PB1 and K1 (Figure 3.46b and d). Calcite saturation increases as pH(H_2O) increases where calcite reaches super saturation above pH(H_2O) 8. Gypsum saturation was not pH(H_2O) dependent and no significant correlation (P=0.270/0.130) between gypsum saturation indices and pH(H_2O) existed in both PB1 and K1 (Figure 3.46c). Quartz and amorphous Si saturation indices showed a strong positive correlation with pH(H_2O) in PB1 and shows an increase in saturation as pH increases (Figure 3.46e and f). In K1, quarts and amorphous Si saturation indices were not significantly (P=0.050) or weakly (r_s=-0.27; P=0.049) correlated with pH (Figure 3.46e and f). This suggests an indirect or secondary cause for the strong correlation in saturation with pH in PB1.

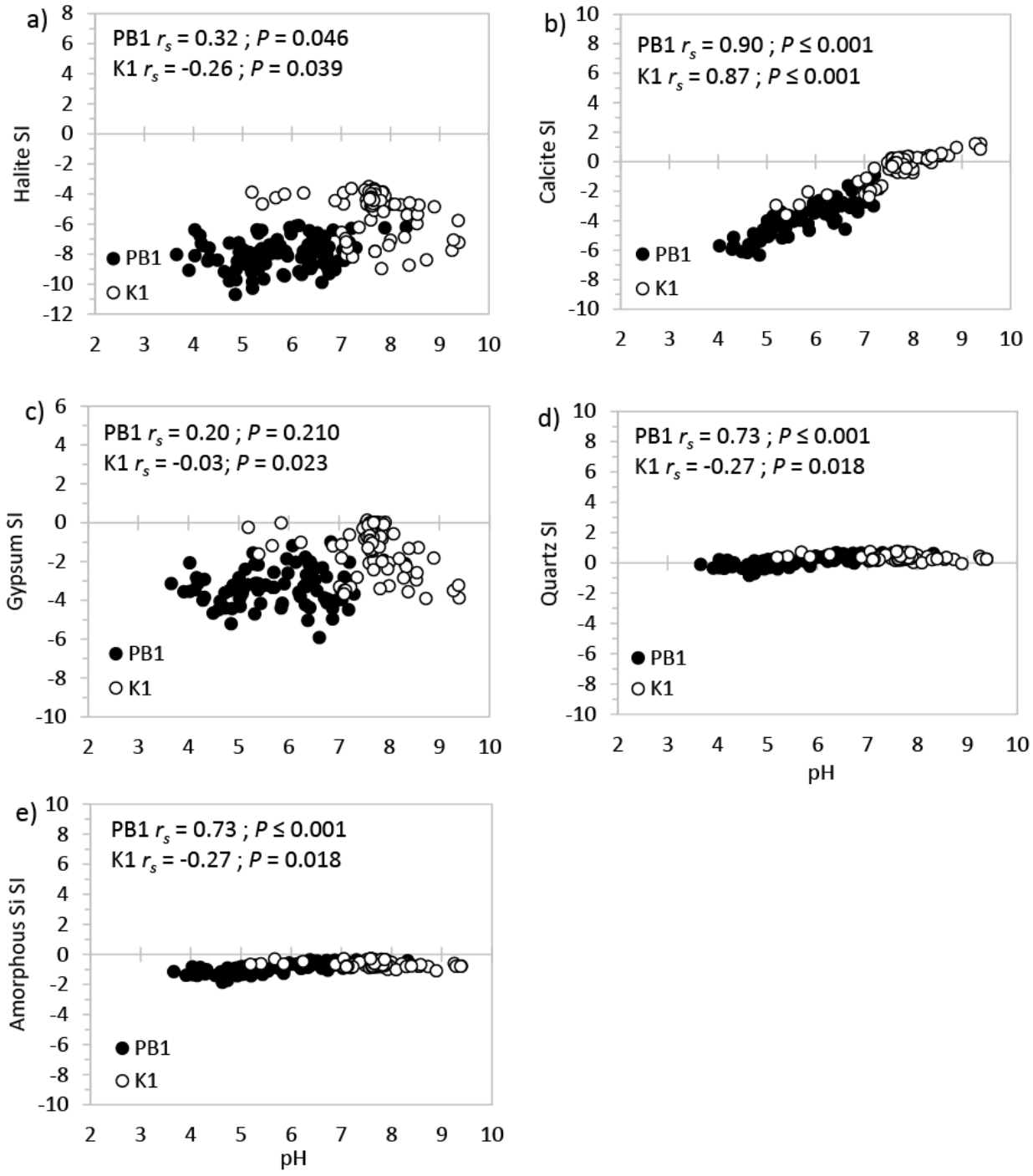

Figure 3.46: Saturation indices of a) halite, b) calcite, c) gypsum, d) quartz, and e) amorphous silica, against the pH(H_2O) for the 1:1 soil:water extracts of the heuweltjies in Piketberg (PB1) (black) and Klawer (K1) (white).

4 Discussion

4.1 Heuweltjie characterisation

4.1.1 Soil texture

Sandy loam or loamy sand textures of the Piketberg and Klawer heuweltjies indicate soil textures typical of the area. Ellis (1988) found that soils were predominantly sandy or loamy in the southern parts of the West Coast and the Knersvlakte. Elevated clay and silt contents, and finer textures in the topsoil of both Piketberg and Klawer heuweltjie soils compared to their inter-heuweltjie soils is consistent with findings reported of other heuweltjies (Ellis, 2002; Francis et al., 2007; Vermooten, 2019). The finer sand grade of the Piketberg and Klawer heuweltjie topsoils compared to inter-heuweltjie topsoil is also observed in heuweltjies of Namaqualand (Vermooten, 2019). The elevated levels of clay in termite mounds and surrounding topsoil have been attributed to transport of soil from subsurface horizons for maintenance of mound structure and other physiological functions such as foraging tunnels and chambers (Turner et al., 2006; Fey et al., 2010b). Gravel and stones are left behind in the deeper soil horizons because of their size resulting in the sorting of sediments through termite and other associated faunal activity (Fey et al., 2010b).

Vermooten (2019) also found that heuweltjie soils of the Namaqualand became coarser with depth when nearing dorbank in subsurface horizons as in both Klawer and Piketberg mounds. Particle size has an inverse effect on capillary rise (Yin et al., 2016). Coarse textured material contains larger particles, and therefore pores, which would not allow for significant capillary rise of water (Yin et al., 2016). Consequently, the coarse textured sandy subsoils and large macropores in both heuweltjies (termite channels, rodent burrows and fractured dorbank) would not allow water to enter the system through capillary rise but would rather facilitate downward preferential flow of solutes in mounds (Beven and Germann, 2013).

4.1.2 Mineralogy

The clay minerals of quartz and kaolinite of inter-heuweltjie soils in Piketberg and additional illite in Klawer are consistent with the findings of the winter rainfall areas of the West Coast (Bühmann et al., 2004). These clay minerals are not particularly rich in Ca or Mg and are not sodic, as weathering of sodic and Ca-rich parent material rather yields montmorillonite (Deer et al., 1966). Heuweltjie soils of Piketberg and Klawer show similar clay phase assemblages to

inter-heuweltjie soils but are additionally enriched in calcite, localised sepiolite and occasionally gypsum (in Klawer) (Figure 3.35 and Figure 8.18). Gypsum was also identified in heuweltjies located in the Buffels River catchment (Vermooten, 2019). In the study done on a heuweltjie near Papendorp, 70 km from the K1 heuweltjie at Klawer, no gypsum was found in the mound soils, however, sepiolite and palygorskite was identified (Francis et al., 2012a).

The presence of calcite in heuweltjie soils and absence thereof in inter-mound soils is consistent with the pattern observed in heuweltjie landscapes (Moore and Picker, 1991; Ellis, 2002; Potts et al., 2009; Francis et al., 2013; Schmiedel et al., 2016; Francis and Poch, 2019; McAuliffe et al., 2019a; Vermooten, 2019). Another carbonate mineral identified in the Piketberg mound (profile PB1W-16-180) was aragonite (Figure 3.28). Aragonite has not been identified in heuweltjies or termite mounds before and is more commonly found in shells of molluscs, pearls, and in caves (Deer et al., 1966). Francis (2008) also found aragonite in soils of fossil beaches in the Namaqualand. The primary precipitation of $CaCO_3$ from seawater occurs as the metastable form, aragonite and preferential aragonite precipitation only occurs at Mg:Ca ratios >2 (Sun et al., 2015). It is possible that the presence of sulphates and Mg favoured the precipitation of aragonite in small amounts in the Piketberg mound (Railsback, 2006).

4.2 Net direction of solute movement

4.2.1 Spatial chemical profiles of heuweltjies

The measured EC_a in the EMI survey indicates both the variation and the spatial distribution of salts in heuweltjies (van Gend et al., 2021). EMI survey results of mounds in Piketberg are similar to those generated in the more arid and saline soils of the Buffels River catchment (van Gend et al., 2021). This confirms that heuweltjie soils consistently contain higher concentrations of salts compared to inter-mound soils (Moore and Picker, 1991; Francis et al., 2013; van Gend et al., 2021). The EC_a of mounds at the Piketberg site showed an increase in EC from 25 to 50 cm depths (Figure 3.37 and Figure 8.19). This suggests the downward movement of salts in the heuweltjies of the Piketberg site. However, EC showed a decrease from 50 to 90 cm depth in the survey of Piketberg which was not observed in the survey of Buffels River (van Gend et al., 2021). The EC_a trends also differed from the 1:1 soil water EC_w trends of samples collected from the excavated heuweltjie, that showed a consistent increase in EC with depth (Figure 3.38b and Figure 8.20b). The decrease in EC_a of the EMI survey at 90 cm depth could be explained by the presence of the gravelly colluvium or nodular dorbank starting at similar depths in heuweltjies, assuming that the morphologies are similar to those of

the excavated mound (Figure 3.3). The presence of an insulating gravel layer is known to cause a reduction in the EC_a and is likely the explanation for the decrease in EC at 90 cm (Friedman, 2005; Abdu et al., 2017; Heil and Schmidhalter, 2019). EC_w (maximum 161.8 mS/m) measurements were much higher compared to EC_a (maximum 30.9 mS/m). However, both EC_a and EC_w spatial trends show an increased EC in heuweltjie centres. A gradual lateral decrease occurs from the centre to the lowest EC values in the inter-heuweltjie soils.

Ion concentrations of Na, Mg, K, Ca, Cl, and SO_4 had an overall significant increase with depth in the soils of the Piketberg and Klawer mounds (Table 3.1 and Table 3.2) and was highest in the centre of the heuweltjies (Figure 3.38 and Figure 3.42). Both Piketberg and Klawer heuweltjies showed pH(H_2O) trends consistent with previous studies indicating higher pH values in the mound centre compared to inter-mound soils (Kunz, Hoffman and Weber, 2012; Schmiedel *et al.*, 2016; McAuliffe *et al.*, 2019a). The lowest pH(H_2O) values were found in the inter-heuweltjie soils for both mounds and the highest pH(H_2O) values were present in the centre of both mounds (Figure 3.38a, Figure 3.41a and Figure 8.20a). In the Klawer mound, pH(H_2O) showed a significant negative correlation with EC, Na, and Cl and a strong positive correlation with alkalinity (Table 3.2). pH(H_2O) values also exceed 8.5 in the topsoil in the centre of the heuweltjie (Figure 3.41a). This suggests that the process of alkalinisation (Schaetzl and Anderson, 2005) is occurring in topsoil of the centre of the heuweltjie. Neutral salts are mobilised in the soil during alkalinisation causing a decrease in EC. However, exchange complexes of clay minerals maintain Na in excess which causes the soil pH to increase as charge balance is kept through the carbonate equilibria (van Breemen et al., 1983; Schaetzl and Anderson, 2005). Cl would migrate downward resulting in a pH increase in the topsoil and a decreased pH in the subsoil of the heuweltjie centre due to the presence of neutral salts and the process of salinisation (Schaetzl and Anderson, 2005). In the Piketberg mound, pH(H_2O) remains below 8.5 and is not negatively correlated with EC, Na, or Cl. However, high pH(H_2O) and corresponding low EC in the centre of the Piketberg mound between 14 and 24 m cross-section distances suggests a similar trend is occurring (Figure 3.38a and Figure 8.20a).

Dissolved Si trends suggest the influence of pH(H_2O) on mobilisation. In both the Piketberg and Klawer mounds, the highest dissolved Si concentrations are associated with dorbank, as expected (Ellis, 1988, 2002; Francis, 2008). In the heuweltjie of Piketberg, the positive correlation of Si with depth in the centre of the mound suggests that the pH(H_2O) close to 8.5 in the centre increases the mobility of Si (Schaetzl and Anderson, 2005). The increased pH aids the migration of Si (Ellis, 1988) towards the base of the heuweltjie along with other salts

(Figure 3.39i and Figure 8.20i). Lower pH(H_2O) values and the lack of Si cemented horizons in the inter-heuweltjie soils explain the low Si concentration in these soils (Drees et al., 1989). In the Klawer heuweltjie, pH(H_2O) values exceed 9 in the centre of the mound which suggests the mobilisation of Si to move downward through the centre of the mound where the permeable, fractured dorbank and high pH allows dissolved Si to be leached downward with salts (Figures 3.39a and 3.40i). Contrasting to the latter, lower pH values in the heuweltjie edges and inter-mound soils combined with impermeable platy dorbank prevents the mobilisation and leaching of Si. Si is retained in the platy dorbank on the edges and inter-mound soils resulting in higher concentrations (Figure 3.41a and Figure 3.42i). Vermooten (2019) found that heuweltjie pH(H_2O) was highest in inter-mound topsoil resulting in Si and salt mobilisation (via alkalinisation) from the inter-mound soils toward the mound centre. However, both this study and that of Vermooten (2019) showed pH(H_2O) trends consistent with the downward migration of salts through the centre of the heuweltjie.

Amorphous Si saturation also increases with depth and coincides with the presence of dorbank (Figure 3.40a, Figure 3.43a and Figure 8.21a), suggesting that the dorbank is in phase with the current pedochemical environment. However, it would then be expected that Amorphous Si would show saturation in the areas corresponding to dorbank. This is because 1:1 soil:water extracts were used and one could expect amorphous Si saturation if saturated pastes were used, giving a more accurate representation of the current pedochemical environment (Sonmez et al., 2008; Aboukila and Norton, 2017). Additionally, saturation indices of the other minerals in this study should also be considered bearing the difference between 1:1 soil: water extracts and saturated pastes in mind.

Halite remained undersaturated throughout all the heuweltjie profiles in Piketberg and Klawer. Gypsum remained undersaturated throughout the Piketberg mound and only a few samples were saturated with gypsum in the Klawer mound as confirmed by the mineralogy (Figure 3.35). Calcite reached saturation in both mounds and can be validated by its presence in the mineralogy and field observations (Figure 3.28 and Figure 3.35). Of the three minerals, halite is most soluble followed by gypsum and lastly calcite. Therefore, the depth at which these minerals are most saturated would give a good indication of the net direction of water movement. Higher halite saturation indices occur at the base of both Piketberg and Klawer heuweltjie trenches at greater depths compared to the highest gypsum and calcite saturation indices (Figure 3.40, Figure 3.43 and Figure 8.21). In addition, gypsum saturation indices are higher at greater depths compared to calcite saturation indices in the west wall of the Piketberg

mound and the Klawer mound (Figure 3.41d and Figure 8.21d). Since gypsum is more soluble than calcite, gypsum would precipitate at greater depths than calcite if the net water movement occurs downward within the heuweltjies (Casby-Horton et al., 2015). Therefore, given the downward separation of increasingly soluble minerals, water is moving in a downward direction in both Piketberg and Klawer mounds. Similariy, a net downward movement of water was observed in heuweltjies of the Buffels River catchment (Vermooten, 2019).

Since the depth to the calcite horizon is proportional to the mean annual precipitation (Egli and Fitze, 2001; Zamanian et al., 2016), a greater depth of leaching occurs in Piketberg due to higher mean annual precipitation compared to Klawer. The depths at which calcite and gypsum are saturated in Piketberg and Klawer therefore, manifests differently due to mean annual precipitation differences. In the Piketberg heuweltjie, calcite reaches saturation at greater depths compared to the mound in Klawer (Figure 3.40, Figure 3.43 and Figure 8.21), similarly, gypsum, reaches saturation at shallower depths in the Klawer heuweltjie compared to gypsum that remained unsaturated in the Piketberg heuweltjie (Figure 3.40, Figure 3.43 and Figure 8.21).

4.3 Sources and preferential movement of salts

Both mounds showed strong evidence of salt transport within biogenic features. In Piketberg EC, Na, Cl, Ca, SO_4, Mg, K, and dissolved Si show a downward leaching gradient from concentrated areas of termite channels, frass piles and rodent burrows and then further through the loose, gravelly dorbank in the centre of the mound (Figure 3.38, Figure 3.39 and Figure 8.20). The large channel between profiles PB1E-16 to PB1E-18 and rodent food pile at profile PB1E-21 clearly shows the downward leaching of salts from the interpolated maps of EC, Na, Cl, Ca, SO_4, and Mg (Figure 3.38 and Figure 3.39). In Klawer the EC shows a clear leaching path where salts are moving from active termite channels in the vesicular dorbank, through the fractured and granular dorbank to the base of the trench in the K1-15 profile (Figure 3.41b). Between profiles K1-18 to K1-21 preferential flow of solutes can be observed to occur from vesicular dorbank associated with many channels, through fractured platy and granular dorbank to the base of the trench (Figure 3.41b). The same preferential flow paths are observed for Na, Cl, Mg, and K (Figure 3.41 and Figure 3.43). Similarly, preferential flow of Ca and SO_4 seems to be occurring through the vesicular dorbank between profiles K1-13 to K1-23 and an active termite channel at profile K1-15 to the base of the trench (Figure 3.41e and f).

The loose, gravelly dorbank, fractured platy dorbank, high concentration of indurated termite channels, and rodent burrows in the centre of heuweltjies create preferential flow for water and accompanying solutes by serving as conduits during large rainfall events. These preferential areas of water and solute flow magnify the process of leaching compared to the surrounding soils (Beven and Germann, 2013). As the centre of the heuweltjie has more porous soils, solutes preferentially move through these profiles and cease movement at textural discontinuities, such as denser channel linings, or when the wetting front stops (Beven and Germann, 2013). Additionally, large animal burrows on the surface of the heuweltjies (Figure 4.1) would harvest water during the winter rainfall season. The water would then be channelled into the mound

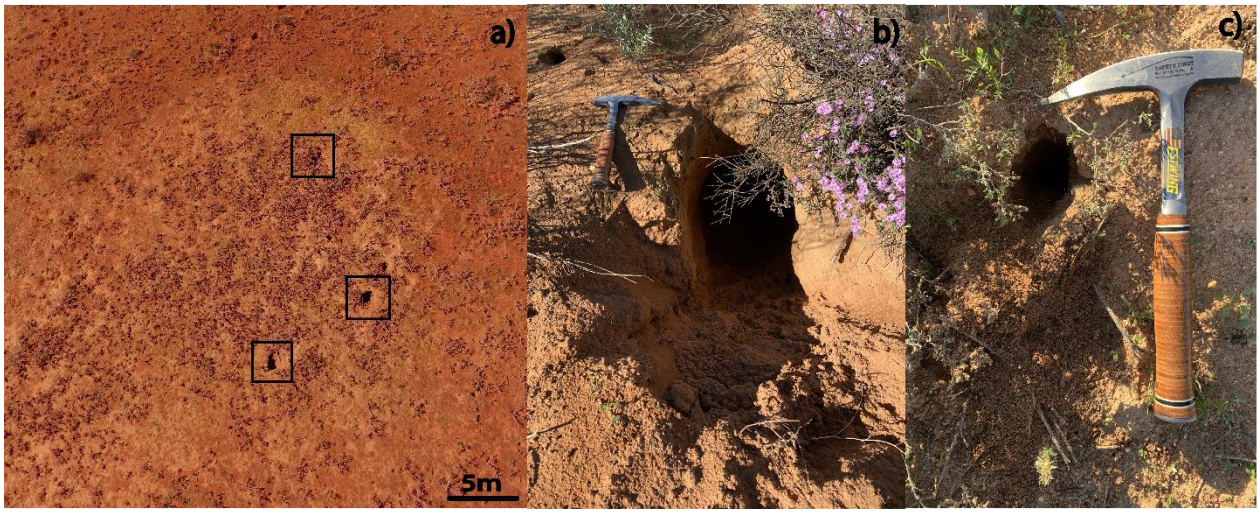

Figure 4.1: a) Large animal burrows (indicated with black boxes) of a heuweltjie at the Klawer site. b) and c) Animal burrows observed on heuweltjies of the Piketberg site.

resulting in salts in the heuweltjie being flushed towards the groundwater system due to the large number of preferential flow pathways.

The highest concentrations of all ions, EC, and alkalinity were associated with biogenic features such as termite channels, frass chambers, and rodent burrows. Most notable is the concentration of Ca in the Piketberg mound, where the highest concentrations are almost always associated with abundant termite channels and rodent food piles (Figure 3.38, Figure 3.39 and Figure 8.20). The higher EC, and ion concentrations of the Klawer mound were also associated with soils where biogenic activity was prevalent such as the vesicular dorbank with abundant channels or below active termite channels (Figure 3.41 and Figure 3.42). The Mg, Ca and SO_4 concentrations of the Klawer mound were prevalent as these ions were clearly concentrated in the centre of the mound where most termite channels were observed in the vesicular and gravelly dorbank (Figure 3.41 and Figure 3.42).

This suggests that termites and rodents play a direct role in the accumulation of salts within the heuweltjie soils. Elevated salt levels could be attributed to termites bringing Na, Cl, Ca, Mg, K, SO_4, and Si rich plant material into the soil (Ellis, 2002; Francis et al., 2013). This would allow for the accumulation of salt-rich plant material in channels and chambers and periodic flushing of salts during rainfall events. Ion accumulation is also evident in the absence of concentrated zones of ions in inter-heuweltjie soils where biogenic features are scarce or lacking. However, it is also possible that the elevated ion concentrations could be the result of the faster drying rate of channels and tunnels. The large voids created by burrows and channels would arrest water flow and allow salts to remain behind as the water evaporates into the channels. This is particularly clear for calcite in the Piketberg heuweltjie where precipitation at textural boundaries occurred above active termite channels or below channels acting as solute conduits (Figure 3.40 and Figure 8.20). The elevated ion concentrations observed for biogenic features could therefore have a dual origin. Preferential flow paths will remain wetter than the rest of the soil matrix since water would move freely through these paths (Liu et al., 1995). It is possible that preferential flow would allow rapid draining of rainfall and prevent the leaching of salts from the soil matrix. This would cause the salts to remain in the heuweltjie soil matrix. However, since almost all ions show an increase with depth throughout the heuweltjie soil matrix it can be assumed that leaching does occur in the soil matrix of both heuweltjies. Infiltration studies on termite mounds using dyes (for example Chen et al. (2019)), would be beneficial to determine the extent and rate of leaching, preferential flow and runoff that occurs within heuweltjies. The presence of gypsum in the Klawer mound can also be ascribed to sufficient concentrations of Ca and SO_4 for precipitation to occur, based on corresponding ion concentrations and gypsum saturation indices (Figure 3.41e, f and Figure 3.43d). It has been proposed that *M. viator* carries and stores Ca-rich plant material in heuweljies (Midgley and Hoffman, 1991; Moore and Picker, 1991; Francis et al., 2013), leading to the build-up of bases and formation of a (petro)calcic (Ellis, 2002) horizons or localised sepiolitic areas where plant material is Mg-enriched (Francis et al., 2013). Studies by Kunz et al. (2012), McAuliffe et al. (2014) and McAuliffe et al. (2019a) suggested the same. Therefore, it is also likely that termites play a direct role in the accumulation of sufficient ions through plant material for minerals such as gypsum, sepiolite and calcite to precipitate in the centre of the mound.

Although many studies allude to termites being responsible for salt accumulation in heuweltjies, it is still unclear if in fact the salts in heuweltjies can be attributed to termites due

to the complex nature of heuweltjie systems. Plants of arid and semi-arid regions can contain high salt concentrations such as *Mesembryanthemum crystallinum* (Bartels and Sunkar, 2005) observed in abundance on heuweltjie soils of the mounds in Klawer during this study. However, no study has indicated whether the salts, introduced to the soil through termites carrying plant material, originate from plants accumulating salt from the soil, or due to salts accumulating on plant surfaces through atmospheric deposition. Therefore, additional research is necessary to determine the source and accumulation of salts in plants surrounding heuweltjies and consequently the soils of heuweltjies. A parallel study of Vermonti (in preparation) is investigating salts associated with harvested vegetation.

Vermooten (2019), found clay, feldspars, and gypsum associated with termite excrement in a sample collected within a heuweltjie in Buffels River but no gypsum was identified in the soil surrounding the frass chamber. It was speculated that the termites may consume some minerals in the soils unintentionally and transfer them throughout the heuweltjie via their excrement. This speculation was supported by the study of Francis *et al.* (2013) that indicated even though *M. viator* is not a soil feeding species it redistributes soil and minerals throughout mound soils. Given that broad kaolinite peaks, and sharp quartz peaks were identified in the XRD pattern of termites sampled at profile PB1-22.5 (Figure 3.29) in Piketberg, the presence thereof could also be attributed to redistribution of minerals by termites. Furthermore, the presence of feldspars and clay minerals in termite excrement also allude to termite mediated soil transport and it is possible that termites unintentionally ingest minerals whilst moving soil. The identification of Ca oxalate in the mineralogy of termite excrement and frass piles in both Klawer and Piketberg further alludes to the role of termites in concentrating minerals and ions within heuweltjies. The occurrence of Ca oxalate in the termite frass piles bears further significance due to its role in the oxalate-carbonate pathway (OCP) (Uren, 2018). Although still speculative, the role of the OCP has been suggested to occur in heuweltjies and the role in Ca oxalate as a precursor for calcium carbonate in heuweltjie soils has been previously proposed (Francis et al., 2013; Francis and Poch, 2019; McAuliffe et al., 2019a). The identification of Ca oxalate in termite frass piles in both Piketberg and Klawer adds to the possible ubiquitous nature of Ca oxalate associated with heuweltjies. This adds further evidence to the possible role of the OCP and implied carbon sequestration (Uren, 2018) in heuweltjies.

An alternative hypothesis is that the source of salts for both heuweltjies in Piketberg and Klawer could originate from the groundwater. This is especially plausible due the winter

rainfall climate of the study areas and the possible development of a perched water table during the wet season and consequent fluctuation during seasonal dry and wet periods. A fluctuating groundwater table can aggravate the salinisation process in the soil profile (Ibrahimi et al., 2014). Saline groundwater enters the soil and is further transported to the rootzone through capillary rise driven by strong evaporative forces (Hillel, 2004; Ibrahimi et al., 2014). However, if saline groundwater would be responsible for introducing salts in the soils of heuweltjies the sequence of precipitation of increasingly soluble minerals (in order halite, gypsum, calcite) is expected to be the reverse of what is observed in the current study. Accumulation of salts at biogenic features such as the large rodent food chamber in the Piketberg mound (Figure 3.38) and termite channels (Figure 3.38 and Figure 3.41) further eliminates the possibility of groundwater capillary rise contributing to the accumulation of salts within these features. Large biogenic conduits would not be able to facilitate groundwater rise to concentrate salts within rodent or termite nests and burrows. The use of $^{87}Sr/^{86}Sr$ ratios and major ion chemistry of the groundwater in Namaqualand has suggested that salts in the groundwater of the region is linked to dry deposition of marine aerosols (van Gend et al., 2021). In addition, the groundwater salinity levels correlated with salinity levels in heuweltjies and it was proposed that heuweltjie salts (originating from marine aerosols) are flushed to the groundwater system during sporadic precipitation events and that the uprise of groundwater is not responsible for salinity in the mounds (van Gend et al., 2021).

4.3.1 Chemical signature of salts

It has been established that the parent material does not indicate a possible salt source from the clay mineralogy and groundwater capillary rise is an unlikely source of salts in this study. However, given that the biogenic features strongly corresponded to salt accumulation it is likely that salts are brought into heuweltjies through foraging fauna. This suggests that the source of salts is likely to come from the surface. Marine aerosols are known to have a strong influence in the region (Smith and Compton, 2004; Soderberg and Compton, 2007; Francis et al., 2020). Comparing the salt signature of heuweltjies to the seawater dilution line can be used to assess if the source of salts is in fact of marine origin.

Cl^- is a conservative solute because anion exchange is minor, it remains in solution until halite saturation and if it is precipitated it is redissolved quantitatively by subsequent wetting (Eugster and Jones, 1979). Conservative solutes can be used to monitor the concentrations of non-conservative ions (K^+, Ca^{2+}, Mg^{2+}, SO_4^{2-}, and HCO_3^-) in solution, that are influenced by

removal mechanisms such as degassing, precipitation of minerals, and ion sorption (Eugster and Jones, 1979). These mechanisms function across the full evaporative concentration with slopes less than that of the conservative solutes (Eugster and Jones, 1979). In the present study, halite remained unsaturated at all Cl^- concentrations for both Piketberg and Klawer heuweltjie ranges (Figure 3.45a). Despite possible exchange reactions Na^+ behaved conservatively in both heuweltjie ranges (Figure 3.44a) and linear relationships are evident in the ranges of both heuweltjies (Figure 3.44). K^+, Ca^{2+}, Mg^{2+}, and SO_4^{2-} activities all showed a significant, linear increase as Cl^- activity increased but at slopes less than that of the conservative solute Na^+ (Figure 3.44a to h).

In both Piketberg and Klawer hueweltjies, ratios of Na^+/Cl^- and Mg^{2+}/Cl^- ratios were similar to seawater across the entire concentration range (Figure 3.44a and d). The strong marine signature indicates that these ions originate from a seawater source. The wider coastal region displays similar Na^+/Cl^- and Mg^{2+}/Cl^- ratios, following the seawater dilution line (Smith and Compton, 2004; Soderberg and Compton, 2007; Francis, 2008; Francis et al., 2020). Heuweltjies of the Buffels River also showed similar Na^+/Cl^- and Mg^{2+}/Cl^- marine signatures (Vermooten, 2019). Ca^{2+}/Cl^- and SO_4^{2-}/Cl^- ratios in the Piketberg and Klawer heuweltjies were slightly elevated compared to the ratios of seawater (Figure 3.44c and e). Elevated Ca^{2+}/Cl^-, K^+/Cl^- and SO_4^{2-}/Cl^- ratios compared to seawater were also found in Citrusdal, located in the Boontjies River subcatchment of the Olifants/Doorn drainage basin (Soderberg, 2003; Soderberg and Compton, 2007). Elevated Ca^{2+}/Cl^- and K^+/Cl^- ratios were proposed to be derived from the land through windblown particles (mainly clays) that are dissolved by rainwater through rainout and washout processes (Soderberg, 2003; Soderberg and Compton, 2007). Dry Berg Winds from the interior of southern Africa potentially carry these particles as dust to the Atlantic coast during winter, depositing nutrient rich clay minerals in this coastal region (Soderberg and Compton, 2007). Soderberg and Compton (2007) suggested that K^+ inputs are also likely derived from inputs of organic matter. Additionally, the elevated SO_4^{2-}/Cl^- ratios compared to seawater can be attributed to atmospheric tranport of aerosols derived from the oxidation of dimethyl sulphide originating from the upwelled waters of the Benguela Current (Eckardt and Spiro, 1999). This was also proposed to be the cause of elevated SO_4^{2-}/Cl^- ratios in the Citrusdal area (Soderberg and Compton, 2007). The heuweltjie salts in the Olifants/Doorn catchment is therefore derived from marine aerosols and additionally possibly windblown particles. However, this does not explain the concentration of salts in heuweltjie

centres and lack thereof in inter-heuweltjie soils as surface deposition of salts would allow for a more even distribution throughout the soils.

4.3.2 Trends relating to mineral saturation

Calcite, being the least soluble followed by gypsum and then halite, was saturated over the entire Cl^- range for the Klawer mound (Figure 3.45b). This is consistent with field observations and mineralogy that indicated calcite presence in most samples of the Klawer heuweltjie. The majority samples of the Klawer mound reached calcite saturation at log[Cl^-] >-1.5 (Figure 3.45b). This parallels Ca^{2+} activities (Figure 3.44c) that was highest at log[Cl^-] >-1.5 and HCO_3^- activities (Figure 3.44f) that showed a decrease in the Klawer mound at log[Cl^-] >-1.5. Francis et al. (2020) found increasing Ca^{2+} and decreasing HCO_3^- in coastal soils containing calcite. The decrease in concentration of HCO_3^- in K1 (Figure 3.44f) and corresponding increase in Ca^{2+} is consistent with its removal from solution, during equilibrium precipitation of calcite (Eugster and Jones, 1979). Decreasing HCO_3^- activities accompanied by increased Ca^{2+} is consistent with calcite precipitation at the first 'chemical divide' in the Hardie-Eugster model of brine evolution (Hardie and Eugster, 1970; Eugster and Jones, 1979). Furthermore, calcite saturation increased at a ratio less than 1:1 in Klawer and saturation even decreased slightly at the highest degree of enrichment (log[Cl^-] >-1.5) for some samples. Eugster and Jones, (1979) stated that decreasing HCO_3^- activities at increased ion concentrations, accompanied by a decrease in calcite saturation indicates that HCO_3^- is the limiting factor in calcite precipitation. The precipitation of calcite further affects the ratios of Ca^{2+}/Cl^- and HCO_3^-/Cl^- away from the conservative ion slope of Na-Cl causing a change in the original marine ratios.

In the Piketberg range, calcite saturation increases with increased Cl^- concentration and only three samples are at or near saturation around log[Cl^-] = -2.2 (Figure 3.45b). This is consistent with only a few profiles in the centre of the Piketberg mound showing calcite saturation and most of the heuweltjie soils remaining unsaturated with regards to calcite (Figure 3.40c and Figure 8.21c). Furthermore, HCO_3^- concentrations remain unchanged (Figure 3.44f) over the full range of concentration since calcite precipitation does not occur to such an extent that it caused a significant decrease in HCO_3^-/Cl^- ratios (Figure 3.44f).

As the decrease in HCO_3^- concentration becomes the limiting factor for calcite precipitation around log[Cl^-] >-1.5 (Figure 3.44f) it is possible that Ca^{2+} becomes available for gypsum precipitation to take place (Francis et al., 2020) in the Klawer mound. This is supported by the increase in gypsum saturation with degree of concentration and eventual equilibrium

precipitation around log[Cl^-] >-1.5 (Figure 3.45c) in the Klawer mound and the corresponding slight decrease in calcite saturation at around log[Cl^-] >-1.5 (Figure 3.45c). Furthermore, Ca^{2+}/Cl^- and SO_4^{2-}/Cl^- ratios of Klawer were affected away from original 1:1 ratios and Na-Cl slope around log[Cl^-] >-1.5 showing that gypsum precipitation limits any further increase of Ca^{2+} and SO_4^{2-}. Gypsum saturation is consistent with the mineralogy where a few samples in the centre of K1 showed the presence of gypsum (Figure 3.35). For the Piketberg heuweltjie, gypsum saturation increased in a 1:1 ratio as the degree of evaporation increased but remained unsaturated throughout all samples.

Figure 3.46 clearly shows that pH in the heuweltjie soils is controlled by calcite and vice versa as calcite precipitation is limited to pH values above 8. In addition, only calcite (Figure 3.46b) showed a significant increase in saturation with increased pH(H_2O) compared to halite, gypsum, quartz and amorphous Si saturation (Figure 3.46a, c to e). The common ion effect between calcite and gypsum can again be observed in the SI vs pH(H_2O) graphs through the increase of calcite saturation above pH(H_2O) 8 (Figure 3.46b) and corresponding decrease in gypsum saturation above pH(H_2O) 8 (Figure 3.46c).

In the Piketberg mound, both quartz and amorphous Si showed a positive correlation with pH(H_2O) (Figure 3.46a, c to e). A plausible explanation is that the highest degree of calcite saturation and H_4SiO_4 concentrations were both associated with gravelly dorbank in the Piketberg mound resulting in a covariation. The positive correlation of quartz and amorphous Si with pH(H_2O) is therefore mainly a result of the corresponding calcite impregnation in the gravelly dorbank in the centre of the mound and not necessarily because of a pH increase as most pH(H_2O) values fall below 8.5. The significant negative correlation of quartz and amorphous Si in the Klawer mound is a secondary effect of calcite saturation. Calcite saturation, and consequently pH, is highest in the centre of K1 (Figure 3.43c). H_4SiO_4 solubility increases above pH 8.5 (Schaetzl and Anderson, 2005) and this results in the negative relationship between quartz and amorphous Si with pH. Quartz and amorphous Si saturation is directly dependent on the concentration of the uncharged solute, H_4SiO_4, and their solubilities are expressed only in terms of this aqueous species. Therefore, the best explanation for mostly unchanged H_4SiO_4 concentrations with increased ion concentration in both Piketberg and Klawer heuweltjies is that it has reached equilibrium with quartz and amorphous Si (Figure 3.46d and e). This is consistent with the observed morphology (dorbank) suggesting that dorbank is in phase with the current pedochemical environment and is not relict. Sepiolite,

quartz and amorphous Si have been proposed to regulate the H_4SiO_4 concentration in the Namaqualand soil system (Francis et al., 2020).

4.4 Implications of heuweltjie chemistry in the Olifants/Doorn catchment

Land management is intrinsically related to water and because large areas of the Olifants/Doorn catchment constitutes large and small scale farms, farming enterprises have to take a number of variables into consideration when assessing the impact on water sources when developing land use plans (Knüppe and Meissner, 2016). Soil constitutes a major factor of these variables included for consideration. Because the Olifants/Doon catchment contains heuweltjies as a variable in the soil factor of land management, it is important to incorporate the possible influence heuweltjies could have on water resources during land use. In the present study, the farm located in Piketberg manages the occurrence of salt affected heuweltjie soils and the adverse effect of these soils on crop productivity and health by removing the carbonate horizon and essentially the centre of the heuweltjie and filling it up with soil from adjacent areas. This seems to be the only solution to cultivating perennial type crops on heuweltjie soils. However, this is an extremely expensive and time-consuming operation. Many farmers deep rip heuweltjies for annual and perennial crop production and it is unclear if this would aggravate the transfer of salts to groundwater. It is also uncertain what the influence of continuous tilling would be on the lateral and vertical redistribution of salts and how it would affect less saline inter-mound soils. Another alternative would be to apply heavy or continuous irrigation to try and wash the salts from the soil. This would in turn, given the findings of the current and previous (Vermooten, 2019; van Gend et al., 2021) studies, possibly aggravate the salinisation of groundwater in the region. The best solution to adapt to heuwetjie soils would be to work and plant around them. This would constitute unconventional farming practices but could be the only solution to the heuweltjie-human interaction issue.

The present study highlights the often neglected influence termites have on the larger soil environment with reference to soil profile development and hydrology. Mound soils are a stark contrast to the shallow inter-mound soils that gives a more accurate representation of the surrounding pedogenic environment. Several studies highlight the increased rate of water infiltration and microporosity of soils affected by termites (Léonard and Rajot, 2001; Bargues Tobella et al., 2014; Ahmed II et al., 2019). Research indicating that hydrological properties of termite mounds are contributing to groundwater chemistry and recharge is receiving increased attention (Vogel et al., 2004; Bargues Tobella et al., 2014; Mills and Sirami, 2018; Ahmed II

et al., 2019). However, preferential flow is not observed in all termite affected soils. Conical mounds with steep slopes, fine textures and crusts repel water preventing leaching and allowing solutes to accumulate in mounds (Watson, 1969; Erens et al., 2015), Heuweltjies are dome shaped and should theoretically also allow most rainwater to be directed away from the centre. However, large faunal burrows and channels connected to the mound surface retain water and funnel solutes preferentially through the mound. The ecosystem hotspot created by heuweltjies therefor allows for greater leaching efficiency compared to surrounding soils. The effect heuweltjies have on groundwater recharge is difficult to measure even though several studies on termite mounds indicate increased infiltration and porosity of mound soils (Léonard and Rajot, 2001; Jouquet et al., 2016). However, investigation into termite affected soil chemistry, downward movement of salts and the groundwater chemistry would provide support to the possible role of termite affected soils in groundwater recharge. The association of termite mounds with shallow groundwater (Ahmed II et al., 2019) and their abundance in arid and semi-arid landscapes warrant their inclusion in groundwater quality research.

If salts in heuweltjies and other termite affected soils are being flushed to the groundwater during precipitation events, mounds would have an inevitable contribution to groundwater salinisation. However, if increasingly saline groundwater is used for agricultural purposes on already salt affected heuweltjie soils, a serious threat awaits the groundwater quality of the Olifants/Doorn catchment and larger West Coast.

5 Conclusions

Heuweltjie soils show a large degree of bioturbation as many channels, burrows, and frass chambers. The Piketberg and Klawer heuweltjies have sandy soil textures typical of the area but are enriched with clay and silt compared to inter-mound soils. The increased coarse texture of mound soils with depth and large macropores excluded groundwater capillary rise as a source for salt concentration in mounds. Both the heuweltjies were enriched with calcite compared to inter-mound soils, and in Klawer, gypsum was present exclusively in heuweltjie soils of the mound centre. Clay mineralogy of mound soils showed quartz, kaolinite and additionally illite in Klawer, indicating that heuweltjie salts are unlikely significantly derived from the parent material.

Heuweltjies in the Olifants/Doorn catchment have salt concentrations that are markedly higher compared to inter-heuweltjie soils. Major ion concentrations of Na^+, Cl^-, Mg^{2+}, Ca^{2+}, SO_4^{2-} and EC increased with depth in both mounds. Saturation indices of minerals from solution modelling supported field observations and mineralogy. The vertical distribution of increasingly soluble minerals of calcite and gypsum indicated that net water movement occurs downward within both mounds of the study, potentially transferring salts from heuweltjie soils to the groundwater via preferential flow. This suggests that in both the hot-summer Mediterranean climate of Piketberg and hot, semi-arid climate of Klawer the net direction of water movement is downward. These results show similar trends observed in the more arid Buffels River catchment (Vermooten, 2019; van Gend et al., 2021), and suggests that heuweltjie salts are moving downward in both highly arid and higher rainfall regions. Gypsum remained unsaturated and calcite was saturated at greater depths in the mound of Piketberg compared to the mound in Klawer due to a greater mean annual precipitation in Piketberg. Salts in the heuweltjies of higher rainfall therefore have greater leaching potential and chance of entering the groundwater system.

The solutes in these heuweltjies show a marine signature. In Klawer, the precipitation of calcite and gypsum in heuweltjies adjusted the ratios of Ca^{2+}/Cl^-, HCO_3^-/Cl^- and SO_4^{2-}/Cl^- away from their original marine ratios. In Piketberg, calcite precipitation was only observed in a few profiles in the mound centre and did not affect the Ca^{2+}/Cl^- and HCO_3^-/Cl^- ratios away from their marine signature. The pH(H_2O) of both heuweltjies was highest in the centre of the mound. Mineral saturation plotted against pH(H_2O) clearly showed that the pH of mounds is controlled by calcite and vice versa. Salts in heuweltjies are not evenly distributed as would be

expected by even deposition of marine aerosols. Heuweltjie salts are rather concentrated in hotspots associated with biogenic features such as termite channels and rodent burrows, indicating that faunal activity is likely responsible for the concentration of salts from the surface to mound centres. The high concentrations of soluble ions associated with termite channels and rodent burrows indicate that termites and rodents play a part in concentrating salts in heuweltjies by bringing Na^{+}, Cl^{-}, Mg^{2+}, Ca^{2+} and SO_4^{2-} into soils. Interconnected preferential flow paths in mound soils created by faunal activity aid in the movement of these solutes towards the groundwater.

This study adds strong evidence to the hypothesis that heuweltjie salts are generated within mounds, possibly through biological activity, and are translocated to the groundwater. This study further supports the important impact of termites in the pedogenic environment and groundwater of arid to semi-arid landscapes. The findings in this study constitutes further research on the impact of termite affected soils in groundwater salinisation of the larger West Coast and southern-Africa.

Further groundwater studies are needed in the Olifants/Doorn catchment to correlate groundwater chemistry with the chemical signature of heuweltjies. This would verify if salts, moving downward in heuweltjies, are entering the groundwater system in the catchment and the extent to which heuweltjies are affecting groundwater chemistry in the West Coast. The source of heuweltjie salts should be investigated by focusing on faunal activity and the influence of termites and other organisms on introducing marine derived aerosols to mound soils. Research on the impact of land use and farming practices on salt movement in heuweltjies could aid in understanding factors that aggravate salinisation and help improve land management strategies. The presence of Ca oxalate associated with biogenic features of termites warrants further investigation as heuweltjies could be potential carbon sinks in the West Coast. Carbon sinks would become increasingly important as climate change becomes a greater threat to South Africa.

6 References

Abdu, H., D.A. Robinson, J. Boettinger, and S.B. Jones. 2017. Electromagnetic induction mapping at varied soil moisture reveals field-scale soil textural patterns and gravel lenses. *Front. Agric. Sci. Eng.* 4(2): 135–145. doi: 10.15302/J-FASE-2017143.

Aboukila, E.F., and J.B. Norton. 2017. Estimation of saturated soil paste salinity from soil-water extracts. *Soil Sci.* 182(3): 107–113. doi: 10.1097/SS.0000000000000197.

Ahmed II, J.B., B. Pradhan, S. Mansor, Z.M. Yusoff, and S.A. Ekpo. 2019. Aquifer potential assessment in termites manifested locales using geo-electrical and surface hydraulic measurement parameters. *Sensors* 19: 1–17. doi: 10.3390/s19092107.

Alvarez, M. del P., E. Carol, and C. Dapeña. 2015. The role of evapotranspiration in the groundwater hydrochemistry of an arid coastal wetland (Península Valdés, Argentina). *Sci. Total Environ.* 506–507: 299–307. doi: 10.1016/j.scitotenv.2014.11.028.

Anscombe, F.J. 1973. Graphs in statistical analysis. *Am. Stat.* 27(1): 17–21. https://www.jstor.org/stable/2682899 (accessed 11 June 2021).

Appelo, C.A.J., and D. Postma. 2005. Geochemistry, groundwater and pollution. 2nd ed. A.A. Balkema, Amsterdam, the Netherlands.

Archer, E., J. Conrad, Z. Münch, D. Opperman, M. Tadross, and J. Venter. 2009. Climate change, groundwater and intensive commercial farming in the semi-arid northern Sandveld, South Africa. *J. Integr. Environ. Sci.* 6(2): 139–155. doi: 10.1080/19438150902916589.

Bargues Tobella, A., H. Reese, A. Almaw, J. Bayala, A. Malmer, H. Laudon, and U. Ilstedt. 2014. The effect of trees on preferential flow and soil infiltrability in an agroforestry parkland in semiarid Burkina Faso. *Water Resour. Res.* 50: 3342–3354. doi: 10.1002/2013WR015197.

Barnes, C.J., G. Jacobson, and G.D. Smith. 1992. The origin of high-nitrate ground waters in the Australian arid zone. *J. Hydrol.* 137(1–4): 181–197. doi: 10.1016/0022-1694(92)90055-Z.

Bartels, D., and R. Sunkar. 2005. Drought and Salt Tolerance in Plants. *CRC. Crit. Rev. Plant Sci.* 24(1): 23–58. doi: 10.1080/07352680590910410.

Beck, H.E., N.E. Zimmermann, T.R. Mcvicar, N. Vergopolan, A. Berg, and E.F. Wood. 2018. Data Descriptor: Present and future Köppen-Geiger climate classification maps at 1-km resolution. doi: 10.1038/sdata.2018.214.

Bekker, S.J., J.E. Hoffman, S.M. Jacobs, A.E. Strever, and J.L. Van Zyl. 2016. Ecophysiology, vigour, berry and wine characteristics of grape-vines growing on and off heuweltjies. *S. Afr. J. Enol. Vitic* 37(2): 176–192.

Bergh, E.W., and J.S. Compton. 2015. A one-year post-fire record of macronutrient cycling in a mountain sandstone fynbos ecosystem, South Africa. *South African J. Bot.* 97: 48–58. doi: 10.1016/J.SAJB.2014.11.010.

Beven, K., and P. Germann. 2013. Macropores and water flow in soils revisited. *Water Resour. Res.* 49(6): 3071–3092. doi: 10.1002/WRCR.20156.

Blum, J.D., C.A. Gazis, A.D. Jacobson, and C.P. Chamberlain. 1998. Carbonate versus silicate weathering in the Raikhot watershed within the High Himalayan Crystalline Series. *Geology* 26(5): 411–414. doi: 10.1130/0091-7613(1998)026<0411:CVSWIT>2.3.CO;2.

Booi, N. 2011. Structure and function of heuweltjies across a rainfall gradient in the South-Western Cape. (MSc. Thesis).

Botha, G.A. 2021. Cenozoic stratigraphy of South Africa: current challenges and future possibilities. *South African J. Geol.* doi: 10.25131/sajg.124.0054.

Bouchaou, L., J.L. Michelot, A. Vengosh, Y. Hsissou, M. Qurtobi, C.B. Gaye, T.D. Bullen, et al. 2008. Application of multiple isotopic and geochemicaltracers for investigation of recharge, salinisation,and residence time of water in the Souss–Massaaquifer, southwest of Morocco. *J. Hydrol.* 352: 267–287. doi: 10.1016/j.jhydrol.2008.01.022.

van Breemen, N., J. Mulder, and C.T. Driscoll. 1983. Acidification and alkalinization of soils. *Plant Soil* 75(3): 283–308. doi: 10.1007/BF02369968.

Bühmann, C., J.P. Nell, M. Samadi, and C. Bohmann. 2004. Clay mineral associations in soils formed under Mediterranean-type climate in South Africa. *South African J. Plant Soil* 21(3): 166–170. doi: 10.1080/02571862.2004.10635043.

Bui, E.N. 2013. Soil salinity: A neglected factor in plant ecology and biogeography. *J. Arid Environ.* 92: 14–25. doi: 10.1016/J.JARIDENV.2012.12.014.

Caruso, J.C., and N. Cliff. 1997. Empirical size, coverage, and power of confidence intervals for Spearman's rho. *Educ. Psychol. Meas.* 57(4): 637–654. doi: 10.1177/0013164497057004009.

Casby-Horton, S., J. Herrero, and N.A. Rolong. 2015. Gypsum soils—Their morphology, classification, function, and landscapes. *Adv. Agron.* 130: 231–290. doi: 10.1016/BS.AGRON.2014.10.002.

Chase, M.W. 1998. NIST-JANAF Thermochemical tables. 4th ed. American Institute of Physics.

Chen, C., J. Wu, X. Zhu, X. Jiang, W. Liu, et al. 2019. Hydrological characteristics and functions of termite mounds in areas with clear dry and rainy seasons. Agric. Ecosyst. Environ. 277(February): 25–35. doi: 10.1016/j.agee.2019.03.001.

Coaton, W., and J. Sheasby. 1974. National survey of the Isoptera of southern Africa. 6. The genus Microhodotermes Sjöstedt (Hodotermitidae). *Cimbebasia* 3(6): 47–59.

Cowling, R.M., K.J. Esler, and P.W. Rundel. 1999. Namaqualand, South Africa – An overview of a unique winter-rainfall desert ecosystem. *Plant Ecol.* 142: 3–21.

Cramer, M.D., and N.N. Barger. 2014. Are mima-like mounds the consequence of long-term stability of vegetation spatial patterning? *Palaeogeogr. Palaeoclimatol. Palaeoecol.* 409: 72–83. doi: 10.1016/j.palaeo.2014.04.026.

Cramer, M.D., J.R.C. von Holdt, V.M. Uys, and J.J. Midgley. 2017. The present and likely past climatic distribution of the termite Microhodotermes viator in relation to the distribution of heuweltjies. *J. Arid Environ.* 146: 35–43. doi: 10.1016/j.jaridenv.2017.07.010.

Cramer, M.D., and J.J. Midgley. 2015. The distribution and spatial patterning of mima-like mounds in South Africa suggests genesis through vegetation induced aeolian sediment deposition. *J. Arid Environ.* 119: 16–26. doi: 10.1016/j.jaridenv.2015.03.011.

Daliakopoulos, I.N., I.K. Tsanis, A. Koutroulis, N.N. Kourgialas, A.E. Varouchakis, G.P. Karatzas, and C.J. Ritsema. 2016. The threat of soil salinity: A European scale review. *Sci. Total Environ.* 573: 727–739. doi: 10.1016/j.scitotenv.2016.08.177.

Davis, C.L., M.T. Hoffman, and W. Roberts. 2016. Recent trends in the climate of Namaqualand, a megadiverse arid region of South Africa. *S. Afr. J. Sci.* 112(3–4): 1–9. doi: 10.17159/SAJS.2016/20150217.

DEA. 2013. Long-term adaptation scenarios flagship research programme (LTAS) for South Africa. Pretoria, South Africa.

Deer, W.A., R.A. Howie, and J. Zussman. 1966. An introduction to the rock forming minerals. Longman Group Limited, London.

Desmet, P.G. 2007. Namaqualand-A brief overview of the physical and floristic environment. *J. Arid Environ.* 70(4): 570–587. doi: 10.1016/j.jaridenv.2006.11.019.

Dingle, R.V., W.G. Siesser, and A.R. Newton. 1983. Mesozoic and Tertiary geology of southern Africa. A.A. Balkema, Rotterdam.

Drees, L.R., L.P. Wilding, N.E. Smeck, and A.L. Senkayi. 1989. Silica in soils: Quartz and disordered silica polymorphs. In: Dixon, J. B., Weed, S.B., editor, Minerals in soil environments. Madison, WI. p. 913–974

DWAF. 2005. Olifants/Doorn water management area: Internal strategic perspective. DWAF Report No P WMA 17/000/00/0305, Prepared by Ninham Shand Consulting Services (Pty) Ltd as a Part of the Olifants/Doorn River Basin Study. South Africa, Cape Town.

Eckardt, F.D., and B. Spiro. 1999. The origin of sulphur in gypsum and dissolved sulphate in the Central Namib Desert, Namibia. *Sediment. Geol.* 123(3–4): 255–273. doi: 10.1016/S0037-0738(98)00137-7.

Egli, M., and P. Fitze. 2001. Quantitative aspects of carbonate leaching of soils with differing ages and climates. *Catena* 46(1): 35–62. doi: 10.1016/S0341-8162(01)00154-0.

Ellis, F. 1988. Die Gronde van die Karoo. (Ph.D Thesis).

Ellis, F. 2001. Land degradation on old landsurfaces affected by termite activity in arid and semi-arid regions of South Africa. (September): 1–6.

Ellis, F. 2002. Contribution of termites to the formation of hardpans in soils of arid and semi-arid regions of South Africa. Paper delivered at the 17th World Congress of Soil Science. Bangkok, Thailand

Ellis, F., and J.J.N. Lambrechts. 1994. Dorbank, a reddish brown hardpan of South Africa: a proto-silcrete? 15th World Congress of Soil Science. Acaoulco, Mexico

Erens, H., B.B. Mujinya, F. Mees, G. Baert, P. Boeckx, F. Malaisse, and E. Van Ranst. 2015. The origin and implications of variations in soil-related properties within Macrotermes

falciger mounds. *Geoderma* 249–250: 40–50. doi: 10.1016/j.geoderma.2015.03.003.

Eugster, H.P., and B.F. Jones. 1979. Behavior of major solutes during closed basin- lakes brine evolution. *Am. J. Sci.* 279(6): 609–631. doi: 10.2475/ajs.279.6.609.

FAO. 1990. Management of Gypsiferous Soils (FAO soils, editor). Rome, Italy.

FAO. 2006. Guidelines for soil description. 4th ed. Rome.

Fey, M., J. Hughes, J. Lambrechts, and T. Dohse. 2010a. The soil groups : distribution, properties, classification, genesis and use. Soils of South Africa. Cambridge University Press, Singapore. p. 18–147

Fey, M., J. Hughes, J. Lambrechts, A. Milewski, and A. Mills. 2010b. Animals in soil environments. Soils of South Africa. Cambridge University Press, Singapore. p. 148–175

Francis, M.L. 2008. Soil Formation on the Namaqualand Coastal Plain. (Ph.D Thesis). https://scholar.sun.ac.za:443/handle/10019.1/1182 (accessed 26 May 2021).

Francis, M.L. 2019. Effect of sepiolite and palygorskite on plant available water in Arenosols of Namaqualand, South Africa. *Geoderma Reg.* 17: doi: 10.1016/j.geodrs.2019.e00222.

Francis, M.L., F. Ellis, J.J.N. Lambrechts, and R.M. Poch. 2013. A micromorphological view through a Namaqualand termitaria (Heuweltjie, a Mima-like mound). *Catena* 100(January): 57–73. doi: 10.1016/j.catena.2012.08.004.

Francis, M.L., M. V. Fey, F. Ellis, and M. Poch. 2012. Petroduric and 'petrosepiolitic' horizons in soils of Namaqualand, South Africa. *Spanish J. Soil Sci.* 2(1): 8–25. doi: 10.3232/SJSS.2012.V2.N1.01.

Francis, M.L., M. V. Fey, H.P. Prinsloo, F. Ellis, A.J. Mills, and T. V. Medinski. 2007. Soils of Namaqualand: Compensations for aridity. *J. Arid Environ.* 70(4): 588–603. doi: 10.1016/j.jaridenv.2006.12.028.

Francis, M.L., T.O. Majodina, and C.E. Clarke. 2020. A geographic expression of the sepiolite-palygorskite continuum in soils of northwest South Africa. *Geoderma.* 379: 114615. doi: 10.1016/j.geoderma.2020.114615.

Francis, M.L., and R.M. Poch. 2019. Calcite accumulation in a South African heuweltjie: Role of the termite Microhodotermes viator and oribatid mites. *J. Arid Environ.* 170(103981): 1–10. doi: 10.1016/j.jaridenv.2019.05.009.

Friedman, S.P. 2005. Soil properties influencing apparent electrical conductivity: A review. *Comput. Electron. Agric.* 46: 45–70. doi: 10.1016/j.compag.2004.11.001.

Gamboa, C., L. Godfrey, C. Herrera, E. Custodio, and A. Soler. 2019. The origin of solutes in groundwater in a hyper-arid environment: A chemical and multi-isotope approach in the Atacama Desert, Chile. *Sci. Total Environ.* 690: 329–351. doi: 10.1016/j.scitotenv.2019.06.356.

Garvin, D., V.B. Parker, and H.J. White, Jr. 1987. CODATA Thermodynamic tables: Selections for some compounds of calcium and related mixtures, a prototype set of tables. Hemisphere Pub. Corp, Washington, D.C.

van Gend, J., M.L. Francis, A.P. Watson, L. Palcsu, A. Horváth, P.H. Macey, P. le Roux, et al. 2021. Saline groundwater in the Buffels River catchment, Namaqualand, South Africa: A new look at an old problem. *Sci. Total Environ.* 762. doi: 10.1016/j.scitotenv.2020.143140.

Goovaerts, P. 1997. Geostatistics for natural resources evaluation. Oxford University Press, New York.

Gresse, P.G. 1986. The tectonosedimentary history of the Vanrhynsdorp Group.(Ph.D Thesis).

Gunnarsson, I., and S. Arnórsson. 2000. Amorphous silica solubility and the thermodynamic properties of H4SiO4° in the range of 0°to 350°C at P(sat). *Geochim. Cosmochim. Acta* 64(13): 2295–2307. doi: 10.1016/S0016-7037(99)00426-3.

Hardie, L.A., and H.P. Eugster. 1970. The Evolution of Closed-basin brines. *Miner. Soc Amer Spec Pap* 3: 273–290.

Heil, K., and U. Schmidhalter. 2019. Theory and guidelines for the application of the geophysical sensor EM38. *Sensors* 19(4293): 1–26. doi: 10.3390/s19194293.

Hemingway, B.S., and R.A. Robie. 1994. Enthalpy and Gibbs energy of formation of dolomite, $CaMg(C0_3)_2$, at 298.15 K from HC1 solution calorimetry. Reston, VA.

Hillel, D. 2004. Introduction to envirnmental soil physics. Elsevier Academic Press, Oxford.

Huang, T., S. Yang, J. Liu, and Z. Li. 2016. How much information can soil solute profiles reveal about groundwater recharge? *Geosci. J. 2016 204* 20(4): 495–502. doi: 10.1007/S12303-015-0069-3.

Huber, S., G. Prokop, D. Arrouays, G. Banko, A. Bispo, R.J.A. Jones, M.G. Kibblewhite, et al. 2008. Environmental assessment of soil for monitoring. Volume I, Indicators & criteria. EUR 23490. Office for the Official Publications of the European Communities, Luxembourg.

Ibrahimi, M.K., T. Miyazaki, T. Nishimura, and H. Imoto. 2014. Contribution of shallow groundwater rapid fluctuation to soil salinisation under arid and semiarid climate. *Arab. J. Geosci.* 7(9): 3901–3911. doi: 10.1007/S12517-013-1084-1/FIGURES/14.

Johnson, M.R., C.. Anhauesser, and R.J. Thomas. 2006. The geology of South Africa. Geological Society of South Africa, Pretoria.

Jones, R.L., and G.B. Dreher. 1996. Silicon. Methods of Soil Analysis. Part 3. Chemical Methods-SSSA Book Series no. 5. Soil Science Society of America and American Society of Agronomy, Madison, WI 53711, USA. Methods. p. 627–637

Jones, L.H.P., and K.A. Handreck. 1963. Effects of iron and aluminium oxides on silica in solution in soils. *Nature* 198(4883): 852–853. doi: 10.1038/198852a0.

Jouquet, P., N. Bottinelli, R.R. Shanbhag, T. Bourguignon, S. Traoré, and S.A. Abbasi. 2016. Termites: The neglected soil engineers of tropical soils. *Soil Sci.* 181(3–4): 157–165. doi: 10.1097/SS.0000000000000119.

Jürgens, N. 1991. A new approach to the Namib Region - I: Phytogeographic subdivision. *Vegetation* 97(1): 21–38. doi: 10.1007/BF00033899.

Knüppe, K., and R. Meissner. 2016. Drivers and barriers towards sustainable water and land management in the Olifants-Doorn water management area, South Africa. *Environ. Dev.* 20: 3–14. doi: 10.1016/J.ENVDEV.2016.09.002.

Kowalski, C.J. 1972. On the Effects of non-normality on the distribution of the sample product-moment correlation coefficient. *J. R. Stat. Soc.* 21(1): 1–12. doi: 10.2307/2346598.

Kunz, N.S., M.T. Hoffman, and B. Weber. 2012. Effects of heuweltjies and utilization on vegetation patterns in the Succulent Karoo, South Africa. *J. Arid Environ.* 87: 198–205. doi: 10.1016/J.JARIDENV.2012.05.007.

Lambrechts, J.J.N. 1983. Soils, soil processes and soil distribution in the Fynbos region: An introduction. South African Scientific Programs Report 75.

Lambrechts, J.J.N., J. Van Zyl, F. Ellis, and B.H.A. Schloms. 1978. Grondkode en kaartsimbool vir detail kartering in die Winterreënstreek.

Léonard, J., and J.L. Rajot. 2001. Influence of termites on runoff and infiltration: Quantification and analysis. *Geoderma* 104: 17–40. doi: 10.1016/S0016-7061(01)00054-4.

Lin, Z.Q., and G.S. Bañuuelos. 2015. Soil salination indicators. *Environ. Indic.*: 319–330. doi: 10.1007/978-94-017-9499-2_20.

Liu, Y., J.Y. Parlange, and T.S. Steenhuis. 1995. A soil water hysteresis model for fingered flow data. Water Resour. Res. 31(9): 2263–2266.

Lovegrove, B.G., and W.R. Siegfried. 1986. Distribution and formation of Mima-like earth mounds in the western Cape Province of South Africa. *S. Afr. J. Sci.* 82(8): 432–436.

Lovegrove, B.G., and W.R. Siegfried. 1989. Spacing and origin(s) of Mma-like earth mounds in the Cape Province of South Africa. *S. Afr. J. Sci.* 85: 108–112.

Luther-Mosebach, J., J. Dengler, U. Schmiedel, I.U. Röwer, T. Labitzky, and A. Gröngröft. 2012. A first formal classification of the Hardeveld vegetation in Namaqualand, South Africa. *Appl. Veg. Sci.* 15(3): 401–431. doi: 10.1111/J.1654-109X.2011.01173.X.

McAuliffe, J.R., M.T. Hoffman, L.D. McFadden, W. Bell, S. Jack, M.P. King, and V. Nixon. 2019a. Landscape patterning created by the southern harvester termite, Microhodotermes viator: Spatial dispersion of colonies and alteration of soils. *J. Arid Environ.* 162: 26–34. doi: 10.1016/j.jaridenv.2018.11.010.

McAuliffe, J.R., M.T. Hoffman, L.D. McFadden, S. Jack, W. Bell, and M.P. King. 2019b. Whether or not heuweltjies: Context-dependent ecosystem engineering by the southern harvester termite, Microhodotermes viator. *J. Arid Environ.* 163: 26–33. doi: 10.1016/j.jaridenv.2018.11.012.

McAuliffe, J.R., L.D. McFadden, and M.T. Hoffman. 2018. Role of Aeolian Dust in Shaping Landscapes and Soils of Arid and Semi-Arid South Africa. *Geosciences* 8: 1–34. doi: 10.3390/geosciences8050171.

McAuliffe, J.R., M. Timm Hoffman, L.D. McFadden, and M.P. King. 2014. Role of aeolian sediment accretion in the formation of heuweltjie earth mounds, western South Africa. *Earth Surf. Process. Landforms* 39(14): 1900–1912. doi: 10.1002/esp.3583.

McKenzie, R.C., C.H. Sprout, and N.F. Clark. 1983. The relationship of the yield of irrigated barley to soil salinity as measured by several methods. *Can. J. Soil Sci.* (63): 519–528.

Midgley, J.J., C. Harris, H. Hesse, and A. Swift. 2002. Heuweltjie age and vegetation change based on * 13 C and 14 C analyses. *S. Afr. J. Sci.* 98: 202–204.

Midgley, G., and T. Hoffman. 1991. Heuweltjies: nutrient factories. *Veld Flora* 77(3): 72–75. doi: 10.10520/AJA00423203_3254.

Midgley, G.F., and C.F. Musil. 1990. Substrate effects of zoogenic soil mounds on vegetation composition in the Worcester – Robertson valley, Cape Province. *South African J. Bot.* 56(2): 158–166. doi: 10.1016/S0254-6299(16)31083-3.

Mifsud, A., V. Fornés, F. Huertas, E. Barahona, and J. Linares. 1979. Test de couleur pour la sepiolite. *Clay Miner.* 14: 247–248.

Miller, J.A., A.P. Watson, M. Fleischer, A. Eilers, N.T. Sigidi, J. van Gend, J. van Rooyen, et al. 2018. Groundwater quality, quantity, and recharge estimation on the West Coast of South Africa. *Biodivers. Ecol.* 6: 86–95. doi: 10.7809/b-e.00309.

Mills, A.J., and C. Sirami. 2018. Nutrient enrichment of ecosystems by fungus-growing versus non-fungus-growing termites. *J. Trop. Ecol.* 34(6): 385–389. doi: 10.1017/S0266467418000330.

Moore, J.M., and M.D. Picker. 1991. Heuweltjies (earth mounds) in the Clanwilliam district, Cape Province, South Africa: 4000-year-old termite nests. *Oecologia* 86(3): 424–432. doi: 10.1007/BF00317612.

Mucina, L., and M.C. Rutherford. 2006. The vegetation of South Africa, Lesotho and Swaziland. *Strelitzia* 19. South African National Biodiversity Institute, Pretoria.

Murphy, J., and J.P. Riley. 1962. A Modified Single Solution Method for the Determination of Phosphate in Natural Waters. *Anal. Chim. Acta* 27: 31–36.

Nancollas, G.H. 1984. The Nucleation and Growth of Phosphate Minerals. In: Nriagu, D.J.O. and Moore, P.D.P.B., editors, Phosphate Minerals. Springer, Berlin, Heidelberg

Nell, J.P., and C.W. van Huyssteen. 2014. Geology and groundwater regions to quantify primary salinity, sodicity and alkalinity in South African soils. *South African J. Plant Soil* 31(3): 127–135. doi: 10.1080/02571862.2014.921940.

Nordstrom, D.K., L.N. Plummer, T.M.L. Wigley, T.J. Wolery, J.W. Ball, E.A. Jenne, R.L. Bassett, et al. 1979. A comparison of computerized chemical models for equilibrium calculations in aqueous systems. Jenne; Chemical Modeling in Aqueous Systems, Speciation, Sorption, Solubility, and Kinetics, Symposium Series 93. American Chemical Society, Washington, D.C. p. 857–892

Papadopoulos, I. 1984. Effect of sulphate waters on soil salinity, growth and yield of tomatoes. *Plant Soil* 81(3): 353–361. doi: 10.1007/BF02323050.

Parkhurst, D.L., and C.A.J. Appelo. 2013. USGS - Description of input and examples for PHREEQC Version 3—A computer program for speciation, batch-reaction, one-dimensional transport, and inverse geochemical calculations. *U.S. Geol. Surv. Tech. Methods*: 497. https://pubs.usgs.gov/tm/06/a43/ (accessed 8 June 2021).

Partridge, T.C., and R.R. Maud. 1987. Geomorphic evolution of southern Africa since the Mesozoic. 90(2): 179–208.

Picker, M.D., M.T. Hoffman, and B. Leverton. 2007. Density of Microhodotermes viator (Hodotermitidae) mounds in southern Africa in relation to rainfall and vegetative productivity gradients. *J. Zool.* 271(1): 37–44. doi: 10.1111/j.1469-7998.2006.00189.x.

Pitman, M.G., and A. Läuchli. 2002. Global impact of salinity and agricultural ecosystems. In: Läuchli A and Lüttge U, editors. Springer, Dordrecht

Plummer, L.N., and E. Busenberg. 1982. The solubilities of calcite, aragonite and vaterite in CO2-H2O solutions between 0 and 90°C, and an evaluation of the aqueous model for the system CaCO3-CO2-H2O. *Geochim. Cosmochim. Acta* 46(6): 1011–1040. doi: 10.1016/0016-7037(82)90056-4.

Potts, A.J., J.J. Midgley, and C. Harris. 2009. Stable isotope and 14C study of biogenic calcrete in a termite mound, Western Cape, South Africa, and its palaeoenvironmental significanc. *Quat. Res.* 72: 258–264. doi: 10.1016/j.yqres.2009.04.008.

Railsback, L.B. 2006. Some fundamentals of mineralogy and geochemistry. *Dep. Geol. Univ. Georg.* http://railsback.org/FundamentalsIndex.html (accessed 28 November 2021).

Rhoades, J.D. 1996. Electrical conductivity and total dissolved solids. Methods of Soil Analysis. Part 3. Chemical Methods-SSSA Book Series no. 5. American Society of Agronomy, Madison, USA. p. 417–435

Rhoades, J.D., N.A. Manteghi, P.J. Shouse, and W.J. Alves. 1989. Estimating soil salinity from saturated soil-paste electrical conductivity. *Soil Sci. Soc. Am. J.* 53(2): 428–433. doi: 10.2136/sssaj1989.03615995005300020019x.

Richet, P., Y. Bottinga, L. Denielou, J.P. Petitet, and C. Tequi. 1982. Thermodynamic properties of quartz, cristobalite and amorphous SiO2: drop calorimetry measurements between 1000 and 1800 K and a review from 0 to 2000 K. *Geochim. Cosmochim. Acta* 46(12): 2639–2658. doi: 10.1016/0016-7037(82)90383-0.

Roberts, D., T. Matthews, A. Herries, C. Boulter, L. Scott, C. Dondo, P. Mtembi, et al. 2011. Regional and global context of the Late Cenozoic Langebaanweg (LBW) palaeontological site: West Coast of South Africa. *Earth-Science Rev.* 106: 191–214.

van Rooyen, J.M., S. Veltman, F. Botha, and J. Matthee. 2021. Groundwater resource exploration & development - Focus on groundwater to support surface water supply in the Lower Olifants River, South Africa. *J. African Earth Sci.* 180: 1–13. doi: 10.1016/j.jafrearsci.2021.104179.

Rozendaal, A., P.G. Gresse, R. Scheepers, and C.H. De Beer. 1994. Structural setting of the Riviera W-Mo deposit, Western Cape, South Africa. *S.AfrJ.Geol* (2): 184–195.

SACS (South African Committee for Stratigraphy). 1980. Stratigraphy of South Africa Part 1: Lithostratigraphy of the Republic of South Africa, South West Africa/Namibia and the Republics of Bophuthatswana, Transkei and Venda. Handbook Geological Survey South Africa, Pretoria.

Salama, R.B., C.J. Otto, and R.W. Fitzpatrick. 1999. Contributions of groundwater conditions to soil and water salinisation. *Hydrogeol. J.* 7: 46–64. http://link.springer.de/link/service/journals/10040 (accessed 27 September 2021).

SASSCAL. 2021. Weather stations in South Africa. https://www.sasscal.org/wp-content/uploads/2020/11/waternet-poster-sasscal-weathernet.pdf (accessed 25 May 2021).

Schaetzl, R., and S. Anderson. 2005. Soils: Genesis and geomorphology. Cambridge University Press, New York.

Schmiedel, U., N. Kühne, A. Twerski, and J. Oldeland. 2015. Small-scale soil patterns drive sharp boundaries between succulent “dwarf” biomes (or habitats) in the arid Succulent

Karoo, South Africa. *South African J. Bot.* 101: 129–138. doi: 10.1016/j.sajb.2015.05.001.

Schmiedel, U., I.U. Röwer, J. Luther-Mosebach, J. Dengler, J. Oldeland, and A. Gröngröft. 2016. Effect of grazing on vegetation and soil of the heuweltjieveld in the Succulent Karoo, South Africa. *Acta Oecologica* 77: 27–36. doi: 10.1016/j.actao.2016.08.012.

Schober, P., and L.A. Schwarte. 2018. Correlation coefficients: Appropriate use and interpretation. *Anesth. Analg.* 126(5): 1763–1768. doi: 10.1213/ANE.0000000000002864.

Smith, M., and J.S. Compton. 2004. Origin and evolution of major salts in the Darling pans, Western Cape, South Africa. *Appl. Geochemistry* 19: 645–664. doi: 10.1016/j.apgeochem.2003.10.003.

Soderberg, K. 2003. Geochemistry of the fynbos ecosystem in a Table Mountain Group sub-catchment of the Olifants River/ Western Cape/ South Africa. (MSc.Thesis).

Soderberg, K., and J.S. Compton. 2007. Dust as a nutrient source for Fynbos ecosystems, South Africa. *Ecosystems* (10): 550–561. doi: 10.1007/s10021-007-9032-0.

Soil Classification Working Group. 1991. Methods of Analysis. Soil classification: A taxonomic system for South Africa. 2nd ed. The Department of Agricultural Development Republic of South Africa, Pretoria. p. 194–197

Sommer, M., D. Kaczorek, Y. Kuzyakov, and J. Breuer. 2006. Review Article Silicon pools and fluxes in soils and landscapes-a review. *J. Plant Nutr Soil Sci* 169: 310–329. doi: 10.1002/jpln.200521981.

Sonmez, S., D. Buyuktas, F. Okturen, and S. Citak. 2008. Assessment of different soil to water ratios (1:1, 1:2.5, 1:5) in soil salinity studies. *Geoderma* 144(1–2): 361–369. doi: 10.1016/j.geoderma.2007.12.005.

Stoessell, R.K. 1988. 25°C and 1 atm dissolution experiments of sepiolite and kerolite. *Geochim. Cosmochim. Acta* 52(2): 365–374. doi: 10.1016/0016-7037(88)90092-0.

Sun, W., S. Jayaraman, W. Chen, and K.A. Persson. 2015. Correction for "Nucleation of metastable aragonite CaCO3 in seawater. *Proc Natl Acad Sci* 11: 3199–3204. doi: 10.1073/pnas.1423898112.

Tabatabai, M.A. 1987. Physicochemical Fate of Sulfate in Soils. *JAPCA* 37(1): 34–38. doi: 10.1080/08940630.1987.10466197.

Turner, S., E. Marais, M. Vinte, A. Mudengpand, and W. Park. 2006. Termites , water and soils. Agricola 16: 40–45. https://www.esf.edu/efb/turner/publication pdfs/Termites water and soils pub.pdf.

United States Salinity Laboratory Staff. 1954. Diagnosis and improvement of saline and alkali soils. Agricultural Handbook. Rev. United States Department of Agriculture, Washington, DC

Uren, N.C. 2018. Calcium oxalate in soils, its origins and fate-a review. *Soil Res.* 56(5): 443–450. doi: 10.1071/SR17244.

USDA. 1954. Diagnoses and improvement of saline and alkali soils. Diagnoses. Superintendent of Documents, U. S. Government Printing Office, Riverside, CA, USA.

Vengosh, A. 2014. Salinisation and saline environments. Elsevier Ltd. p. 325–378

Vengosh, A., and E. Rosenthal. 1994. Saline groundwater in Israel: Its bearing on the water crisis in the country. *J. Hydrol.* 156(2): 389-430.

Vengosh, A., A.J. Spivack, Y. Artzi, and A. Ayalon. 1999. Geochemical and boron, strontium, and oxygen isotopic constraints on the origin of the salinity in groundwater from the Mediterranean Coast of Israel. *Water Resour. Res.* 35(6): 1877–1894. doi: 10.1029/1999WR900024.

Vermooten, M. 2019. Investigation of heuweltjie structure and soil chemistry in the Buffels River valley and implications for transfer of salts to groundwater. (MSc. Thesis).

Vogel, H., K. Mokokwe, and T. Setloboko. 2004. Nitrate hotspots and salinity levels in groundwater in the Central District of Botswana. Lobatse, Botswana.

Watson, J.P. 1969. Water movement in two Termite mounds in Rhodesia. *J. Ecol.* 56: 441–451.

Watson, A., A. Eilers, and J.A. Miller. 2020a. Recharge estimation using CMB and environmental isotopes in the Verlorenvlei Estuarine System , South Africa and implications for groundwater sustainability in a semi-arid agricultural region. *Water* 12(1362): 1–26. doi: 10.3390/w12051362.

Watson, A., S. Kralisch, A. Künne, M. Fink, and J. Miller. 2020b. Impact of precipitation data density and duration on simulated flow dynamics and implications for ecohydrological modelling in semi-arid catchments in Southern Africa. *J. Hydrol.* 590. doi: 10.1016/j.jhydrol.2020.125280.

WRB. 2014. World Reference Base for Soil Resources. World Soil Resources Reports 106.

Yang, H., C. Li, C. Wei, M. Li, X. Li, Z. Deng, and G. Fan. 2015. Molybdenum blue photometry method for the determination of colloidal silica and soluble silica in leaching solution. *Anal. Methods* 7(13): 5462–5467. doi: 10.1039/c5ay01306b.

Yin, S. hua, L. ming Wang, X. Chen, and A. xiang Wu. 2016. Effect of ore size and heap porosity on capillary process inside leaching heap. *Trans. Nonferrous Met. Soc. China* 26(3): 835–841. doi: 10.1016/S1003-6326(16)64174-2.

Zamanian, K., K. Pustovoytov, and Y. Kuzyakov. 2016. Pedogenic carbonates: Forms and formation processes. *Earth Surf. Process. Landforms*. 157: 1–17. doi: 10.1016/j.earscirev.2016.03.003. doi: 10.1016/j.earscirev.2016.03.003.

Zhang, H., J.L. Schroder, J.J. Pittman, J.J. Wang, and M.E. Payton. 2005. Soil salinity using saturated paste and 1:1 soil to water extracts. *Soil Sci. Soc. Am. J.* 69(4): 1146–1151. doi: 10.2136/sssaj2004.0267.

Ziervogel, G., M. New, E. Archer van Garderen, G. Midgley, A. Taylor, R. Hamann, S. Stuart-Hill, et al. 2014. Climate change impacts and adaptation in South Africa. *Wiley Interdiscip. Rev. Clim. Chang.* 5(5): 605–620. doi: 10.1002/WCC.295/FORMAT/PDF.

7 Appendix A

7.1 Vaiogram parameters PB1E

pH(H_2O) had the best correlation horizontally (0˚) and data followed a normal distribution. EC, Na, Cl, SO_4, Ca, Mg, and K showed the best correlation diagonally (-60˚) and all the datasets were skewed right. Dissolved Si and alkalinity had the best correlation vertically (90˚ and -90˚) and both datasets were skewed right. Amorphous silica and halite had the best correlation vertically (90˚ and -90˚) and both datasets followed a normal distribution. Gypsum and calcite had the best correlation diagonally (-60˚) and both datasets were distributed normally.

Table 7.1: Variogram parameters of best fit set for all ion and SI data during Kriging of PB1E data for interpolated maps.

PB1E	Model fit	Direction of best fit (˚)	Tolerance (˚)	Coefficient of determination (R^2)	Skewness (Distribution)
EC	Linear	-60	30	0.175	Right
pH(H_2O)	Linear	0	30	0.087	Evenly skewed
Sodium	Linear	-60	30	0.198	Right
Chloride	Linear	-60	30	0.150	Right
Sulphate	Linear	-60	30	0.169	Right
Dissolved Silica	Linear	90	30	0.073	Right
Calcium	Linear	-60	30	0.045	Right
Magnesium	Linear	-60	30	0.068	Right
Potassium	Linear	-60	30	0.110	Right
Alkalinity	Linear	-90	30	0.042	Right
Amorphous Silica	Linear	90	30	0.018	Normal
Gypsum	Linear	-60	30	0.072	Normal
Calcite	Linear	-60	30	0.020	Normal
Halite	Linear	-90	30	0.185	Normal

7.2 Variogram parameters PB1W

EC had the best correlation diagonally (-60˚) and data was skewed right. pH(H_2O) and dissolved silica had the best correlation horizontally (0˚) and all datasets were distributed normally. Na, Cl, Ca, Mg, and K had the best correlation vertically (-90˚) and all datasets were skewed right. SO_4, alkalinity, gypsum, and calcite had the best correlation horizontally (0˚) and all datasets were skewed right. Amorphous silica had the best correlation diagonally (30˚) and data was skewed left. Halite had the best correlation vertically (-90˚) and data was distributed normally.

Table 7.2: Variogram parameters of best fit set for all ion and SI data during Kriging of PB1W data for interpolated maps.

PB1W	Model fit	Direction of best fit (˚)	Tolerance (˚)	Coefficient of determination (R^2)	Skewness (Distribution)
EC	Linear	-60	30	0.156	Right
pH(H_2O)	Linear	0	30	0.472	Normal
Sodium	Linear	-90	30	0.204	Right
Chloride	Linear	-90	30	0.056	Right
Sulphate	Linear	0	30	0.145	Right
Dissolved Silica	Linear	0	30	0.509	Right
Calcium	Linear	-90	30	0.085	Right
Magnesium	Linear	-90	30	0.082	Right
Potassium	Linear	-90	30	0.017	Right
Alkalinity	Linear	0	30	0.106	Right
Amorphous Silica	Linear	30	30	0.664	Left
Gypsum	Linear	-90	30	0.239	Right
Calcite	Linear	-90	30	0.374	Right
Halite	Linear	-90	30	0.209	Left

7.3 Variogram parameters K1

EC had the best correlation horizontally (0˚) and followed a normal distribution. pH(H_2O), and halite had the best correlation diagonally (30˚) and all datasets were skewed left. Na, Cl, and K had the best correlation diagonally (30˚) and all datasets were skewed right. SO_4, Ca, and alkalinity had the best correlation horizontally (0˚) and datasets were skewed right. Dissolved silica had the best correlation diagonally (-30˚) and data was skewed right. Mg had the best correlation diagonally (45˚) and data was skewed right. Amorphous silica had the best correlation diagonally (-30˚) and data followed a normal distribution. Gypsum had the best correlation horizontally (0˚) and data was skewed left. Calcite had the best correlation diagonally (45˚) and data was skewed left.

Table 7.3: Variogram parameters of best fit set for all ion and SI data during Kriging of K1 data for interpolated maps.

K1	Model fit	Direction of best fit (˚)	Tolerance (˚)	Coefficient of determination (R^2)	Skewness (Distribution)
EC	Linear	0	30	0.549	Normal
pH(H_2O)	Linear	30	30	0.173	Left
Sodium	Linear	30	30	0.605	Right
Chloride	Linear	30	30	0.616	Right
Sulphate	Linear	0	30	0.083	Right
Dissolved Silica	Linear	-30	30	0.010	Right
Calcium	Linear	0	30	0.090	Right
Magnesium	Linear	45	30	0.373	Right
Potassium	Linear	30	30	0.514	Right
Alkalinity	Linear	0	30	0.135	Right
Amorphous Silica	Linear	-30	30	0.022	Right
Gypsum	Linear	0	30	0.330	Left
Calcite	Linear	0	30	0.083	Left

Halite	Linear	30	30	0.503	Left

8 Appendix B

8.1 Heuweltjie screening

Table 8.1: Kruskal-Wallis tests statistics, P-values, and post hoc Nemenyi comparisons of EC (uS/cm) and pH of topsoil by sample location and subsoil by sample location of heuweltjies in Piketberg (PB) and Klawer (K).

Topsoil (0-20 cm)		*Heuweltjie centre*	*Heuweltjie side*	*Inter-heuweltjie*	*P*	$\chi^2_{(2)}$	Shapiro-Wilk *P*
PB	pH	A	AB	B	**0.015**	8.42	0.002
	EC	a	b	b	**0.012**	8.89	0.000
K	pH	A	A	B	**0.000**	16.22	0.112
	EC	a	b	ab	**0.034**	6.76	0.004
Subsoil (>20 cm)							
PB	pH	C	D	D	**0.024**	7.50	0.001
	EC	c	d	d	**0.001**	13.52	0.000
K	pH	C	C	-	0.424	0.64	0.478
	EC	c	c	-	0.155	2.02	0.002

8.1.1 Piketberg

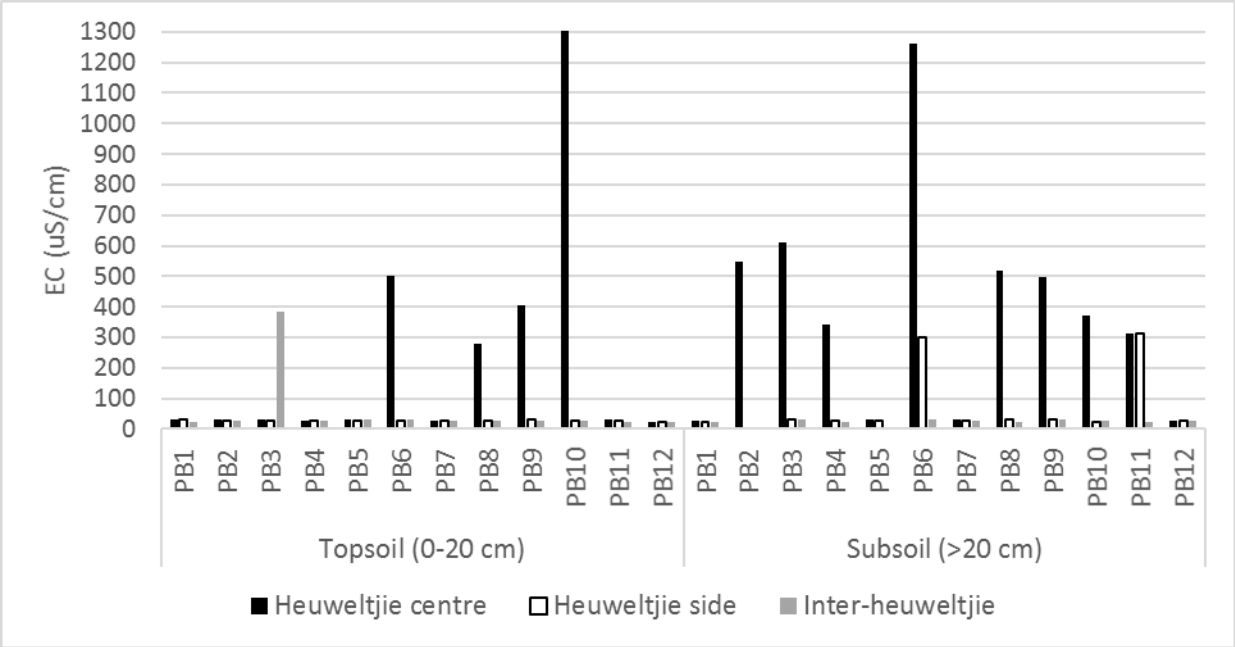

Figure 8.1: The EC (uS/cm) of the centre, side, and inter-heuweltjie topsoil and subsoil of twelve heuweltjies screened in Piketberg.

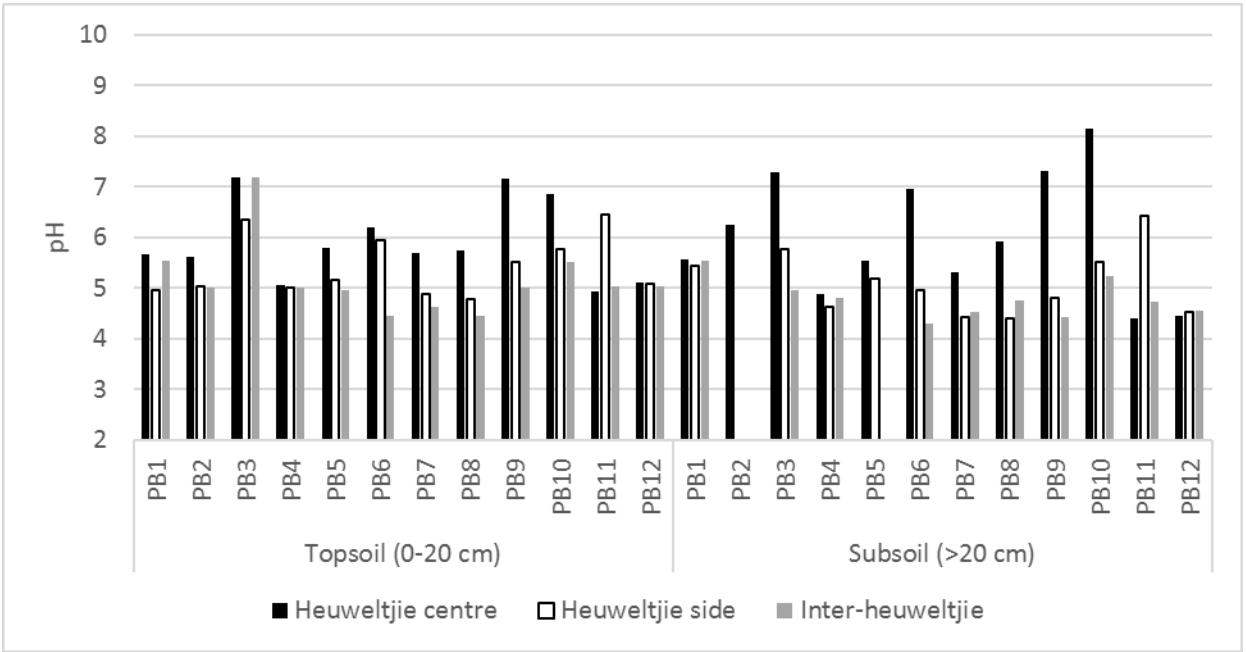

Figure 8.2: The pH of the centre, side, and inter-heuweltjie topsoil and subsoil of twelve heuweltjies screened in Piketberg.

8.1.2 Klawer

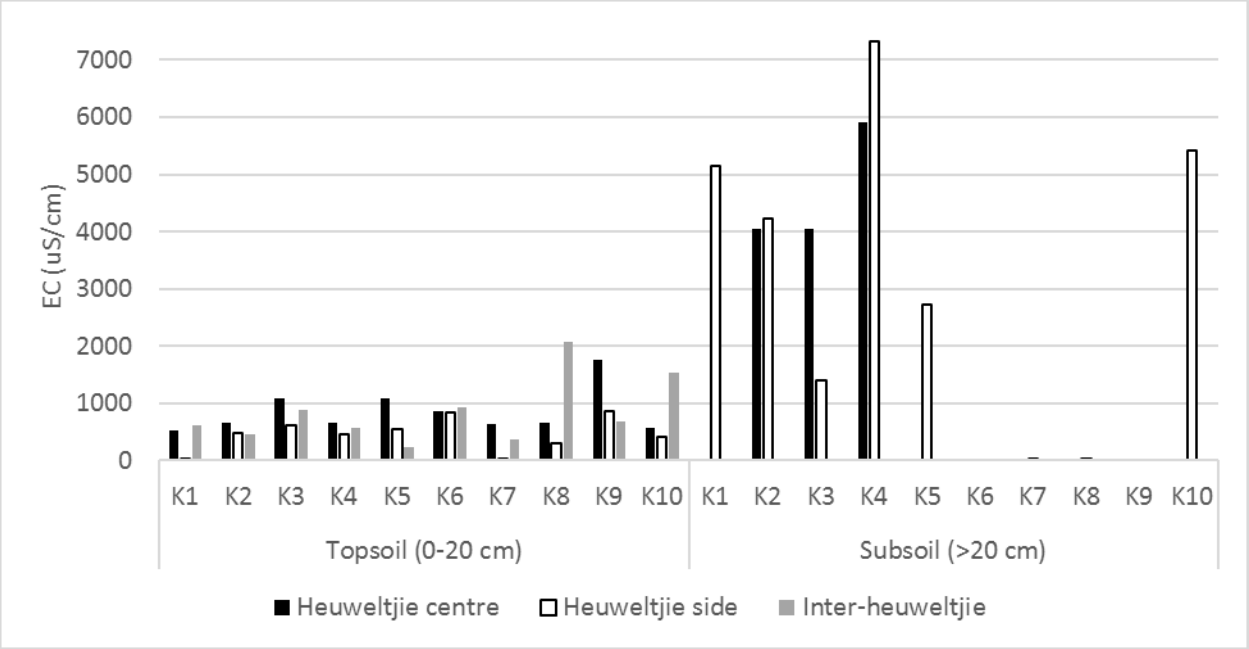

Figure 8.3: The EC (uS/cm) of the centre, side, and inter-heuweltjie topsoil and subsoil of ten heuweltjies screened in Klawer.

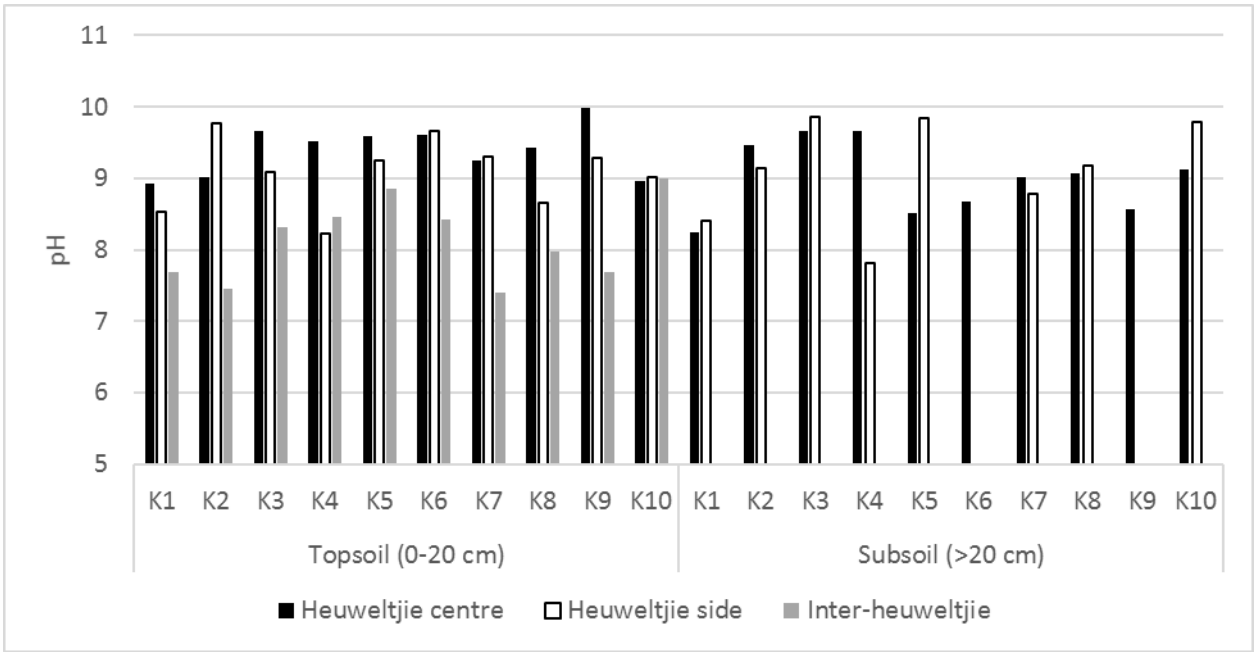

Figure 8.4: The pH of the centre, side, and inter-heuweltjie topsoil and subsoil of ten heuweltjies screened in Klawer.

8.2 Detailed soil profile descriptions

In the following tables, detailed horizon descriptions are given along with assigned diagnostic horizons according to both the South African taxonomic system of soil classification (Soil Classification Working Group, 1991) and Guidelines for Soil Description (FAO, 2006).

In Guidelines for Soil Description (FAO, 2006); Bw = weathered B-horizon, shows development of colour or structure; Bt = illuvial accumulation of silicate clay; in B/C-horizons; Bk = accumulation of pedogenetic carbonates in the B-horizon; Bqm = pedogenetic silica cementation or induration in the B-horizon; Bkqm = pedogenetic carbonate and silica cementation or induration in B-horizon; UC1 = unconsolidated colluvial slope deposits; If more than one of the same horizon is present within a profile, horizons are distinguished using numbers e.g. Bw1, Bw2, Bw3 (FAO, 2006).

In the South African taxonomic system of soil classification, numerical values of 1-3 following a cemented horizon code indicates the degree of cementation ranging from; hard (1) for moderate cementation, very hard (2) for moderate to high degree of cementation, to extremely hard (3) for massive and/or continuously platy with no fracture planes, as described in the soil code by (Lambrechts et al., 1978).

8.2.1 Piketberg

Table 8.2: Detailed description of each horizon within profile PB1E-4.

East wall Profile PB1E-4	**August 2020**	**Diagnostic horizon**
Depth (cm)		
0-20	Dry, loose, massive apedal, many medium and fine roots, few fine pores, very pale brown (10YR7/4), medium sand (5% clay), <2% gravel, slightly hydrophobic, -ve 10% HCl reaction, gradual transition to	Orthic A A
20-75	Dry, slightly firm, massive apedal, few roots, few medium pores, brownish yellow (10YR6/6), slight cutans, medium sand (5-7% clay), <2% gravel, -ve 10% HCl reaction, abrupt transition to	Neocutanic B Bw
75-160+	Dry, loose, very few roots, abundant medium and fine pores, yellow (10YR7/6), medium sandy loam (10-12% clay), 60% coarse fragments (gravel 2cm, stones 7cm, and rocks >15cm), transported colluvium material with pockets of red clay tongues with coarse grained material, discontinuous with clay pockets (15-20% clay), -ve 10% HCl reaction	Colluvium UC1 (unconsolidated colluvial material)

Table 8.3: Detailed description of each horizon within profile PB1E-13.

East wall Profile PB1E-13	**August 2020**	**Diagnostic horizon**
Depth (cm)	*Frass chamber at 20cm, concentrated channels (possible paleo nest) at 30-80cm, many carbonate and Mn coated large termite channels 100+ cm	
0-20	Dry, loose, massive apedal, abundant medium and fine roots, few fine pores, very pale brown (10YR7/4), medium/fine sand (5% clay), <2% gravel, -ve 10% HCl reaction, gradual transition to	Orthic A A
20-50	Dry, slightly hard, massive apedal, common medium fine roots, occasional termite channels with frass, few clay cutans, reddish yellow (7.5YR7/6), few hard, indurated soil spheres, medium sand (5-10% clay), <2% gravel, -ve 10% HCl reaction, gradual transition to	Neocutanic B1 Bw1
50-80	Dry, slightly hard, massive apedal, many medium fine roots, few clay cutans, reddish yellow (7.5YR7/6), medium sand (5-10% clay), <2% gravel, -ve 10% HCl reaction, abrupt transition to	Neocutanic B2 Bw2
80-100	Dry, single grained, apedal, nodular, common medium roots, many coarse and medium pores/ termite channels, reddish yellow (7.5YR6/8), medium sand (5-10% clay), 60% gravel (2cm) indurated by dorbank, fragmented/fractured dorbank with many Mn coatings (Db1), -ve 10% HCl reaction, abrupt transition to	Dorbank (Db1) Bqm
100-125+	Dry, very hard, indurated, discontinuous, many fine/medium roots, abundant fine, medium, and coarse pores, abundant termite channels, reddish yellow (7.5YR6/6), carbonate coatings, moderate +ve 10% HCl reaction	Calcareous dorbank (Db2) Bkqm

Table 8.4: Detailed description of each horizon within profile PB1E-19.

East wall Profile PB1E-19	**August 2020**	**Diagnostic horizon**
Depth (cm)	*Rodent burrows and food chambers 20-100 cm	
0-20	Dry, slightly hard, massive, few medium and fine roots, few fine pores, medium/fine loamy sand (7-10% clay), light yellowish-brown (10YR6/4), <2% gravel, -ve 10% HCl reaction, gradual transition to	Orthic A A
20-60	Dry, hard, massive, many medium pores, few medium and fine roots, rare large burrows, medium loamy sand (12% clay), strong brown (7.5YR5/6), few clay cutans, <2% gravel, -ve 10% HCl reaction, gradual transition to	Neocutanic B1 Bw1
60-80	Dry, hard, massive, many medium pores, many medium roots, rare large burrows, medium sand (12% clay), strong brown (7.5YR5/6), few clay cutans, 5% gravel indurated by dorbank (few dorbank nodules), -ve 10% HCl reaction, clear transition to	Neocutanic B2 Bw2
80-145	Dry, loose, single grained apedal, few medium roots, few medium pores, rare large burrows, fine sand (7% clay), reddish yellow (7.5YR6/8), 40% gravel (fine and medium) indurated by dorbank, fragmented/fractured nodular dorbank with many Mn coatings, -ve 10% HCl reaction, abrupt transition to	Dorbank (Db1) Bqm1
145-170	Dry, hard, indurated nodular gravelly dorbank, many fine roots, many channels, occasional insect casts, few Mn oxide coatings, reddish yellow (7.5YR7/6), -ve 10% HCl reaction, clear transition to	Dorbank (Db1) Bqm2
170-200+	Dry, loose gravel, transported colluvium	C-horizon

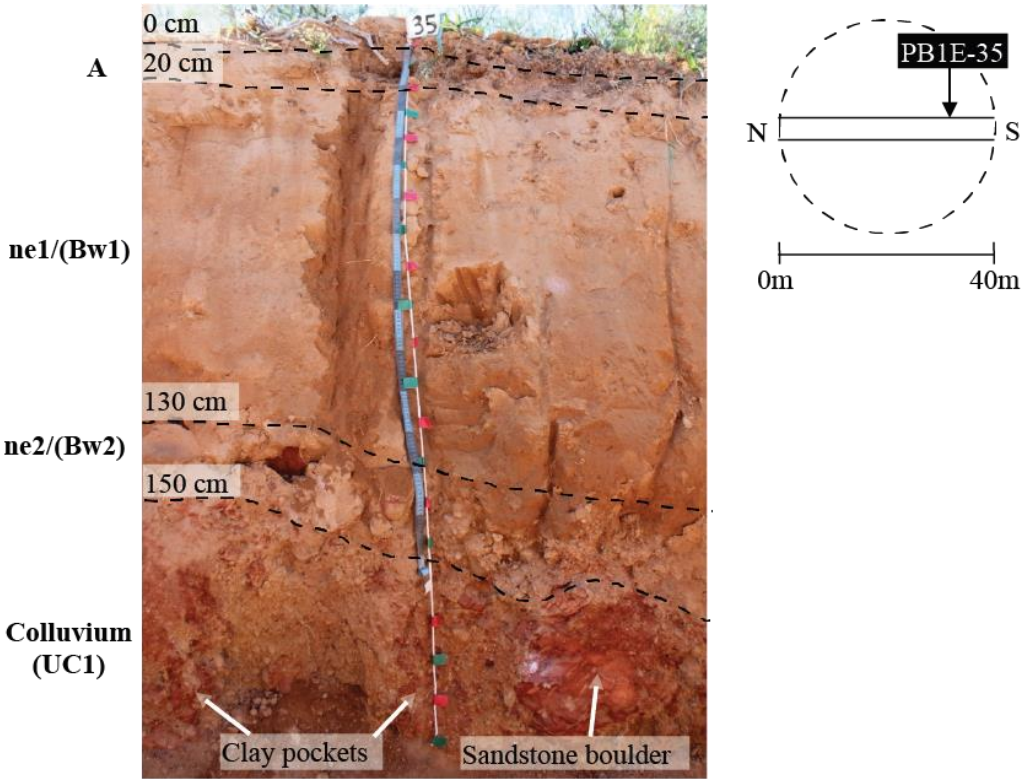

Figure 8.5:Detailed image of inter-heuweltjie modal profile at PB1E-35. Ne/Bw= neocutanic/weathered B-horizon showing signs of colour development; UC1= unconsolidated colluvial slope deposit.

Table 8.5: Detailed description of each horizon within profile PB1E-35.

East wall Profile PB1E-35	**August 2020**	**Diagnostic horizon**
Depth (cm)		
0-20	Dry, loose, single grained apedal, abundant fine and medium roots, many medium pores and channels, medium/fine sand (5% clay), very pale brown (10YR7/4), <2% gravel, -ve 10% HCl reaction, gradual transition	Orthic A A
20-130	Dry, slightly hard, massive apedal, few medium and fine roots, few medium and fine pores, medium/fine sand (5% clay), reddish yellow (7.5YR7/6), few clay cutans, <2% gravel, -ve 10% HCl reaction, abrupt transition	Neocutanic B1 Bw1
130-150	Dry, slightly hard, massive apedal, many medium and fine roots, few fine and medium pores, medium/fine sand (7% clay), pink (7.5YR7/4), few clay cutans, 60% stone (10-15cm), -ve 10% HCl reaction, abrupt transition	Neocutanic B2 Bw2
150-190+	Dry, very hard, weak fine subangular blocky, reddish yellow (7.5YR7/6), clay conglomerate, with red clay pockets (10-12% clay) between coarse material tongues, -ve 10% HCl reaction	Colluvium UC1

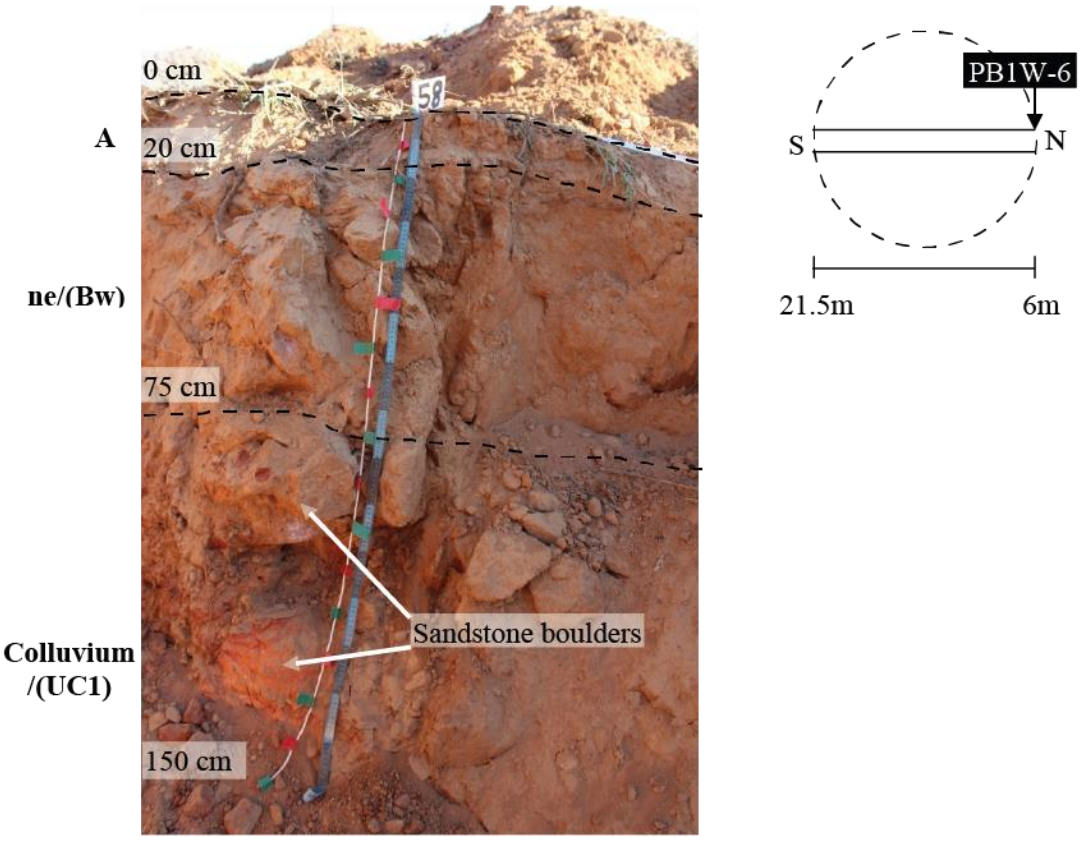

Figure 8.6: Detailed image of inter-heuweltjie modal profile at PB1W-6. Ne/Bw= neocutanic /weathered B-horizon showing signs of colour development; UC1= unconsolidated colluvial slope deposit.

Table 8.6: Detailed description of each horizon within profile PB1W-6.

West wall Profile PB1W-6	**August 2020**	**Diagnostic horizon**
Depth (cm)		
0-20	Dry, loose, singular grained apedal, few medium and fine roots, few medium and fine pores, fine/medium sand (5% clay), light brown (7.5YR6/4), <2% gravel, -ve 10% HCl reaction, gradual transition to	Orthic A A
20-75	Dry, slightly hard, massive apedal, few medium and fine roots, common medium channels/pores, medium/fine sand (7% clay), pink (7.5YR7/4), few clay cutans, <2% gravel, -ve 10% HCl reaction, abrupt transition to	Neocutanic B1 Bw
75-150+	Dry, loose, few medium and fine roots, few channels, medium/fine sand (7% clay), reddish yellow (7.5YR7/6), transported colluvium material, 60% stones and boulders, -ve 10% HCl reaction	Colluvium (UC1)

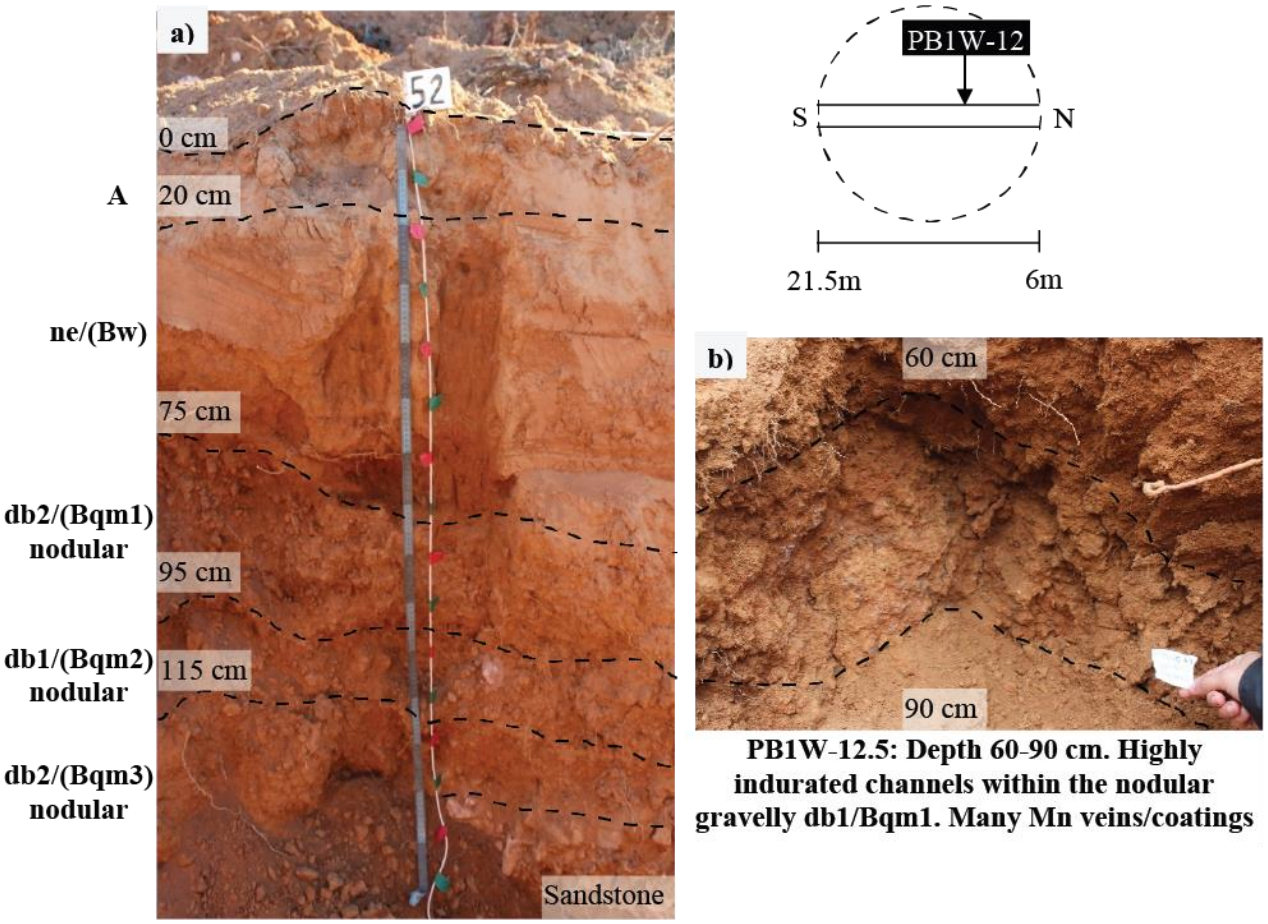

PB1W-12.5: Depth 60-90 cm. Highly indurated channels within the nodular gravelly db1/Bqm1. Many Mn veins/coatings

Figure 8.7: Detailed image of heuweltjie modal profile at PB1W-12. a) Shows entire profile at PB1E-12; b) Indurated channels with many Mn coats/veins between 60-90 cm within the nodular gravelly db2/Bqm1 at PB1W-12.5. Ne/Bw= neocutanic/weathered B-horizon showing signs of colour development; db/Bqm= moderate (db1) to high (db2) Si cementation or induration

Table 8.7: Detailed description of each horizon within profile PB1W-12.

West wall Profile PB1W-12	**August 2020**	**Diagnostic horizon**
Depth (cm)	*Indurated channels 60-90 cm (12.5m)	
0-20	Dry, loose, massive apedal, common medium roots, few fine roots, few fine pores, medium/fine sand (5% clay), light brown (7.5YR6/4), few clay cutans, <2% gravel, -ve 10% HCl reaction, gradual transition to	Orthic A A
20-75	Dry, slightly hard, massive apedal, common medium/fine roots, common medium pores, termite frass, few slight mottles and indurated nodules at Db transition, medium/fine sand (7% clay), reddish yellow (7.5YR6/6), few clay cutans, <2% gravel, -ve 10% HCl reaction, abrupt transition to	Neocutanic B Bw
75-95	Dry, hard, indurated massive apedal, few fine and medium pores, few medium roots, gravelly nodular Si cementation, reddish yellow (7.5YR6/8), -ve 10% HCl reaction, abrupt transition to	Dorbank (Db2) Bqm1
95-115	Dry, loose, indurated gravel, common medium roots, few medium/fine pores, medium sand (5% clay), strong brown (7.5YR5/8), nodular Si cementation, abrupt transition to	Dorbank (Db1) Bqm2
115-145+	Dry, very hard, apedal, indurated gravel, many fine and medium roots, many fine and medium pores, strong brown (7.5YR5/8) fractured nodular and gravelly dorbank, -ve 10% HCl reaction	Dorbank (Db2) Bqm3

Table 8.8: Detailed description of each horizon within profile PB1W-15.

West wall Profile PB1W-15	**August 2020**	**Diagnostic horizon**
Depth (cm)	*Possible old nest area between 65-145 cm	
0-10	Removed by excavator	Disturbed
10-20	Dry, loose, massive apedal, many medium and fine roots, sandy loam (12% clay), light brown (7.5YR6/4), <2% gravel, -ve 10% HCl reaction, gradual transition to	Orthic A A
20-65	Dry, hard, slightly indurated (proto dorbank), many medium and fine roots, many medium and fine pores, loam (15% clay), light brown (7.5YR6/4), few clay cutans, -ve 10% HCl reaction, clear transition to	Neocutanic B Bw
65-80	Dry, hard, nodular dorbank, many medium roots, many fine and medium pores, strong brown (7.5YR5/8), -ve 10% HCl reaction, gradual transition to	Dorbank (Db1) Bqm1
80-130	Dry, soft, friable, many medium and fine roots, many medium and fine pores, and channels, fine subangular blocky indurated dorbank nodules, possible nest area, loam (15% clay), strong brown (7.5YR5/8), 50% fine gravel, -ve 10% HCl reaction, gradual transition to	Dorbank (Db1) Bqm2
130-145	Dry, hard, indurated fractured dorbank, many medium and fine roots, many medium channels, many nodules and gravel, strong brown (7.5YR5/8), slight +ve 10% HCl reaction, gradual transition to	Calcareous dorbank (Db1) Bkqm1
145-160	Dry, very hard, highly indurated, old nest material, many medium channels and horizontal burrows, light brown (7.5YR6/4), moderate +ve 10% HCl reaction, clear transition to	Calcareous dorbank (Db2) Bkqm2
160+	Weathering sandstone	C-horizon

8.2.2 Klawer

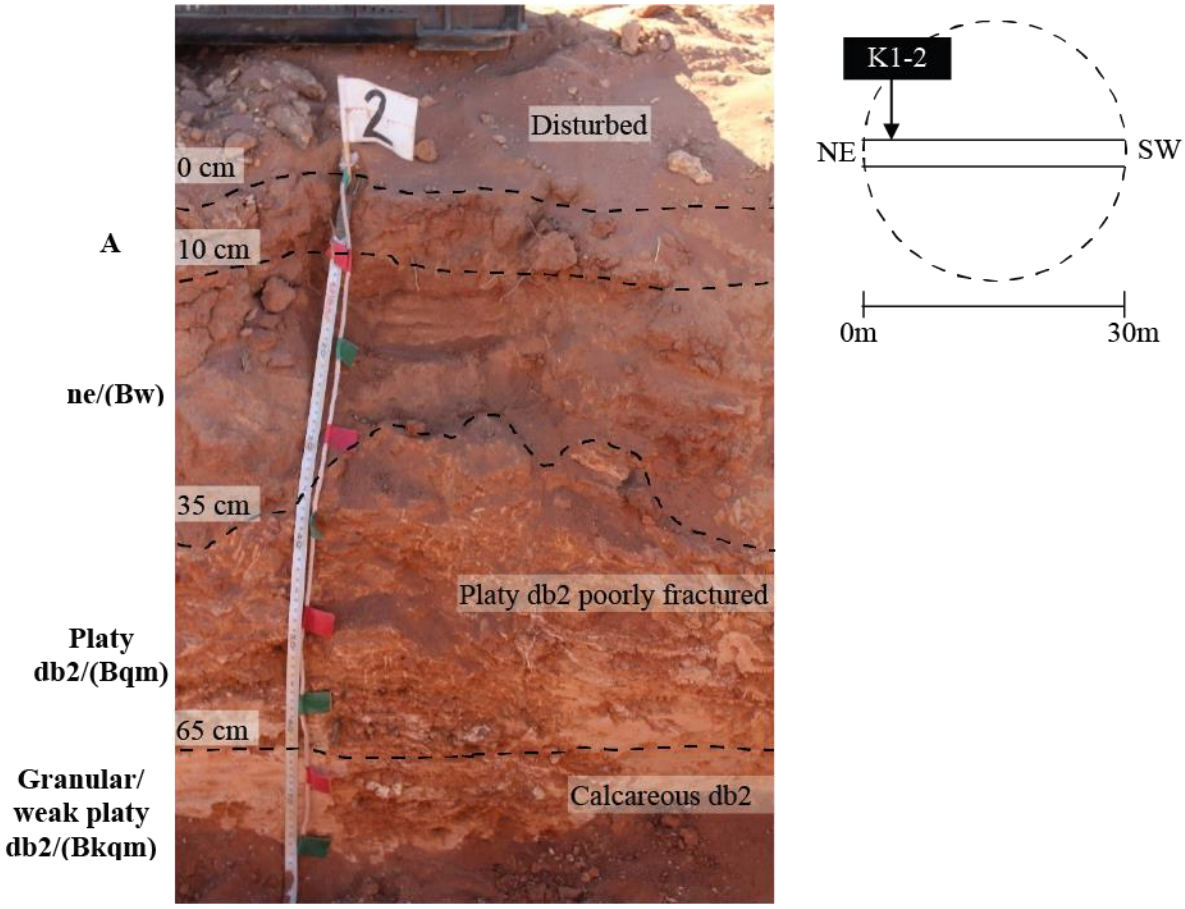

Figure 8.8: Detailed image of inter-heuweltjie modal profile at K1-2. Ne/Bw= neocutanic /weathered B-horizon showing signs of colour development; db2/Bqm= highly indurated, Si-cementation; calcareous db2/Bkqm= highly indurated, carbonate and Si cementation

Table 8.9: Detailed description of each horizon within profile K1-2.

East wall Profile K1-2	**November 2020**	**Diagnostic horizon**
Depth (cm)		
0-10	Dry, loose, massive apedal, many fine and coarse roots, many very fine and fine pores, yellowish red (5YR5/8), medium sand (5% clay), very few gravel (<15%), no mottles, few clay cutans, -ve 10% HCl reaction, gradual transition to	Orthic A A
10-35	Dry, slightly hard, massive apedal, few fine and coarse roots, common fine pores, yellowish red (5YR5/6), medium loamy sand (10% clay), very few gravel (<15%), no mottles, few clay cutans, -ve 10% HCl reaction, abrupt transition to	Neocutanic B Bw
35-65	Dry, hard, continuous, weak massive, no roots, few fine pores, reddish yellow (5YR6/8), moderate laminar cementation, many grey, white and black Si and Mn mottles, many clay and Si cutans, -ve 10% HCl reaction, gradual transition to	Dorbank (Db2) Bqm
65-75+	Dry, hard, continuous, weak massive, no roots, few fine pores, reddish yellow (5YR6/8), moderate laminar cementation, many grey, white and black Si with localised sepiolite and Mn mottles, many clay cutans, weak +ve 10% HCl reaction at 65-75cm	Calcareous Dorbank (Db2) Bkqm

Table 8.10: Detailed description of each horizon within profile K1-8.

East wall Profile K1-8	**November 2020**	**Diagnostic horizon**
Depth (cm)		
0-20	Dry, loose, massive apedal, few fine and coarse roots, few medium and common fine pores, reddish yellow (7.5YR6/6), loamy sand (12.5% clay), very few gravel (<15%), no mottles, few clay cutans, -ve 10% HCl reaction, gradual transition to	Orthic A A
20-43	Dry, loose, massive apedal, common fine and coarse roots, few fine and medium pores, yellowish red (5YR5/6), few clay cutans, medium loamy sand (12.5% clay), very few gravel (<15%), -ve 10% HCl reaction, clear transition to	Neocutanic B1 Bw1
43-64	Dry, slightly hard, massive apedal, discontinuous, moderate nodular pan Si cementation, common fine and coarse roots, many fine and common medium pores, yellowish red (5YR5/6), medium loamy sand (12.5% clay), common (15-35%) coarse gravel and medium biocasts, no mottles, few clay cutans, -ve 10% HCl reaction, abrupt transition to	Neocutanic B2 Bw2
64-145+	Dry, hard, weak massive, continuous, moderate laminar cementation, no roots, common fine and many medium pores, yellowish red (5YR5/6), indurated material, many grey, white and black Si with localised sepiolite and Mn mottles, -ve 10% HCl reaction	Dorbank (db2) Bqm

Table 8.11: Detailed description of each horizon within profile K1-11.

East wall Profile K1-11	**November 2020**	**Diagnostic horizon**
Depth (cm)	*Frass chamber at 65 cm	
0-10	Dry, loose, massive apedal, many fine and coarse roots, few fine pores, reddish yellow (7.5YR7/6), fine loamy sand (13% clay), few gravel (15-25%), no mottles, few clay cutans, -ve 10% HCl reaction, gradual transition to	Orthic A A
10-65	Dry, loose, massive apedal, abundant fine and coarse roots, few fine and common medium pores, reddish yellow (5YR6/6), fine to medium loamy sand (12% clay), few gravel (15-25%), no mottles, few clay cutans, moderate +ve 10% HCl reaction, abrupt transition to	Neocarbonate B1 Bk
50-110	Dry, hard, discontinuous, moderate vesicular Si and carbonate cementation, few fine and coarse roots, common medium pores, yellowish red (5YR5/6), indurated material, few gravel (15-25%), very many coarse pedotubules and biocasts, no mottles, many carbonate and Si cutans, strong +ve 10% HCl reaction, abrupt transition to	Calcareous dorbank (Db1) Bkqm1
95-170	Dry, hard, moderate platy, continuous, moderate laminar silica cementation, no roots, common fine and many medium pores, red (2.5YR4/6), indurated material, few gravel (15-25%), common coarse distinct black and white mottles of Mn and Si with localised sepiolite, many carbonate cutans, slight +ve 10% HCl reaction, gradual transition to	Calcareous dorbank (Db2) Bkqm2
170-270+	Dry, slightly hard, weak granular, continuous, slight nodular pan silica cementation, no roots, few fine and medium pores, yellowish red (5YR5/6), indurated material, many coarse gravel (50-90%) of mixed shapes and medium lime nodules, many medium, distinct, black, blueish black and white mottels of Mn and Si with localised sepiolite, many carbonate cutans, strong +ve 10% HCl reaction	Unconsolidated material, without signs of wetness/ Neocarbonate B2 Bkqm3

Table 8.12: Detailed description of each horizon within profile K1-17.

East wall Profile K1-17	**November 2020**	**Diagnostic horizon**
Depth (cm)	*New indurated termite channels at 40 cm and 100 cm	
0-25	Dry, loose, massive apedal, common fine and coarse roots, common fine pores, yellowish red (5YR5/6), fine loamy sand (13% clay), no gravel, no mottles, few clay cutans, moderate +ve 10% HCl reaction, gradual transition to	Orthic A A
25-75	Dry, loose, massive apedal, many fine and coarse roots, common fine pores, reddish yellow (5YR6/6), fine sandy loam (15% clay), very few gravel (<15%), no mottles, few clay cutans, strong +ve 10% HCl reaction, clear transition to	Neocarbonate B Bk
75-120	Dry, slightly hard, discontinuous, moderate vesicular silica and carbonate cementation, few fine and coarse roots, many medium and fine pores, reddish yellow (5YR6/6), indurated material, very few gravel (<15%), very many coarse pedotubules and biocasts, no mottles, many carbonate and Si (with localised sepiolite) cutans, moderate localised +ve 10% HCl reaction, abrupt transition to	Dorbank (db1) Bkqm1
120-195	Dry, hard, strong platy, continuous, strong laminar silica and carbonate cementation, highly fractured, no roots, many fine and many medium pores, reddish yellow (5YR6/8), indurated material, few gravel (15-25%), many distinct medium and coarse red, black and white Mn and lime-silica mottles with localised sepiolite, many carbonate cutans, moderate +ve 10% HCl reaction, gradual transition to	Dorbank (db2) Bkqm2
195-235	Dry, slightly hard, massive, discontinuous, slight nodular pan silica cementation, no roots, many fine and medium pores, yellowish red (5YR5/6), indurated material, visible powdery white carbonates, many coarse gravel (50-90%) of mixed shapes and medium lime nodules, many distinct fine and	Unconsolidated material, without signs of wetness/ Soft carbonate Bkqm3

	medium red, black, and white Mn, and lime-silica mottles with localised sepiolite, many carbonate cutans, strong +ve 10% HCl reaction, gradual transition to	
235-335+	Dry, slightly hard, weak granular, discontinuous, slight nodular pan silica cementation, no roots, many fine and medium pores, pinkish grey (5YR7/2), indurated material, visible powdery carbonates, many coarse gravel (50-90%) of mixed shapes and medium lime nodules, many distinct fine and medium red, black, and white Mn, and lime-silica mottles with localised sepiolite, many carbonate cutans, strong +ve 10% HCl reaction	Unconsolidated material, without signs of wetness/ Soft carbonate Bkqm4

Table 8.13: Detailed description of each horizon within profile K1-21.

East wall Profile K1-21	**November 2020**	**Diagnostic horizon**
Depth (cm)	*Active termite channels between 65-75 cm	
0-10	Dry, loose, massive apedal, few fine and coarse roots, few fine and medium pores, strong brown (7.5YR5/6), fine loamy sand (13% clay), no gravel, no mottles, few clay cutans, slight +ve 10% HCl reaction, clear transition to	Orthic A
10-50	Dry, loose, massive apedal, many fine and coarse roots, many fine and medium pores, strong brown (7.5YR5/6), fine sandy loam (15% clay), few coarse gravel (15-25%), no mottles, many carbonate and Si cutans, moderate +ve 10% HCl reaction, gradual transition to	Neocarbonate B1 Bk1
50-100	Dry, soft, massive apedal, few fine and coarse roots, many medium and fine pores, pink (7.5YR7/4), fine sandy loam (15% clay), few coarse gravel (15-25%), many coarse pedotubules and biocasts, discontinuous, slight vesicular silica and lime cementation, many carbonate cutans, strong +ve 10% HCl reaction, gradual transition to	Neocarbonate B2 Bk2

100-130	Dry, hard, massive, discontinuous, moderate vesicular silica and lime cementation, no roots, many fine and many medium pores, reddish yellow (5YR7/6), indurated material, few gravel (15-25%), many coarse pedotubules and biocasts, common distinct medium red lime-silica mottles with localised sepiolite, many carbonate cutans, strong +ve 10% HCl reaction, abrupt transition to	Hard carbonate (Hk1) Bkqm1
130-180	Dry, hard, strong platy, continuous, strong laminar lime, and silica cementation, fractured, no roots, many fine and medium pores, reddish yellow (5YR6/8), indurated material, few gravel (15-25%), many hard coarse calcite nodules, many MnO2 coated green nodules, many distinct fine and medium red, black, and white Mn, and lime-silica mottles with localised sepiolite, many carbonate cutans, moderate +ve 10% HCl reaction, clear transition to	Dorbank (db2) Bkqm2
180-310+	Dry, slightly hard, weak granular, continuous, moderate nodular pan silica cementation, no roots, many fine and medium pores, yellowish red (5YR5/8), indurated material, many coarse gravel (50-90%) of mixed shapes and medium calcite nodules, many MnO2 coated green nodules, many distinct fine and medium red, black, and white Mn, and lime-silica mottles with localised sepiolite, many carbonate cutans, strong +ve 10% HCl reaction.	Unconsolidated material, without signs of wetness/ Neocarbonate B3 Bkqm3

Table 8.14: Detailed description of each horizon within profile K1-26.

East wall Profile K1-26	**November 2020**	**Diagnostic horizon**
Depth (cm)	*Frass chamber (25 cm), rodent food pile (25 cm) and active rodent at bottom during excavation	
0-10	Dry, loose, massive apedal, few fine and coarse roots, few fine and medium pores, red (2.5YR4/6), fine loamy sand (11% clay), no gravel, no mottles, few clay cutans, -ve 10% HCl reaction, gradual transition to	Orthic A A
10-35	Dry, loose, massive apedal, few fine and coarse roots, common fine and medium pores, red (2.5YR4/8), fine to medium loamy sand (12.5% clay), very few gravel (<15%), no mottles, few clay cutans, -ve 10% HCl reaction, abrupt transition to	Neocutanic B Bw
35-45	Dry, slightly hard, massive apedal, discontinuous, slight massive silica cementation, no roots, common fine and medium pores, yellowish red (5YR5/8), indurated material, very few gravel (<15%), few faint medium reddish brown and white Si mottles with localised sepiolite, few clay cutans, -ve 10% HCl reaction, abrupt transition to	Dorbank (db1) Bqm1
45-150	Dry, hard, strong platy, continuous, no roots, few fine and common medium pores, yellowish red (5YR5/8), indurated material, very few gravel (<15%), strong laminar silica cementation, common coarse distinct black, reddish brown and white Mn and Si mottles with localised sepiolite, many clay cutans, -ve 10% HCl reaction, clear transition to	Dorbank (db2) Bqm2
150-275+	Dry, slightly hard, moderate granular, continuous, slight nodular pan silica cementation, no roots, few fine and medium pores, yellowish red (5YR5/8), indurated material, many coarse gravel (50-90%) of mixed shapes and medium calcite nodules, common distinct fine and medium black, reddish brown and white Mn and Si mottles with localised sepiolite, common clay cutans, few carbonate cutans, slight +ve 10% HCl reaction	Unconsolidated material, without signs of wetness/ Neocarbonate B Bkqm

Table 8.15: Detailed description of each horizon within profile K1-30.

East wall Profile K1-30	**November 2020**	**Diagnostic horizon**
Depth (cm)		
0-10	Dry, loose, massive apedal, common fine and coarse roots, few fine and medium pores, yellowish red (5YR5/6), fine/medium loamy sand (10% clay), very few gravel (<15%), no mottles, few clay cutans, -ve 10% HCl reaction, clear transition to	Orthic A A
10-30	Dry, loose, massive apedal, few fine and coarse roots, common fine and medium pores, strong brown (7.5YR4/6), fine/medium loamy sand (13% clay), very few gravel (<15%), few faint fine black and brown mottles, few clay cutans, -ve 10% HCl reaction, abrupt transition to	Neocutanic B Bw
30-95	Dry, hard, strong platy, continuous, strong laminar Si cementation, no fractures, no roots, many fine and common medium pores, light reddish brown (5YR6/4), indurated material, very few gravel (<15%), many distinct coarse black, blueish black, brown, and white Mn and Si mottles with localised sepiolite, -ve 10% HCl reaction, clear transition to	Dorbank (db3) Bqm
95-120+	Dry, slightly hard, strong granular, continuous, moderate nodular pan lime and silica cementation, no roots, many fine and common medium pores, reddish yellow (5YR6/6), indurated material, many coarse gravel (50-90%) of mixed shapes and coarse lime nodules, many distinct coarse black, brown, and white Mn and lime-silica mottles with localised sepiolite, common carbonate cutans, moderate localised +ve 10% HCl reaction	Dorbank (db3) Bkqm

8.3 Mineralogy

This section contains XRD patterns of the clay mineralogy omitted in section 3.5.1.

8.3.1 Piketberg clay extract mineralogy

8.3.1.1 Inter-heuweltjie clay extract mineralogy

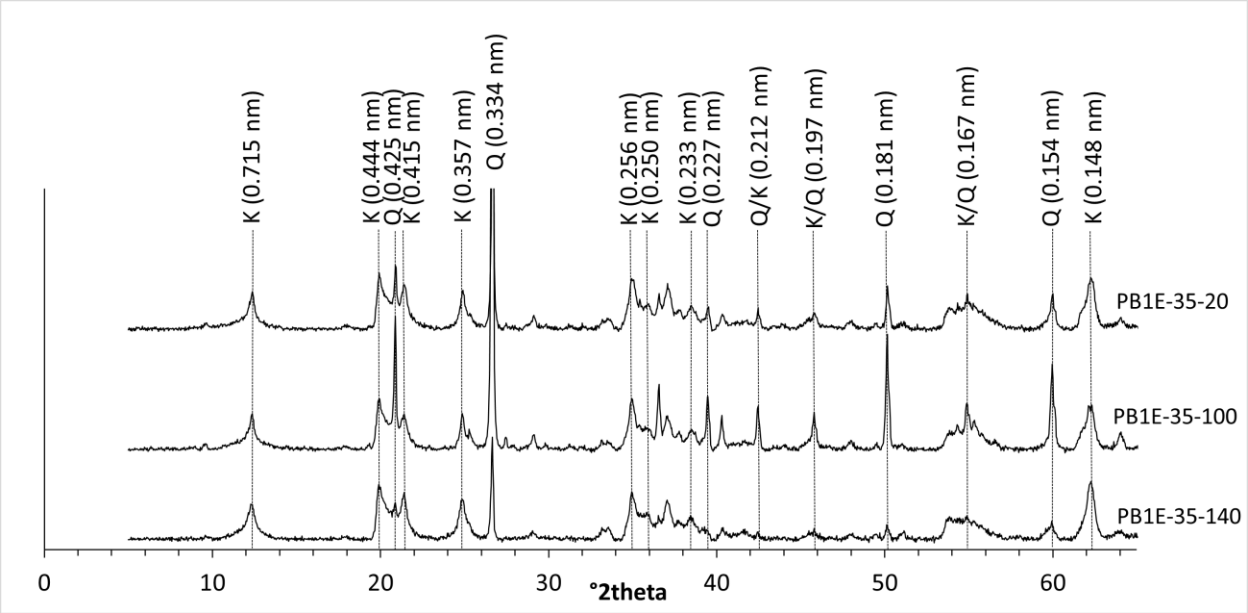

Figure 8.9: XRD pattern indicating peaks labelled with d-spacings (nm) of the $MgCl_2$ treated clay extracts of the inter-heuweltjie soil at profile PB1E-35 (K=kaolinite, Q=quartz).

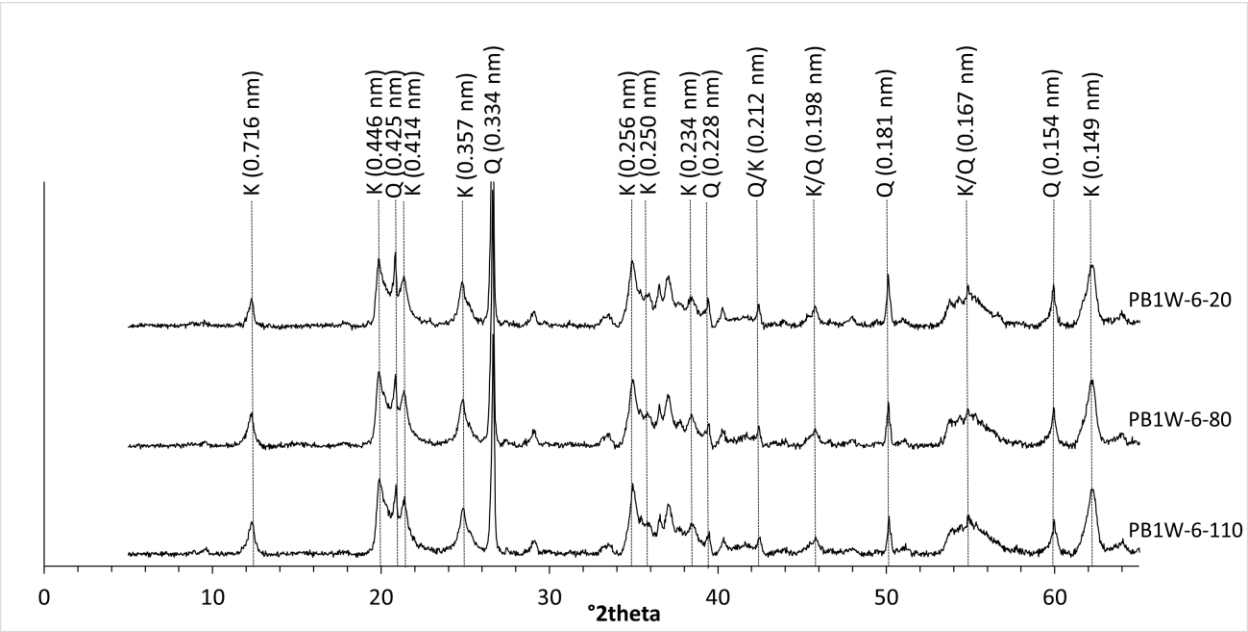

Figure 8.10: XRD pattern indicating peaks labelled with d-spacings (nm) of the $MgCl_2$ treated clay extracts of the inter-heuweltjie soil at profile PB1W-6 (K=kaolinite, Q=quartz).

8.3.1.2 Heuweltjie clay extract mineralogy

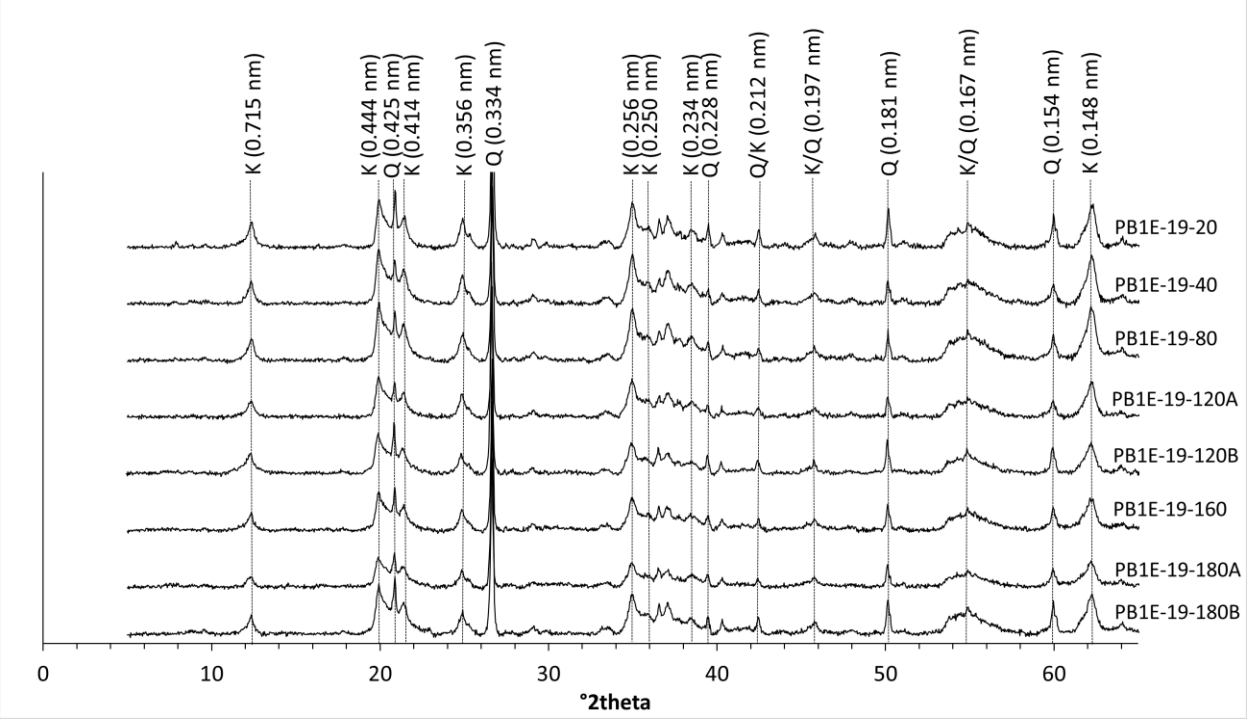

Figure 8.11: XRD pattern indicating peaks labelled with d-spacings (nm) of the $MgCl_2$ treated clay extracts of the heuweltjie soil at profile PB1E-19 (K=kaolinite, Q=quartz).

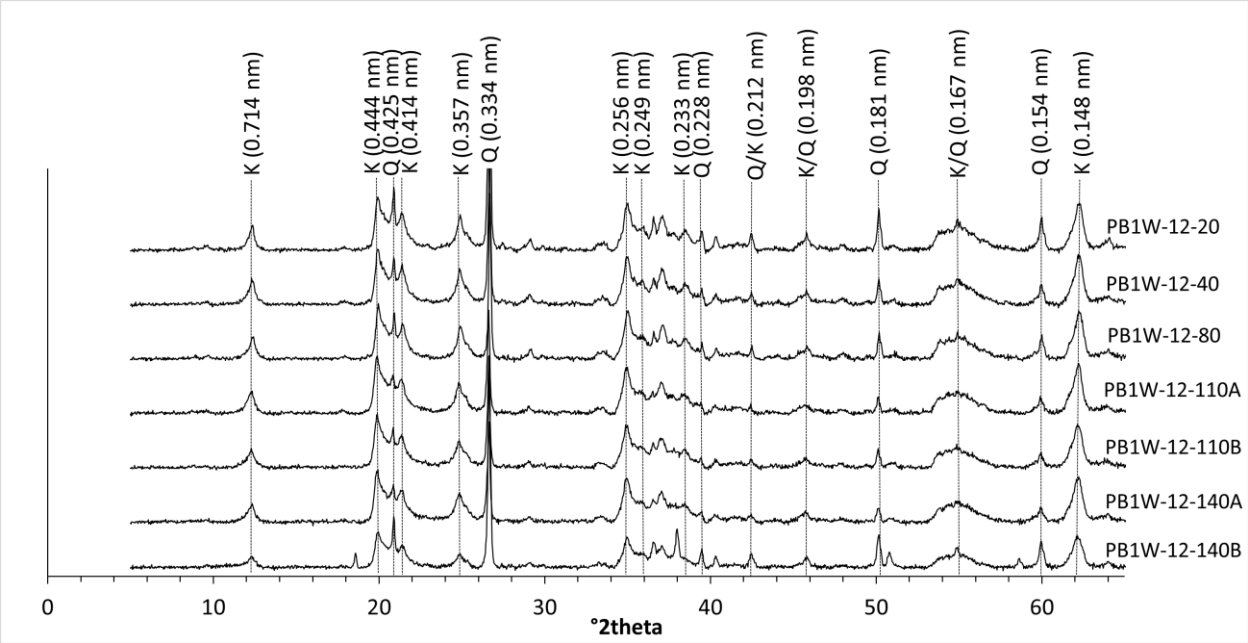

Figure 8.12: XRD pattern indicating peaks labelled with d-spacings (nm) of the $MgCl_2$ treated clay extracts of the heuweltjie soil at profile PB1W-12 (K=kaolinite, Q=quartz).

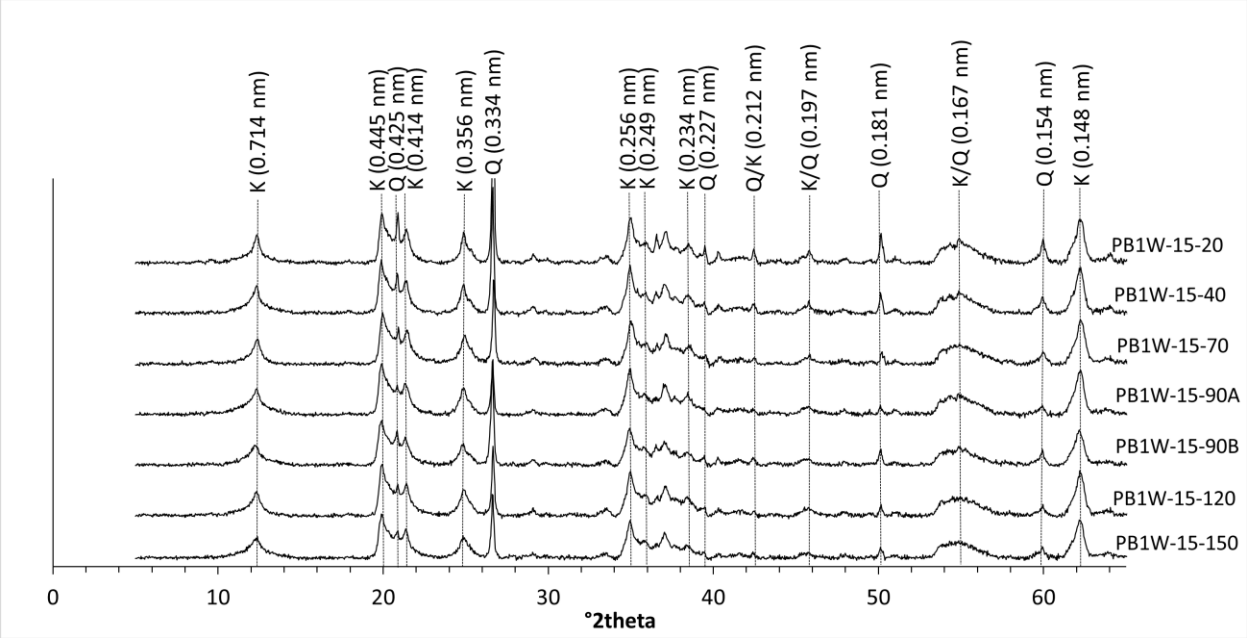

Figure 8.13: XRD pattern indicating peaks labelled with d-spacings (nm) of the $MgCl_2$ treated clay extracts of the heuweltjie soil at profile PB1W-15 (K=kaolinite, Q=quartz).

8.3.2 Klawer clay extract mineralogy

8.3.2.1 Inter-heuweltjie clay extract mineralogy

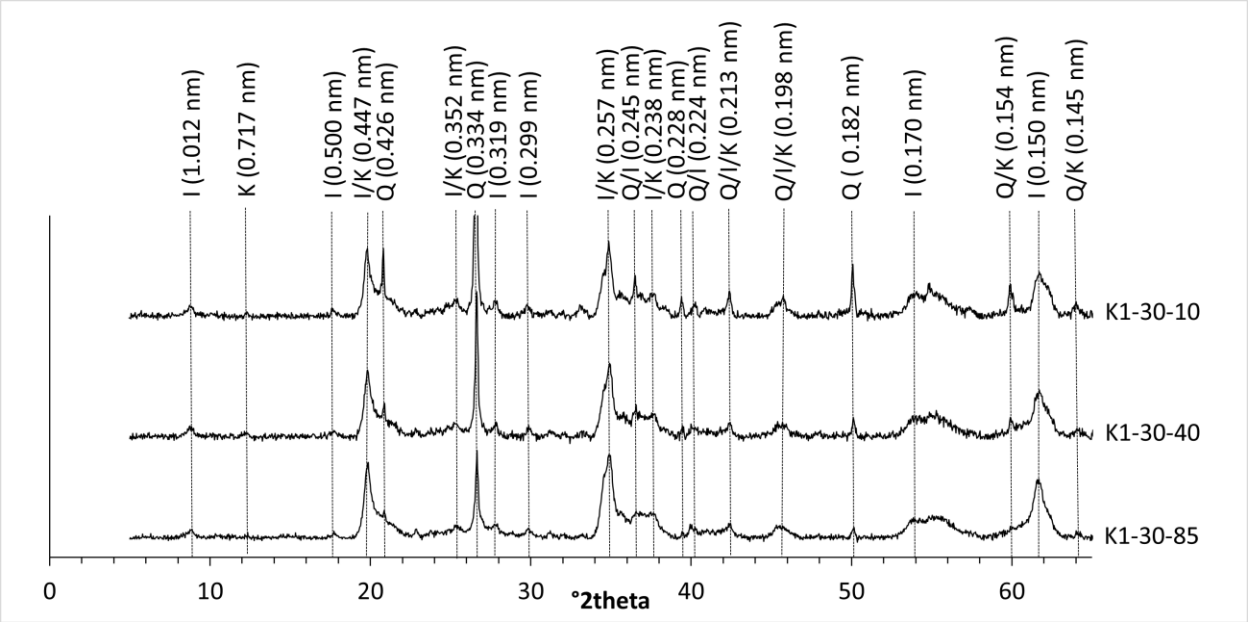

Figure 8.14: XRD pattern indicating peaks labelled with d-spacings (nm) of the $MgCl_2$ treated clay extracts of the inter-heuweltjie soil at profile K1-30 (I=illite, K=kaolinite, Q=quartz).

8.3.2.2 Heuweltjie clay extract mineralogy

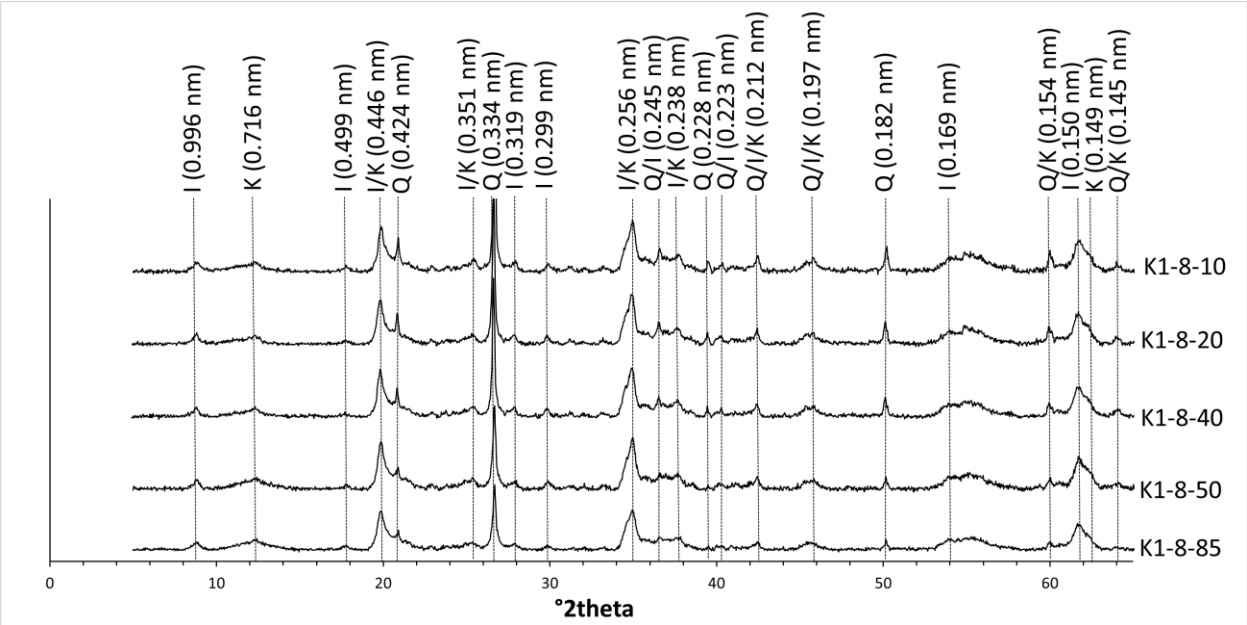

Figure 8.15: XRD pattern indicating peaks labelled with d-spacings (nm) of the $MgCl_2$ treated clay extracts of the heuweltjie soil at profile K1-8 (I=illite; K=kaolinite, Q=quartz).

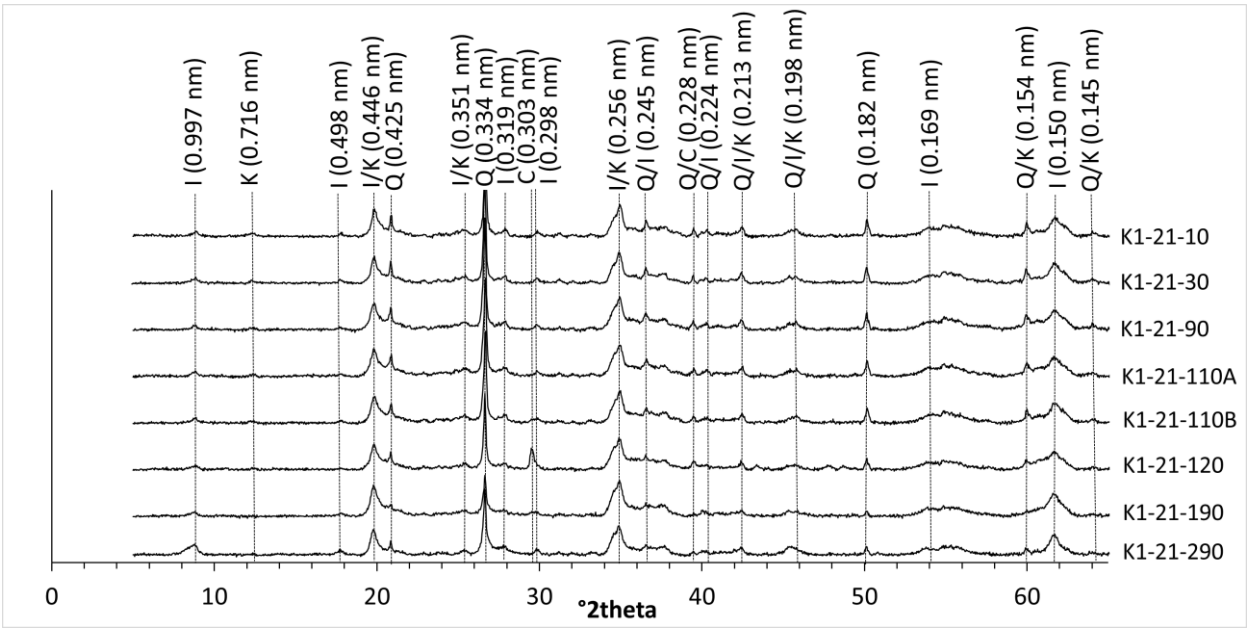

Figure 8.16: XRD pattern indicating peaks labelled with d-spacings (nm) of the $MgCl_2$ treated clay extracts of the heuweltjie soil at profile K1-21 (I=illite; K=kaolinite; Q=quartz; C=calcite).

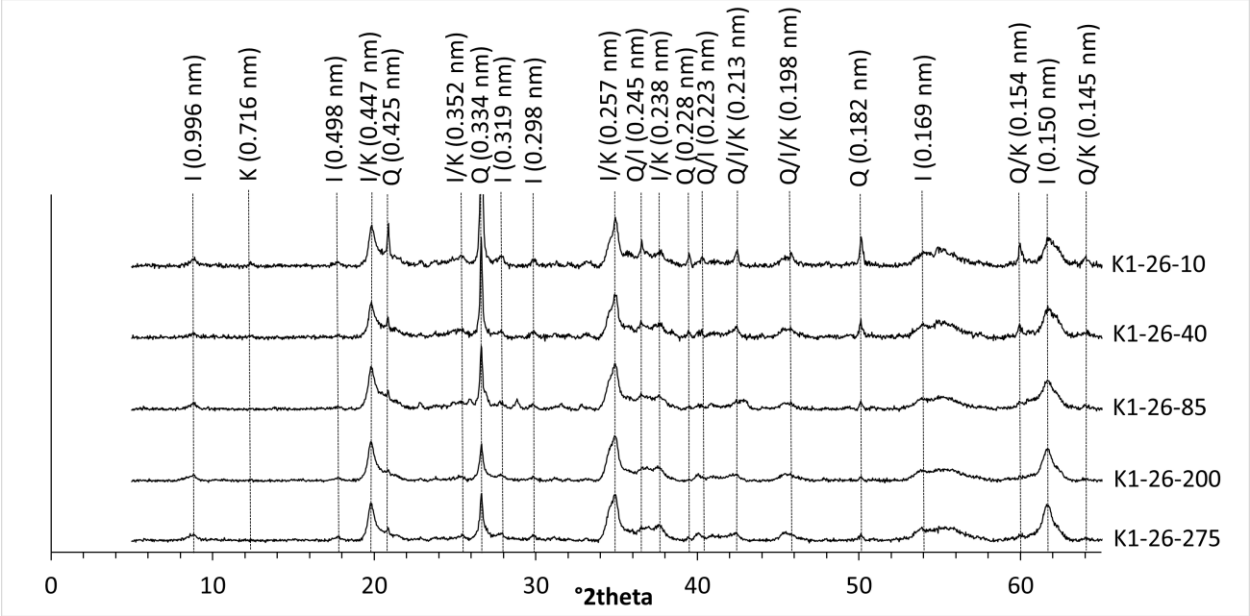

Figure 8.17: XRD pattern indicating peaks labelled with d-spacings (nm) of the MgCl2 treated clay extracts of the heuweltjie soil at profile K1-26 (I=illite; K=kaolinite, Q=quartz).

8.3.3 Klawer bulk sample mineralogy

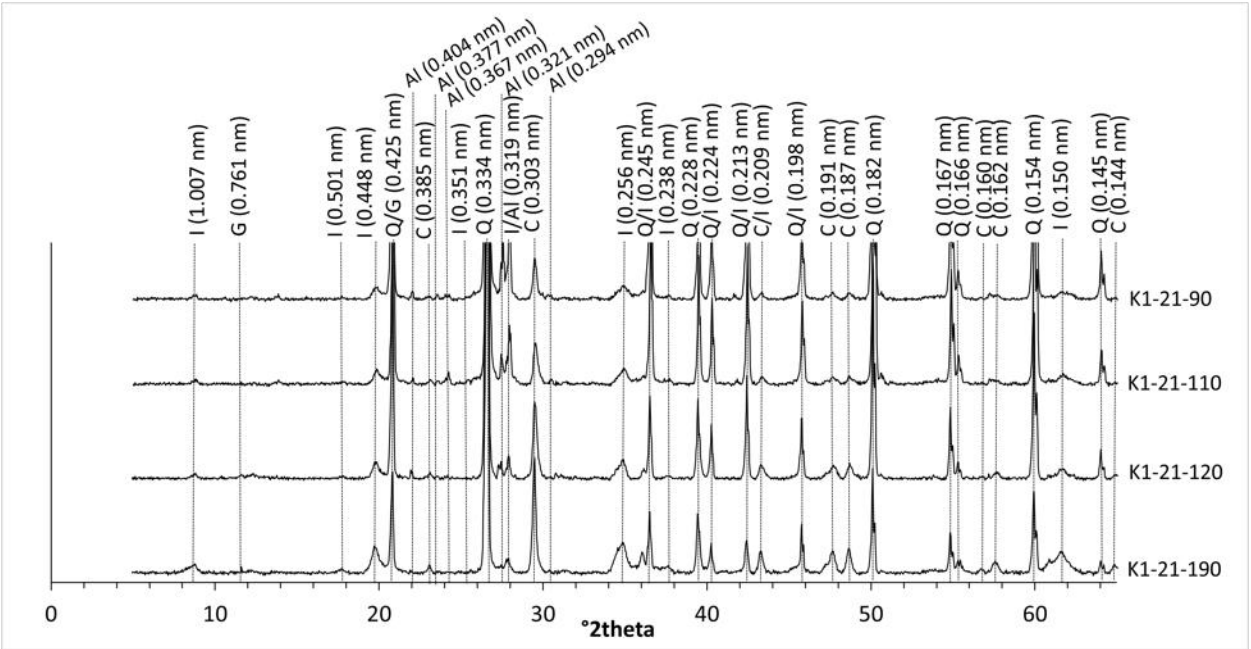

Figure 8.18: XRD pattern indicating peaks labelled with d-spacings (nm) of the untreated bulk samples of the heuweltjie profile K1-21 (I=illite, G=gypsum, Q=quartz, C=calcite, Al=albite).

8.4 EMI survey of single mound

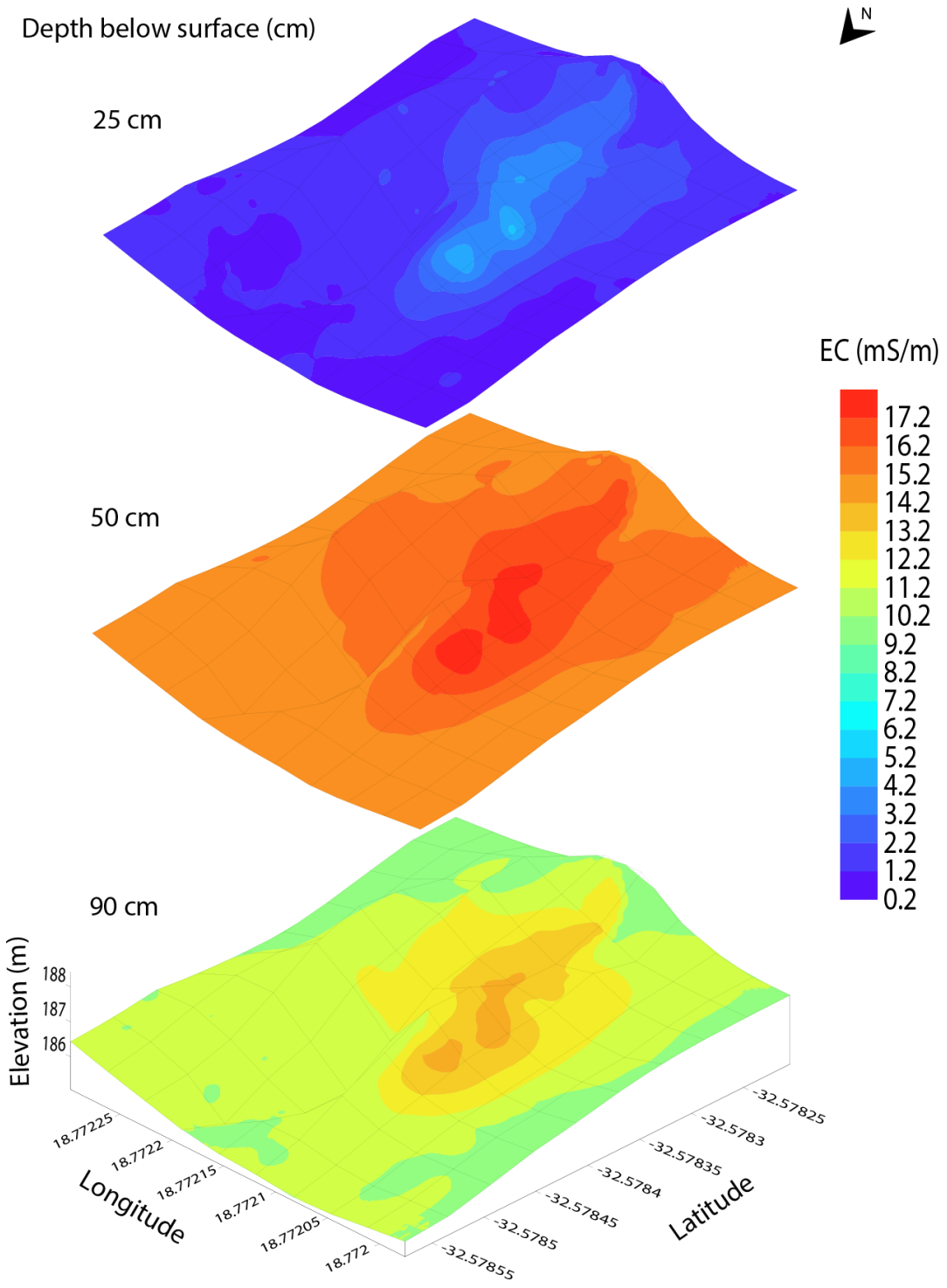

Figure 8.19: EC (mS/cm) of a single heuweltjie in Piketberg indicating the relationship of EC with elevation at depths of 25, 50 and 90 cm.

8.5 Interpolated maps of PB1W

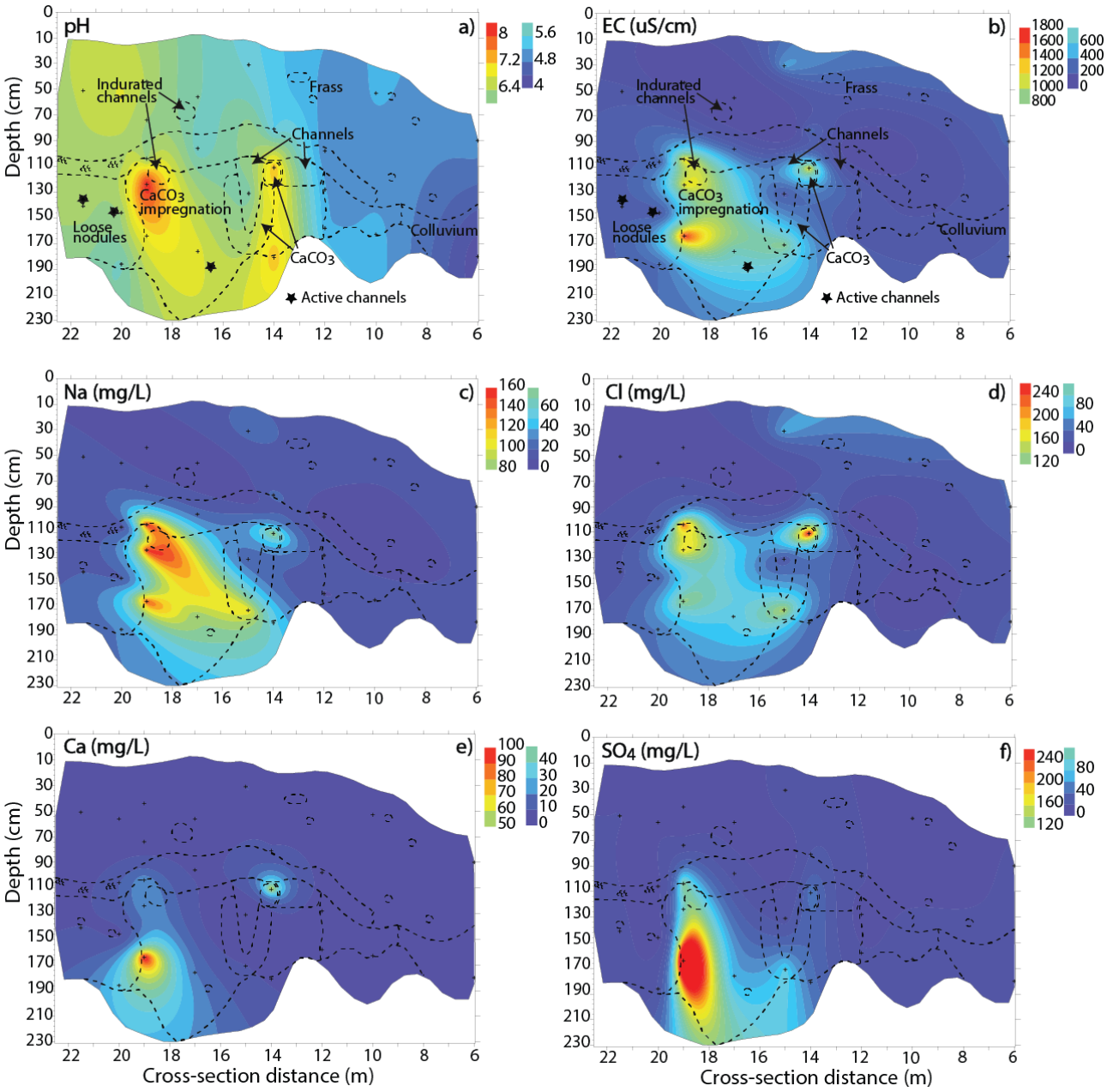

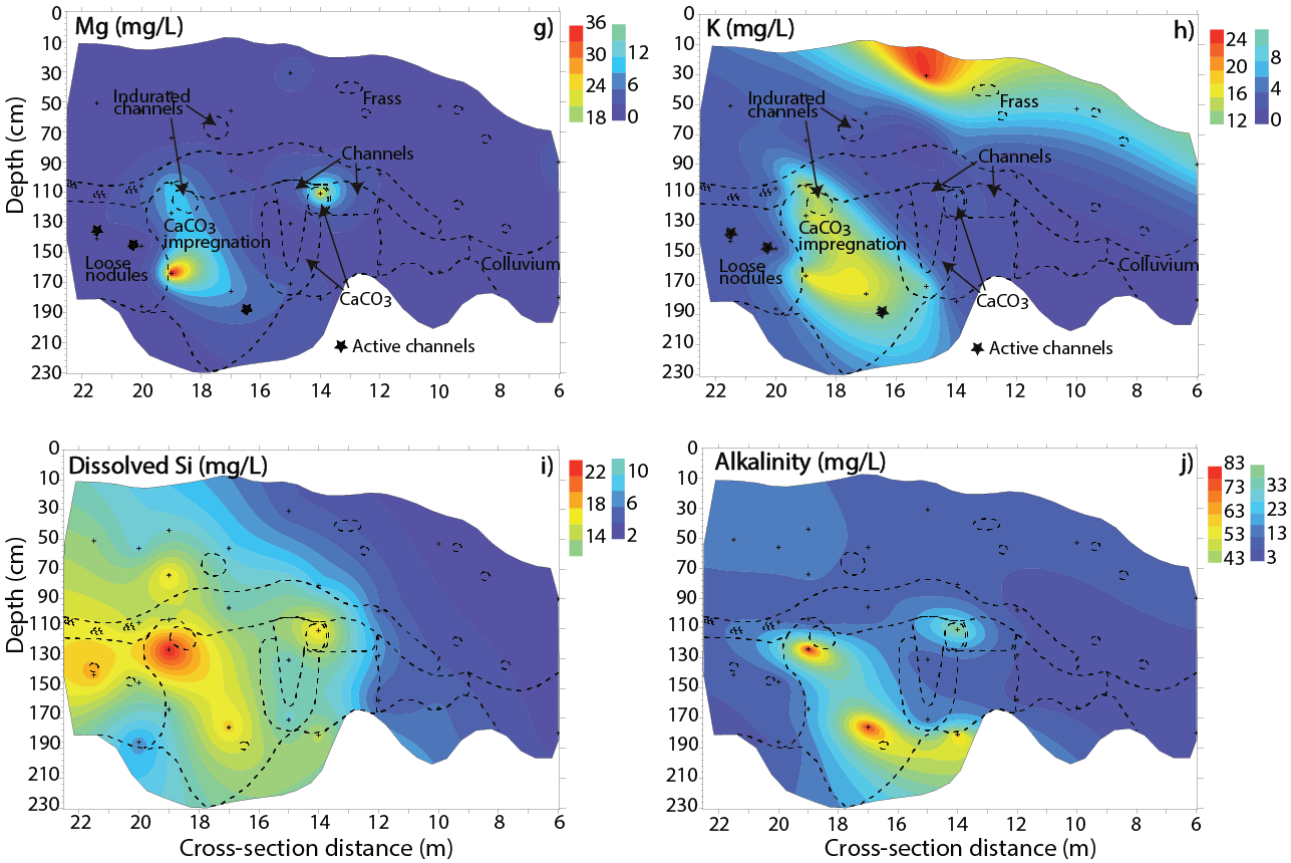

Figure 8.20: Interpolated maps of the west wall of the heuweltjie in Piketberg (PB1W) for a) pH, b) EC, concentrations; c) Na, d) Cl, e) Ca, f) SO4, g) Mg, h) K, i) Dissolved Si, and j) Alkalinity.

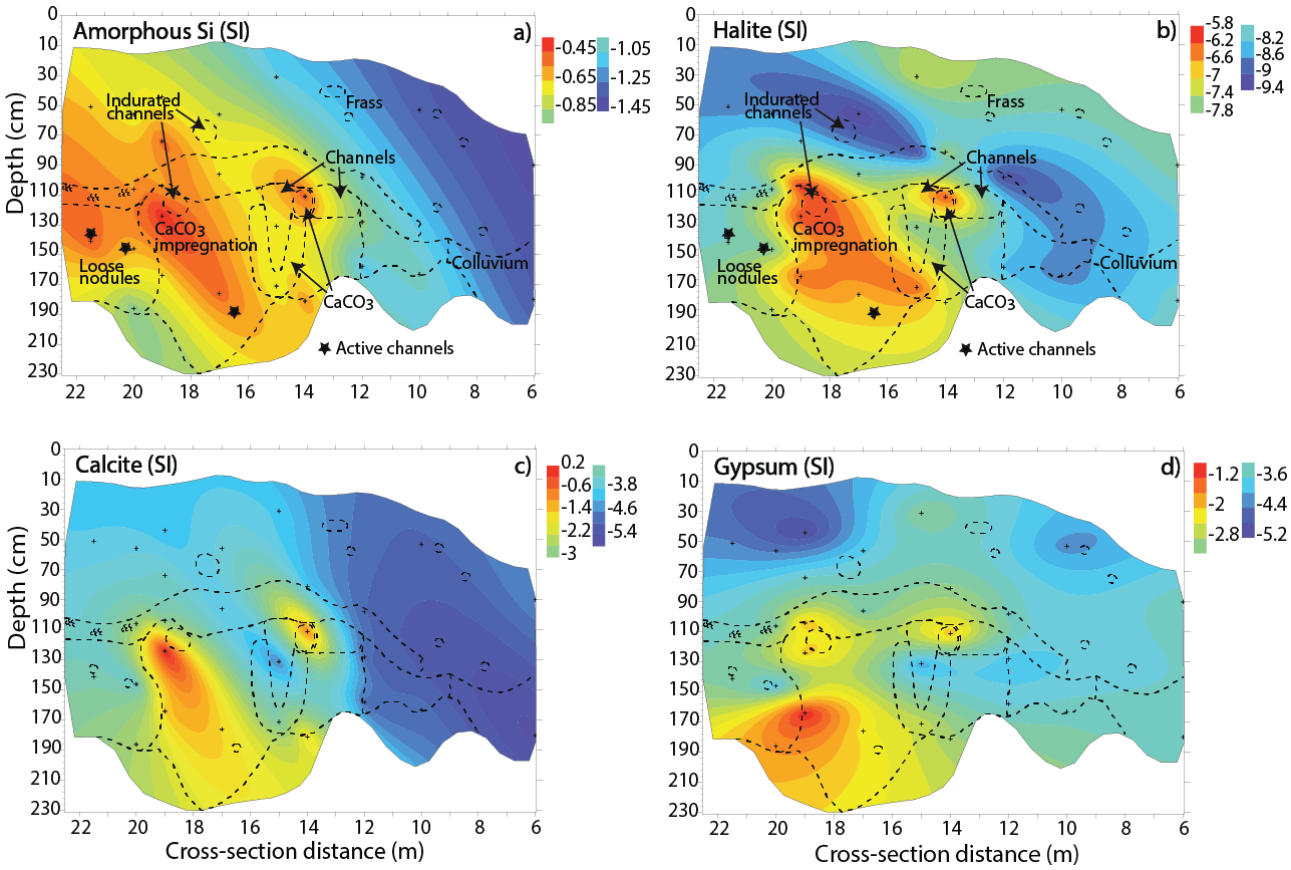

Figure 8.21:Interpolated maps of the west wall of the heuweltjie in Piketberg (PB1W) for saturation indices of a) amorphous silica, b) halite, c) calcite, and d) gypsum.

9 Appendix C

Tables containing raw data of this thesis.

Table 9.1: Particle size analysis and texture classes of modal profiles sampled in PB1E.

PB1E Sample ID	% Sand	% Silt	% Clay	Texture class
PB1E-4-20	80.09	13.89	6.02	Coarse Loamy Sand
PB1E-4-40	77.79	14.09	8.12	Medium Loamy Sand
PB1E-4-80	78.05	14.25	7.70	Coarse Loamy Sand
PB1E-4-140	77.16	12.71	10.13	Coarse Sandy Loam
PB1E-13-20	74.40	15.74	9.87	Medium Sandy Loam
PB1E-13-40	73.84	15.01	11.15	Medium Sandy Loam
PB1E-13-60	72.55	15.45	12.01	Medium Sandy Loam
PB1E-13-80	76.13	14.72	9.15	Medium Sandy Loam
PB1E-13-100 Db1	90.94	7.60	1.46	Coarse Sand
PB1E-13-110A	87.57	11.16	1.27	Coarse Sand
PB1E-13-110B Db1	91.33	7.57	1.10	Coarse Sand
PB1E-19-20	72.26	18.98	8.76	Medium Sandy Loam
PB1E-19-40	68.48	17.67	13.86	Medium Sandy Loam
PB1E-19-80	66.35	19.21	14.45	Medium Sandy Loam
PB1E-19-120A	83.31	15.13	1.56	Medium Loamy Sand
PB1E-19-120B Db1	87.01	11.19	1.80	Coarse Sand
PB1E-19-160 Db1	87.13	11.74	1.13	Coarse Sand
PB1E-19-180A	86.52	12.54	0.94	Coarse Sand
PB1E-19-180B Db1	90.38	8.48	1.14	Coarse Sand
PB1E-35-20	80.93	11.97	7.10	Coarse Loamy Sand
PB1E-35-100	74.96	15.47	9.57	Medium Sandy Loam
PB1E-35-160	65.56	13.82	20.62	Coarse Sandy Clay Loam

Table 9.2: Particle size analysis and texture classes of modal profiles sampled in PB1W.

PB1W Sample ID	% Sand	% Silt	% Clay	Texture class
PB1W-15-20	71.37	17.99	10.64	Medium Sandy Loam
PB1W-15-40	67.46	17.54	14.99	Medium Sandy Loam
PB1W-15-70	72.19	17.57	10.24	Medium Sandy Loam
PB1W-15-90A	77.07	14.63	8.29	Medium Sandy Loam
PB1-15-90B Db1	88.15	10.01	1.84	Coarse sand
PB1W-15-120 Db1	82.00	12.71	5.28	Coarse Loamy Sand
PB1W-15-150 Db2	85.17	12.76	2.07	Coarse Loamy Sand
PB1W-12-20	74.87	17.10	8.03	Medium Sandy Loam
PB1W-12-40	72.91	14.47	12.63	Medium Sandy Loam
PB1W-12-80	72.93	15.06	12.00	Medium Sandy Loam
PB1W-12-110A	77.76	14.54	7.70	Medium Loamy Sand
PB1W-12-110B Db1	88.37	9.66	1.97	Coarse Sand
PB1W-12-140A	84.17	13.55	2.29	Coarse Loamy Sand
PB1W-12-140B Db1	90.43	8.64	0.93	Coarse Sand
PB1W-6-20	80.90	12.65	6.45	Medium Loamy Sand
PB1W-6-80	80.61	10.93	8.47	Coarse Loamy Sand
PB1W-6-110	77.68	11.49	10.83	Medium Sandy Loam

Table 9.3: Particle size analysis and texture classes of modal profiles sampled in K1.

K1 Sample ID	% Sand	% Silt	% Clay	Texture class
K1-2-10	76.51	15.67	7.82	Medium Sandy Loam
K1-2-30	87.60	9.48	2.92	Coarse Sand

K1-8-10	71.59	18.25	10.17	Fine Sandy Loam
K1-8-20	72.16	18.79	9.06	Fine Sandy Loam
K1-8-40 Gravelly Db1	77.52	14.87	7.60	Medium Sandy Loam
K1-8-50 Platy Db2	84.43	10.26	5.31	Coarse Loamy Sand
K1-8-95 Platy Db2	86.27	9.56	4.17	Coarse Loamy Sand
K1-11-10	73.86	18.62	7.52	Fine Sandy Loam
K1-11-60	77.17	18.62	4.20	Fine Loamy Sand
K1-11-90 Vesicular Db1	85.84	12.08	2.08	Coarse Loamy Sand
K1-11-130 Platy Db2	89.86	7.20	2.94	Coarse Sand
K1-11-210 Granular Db1	81.71	10.64	7.65	Coarse Loamy Sand
K1-11-275 Granular Db1	63.76	15.66	20.58	Coarse Sandy Clay Loam
K1-17-10	74.28	19.01	6.71	Fine Sandy Loam
K1-17-40	72.41	20.70	6.89	Fine Sandy Loam
K1-17-80	71.25	21.12	7.63	Fine Sandy Loam
K1-17-100 Gravelly Db1	72.19	20.26	7.54	Fine Sandy Loam
K1-17-160 Platy Db2	85.77	10.14	4.09	Coarse Loamy Sand
K1-17-200 Granular Db1	80.73	12.36	6.91	Coarse Loamy Sand
K1-17-280 Granular Db1	72.22	13.00	14.78	Coarse Sandy Loam
K1-17-305 Granular Db1	66.39	16.47	17.14	Coarse Sandy Loam
K1-21-10	74.31	17.67	8.02	Fine Sandy Loam
K1-21-30	74.27	19.18	6.55	Fine Sandy Loam
K1-21-90 Gravelly Db1	76.31	18.92	4.77	Fine Loamy Sand
K1-21-110A	75.21	18.63	6.17	Fine Sandy Loam
K1-21-110B Vesic Db1	77.51	17.45	5.04	Medium Loamy Sand

K1-21-120 Platy Db2	81.68	14.24	4.08	Coarse Loamy Sand
K1-21-190 Granular Db1	80.18	13.81	6.01	Coarse Loamy Sand
K1-26-10	80.92	13.73	5.36	Fine Loamy Sand
K1-26-40	72.49	17.88	9.63	Fine Sandy Loam
K1-26-85 Platy Db2	83.96	13.25	2.79	Coarse Loamy Sand
K1-26-200 Granular Db1	69.42	13.42	17.17	Coarse Sandy Loam
K1-30-10	83.25	12.15	4.60	Medium Loamy Sand
K1-30-40 Platy Db3	88.28	9.27	2.45	Coarse Sand
K1-30-85 Platy Db3	83.47	11.93	4.61	Coarse Loamy Sand

Table 9.4: pH(H_2O) and EC (uS/cm) data of the Piketberg heuweltjie (PB1). Samples containing both soil and indurated material were separated as A and B respectively.

Sample ID	pH (H_2O)	EC (uS/cm)	Sample ID	pH (H_2O)	EC (uS/cm)
PB1E-1-20	5,2	11,0	PB1E-21-20	7,2	186,4
PB1E-1-90	4,5	150,8	PB1E-21-70	6,4	744,0
PB1E-4-20	5,2	10,8	PB1E-21-110A	6,3	558,0
PB1E-4-40	4,9	10,3	PB1E-21-150B	6,4	408,0
PB1E-4-100-140	4,3	197,2	PB1E-24-20	5,5	127,8
PB1E-8-20	4,9	106,4	PB1E-24-80	5,7	173,6
PB1E-8-80	4,3	211,4	PB1E-24-160	6,4	168,6
PB1E-8-80-110	4,2	426,0	PB1E-27-20	5,9	11,4
PB1E-10-20	5,3	11,2	PB1E-27-100	4,9	129,4
PB1E-10-60	4,9	10,4	PB1E-27-160	5,3	191,4
PB1E-10-140	4,2	424,0	PB1E-27-200B	5,4	124,6
PB1E-10-140-160A	4,3	290,4	PB1E-30-20	5,2	10,3
PB1E-12-20	5,6	176,6	PB1E-30-100	4,1	578,0
PB1E-12-60	5,3	11,2	PB1E-30-190-200	4,0	946,0
PB1E-12-100	4,7	293,6	PB1E-35-20	4,7	11,6
PB1E-12-120-140B	4,9	298,6	PB1E-35-160-200	3,7	305,6
PB1E-13-20	5,9	219,2	PB1E-40-20	4,6	118,4
PB1E-13-40	5,1	344,0	PB1E-40-100-110	3,9	135,8
PB1E-13-80	5,0	395,4	PB1W-6-20	4,9	216,2
PB1E-13-100	5,2	156,8	PB1W-6-110	4,0	165,0
PB1E-13-110-130B	5,4	113,4	PB1W-10-20	5,0	179,6

PB1E-14-20	7,0	271,4	PB1W-10-130B	5,1	115,0
PB1E-14-40	6,8	11,2	PB1W-12-20	5,4	10,4
PB1E-14-60	5,7	446,0	PB1W-12-40-60	4,6	10,7
PB1E-14-100	7,1	345,4	PB1W-12-80	4,8	11,5
PB1E-14-140	6,5	290,8	PB1W-12-110B	5,0	158,8
PB1E-16-20	6,8	354,8	PB1W-12-140B	5,1	112,8
PB1E-16-80	6,6	189,0	PB1W-14-60	5,4	234,0
PB1E-16-120A	5,3	1142,0	PB1W-14-90	7,2	1084,0
PB1E-16-120B	5,3	748,0	PB1W-14-160-180	7,2	394,8
PB1E-16-160-180	6,0	604,0	PB1W-15-10	5,5	369,6
PB1E-17-20	6,6	10,7	PB1W-15-60-75	6,1	10,3
PB1E-17-80	6,9	11,3	PB1W-15-80-110B	6,2	10,3
PB1E-17-120A	6,0	1034,0	PB1W-15-110-130	5,9	177,6
PB1E-17-120B	5,4	820,0	PB1W-15-140-150	6,4	786,0
PB1E-17-220	7,9	1180,0	PB1W-17-40	5,8	11,0
PB1E-18-20	6,3	11,3	PB1W-17-80	5,7	221,2
PB1E-18-60	7,0	125,2	PB1W-17-160	6,7	662,0
PB1E-18-100B	6,7	181,6	PB1W-19-20	6,4	11,1
PB1E-18-120-130	7,3	245,8	PB1W-19-50	6,2	135,0
PB1E-18-220B	6,5	766,0	PB1W-19-80A	6,1	1576,0
PB1E-19-20	6,7	119,0	PB1W-19-80B	6,1	1132,0
PB1E-19-40	6,8	11,1	PB1W-19-100	8,3	1094,0
PB1E-19-80	6,4	231,6	PB1W-19-140A	6,8	1618,0
PB1E-19-120B	6,4	163,4	PB1W-20-20	6,6	118,6
PB1E-19-160	7,1	107,0	PB1W-20-60	6,3	225,4
PB1E-19-180A	6,9	10,9	PB1W-20-100A	6,2	166,2
			PB1W-20-140B	5,8	250,6
			PB1W-21.5-20	6,4	121,0
			PB1W-21.5-100B	6,3	188,6

Table 9.5:Anion, cation, dissolved Si and alkalinity data (mg/L) of the heuweltjie in Piketberg (PB1). Samples containing both soil and indurated material were separated as A and B respectively.

	Concentration mg/L								
Sample ID	Cl^-	$SO4^{2-}$	Alkalinity	PO_4^{3-}	Ca^{2+}	K^+	Mg^{2+}	Na^+	Dissolved Si
PB1E-1-20	5,7	5,6	7,6	0,0	0,0	4,6	0,0	3,6	2,8
PB1E-1-90	17,4	3,9	4,6	0,0	0,7	1,1	0,5	7,5	2,2
PB1E-4-20	2,3	4,6	9,2	0,1	0,0	2,8	0,1	2,0	4,4
PB1E-4-40	1,8	5,6	7,6	0,0	0,1	2,9	0,2	0,4	4,1
PB1E-4-100-140	9,9	10,0	5,2	0,0	1,3	4,0	0,5	12,3	2,8

PB1E-8-20	10,1	4,3	8,2	0,0	1,1	5,0	0,8	3,1	4,1
PB1E-8-80	15,0	6,6	3,4	0,0	2,8	3,0	1,1	11,9	5,3
PB1E-8-80-110	48,6	10,0	0,0	0,0	12,3	3,1	5,8	27,0	7,6
PB1E-10-20	8,6	4,9	11,0	0,1	0,5	7,4	0,1	3,8	3,9
PB1E-10-60	2,2	8,1	7,6	0,0	0,0	1,0	0,0	2,9	5,4
PB1E-10-140	72,6	17,7	0,0	0,0	14,8	2,0	7,3	26,7	3,9
PB1E-10-140-160A	46,4	20,2	4,8	0,0	9,5	2,3	4,5	19,2	4,8
PB1E-12-20	23,5	12,2	13,8	0,1	0,0	11,9	0,0	16,4	6,2
PB1E-12-60	10,2	11,7	9,8	0,0	0,0	3,0	0,0	11,7	9,1
PB1E-12-100	61,2	7,4	8,2	0,0	4,9	1,6	2,2	31,9	7,1
PB1E-12-120-140B	58,2	20,5	7,0	0,0	4,1	1,6	2,7	34,2	7,0
PB1E-13-20	16,9	20,9	22,8	0,1	5,1	11,2	3,2	15,3	9,7
PB1E-13-40	28,5	27,0	11,6	0,1	26,5	6,2	3,8	16,8	9,6
PB1E-13-80	46,7	11,7	8,0	0,0	22,1	2,8	9,6	15,1	8,7
PB1E-13-100	17,0	13,8	7,8	0,0	6,7	1,2	2,2	11,8	10,3
PB1E-13-110-130B	10,5	14,8	8,0	0,0	3,0	1,1	0,8	11,7	8,9
PB1E-14-20	29,1	6,8	45,4	0,2	9,1	21,0	2,6	23,0	6,7
PB1E-14-40	7,1	3,6	16,4	0,1	3,9	1,4	0,0	10,0	14,2
PB1E-14-60	79,2	23,9	8,6	0,0	21,4	0,7	6,9	42,7	15,9
PB1E-14-100	43,1	30,8	46,8	0,0	8,7	3,7	5,1	36,8	18,6
PB1E-14-140	42,6	36,4	13,8	0,0	5,1	2,8	2,4	38,7	13,3
PB1E-16-20	46,0	22,7	34,4	0,1	12,6	27,2	6,9	23,3	7,8
PB1E-16-80	24,4	7,8	16,0	0,0	5,9	2,3	3,3	18,9	15,1
PB1E-16-120A	234,9	141,1	8,8	0,0	63,4	3,7	36,2	72,2	10,5
PB1E-16-120B	161,8	63,6	7,8	0,0	27,2	3,0	18,5	58,8	10,9
PB1E-16-160-180	99,7	68,8	11,4	0,0	7,2	8,0	4,2	86,1	12,3
PB1E-17-20	3,1	1,7	15,2	0,1	0,1	7,1	0,1	1,4	6,7
PB1E-17-80	4,3	5,3	17,0	0,0	0,9	4,2	0,6	7,2	15,1
PB1E-17-120A	225,3	94,2	11,0	0,0	39,8	3,6	23,4	103,5	14,9
PB1E-17-120B	176,1	61,6	6,8	0,0	25,6	3,0	15,4	81,9	10,9
PB1E-17-220	144,1	132,0	77,5	0,0	23,8	14,2	11,9	151,9	25,0
PB1E-18-20	7,2	4,2	15,4	0,1	1,8	6,7	0,5	6,0	7,5
PB1E-18-60	9,9	6,4	20,4	0,1	2,0	3,2	0,7	12,8	14,5
PB1E-18-100B	22,4	7,8	12,8	0,0	2,3	4,3	1,1	13,3	22,5
PB1E-18-120-130	28,6	8,6	40,0	0,0	3,7	6,9	1,0	33,0	24,7
PB1E-18-220B	93,5	95,8	12,4	0,0	10,5	15,2	6,1	105,0	20,7
PB1E-19-20	6,7	3,4	22,2	0,1	0,0	10,0	0,1	5,4	5,0
PB1E-19-40	2,9	3,5	19,0	0,1	2,7	5,9	0,6	6,0	13,7
PB1E-19-80	17,9	17,1	13,6	0,0	7,7	5,1	2,5	20,7	16,6
PB1E-19-120B	17,9	12,7	8,8	0,0	7,9	5,3	2,5	8,5	24,8
PB1E-19-160	11,0	6,1	13,6	0,0	2,3	2,5	0,5	11,9	21,5
PB1E-19-180A	10,1	1,6	13,8	0,0	0,8	2,2	0,1	8,9	23,7
PB1E-21-20	14,0	10,7	31,4	0,2	0,4	5,2	0,2	22,0	7,4
PB1E-21-70	67,4	71,8	14,2	0,0	29,1	17,1	7,4	77,0	13,6

PB1E-21-110A	47,0	97,9	12,0	0,0	40,0	1,8	12,6	34,1	19,4
PB1E-21-150B	39,4	59,2	11,2	0,0	25,0	3,1	10,8	22,2	22,8
PB1E-24-20	8,6	9,4	17,0	0,1	8,1	5,9	1,4	9,7	5,7
PB1E-24-80	27,7	8,7	10,0	0,0	7,6	1,0	2,5	14,8	15,0
PB1E-24-160	14,6	27,2	9,2	0,0	3,6	0,5	1,0	21,6	20,2
PB1E-27-20	3,4	4,3	12,8	0,1	1,1	9,2	0,1	3,5	3,1
PB1E-27-100	8,8	20,6	5,8	0,0	4,0	2,1	1,0	13,3	6,6
PB1E-27-160	23,0	24,7	6,2	0,0	4,4	1,5	1,1	24,0	10,6
PB1E-27-200B	15,8	11,6	6,4	0,0	0,8	1,5	0,0	13,8	7,4
PB1E-30-20	2,4	4,0	8,2	0,0	0,0	3,4	0,0	0,7	2,1
PB1E-30-100	133,9	3,1	0,0	0,0	21,6	3,6	6,0	47,3	2,2
PB1E-30-190-200	173,9	73,0	0,0	0,0	28,8	3,4	13,7	92,9	8,3
PB1E-35-20	3,4	6,9	5,8	0,0	0,7	3,8	0,6	1,6	1,0
PB1E-35-160-200	24,3	14,0	0,0	0,0	9,9	2,4	2,9	13,8	4,0
PB1E-40-20	6,8	8,5	6,0	0,0	1,3	5,2	1,0	3,4	0,8
PB1E-40-100-110	8,7	6,3	0,0	0,0	6,3	1,5	2,4	3,3	2,3
PB1W-6-20	31,5	11,1	11,2	0,1	4,5	9,7	2,3	15,2	2,1
PB1W-6-110	22,4	10,3	3,6	0,0	4,0	0,6	1,7	12,1	2,5
PB1W-10-20	33,4	4,5	9,4	0,0	1,4	8,5	1,2	10,7	2,6
PB1W-10-130B	5,3	18,0	7,2	0,0	2,5	0,3	0,9	13,1	5,2
PB1W-12-20	3,0	2,9	12,0	0,0	0,0	3,0	0,0	2,4	2,6
PB1W-12-40-60	0,0	11,2	7,0	0,0	0,3	1,2	0,1	2,4	3,9
PB1W-12-80	4,0	11,3	6,6	0,0	3,7	1,2	1,9	5,3	5,0
PB1W-12-110B	18,8	6,5	7,6	0,0	2,4	1,2	1,3	12,8	6,5
PB1W-12-140B	13,5	11,0	7,2	0,0	2,6	0,9	0,8	9,5	4,1
PB1W-14-60	32,5	20,7	10,2	0,0	5,3	4,3	1,4	25,2	7,8
PB1W-14-90	245,9	48,9	40,8	0,0	50,9	3,5	24,2	80,9	16,6
PB1W-14-160-180	39,7	44,7	60,1	0,0	4,4	2,5	2,4	53,6	13,5
PB1W-15-10	57,1	19,4	10,0	0,0	5,1	24,9	2,4	25,1	4,4
PB1W-15-60-75	4,6	4,2	9,8	0,1	0,0	0,4	0,0	5,0	10,3
PB1W-15-80-110B	3,7	6,1	8,6	0,0	0,0	0,2	0,0	4,0	6,5
PB1W-15-110-130	23,9	16,4	10,0	0,0	0,6	1,4	0,4	22,0	9,8
PB1W-15-140-150	128,3	84,4	12,8	0,0	5,2	10,5	3,9	108,3	9,6
PB1W-17-40	3,4	6,2	12,0	0,0	0,0	3,7	0,0	4,2	8,4
PB1W-17-80	20,9	15,8	10,0	0,0	4,1	1,9	1,8	25,5	10,7
PB1W-17-160	71,0	66,2	77,5	0,0	15,4	16,1	7,8	81,2	16,6
PB1W-19-20	5,4	3,4	15,0	0,1	0,3	3,0	0,0	6,9	10,0
PB1W-19-50	14,0	13,8	14,2	0,0	2,6	2,2	1,5	14,2	16,3
PB1W-19-80A	171,0	387,1	10,0	0,0	67,1	20,3	23,0	175,1	12,0
PB1W-19-80B	202,3	122,0	8,8	0,0	19,6	15,5	9,3	155,5	13,5
PB1W-19-100	162,5	99,1	80,9	0,0	20,1	14,7	9,0	151,0	22,5
PB1W-19-140A	115,0	486,7	18,4	0,0	91,8	17,2	34,8	144,9	10,6
PB1W-20-20	8,2	8,8	15,0	0,0	0,0	3,3	0,0	10,7	9,4
PB1W-20-60	26,1	7,8	12,4	0,0	9,7	3,7	3,9	14,0	13,7

PB1W-20-100A	30,5	5,6	9,6	0,0	3,8	2,3	0,9	18,0	12,7
PB1W-20-140B	41,1	21,5	8,2	0,0	0,0	3,5	0,3	31,6	6,3
PB1W-21.5-20	4,9	10,2	16,2	0,0	0,5	2,5	0,2	13,3	12,0
PB1W-21.5-100B	18,2	14,6	9,8	0,0	5,1	2,3	2,1	19,9	17,6

Table 9.6: pH(H_2O) and EC (uS/cm) data of the Klawer heuweltjie (K1). Samples containing both soil and indurated material were separated as A and B respectively.

Sample ID	pH (H_2O)	EC (uS/cm)	Sample ID	pH (H_2O)	EC (uS/cm)
K1-2-10	7,0	538,0	K1-18-40-50	8,6	2138,0
K1-2-30-50	5,7	7540,0	K1-18-95-105	7,7	7640,0
K1-4-10	7,1	378,4	K1-18-155-165	7,7	14280,0
K1-4-50-60	5,4	4640,0	K1-18-190-200	7,9	11140,0
K1-7-10	7,6	1588,0	K1-18-295-305	7,7	13040,0
K1-7-90-105	6,2	10560,0	K1-19-10	9,3	588,0
K1-8-10	7,1	4820,0	K1-19-40-50	8,9	3998,0
K1-8-20-30	6,9	6340,0	K1-19-70-80A	7,9	8020,0
K1-8-40-50	5,9	12620,0	K1-19-70-80B	8,1	6060,0
K1-8-50-70	5,2	13380,0	K1-19-10-110A	7,8	8440,0
K1-8-95-110	7,1	10960,0	K1-19-100-110B	7,7	14680,0
K1-11-10	8,0	452,0	K1-19-160-170	7,9	12880,0
K1-11-60-70	8,3	2054,0	K1-19-200-220	7,6	14420,0
K1-11-90-100	8,0	4580,0	K1-19-295-305	7,6	13020,0
K1-11-130-140	7,6	7160,0	K1-21-10	8,3	536,0
K1-11-210-220	7,7	12360,0	K1-21-30-40	9,4	1498,0
K1-11-275-285	7,6	12640,0	K1-21-90-100	8,6	4740,0
K1-13-10	8,5	1232,0	K1-21-110-120A	7,9	7680,0
K1-13-40-50	9,3	404,0	K1-21-110-120B	8,4	5360,0
K1-13-80-90	8,2	4360,0	K1-21-120-140	7,9	10740,0
K1-13-100-110	7,5	8520,0	K1-21-190-205	7,8	11980,0
K1-13-125-135	7,5	7460,0	K1-21-290-305	7,7	13500,0
K1-13-220-230	7,7	14460,0	K1-23-10	7,7	331,0
K1-13-290-300	7,2	16000,0	K1-23-20-30	7,8	155,4
K1-15-10	7,7	432,0	K1-23-90-100A	7,7	3260,0
K1-15-30-40	8,4	249,8	K1-23-90-100B	7,6	4400,0
K1-15-70-80	7,5	6800,0	K1-23-120-150	7,6	9720,0
K1-15-110-120B	7,8	7980,0	K1-23-210-225	7,7	12620,0
K1-15-120-135	7,6	7220,0	K1-23-330-355	7,6	11120,0
K1-15-140-150	7,6	19640,0	K1-26-10	7,1	151,4
K1-15-190-200	7,7	15760,0	K1-26-40-50	7,4	836,0
K1-15-280-290	7,5	15360,0	K1-26-85-95	7,7	5080,0
K1-17-10	8,0	430,0	K1-26-200-210	7,6	8580,0
K1-17-40-50	9,4	606,0	K1-26-275-285	7,6	8180,0

K1-17-80-100	7,6	7480,0	K1-28-10	7,2	154,8
K1-17-100-110	7,6	6880,0	K1-28-20-30	7,1	196,4
K1-17-160-180	7,7	15220,0	K1-28-30-50	7,8	2150,0
K1-17-200-220	7,8	10460,0	K1-28-120-135	7,7	648,0
K1-17-280-295	7,8	10900,0	K1-28-190-200	7,7	6700,0
K1-17-305-315	7,7	10920,0	K1-30-10	7,1	297,6
K1-18-10	8,7	277,2	K1-30-40-50	7,9	2728,0
			K1-30-85-105	7,6	7100,0

Table 9.7: Anion, cation, dissolved Si and alkalinity data (mg/L) of the heuweltjie in Klawer (K1). Samples containing both soil and indurated material were separated as A and B respectively.

	Concentration (mg/L)								
Sample ID	Cl^-	$SO4^{2-}$	Alkalinity	PO_4^{3-}	Ca^{2+}	K^+	Mg^{2+}	Na^+	Dissolved Si
K1-2-10	121,8	14,3	25,2	0,2	6,3	4,8	1,9	84,9	8,3
K1-2-30-50	2254,2	508,9	11,6	0,0	114,8	28,7	150,7	1254,4	26,9
K1-4-10	73,6	18,9	24,2	0,3	0,0	7,2	0,3	53,2	8,0
K1-4-50-60	1264,9	313,3	10,0	0,0	41,8	22,8	44,3	791,5	13,2
K1-7-10	337,5	98,7	73,9	0,8	25,2	34,4	12,7	222,2	10,9
K1-7-90-105	3396,9	690,4	12,8	0,0	159,7	44,2	204,5	1858,1	18,2
K1-8-10	1457,6	113,2	29,6	0,3	71,4	86,3	60,7	691,0	8,1
K1-8-20-30	1892,4	342,6	22,0	0,1	140,1	31,1	128,4	926,9	12,0
K1-8-40-50	3580,2	2365,2	13,6	0,1	853,2	37,1	429,4	1568,2	12,4
K1-8-50-70	4068,3	1842,8	10,0	0,1	579,7	50,6	437,1	1854,4	11,8
K1-8-95-110	3352,0	704,0	39,6	0,1	114,9	47,3	166,5	1960,1	29,1
K1-11-10	49,9	23,2	94,7	0,9	4,3	21,4	2,3	61,0	10,3
K1-11-60-70	525,2	34,8	76,7	0,1	49,7	17,8	8,8	315,3	14,6
K1-11-90-100	1284,2	171,4	54,8	0,1	24,1	30,7	22,2	742,3	16,8
K1-11-130-140	1841,6	734,9	70,9	0,3	104,7	44,2	76,3	1235,9	29,8
K1-11-210-220	3934,6	745,9	52,0	0,1	205,9	90,2	202,8	2144,2	19,9
K1-11-275-285	4027,7	801,4	45,8	0,0	212,6	92,6	225,2	2181,2	14,1
K1-13-10	209,9	23,2	174,2	2,7	12,5	24,5	4,1	203,5	9,4
K1-13-40-50	7,9	4,0	216,2	0,6	0,0	8,8	0,7	82,5	18,0
K1-13-80-90	1234,1	101,1	65,9	0,1	68,1	46,7	18,1	720,3	13,8
K1-13-100-110	1595,8	2444,0	34,8	0,2	651,1	69,8	144,8	1161,1	18,8
K1-13-125-135	1595,7	1264,3	56,5	0,1	116,5	50,2	69,0	1337,9	24,8
K1-13-220-230	4786,8	834,9	55,4	0,1	314,0	120,1	255,1	2502,0	17,6
K1-13-290-300	5037,5	1047,4	47,6	0,1	373,5	112,0	326,9	2597,2	11,4
K1-15-10	23,6	74,4	60,1	0,5	32,5	12,8	7,7	24,9	9,3
K1-15-30-40	2,1	8,2	135,3	0,2	5,7	9,7	2,3	30,8	11,9
K1-15-70-80	1239,5	1647,2	40,2	0,1	505,6	62,6	119,7	847,8	10,0
K1-15-110-120B	1320,4	2360,8	38,4	0,1	660,3	70,0	159,8	988,8	8,3
K1-15-120-135	1041,7	2350,0	35,8	0,1	641,0	62,0	145,7	864,4	14,9
K1-15-140-150	5804,3	3421,0	51,4	0,2	1137,0	127,8	553,9	3230,5	23,5

K1-15-190-200	4897,0	1141,9	60,7	0,1	410,1	127,0	333,7	2654,4	18,1
K1-15-280-290	4603,9	1633,0	44,6	0,1	580,8	118,9	399,5	2349,5	10,0
K1-17-10	41,6	31,0	80,9	0,3	27,0	18,5	7,3	34,3	9,4
K1-17-40-50	22,3	3,3	275,8	0,5	11,6	9,4	1,7	102,2	12,9
K1-17-80-100	1307,8	2245,9	35,2	0,1	709,6	63,5	227,3	760,1	8,1
K1-17-100-110	1095,3	2188,0	35,2	0,1	688,0	65,8	201,5	660,1	8,4
K1-17-160-180	3883,9	3046,3	49,2	0,1	801,5	132,8	474,0	2221,1	20,4
K1-17-200-220	2915,0	995,6	53,8	0,0	275,0	101,9	220,7	1637,9	10,5
K1-17-280-295	3257,2	675,3	45,4	0,1	176,6	112,2	216,5	1719,2	9,3
K1-17-305-315	3260,6	675,7	48,0	0,1	207,3	111,1	238,7	1714,3	8,8
K1-18-10	3,5	2,4	126,5	0,4	9,1	7,4	2,7	41,6	9,4
K1-18-40-50	524,6	34,2	104,9	0,1	24,3	30,6	6,5	348,6	9,7
K1-18-95-105	1397,8	2158,4	35,4	0,2	719,4	51,1	228,9	755,0	9,3
K1-18-155-165	3629,8	2837,1	43,2	0,1	808,8	132,7	444,2	2003,2	16,6
K1-18-190-200	3249,1	773,0	59,5	0,1	240,4	110,7	250,2	1746,6	10,3
K1-18-295-305	4036,9	794,6	49,8	0,1	299,8	122,7	327,3	2050,3	8,8
K1-19-10	37,3	5,4	224,4	0,6	15,1	8,8	2,6	87,5	11,9
K1-19-40-50	951,4	188,0	150,3	0,2	39,4	62,3	14,0	677,4	5,2
K1-19-70-80A	1337,2	2471,8	36,6	0,1	679,4	64,9	209,4	950,6	5,6
K1-19-70-80B	1244,5	1094,7	44,0	0,1	229,3	51,9	126,9	835,2	5,4
K1-19-10-110A	1533,4	2452,3	33,2	0,1	698,6	67,0	245,7	966,8	9,1
K1-19-100-110B	3820,6	2901,1	47,2	0,1	790,1	109,2	468,3	2113,6	12,9
K1-19-160-170	3786,7	1168,6	58,1	0,1	353,7	110,5	330,3	2007,9	14,0
K1-19-200-220	4588,6	827,0	51,0	0,0	315,8	125,5	370,5	2303,7	8,5
K1-19-295-305	3959,0	920,5	43,0	0,0	289,9	114,3	323,4	2022,8	7,4
K1-21-10	70,9	16,5	102,9	1,2	17,4	19,2	6,0	69,7	8,8
K1-21-30-40	282,9	27,4	209,8	0,6	7,3	25,2	2,4	241,5	12,8
K1-21-90-100	1013,5	551,0	92,7	0,1	57,2	34,3	25,0	843,5	12,4
K1-21-110-120A	1223,0	2399,4	38,8	0,0	585,1	60,4	130,5	1045,3	10,0
K1-21-110-120B	1289,6	506,3	80,9	0,0	60,7	37,3	43,8	936,7	9,7
K1-21-120-140	2302,3	2500,3	50,8	0,1	546,5	70,5	204,2	1712,7	13,8
K1-21-190-205	3599,4	939,7	56,1	0,1	275,5	89,6	241,4	1964,0	15,5
K1-21-290-305	4300,6	857,4	44,0	0,0	295,0	104,9	347,7	2112,0	8,1
K1-23-10	25,5	41,5	50,0	0,2	16,6	12,3	9,1	21,7	10,1
K1-23-20-30	4,0	6,0	54,8	0,2	10,1	8,5	4,0	9,6	11,4
K1-23-90-100A	878,4	155,1	46,0	0,0	109,5	4,5	69,7	403,2	16,0
K1-23-90-100B	1311,8	145,7	41,0	0,0	146,8	5,6	104,9	575,4	16,6
K1-23-120-150	2542,4	1749,3	50,0	0,1	694,3	14,6	353,8	1092,9	20,8
K1-23-210-225	2967,3	2929,6	54,2	0,1	708,9	71,8	355,0	1868,5	22,5
K1-23-330-355	3298,5	914,5	44,0	0,0	323,7	78,7	307,2	1663,8	8,4
K1-26-10	19,7	5,3	20,6	0,1	8,6	2,2	1,3	15,7	9,6
K1-26-40-50	179,5	38,7	31,2	0,1	8,3	3,2	3,2	131,2	17,3
K1-26-85-95	1297,8	351,3	58,7	0,3	74,4	23,6	67,0	833,0	26,8
K1-26-200-210	2471,1	596,8	60,5	0,0	210,0	63,2	176,6	1337,9	12,8
K1-26-275-285	2309,3	625,6	56,5	0,0	186,9	59,9	165,6	1252,1	9,6
K1-28-10	16,8	9,8	20,6	0,1	7,0	9,1	1,5	13,0	8,4

K1-28-20-30	32,1	5,2	23,2	0,1	9,5	2,1	2,3	27,5	9,3
K1-28-30-50	467,0	155,0	70,7	0,2	21,7	16,7	17,0	352,6	26,8
K1-28-120-135	1768,8	379,2	71,3	0,1	108,0	47,7	101,1	1015,5	26,6
K1-28-190-200	1835,6	489,7	70,5	0,0	147,9	50,2	121,9	1032,2	14,0
K1-30-10	63,8	6,9	14,4	0,1	4,8	7,4	2,6	36,2	8,5
K1-30-40-50	630,1	177,7	80,1	0,3	22,5	20,1	22,1	458,4	25,4
K1-30-85-105	2044,6	382,5	64,5	0,1	103,5	52,7	112,6	1126,7	29,0